



US Army Corps  
of Engineers  
Waterways Experiment  
Station

AD-A285 193

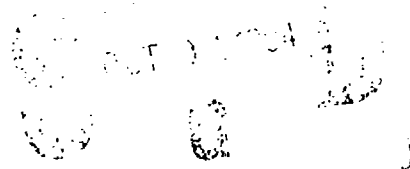


Technical Report GL-94-29  
August 1994

# Normalization and Prediction of Geotechnical Properties Using the Cone Penetrometer Test (CPT)

by *Richard S. Olsen*

DTIC REPORT UNCLASSIFIED &



Approved For Public Release; Distribution Is Unlimited

94

94-31531



Prepared for Headquarters, U.S. Army Corps of Engineers

The contents of this report are not to be used for advertising, publication, or promotional purposes. Citation of trade names does not constitute an official endorsement or approval of the use of such commercial products.



PRINTED ON RECYCLED PAPER

# Normalization and Prediction of Geotechnical Properties Using the Cone Penetrometer Test (CPT)

by Richard S. Olsen

U.S. Army Corps of Engineers  
Waterways Experiment Station  
3909 Halls Ferry Road  
Vicksburg, MS 39180-6199

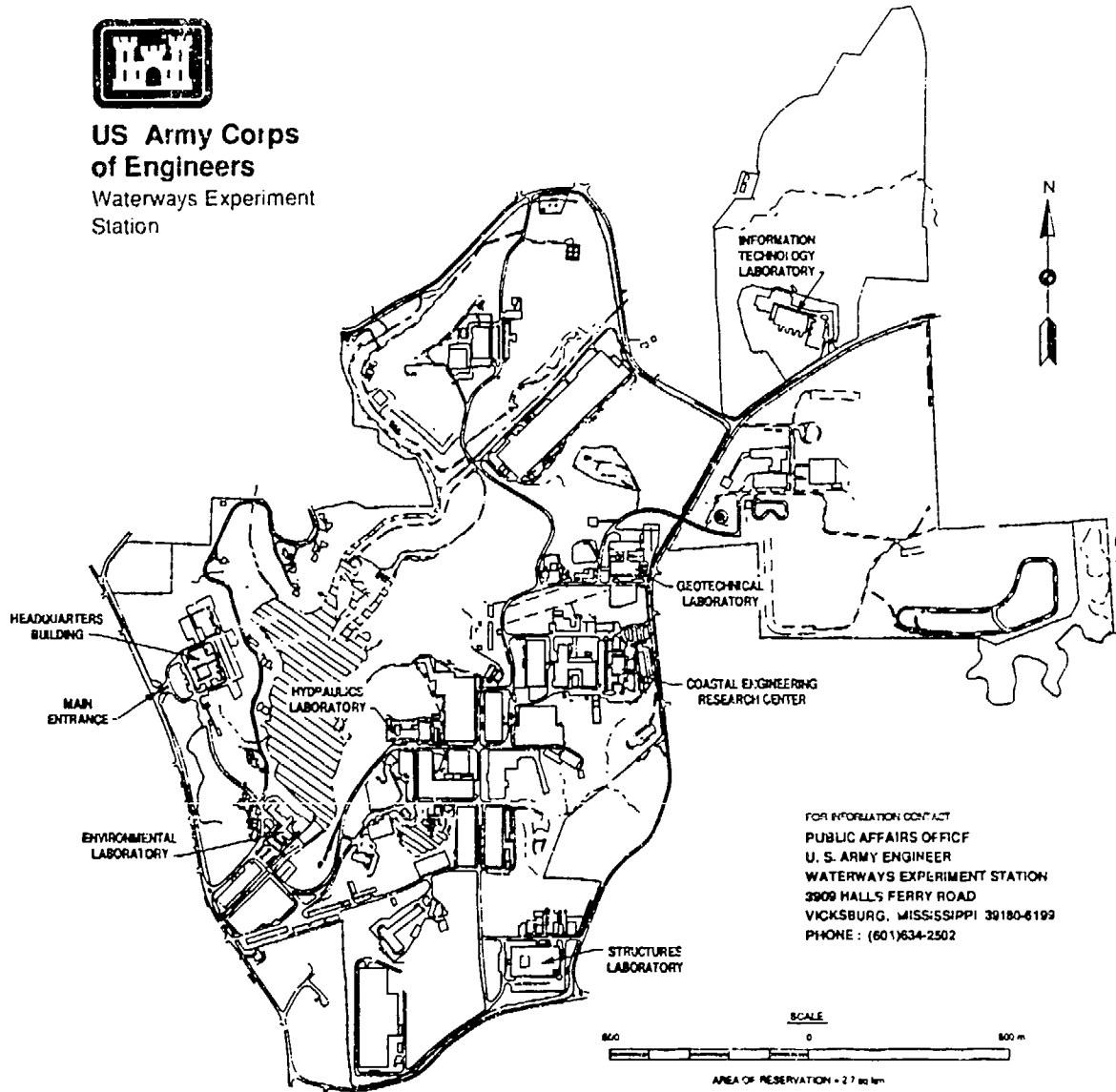
Accession For	
NTIS	CRA&I
DTIC	LAB
Unlimited	
By	
Date	
Availability	
Dist	Avail. or Special
A-1	

Final Report

Approved for public release; distribution is unlimited



**US Army Corps  
of Engineers**  
Waterways Experiment  
Station



### Waterways Experiment Station Cataloging-In-Publication Data

Olsen, Richard S.

Normalization and prediction of geotechnical properties using the cone penetrometer test (CPT) / by Richard S. Olsen ; prepared for U.S. Army Corps of Engineers.

322 p. : ill. ; 28 cm. -- (Technical report. ; GL-94-29)

Includes bibliographic references.

1. Soils -- Testing -- Statistical methods. 2. Soil penetration test. 3. Probability measures. 4. Penetrometer. I. United States. Army. Corps of Engineers. II. U.S. Army Engineer Waterways Experiment Station. IV. Geotechnical Laboratory (U.S.) V. Title. VI. Series: Technical report (U.S. Army Engineer Waterways Experiment Station) ; GL-94-29. TA7 W34 no.GL-94-29

## Preface

The Doctor of Philosophy (Ph.D.) dissertation replicated in this report was written by Dr. Richard S. Olsen, In Situ Evaluation Branch (ISEB), Earthquake Engineering and Geosciences Division (EEGD), Geotechnical Laboratory (GL), Waterways Experiment Station (WES). Dr. Olsen is under the direct supervision of Mr. M. A. Vispi, Chief, ISEB, and general supervision of Dr. A. G. Franklin, Chief, EEGD, and Dr. W. F. Marcuson III, Director, GL.

The dissertation committee chairman at the University of California at Berkeley (UCB) was Prof. James K. Mitchell and the other committee members were Prof. Raymond B. Seed and Prof. H. Frank Morrison. Dr. Olsen was on WES sponsored Long Term Training (LTT) from August 1988 to September 1989 at the UCB campus (he also received his Master of Science degree from UCB in 1977). He passed his written Preliminary Examination in May 1989 and Oral Qualifying Examination in April 1991. He was advanced to candidate for the Ph.D. degree in April 1991 and the final dissertation was submitted to the University on May 20, 1994.

At the time of publication of this report, Director of WES was Dr. Robert W. Whalin. Commander was COL Bruce K. Howard, EN.

*The contents of this report are not to be used for advertising, publication, or promotional purposes. Citation of trade names does not constitute an official endorsement or approval for the use of such commercial products.*

Normalization and Prediction  
of Geotechnical Properties  
Using the Cone Penetrometer Test (CPT)

by

Richard Scott Olsen

B.S.C.E. (Oregon State University) 1976  
M.S. (University of California, Berkeley) 1977

A dissertation submitted in partial satisfaction of the  
requirements for the degree of  
Doctor of Philosophy  
in  
Engineering—Civil Engineering  
in the  
GRADUATE DIVISION  
of the  
UNIVERSITY of CALIFORNIA at BERKELEY

Committee in charge:

Professor James K. Mitchell, Chair  
Professor Raymond B. Seed  
Professor H. Frank Morrison

1994



# Abstract

Normalization and Prediction  
of Geotechnical Properties  
Using the Cone Penetrometer Test (CPT)

by

Richard Scott Olsen  
Doctor of Philosophy in Civil Engineering  
University of California at Berkeley  
Professor James K. Mitchell, Chair

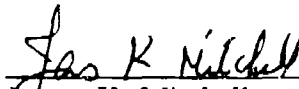
The objectives of this research were to develop techniques for (1) stress normalization of CPT measurements (and geotechnical properties) and (2) CPT prediction of geotechnical properties using cone and sleeve friction resistance values. Stress normalization allows a variable geotechnical property to be reduced to an equivalent value at a standard confining stress.

A new concept, the Stress Focus, was identified which provides a basis for understanding soil strength as a function of confining stress. This study demonstrated that sand friction angles for different initial relative densities converge to a Stress Focus at high confining stress (approximately 100 atm), where the strength behavior is similar to that of a sedimentary rock. Dilation of dense sands decreases with increased confining stress until the Stress Focus is reached, as confirmed using historic high pressure triaxial test data as well with CPT measurements from laboratory chamber tests and uniform soil layers. The paths of convergence to the Stress Focus are exponentially related to confining stress and are the basis for development of CPT cone and sleeve friction resistance normalization techniques. The overburden stress at the Stress Focus is soil type dependent.



The stress exponent for SPT normalization was shown to be equal to the CPT derived stress exponent.

CPT correlations to geotechnical properties were established using both CPT cone resistance and friction ratio. These correlations were based on a large database which was developed for this research effort. Statistical evaluation during the development of these correlations concentrated on excluding biased data. CPT based correlations were established for the following geotechnical properties: SPT blow count, unconsolidated undrained triaxial test strength, field vane shear test strength, and shear wave velocity.

  
\_\_\_\_\_  
James K. Mitchell  
Dissertation Committee Chairman

## Dedication

I wish to thank Professor James K. Mitchell and acknowledge the late H. Bolton Seed for being two of the greatest teachers that I have known. While preparing to return to UC Berkeley for PhD studies from 1982 to 1988 and while attending classes during 1988 and 1989, I was in nearly constant communication with the late H. Bolton Seed. After the death of Professor Seed in 1989, Professor Mitchell became my dissertation chairman and I am very thankful that it was a seamless transition. A special gratitude goes to Professor Mitchell during my class work studies, PhD examinations, research phase and dissertation preparation from 1988 to 1994. He was also instrumental in securing project funding from the Department of Energy. He also read through the massive first draft, providing valuable insight toward shorter final versions. A sincere thanks goes out to Dr. Joseph P. Koester and Dr. A. G. Franklin (Waterways Experiment Station) for their in-depth detailed review of the final draft before it went to committee members. I would also like to express my gratitude to the other members of the committee, Professors Raymond B. Seed and H. Frank Morrison, for their review of this manuscript.

I dedicate this dissertation to my father, Irving E. Olsen, for his contributions to my career. He introduced me to world of geotechnical engineering as a small child. I worked summers on the drafting table, then in the lab, and finally in the field on inspection jobs and logging borholes while still in high school. I'm sure that he would have supported any occupation that I picked, but I enjoyed geotechnical engineering. As the principle-in-charge of the Portland office of Dames & Moore in the late 1960s, his acceptance of the mechanical Dutch cone penetrometer allowed two contractors to start business in the Northwest. It also started my working exposure to Cone Penetrometer Test (CPT) technology. I worked as a helper on both of these CPT rigs during the 1972 to 1974 summers of my high school and college years. My father also planted a seed in my head that the Unified Soil Classification System (USCS) was not enough; the profession needed a good index for soil

strength. I believe that this dissertation points toward the future of using the CPT as a rapid tool for indexing soil strength.

Christine, my enduring partner, best friend and devoted wife, would always remind me that there is an end to the PhD work. She has had to live as the wife of a PhD student and the wife of a full time research engineer. She loves music but would turn it off at night while I worked at this computer. She has gone on numerous vacations and trips by herself, leaving me at home to work on the dissertation.

To Erin, my daughter, for her willingness to adjust to a new school when we moved to Berkeley for my PhD studies and always having to turn down the TV. She understands my needs because she is a good student.

And finally Jonathan, my son, who was two when I went back to school for PhD studies and is now seven. He always wants to be my buddy, to sit on my lap, or to be at my side. He has only known his dad as always needing to work on the dissertation. During the weekends, I would work for 4 hours then we would play for 1/2 an hour. His vocabulary is now filled with words such as data, PC, digitizer, scanner, unstable soil, CPT, and dad's study. I hope that he has seen the effort of hard work—education is what you make of it and it can be fun. Your brain is the most powerful part of the body—exercise it and life becomes fascinating.

This dissertation is also for my professional career. CPT is my profession and the opportunity to write this dissertation has allowed me to revisit fundamental theory to discover new concepts and prove old ideas.

Richard S. Olsen  
May 1994

# Table of Contents

Abstract .....	1
Dedication .....	iii
Table of Contents .....	v
List of Figures .....	x
List of Tables .....	xxii
List of Symbols .....	xxiii
Chapter 1 - Introduction .....	1
• General .....	1
• <i>The CPT Test</i> .....	2
• <i>The CPT Measurements</i> .....	4
• <i>Developing CPT Prediction Relationships for Geotechnical Properties</i> ..	4
• <i>Stratigraphic Influences on CPT Correlations</i> .....	5
• <i>Accounting for Factors that Influence Geotechnical Properties</i> .....	6
• <i>Using CPT based Soil Classification</i> .....	6
• <i>Accounting for Stress Effects in CPT Correlations</i> .....	8
• Outline of Dissertation .....	10
Chapter 2 - Mohr Envelope Curvature and Development of the Stress Focus	
Concept .....	12
• Introduction .....	12
• Baligh Formulation of Curvature Envelope .....	12
• New Strength Normalization Based on Failure Envelope Curvature .....	15
• The Stress Focus Concept .....	16
• Rock Mechanics and Friction Angle at High Confining Stresses .....	18

Chapter 3 - Stress Normalization . . . . .	28
• Introduction . . . . .	28
• The Stress Exponent for Geotechnical Engineering . . . . .	29
• The Stress Focus and Stress Exponent Interrelationship . . . . .	34
• Stress Type and Stress Normalization . . . . .	34
• The Atmospheric Pressure Standard . . . . .	38
Chapter 4 - Developing the Cone Resistance Normalized Formulation . . . . .	39
• Introduction . . . . .	39
• Comparison of Limit Equilibrium and Cavity Expansion Theories . . . . .	40
• Exponential Behavior of the Cone Resistance . . . . .	40
• Development of the Cone Resistance Normalization Formulation . . . . .	44
• <i>Development of the Bearing Capacity Formulation for Clay</i> . . . . .	47
• <i>Development of the Bearing Capacity Formulation for Sand</i> . . . . .	48
• Modification to the Bearing Formulation for Non-linear Exponential Behavior . . . . .	49
• Bearing Stress Formulation for All Soil Types . . . . .	50
Chapter 5 - Cone Resistance Stress Focus—Confirmation Using CPT Chamber Test Data . . . . .	51
• Introduction . . . . .	51
• Interpretation of Large Diameter Test Chamber Data . . . . .	53
• <i>Explanation of the Cone Resistance Stress Focus</i> . . . . .	54
• <i>Shallow and Deep Bearing Stress in Terms of the Stress Focus</i> . . . . .	57
• Using Chamber Data to Establish Trends of Stress Exponent and the Stress Focus . . . . .	60
• <i>Evaluation of the Chamber Data</i> . . . . .	60
• <i>CPT Stress Exponent Evaluation</i> . . . . .	61
• <i>Overconsolidation Effects on the Stress Exponent</i> . . . . .	67

· <i>Chamber Boundary Effects for Dense Sands</i> . . . . .	69
• SPT Chamber Evaluation . . . . .	76
· <i>SPT Chamber Data Plotting</i> . . . . .	77
· <i>SPT Stress Focus and Sand Type</i> . . . . .	77
· <i>Chamber Test Stress Exponent Discussion</i> . . . . .	87
• Conclusion . . . . .	92
Chapter 6 - CPT Prediction of CPT Normalization Parameters—Developed using Uniform Soil Layer Data . . . . .	93
• Introduction . . . . .	93
• Limitations and Merits of Using In Situ Data for Stress Normalization . . . . .	94
• Establishing In Situ Uniform Layer Trends . . . . .	95
• Establishing Cone Resistance Stress Exponents using the CPT Soil Characterization Chart . . . . .	97
· <i>Discussion of Cone Resistance Stress Exponent on the CPT Soil         Characterization Chart</i> . . . . .	99
• Establishment of the Sleeve Friction Resistance Stress Exponent . . . . .	115
· <i>Direct Correlation of Sleeve and Cone Stress Exponents</i> . . . . .	115
• Determining the Soil Type Dependent Stress Focus using Uniform Soil Layer Data . . . . .	119
· <i>Developing the Stress Focus Relationship for Different Soil Types</i> . . . . .	119
· <i>Soil Type Dependent Trend of the Stress Focus</i> . . . . .	125
• Conclusions . . . . .	127
Chapter 7 - Normalization of Selected Geotechnical Properties . . . . .	130
• Introduction . . . . .	130
• Standard Penetration Test (SPT) Normalization . . . . .	130
· <i>Historical SPT Blow Count Normalization</i> . . . . .	131
· <i>SPT Blow Count Normalization</i> . . . . .	133
· <i>Stresses at the SPT Sampler</i> . . . . .	133

- *Mud Stress Influence at the SPT Sampler* . . . . . 136
- *Stresses at the SPT Sampler for Field In Situ conditions* . . . . . 137
- *Stresses at the SPT Sampler for Chamber Testing Conditions* . . . . . 140
- *Conclusion* . . . . . 146
- Normalization of the Shear Wave Velocity . . . . . 148
  - *Introduction* . . . . . 148
  - *Definition of Normalized Maximum Shear Modulus* . . . . . 149
  - *Relating Maximum Shear Modulus to Shear Wave Velocity* . . . . . 149
  - *Relationships of Shear Wave Velocity Stress Exponent to Soil Type* . . . . . 152
  - *Shear Wave Velocity Stress Exponent trend from a Sand Site* . . . . . 153
  - *Relating Stress Exponents for Shear Wave Velocity & Cone Resistance* . . . . . 155
  - *Conclusions* . . . . . 158

Chapter 8 - Development of Correlations for CPT Prediction of Geotechnical

- Properties . . . . . 159
- Introduction . . . . . 159
- The CPT and soil sample database . . . . . 161
- Using the CPT Soil Characterization Chart to Predict Properties . . . . . 161
- Statistics and CPT Correlations . . . . . 162
  - *Bias Error Results from Stratigraphy* . . . . . 164
  - *The Academic Quality Index (AQI)* . . . . . 164
- Developing CPT Predictive Contours . . . . . 168
  - *Use of the AQI for Developing Predictive Contours* . . . . . 170
- CPT Prediction of the SPT blow count . . . . . 174
  - *Introduction* . . . . . 174
  - *SPT Prediction using Both CPT Measurements* . . . . . 175
  - *CPT Prediction of  $N_1$  using the CPT Soil Characterization Chart* . . . . . 178
  - *Discussion of CPT Prediction of the SPT Blow Count* . . . . . 178

• CPT Prediction of Clay Undrained Strength, $S_u$ . . . . .	199
· <i>introduction</i> . . . . .	199
· <i>CPT Prediction of <math>S_u</math></i> . . . . .	199
· <i>Historical Means of Estimating <math>N_k</math> for CPT Prediction of <math>S_u</math></i> . . . . .	200
· <i>Determining <math>S_{u1}</math> using CPT Soil Characterization Chart</i> . . . . .	201
· <i>Establishment of <math>S_{u1}</math> contours on the CPT soil characterization chart</i> . .	203
· <i>Conclusions</i> . . . . .	234
• CPT Prediction of Shear Wave Velocity ( $V_s$ ) . . . . .	239
· <i>Introduction</i> . . . . .	239
· <i>Minimal Stratigraphic Error when <math>V_s</math> Measured by CPT sounding</i> . . . .	239
· <i>Historical use of both CPT Measurements to Predict <math>V_s</math> or <math>G_{max}</math></i> . . . . .	240
· <i>CPT Prediction of <math>V_{s1}</math> using Both CPT Measurements</i> . . . . .	240
· <i>Discussion of CPT prediction of <math>V_{s1}</math></i> . . . . .	248
Chapter 9 - Conclusions . . . . .	260
Reference . . . . .	265
Appendix . . . . .	282



# List of Figures

Figure 1.1	The Cone Penetrometer Test (CPT) system . . . . .	3
Figure 1.2	The CPT soil characterization (Olsen, 1988) . . . . .	7
Figure 1.3	Using of stress normalization for CPT prediction of geotechnical properties . . . . .	9
Figure 2.1	Failure envelope curvature effects for different relative densities and sand types (Baligh, 1976) . . . . .	14
Figure 2.2	Simplified representation of the Stress Focus using the Mohr envelope curvature . . . . .	17
Figure 2.3	Strength Stress Focus described for Chatahoochee sand in terms of friction angle and overburden stress (data from Baligh, 1976) . . .	19
Figure 2.4	Strength Stress Focus described for Sacramento sand in terms of friction angle and overburden stress (data from Baligh (1976)) . .	20
Figure 2.5	Effect of sand type on Stress Focus location . . . . .	21
Figure 2.6	Sacramento sand plotted in terms of strength versus confining stress . . . . .	22
Figure 2.7	Components of shear strength in granular soils (After Mitchell, 1993, and Rowe, 1962) . . . . .	25
Figure 2.8	Proposed interaction of friction angle effects and the Stress Focus concept . . . . .	26
Figure 3.1	Representing geotechnical properties in terms of exponential behavior . . . . .	30
Figure 3.2	Illustrating the parameters to describe the curvature of the failure envelope for geotechnical engineering . . . . .	33
Figure 3.3	Stress Focus expressed using the stress exponent and normalized value . . . . .	35
Figure 4.1	Comparison of the Classical Limit Equilibrium based bearing failure to Cavity Expansion bearing failure . . . . .	41

Figure 4.2	Approximately combining the classical limit equilibrium bearing capacity formulation with non linear Mohr envelope behavior . . .	43
Figure 5.1	Proposed relationship of cone resistance versus vertical effective stress trending for a given sand (or soil) type . . . . .	52
Figure 5.2	Trends of cone resistance versus vertical effective stress for Ticino sand (Baldi, et.al., 1981) . . . . .	55
Figure 5.3	Replotting of Baldi, et.al., 1981 data curves from Figure 5.2 in terms of $\text{Log}_{10}$ net cone resistance versus $\text{Log}_{10}$ vertical effective stress . . . . .	56
Figure 5.4	Annotated description of the cone resistance Stress Focus together with bearing stress divided into vertical expression failure and cavity expansion failure . . . . .	58
Figure 5.5	Correlations between cone resistance and friction angle based on limit equilibrium theories and laboratory chamber tests (Campanella and Robertson, 1983) . . . . .	59
Figure 5.6	Net Cone resistance versus vertical effective stress for Hokksand sand . . . . .	62
Figure 5.7	Net cone resistance versus vertical effective stress for Ticino sand (batch #1) . . . . .	63
Figure 5.8	Net cone resistance versus vertical effective stress for Ticino sand (batch #2) . . . . .	64
Figure 5.9	Net cone resistance versus vertical effective stress for Ticino sand (batch #4) . . . . .	65
Figure 5.10	Stress Focus locations for Hokksund and Ticino sands based on evaluation of laboratory chamber tests . . . . .	66
Figure 5.11	CPT stress exponent range for several sands in terms of the Relative density and CPT cone resistance stress exponent . . . . .	68
Figure 5.12	Relationship of the cone resistance stress exponent for overconsolidated sands in chamber tests . . . . .	70
Figure 5.13	Overconsolidation effects illustrated by comparing the conventional	

	consolidation representation to the observed relationship of cone resistance versus vertical effective stress . . . . .	71
Figure 5.14	Boundary effects on the measured cone resistance level in laboratory chamber test in sand (Parkin and Lunne, 1981) . . . . .	72
Figure 5.15	The reduced cone resistance for dense sands due to "chamber size effects" can be represented with higher stress exponents because all relative densities appear to have a common Stress Focus. . . . .	74
Figure 5.16	Possible modification of the chamber based stress exponent for dense and very dense sands . . . . .	75
Figure 5.17	Cone resistance chamber data for a relative density of 33% for Reid Bedford sand . . . . .	78
Figure 5.18	Cone resistance chamber data for a relative density of 45% for Reid Bedford sand . . . . .	79
Figure 5.19	Cone resistance chamber data for a relative density of 67% for Reid Bedford sand . . . . .	80
Figure 5.20	Cone resistance chamber data for all relative densities for Reid Bedford sand together with the Stress Focus . . . . .	81
Figure 5.21	Cone resistance chamber data for Standard Concrete sand together with the corresponding Stress Focus . . . . .	82
Figure 5.22	Cone resistance chamber data for Platte River sand together with the corresponding Stress Focus . . . . .	83
Figure 5.23	Cone resistance chamber data for one relative density range of Ottawa sand . . . . .	84
Figure 5.24	Cone resistance chamber data trends for Gibbs & Holtz data . . . . .	85
Figure 5.25	Comparison of SPT Stress Focus locations for different sands to the resulting trends of Feldspar percentage and $D_{50}$ . . . . .	86
Figure 5.26	Relationship between relative density and SPT stress exponent for different sands from SPT chamber tests . . . . .	88
Figure 5.27	Comparison of the ranges for CPT and SPT stress exponents from evaluation of chamber data . . . . .	89

Figure 5.28	Relationship between SPT stress exponent and Feldspar percentage at a relative density of 36% for chamber tests . . . . .	90
Figure 5.29	Interrelation of the Stress Focus and the stress exponent (for a very loose sand condition) based on evaluation of CPT cone resistance chamber data for increasing feldspar content . . . . .	91
Figure 6.1	Determining the cone resistance normalization value ( $q_{c1c}$ ) and corresponding stress exponent ( $c$ ) using uniform soil layers . . . . .	96
Figure 6.2	Example of in situ cone resistance data having a uniform soil layer with the stress exponent, $c$ , and normalized cone resistance, $q_{c1c}$ , defined . . . . .	98
Figure 6.3	Using uniform soil layer data to establish cone resistance stress exponent data points on the CPT soil characterization chart . . . . .	100
Figure 6.4	Uniform sand layer at the Holmen, Norway (NGI research site) . . . . .	101
Figure 6.5	Uniform unstable silty clay layers for a Hong Kong Bay deposit (airport replacement project) . . . . .	102
Figure 6.6	Uniform sandy silt layer in the core of Ririe dam (Corps of Engineers) . . . . .	103
Figure 6.7	Uniform sand layer for project code DE-S-R . . . . .	104
Figure 6.8	Uniform silty sand layer in the Aftchafalaya River (dredging study) . . . . .	105
Figure 6.9	Uniform silty clay layer in the Aftchafalaya River (Dredging study) . . . . .	106
Figure 6.10	Uniform silty clay layers of the foundation for Lucky Peak Dam (Corps of Engineers) . . . . .	107
Figure 6.11	Uniform sand layer segment at the McDonalds Farm, Sea Island, Canada . . . . .	108
Figure 6.12	Uniform silty sand layer at Salinas (Old Hilltown), California (USGS research project) . . . . .	109
Figure 6.13	Uniform foundation clay layer (Levee failure investigation) . . . . .	110

Figure 6.14	Establishing contours of cone resistance stress exponent using CPT data from in situ uniform soil layers with constant relative strength	111
Figure 6.15	Comparing soil types from uniform soil layers to the CPT soil classification line (from Olsen, 1988)	112
Figure 6.16	Annotated version of the cone resistance stress exponent chart showing soil zones (and strength character) together with CPT soil characterization line	113
Figure 6.17	Relationship of sleeve friction resistance stress exponent (s) to the cone resistance stress exponent (c) using uniform soil layer data	116
Figure 6.18	Correlation of the s/c ratio (sleeve to cone stress exponents) to the normalized sleeve friction resistance ( $f_{s/c}$ )	118
Figure 6.19	Projections of trends for uniform in situ clay layers in terms of log net cone resistance versus log vertical effective stress	120
Figure 6.20	Compression curves for several clays and silty clays (from Mitchell, 1993; Lambe & Whitman, 1969)	122
Figure 6.21	Replot of selected soil types from Figure 6.20 in using stress normalization format to show that clays have an approximate Stress Focus	123
Figure 6.22	Projections of trends for uniform sand layers in terms of log net cone resistance versus log vertical effective stress	124
Figure 6.23	Projections of trends for uniform soil mixture layers in terms of Log cone resistance versus Log vertical effective stress	126
Figure 6.24	The soil type dependency trend for the Stress Focus based on uniform soil layer and laboratory chamber test evaluation	128
Figure 6.25	Inferences concerning the soil type dependent Stress Focus	129
Figure 7.1	$C_n$ versus vertical effective stress (Kips/ft <sup>2</sup> ) relationship developed by Seed et al. 1983 (Note: 2 Kips/ft <sup>2</sup> = 1 atm)	134
Figure 7.2	Back-calculated SPT $C_N$ parameters from field and laboratory chamber test (Skempton, 1986)	135
Figure 7.3	Mud pressure effects on the SPT sampler	138

Figure 7.4	Drilling mud pressure effects for the SPT sampler in field boreholes . . . . .	139
Figure 7.5	Stress effects on the SPT sampler for historical laboratory chamber tests due to a constant drilling mud stress at differing confining stress levels . . . . .	141
Figure 7.6	Comparison of confining stress surrounding the SPT sampler (or CPT probe) for chamber and field conditions . . . . .	145
Figure 7.7	Comparison of the ranges for CPT and SPT stress exponents from evaluation of chamber data . . . . .	147
Figure 7.8	Shear wave velocity versus depth for intermediate and saturated firm natural soils (Lee and Campbell, 1985) . . . . .	154
Figure 7.9	Comparing the stress exponent ranges for shear wave velocity and cone resistance . . . . .	157
Figure 8.1	Using CPT measurements to predict geotechnical properties . . . . .	160
Figure 8.2	CPT Soil Characterization chart in terms of the normalized cone resistance and normalized friction ratio (Olsen, 1988) . . . . .	163
Figure 8.3	Hypothetical example showing that soil lenses of differing soil type (or strength) can bias correlations . . . . .	165
Figure 8.4	Definition of a stratigraphic AQI of 76% (i.e. 76% of the soil layers are continuous between the boring and CPT sounding) . . . . .	167
Figure 8.5	Description of a response surface . . . . .	169
Figure 8.6	An illustration of the iterative technique for removing bias data using the AQI index . . . . .	172
Figure 8.7	Example using the Academic Quality Index (AQI) toward establishing the best correlation line by excluding biased data . . . . .	173
Figure 8.8	Comparison of forces on the SPT and CPT devices (Schmertmann, 1979a) . . . . .	176
Figure 8.9	Prediction of the SPT blow count, $N$ , using both CPT measurements (Olsen, 1988) . . . . .	177
Figure 8.10	Prediction of the $N_1=2$ contour on the CPT Soil Characterization	

	Chart . . . . .	179
Figure 8.11	Prediction of the $N_1=4$ contour on the CPT soil characterization chart . . . . .	180
Figure 8.12	Prediction of the $N_1=7$ contour on the CPT Soil Characterization Chart . . . . .	181
Figure 8.13	Prediction of the $N_1=15$ contour on the CPT Soil Characterization Chart . . . . .	182
Figure 8.14	Prediction of the $N_1=25$ contour on the CPT Soil Characterization Chart . . . . .	183
Figure 8.15	Prediction of the $N_1=35$ contour on the CPT Soil Characterization Chart . . . . .	184
Figure 8.16	Prediction of the $N_1=50$ contour on the CPT Soil Characterization Chart . . . . .	185
Figure 8.17	Final plot of the best fit SPT $N_1$ contours on the CPT Soil Characterization Chart . . . . .	186
Figure 8.18	Contours of constant normalized sleeve friction resistance on the CPT soil characterization chart . . . . .	188
Figure 8.19	Example of CPT Prediction of SPT blow count with comparison data (Barkley dam seismic evaluation study, data from Olsen, et al, 1989) . . . . .	190
Figure 8.20	CPT predicted versus measured SPT $N_1$ for the Barkley dam seismic evaluation study (data from Olsen et al., 1989) . . . . .	191
Figure 8.21	CPT predicted versus measured $N_1$ for sites on the East coast of the US (data from project code LE-JN) . . . . .	192
Figure 8.22	CPT predicted versus measured $N_1$ for a CPT sounding through the hydraulic core of Sardis dam . . . . .	193
Figure 8.23	CPT predicted versus measured SPT $N_1$ for a stiff/dense dirty sand site (project code DE-S-R) . . . . .	194
Figure 8.24	CPT predicted versus measured SPT $N_1$ for a site composed of soil mixtures in Tracy California (project code WC-TSS) . . . . .	195

Figure 8.25	CPT predicted versus measured SPT $N_1$ for McDonalds Farm, Sea Island, Richmond, British Columbia, Canada (University of British Columbia research site)(data from Campanella, et al, 1982) . . . . .	196
Figure 8.26	CPT predicted versus measured SPT $N_1$ for the Arcadia Dam seismic evaluation study . . . . .	197
Figure 8.27	CPT predicted versus measured SPT $N_1$ at the Coyote North site (near San Jose) California (data from Martin & Douglas, 1980) . .	198
Figure 8.28	Establishing $S_{u1}$ (i.e. c/p) contours on the CPT soil characterization chart based on bearing theory for clay penetration . . . . .	204
Figure 8.29	Prediction of the $(S_{u1})_{TxUU}=0.1$ contour on the CPT Soil Characterization Chart . . . . .	206
Figure 8.30	Prediction of the $(S_{u1})_{TxUU}=0.25$ contour on the CPT Soil Characterization Chart . . . . .	207
Figure 8.31	Prediction of the $(S_{u1})_{TxUU}=0.31$ contour on the CPT Soil Characterization Chart . . . . .	208
Figure 8.32	Prediction of the $(S_{u1})_{TxUU}=0.39$ contour on the CPT Soil Characterization Chart . . . . .	209
Figure 8.33	Prediction of the $(S_{u1})_{TxUU}=0.54$ contour on the CPT Soil Characterization Chart . . . . .	210
Figure 8.34	Prediction of the $(S_{u1})_{TxUU}=0.80$ contour on the CPT Soil Characterization Chart . . . . .	211
Figure 8.35	Prediction of the $(S_{u1})_{TxUU}=2$ contour on the CPT Soil Characterization Chart . . . . .	212
Figure 8.36	Contours of normalized $(S_{u1})_{TxUU}$ (i.e. $(S_{u1})_{TxUU}/\sigma'_v$ ) on the CPT soil characterization chart for the unconsolidated undrained triaxial strength test . . . . .	213
Figure 8.37	Prediction of the $(S_{u1})_{FVanc} = 0.25$ contour on the CPT soil characterization chart . . . . .	214
Figure 8.38	Prediction of the $(S_{u1})_{FVanc} = 0.31$ contour on the CPT soil characterization chart . . . . .	215



Figure 8.39	Prediction of the $(S_{ul})_{FVane} = 0.54$ contour on the CPT soil characterization chart . . . . .	216
Figure 8.40	Prediction of the $(S_{ul})_{FVane} = 0.80$ contour on the CPT soil characterization chart . . . . .	217
Figure 8.41	Prediction of the $(S_{ul})_{FVane} = 2$ contour on the CPT soil characterization chart . . . . .	218
Figure 8.42	Contours of $(S_{ul})_{FVane}$ (i.e. $(S_u)_{FVane} / \sigma'_v$ ) for the field vane shear on the CPT soil characterization chart . . . . .	219
Figure 8.43	CPT predicted versus measured $(S_{ul})_{TxUU}$ for silty clays from a Fraser River site, Vancouver International Airport, Canada (data from Konrad, et al., 1985) . . . . .	220
Figure 8.44	CPT predicted versus measured $(S_{ul})_{TxUU}$ for silty clay from Limma Mellosa, Sweden (40 km north of Stockholm) (data from Larsson & Mulabdic, 1991) . . . . .	221
Figure 8.45	CPT predicted versus measured $(S_{ul})_{TxUU}$ for San Francisco Bay mud at the Muni Metro turnaround facility (the measured strength data are located at 10 different elevations) (data from Dames & Moore, 1992) . . . . .	222
Figure 8.46	CPT predicted versus measured $(S_{ul})_{TxUU}$ for the Onsoy site in Norway (NGI research site) (the measured strength data are at four different depths) (data from Rød, et al, 1985, Gillespie, et al., 1985) . . . . .	223
Figure 8.47	CPT predicted versus measured $(S_{ul})_{TxUU}$ for San Francisco Bay mud at Hamilton AFB (University of California at Berkeley research site) (data from project code ET-SE) . . . . .	224
Figure 8.48	CPT predicted versus measured $(S_{ul})_{TxUU}$ from Norrköping, Sweden (with measurements at 11 different depths) (a Swedish Geotechnical Institute research site) (data from Larsson and Mulabdic, 1991) . . . . .	225
Figure 8.49	CPT predicted versus measured $(S_{ul})_{TxUU}$ from the Kibernia	

	offshore investigation (data from Konrad, et al., 1991) . . . . .	226
Figure 8.50	CPT predicted versus measured $(S_{u1})_{TxUU}$ for San Francisco bay mud at the muni metro turnaround facility (with measurements from 17 different depths) (data from Dames & Moore, 1985) . . . . .	227
Figure 8.51	CPT predicted versus measured $(S_{u1})_{Fvane}$ for a conference pile load test at Northwestern University in 1988 (with measurements from 12 different depths) (data from Stratigraphics, Inc, 1988) . . . . .	228
Figure 8.52	CPT predicted versus measured $(S_{u1})_{Fvane}$ for a foundation clay layer for the Nerlerk Berm liquefaction slide study . . . . .	229
Figure 8.53	CPT predicted versus measured $(S_{u1})_{Fvane}$ at the Fraser River Delta Bridge, 25 km SW of Vancouver, Canada (with measurements from 11 different depths) (Data from Crawford & Campanella, 1991) . . . . .	230
Figure 8.54	CPT predicted versus measured $(S_{u1})_{Fvane}$ for bay sediments at the Hong Kong Airport replacement at Chek Lap Kok (data from Dames & Moore, 1982) . . . . .	231
Figure 8.55	CPT predicted versus measured $(S_{u1})_{Fvane}$ at Lower 232 Street, Langley, British Columbia, Canada (data from Campanella, et al., 1991) . . . . .	232
Figure 8.56	CPT predicted versus measured $(S_{u1})_{Fvane}$ at Barkley dam within clay lenses (data from Olsen, et al , 1989) . . . . .	233
Figure 8.57	Illustration on how to calculate the Bjerrum $\mu$ correction factor using the predicted $S_{u1}$ contours . . . . .	235
Figure 8.58	Calculated contours of $(\Delta u)_{TxUU}/(S_u)_{FV}$ on the CPT soil characterization chart by taking a ratio of contours on Figure 8.36 to Figure 8.42 . . . . .	236
Figure 8.59	Correlation of PI to the Bjerrum $\mu$ correction factor for determining the undrained strength from field vane shear results (Bjerrum, 1972) . . . . .	237
Figure 8.60	Correlation of $(S_{u1})_{FV}$ to PI to establish the overconsolidation	

	character and then to get the Bjerrum $\mu$ correction factor (Aas, Lacasse, Lunne, and Hoeg, 1985) . . . . .	238
Figure 8.61	CPT prediction of the maximum shear modulus using both of the CPT measurements (Olsen, 1988) . . . . .	241
Figure 8.62	Prediction of $V_{s1} = 150$ ft/sec contour on the CPT soil characterization chart . . . . .	242
Figure 8.63	Prediction of the $V_{s1} = 400$ ft/sec contour on the CPT soil characterization chart . . . . .	243
Figure 8.64	Prediction of the $V_{s1} = 650$ ft/sec contour on the CPT soil characterization chart . . . . .	244
Figure 8.65	Prediction of the $V_{s1} = 900$ ft/sec contour on the CPT soil characterization chart . . . . .	245
Figure 8.66	Prediction of the $V_{s1} = 1200$ ft/sec contour on the CPT soil characterization chart . . . . .	246
Figure 8.67	Contours of normalization shear wave velocity ( $V_{s1}$ ) on the CPT soil characterization chart . . . . .	247
Figure 8.68	CPT predicted versus measured $V_{s1}$ for the Holmen site, Drammen, Norway (NGI research site) (data from Christoffersen and Lunne, 1982; Gillespie, Lunne, and Eidsmoen, 1985) . . . . .	249
Figure 8.69	CPT predicted versus measured $V_{s1}$ for a stiff/dense dirty sand site in the U.S. (project code DE-S-R) . . . . .	250
Figure 8.70	CPT predicted versus measured $V_{s1}$ for the Barkley dam seismic evaluation study (data from Olsen, et al., 1989) . . . . .	251
Figure 8.71	CPT predicted versus measured $V_{s1}$ for a site at Tuktoyaktule, Bugmallit Bay, Beaufort Sea, Canada (data from Campanella, et al., 1987) . . . . .	252
Figure 8.72	CPT predicted versus measured $V_{s1}$ for a uniformly compacted sand (data from project code DN-HIJ2) . . . . .	253
Figure 8.73	CPT predicted versus measured $V_{s1}$ for a site at Onsoy, Norway (NGI research site) . . . . .	254

Figure 8.74	CPT predicted versus measured $V_{s1}$ at Treasure Island, San Francisco, California (data from Hryciw, 1990) . . . . .	255
Figure 8.75	CPT predicted versus measured $V_{s1}$ at the parameter levee area of Santa Cruz, California (data from Hryciw, 1990) . . . . .	256
Figure 8.76	CPT predicted versus measured $V_{s1}$ for the compacted silt core, Lucky Peak dam, Idaho . . . . .	257
Figure 8.77	Illustration why the predicted shear wave velocity contours on the CPT Soil Characterization chart are curved . . . . .	259

## List of Tables

Table 2.1	High pressure friction angles for sedimentary materials (Barton, 1976) . . . . .	23
Table 7.1	Showing the equivalent $(G_{\max})_1$ from historic $G_{\max}$ formulations .	150
Table 7.2	Shear wave velocity parameters determined from data presented by Lee and Campbell (1985) for differing soil conditions . . . . .	153
Table 7.3	Published stress exponents for shear wave velocity . . . . .	156
Table 8.1	Typical $N_k$ values for estimating the unconsolidated undrained strength of clays using the CPT cone resistance (Olsen, 1994) . . .	202

## List of Symbols

<u>Symbol</u>	<u>Definition</u>	<u>Defined on page</u>
$\sigma'_v$	Vertical effective stress	15
$\sigma_{total}$	Total vertical stress	47
atm	Atmospheric pressure designation (approximately 1 ton/ft <sup>2</sup> or 100 KPa)	38
$F_{mean}$	Multiplication factor for $\sigma'_v$ to convert to $\sigma_{mean}$	36
e	General exponent value	32, 35
V	Vertical axes, overburden stress	32, 35
H	Horizontal axes, geotechnical property	32, 35
$H_1$	Normalized H property	32, 35
$H_f$	H at the Stress Focus	34, 35
$\sigma_{fl}$	Confining stress at the Stress Focus for H	34, 35
$q_c$	Measured cone resistance	2, 3
$q_{c1c}$	Normalized cone resistance using stress exponent based on soil character at $\sigma'_v = 1$ atm	49, 96
$(q_c)_{net}$	net cone resistance	47
c	Cone resistance stress exponent	49, 96, 113
$f_s$	Measured sleeve friction resistance	2, 3
$f_{s1c}$	Normalized measured sleeve friction resistance based on soil character at $\sigma'_v = 1$ atm	115
s	Sleeve friction resistance stress exponent	115, 118
FR = $R_f$	Friction ratio (%) (calculated)	6
FR <sub>1c</sub> = $R_{flc}$	Normalized friction ratio using $q_{c1c}$ and $f_{s1c}$	100
$q_{cf}$	Cone resistance at the Stress Focus	54, 58
$\sigma_{fc}$	Vertical effective stress at the cone resistance Stress Focus	54, 58

$q_{cfl}$	Normalized cone resistance Stress Focus	54, 58
$Z_c$ & $Z_\sigma$	General bearing factors	46
$\phi$	Drained friction angle	13
$\phi_f$	Drained friction angle at the Stress Focus	16
$\sigma_{f\phi}$	Vertical effective stress at the friction angle Stress Focus	16
$\tau_1$	Normalized shear strength, atm units	15
$t$	shear strength stress exponent	15
$\phi_\mu$	Material friction angle	24
$\alpha$	Balighs' Mohr failure envelope curvature parameter	13
$N$	Standard Penetration Test (SPT) blow count	76, 132
$N_1$	SPT blow count normalized at $\sigma'_v = 1$ atm	132
$C_N$	SPT normalization factor	67, 132
$(\sigma_{sc})_c$	Vertical effective stress surrounding the SPT sampler for SPT chamber tests	138
$(\sigma_{sc})_f$	Vertical effective stress surrounding the SPT sampler for field situations	138
$(\sigma_{si})_c$	Stress that influences the SPT blow count for SPT chamber tests	138
$(\sigma_{sc})_f$	Stress that influences the SPT blow count for field situations	138
$n$	SPT stress exponent for normalization (from SPT chamber evaluation)	88, 132
$b$	Calculated SPT stress exponent relating $(\sigma_{si})_c$ to $(\sigma_{sc})_c$ (for field SPT blow count normalization) (equals $c$ )	144
$R_m$	Reduction of the confining stresses at the SPT sampler due to the low mud pressure borehole effects for SPT chamber tests (%)	144

$V_s$	Shear wave velocity (units must be specified)	149
$V_{s1}$	Normalized shear wave velocity at $\sigma'_v = 1$ atm (units must be specified)	152
$v$	Shear wave velocity stress exponent	152
fps	feet per second	149
mps	meters per second	149
$G_{max}$	Maximum shear modulus (units must be specified)	149
$(G_{max})_1$	Normalized maximum shear modulus, atm units	149
$m$	Shear modulus stress exponent	149
$S_u$	Undrained cohesive strength (units must be specified)	47, 200
$(S_u)_{TxUU}$	Undrained cohesive strength based on the laboratory triaxial unconsolidated undrained (TxUU) test (units must be specified)	203
$(S_u)_{FVane}$	Undrained cohesive strength based on the field vane (FVane) shear test (units must be specified)	203
$\frac{S_u}{\sigma'_v} = \frac{c}{p} = S_{u1}$	Normalized undrained cohesive strength at $\sigma'_v = 1$ atm	48, 201
$\left(\frac{S_u}{\sigma'_v}\right)_{TxUU}$	$= (S_{u1})_{TxUU}$ Normalized undrained cohesive strength based on the laboratory triaxial unconsolidated undrained (TxUU) test at $\sigma'_v = 1$ atm	203
$\left(\frac{S_u}{\sigma'_v}\right)_{FVane}$	$= (S_{u1})_{FVane}$ Normalized undrained cohesive strength based on the field vane (FVane) shear test at $\sigma'_v = 1$ atm	203
$\mu = \frac{(S_u)_{TxUU}}{(S_u)_{FVane}}$	Bjerrum field vane shear correction factor	205, 236



# Chapter 1

## Introduction

### General

Site characterization, in terms of geotechnical properties, can be the single most important task for geotechnical engineering investigations. Characterization is defined as "To reveal and separate into categories" (Webster's New Collegiate Dictionary, 1975). Once a site has been realistically characterized in terms of geotechnical property distribution, to the needs of a project, the foundation design or foundation performance evaluation (e.g. liquefaction evaluation) can be done with greater economy and reliability. Site characterization by drilling and sampling is economically limited because of the small proportion of the subsurface sampled and the relatively high cost of laboratory tests.

When the Cone Penetrometer Test (CPT) is used for a site investigation, the industry standard practice for CPT data reduction has generally been to use only the CPT cone resistance and calculated friction ratio; The measured dynamic pore pressure is become more common as an additional CPT measurement. Most CPT-based theories are derived either for clay or sand and therefore are not directly applicable in a world of soil mixtures, dirty sands, and silty clays. Use of techniques for CPT prediction of geotechnical properties that are applicable to all soil types (Olsen 1984, 1988, Olsen and Farr, 1986) have been constrained by the limited amount of published verification.

The goal of this research program was to develop improved techniques for CPT prediction of geotechnical properties. This goal was achieved by creating a large database (of CPT and soil test results), developing new stress normalization techniques, accounting for bias error due to stratigraphy changes (between CPT soundings and borings), and finally, by using the CPT soil characterization chart (Olsen, 1988) to develop predictive correlations for Standard Penetration Test (SPT) blow count, clay undrained strengths (laboratory unconsolidated undrained triaxial test and field vane shear test), and shear wave velocity.

### *The CPT Test*

The CPT test is performed by pushing a 3.57 cm (1.4 inch) diameter instrumented probe into the earth at 2 cm/second while simultaneously measuring the cone resistance and sleeve friction resistance, as illustrated in Figure 1.1. Cone resistance ( $q_c$ ) is the axial component of the stress acting on the tip of the probe (10 cm<sup>2</sup> horizontal cross sectional area) and sleeve friction resistance ( $f_s$ ) is the sliding stress developed on a short cylindrical section of steel just above the tip (surface area of 150 cm<sup>2</sup>). The electric CPT has received wide acceptance throughout the world and its use continues to grow. The advantages of the electrical CPT are: fast rate of penetration (production rate up to 600 ft per day), higher accuracy and repeatability (compared to the Standard Penetration Test (SPT)), and use of a computer data acquisition system which allows for computer based evaluation. While there are numerous additional sensors (Figure 1.1) that can be added to a CPT probe (Lieberman, et.al, 1991, Cooper, et.al., 1988, Robertson, et.al., 1986, FUGRO, 1980), approximately 60% of all CPT work in the U.S. is done using only the two basic measurements (i.e.  $q_c$  and  $f_s$ ). The CPT is also becoming the geotechnical tool of choice for investigations where there are local CPT contractors and the site is composed of clays, sands, or soil mixtures containing little or no gravel.

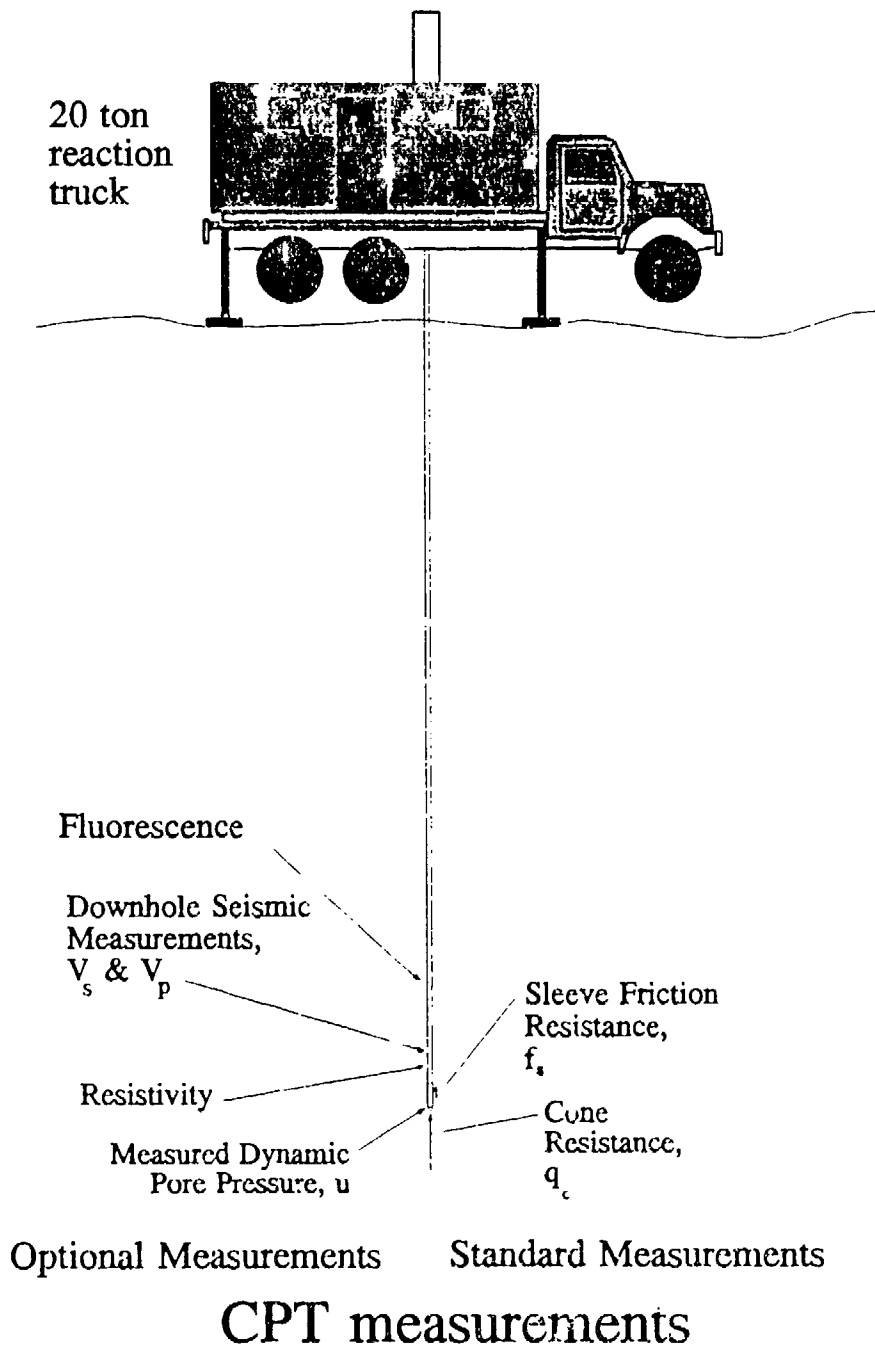


**Figure 1.1** The Cone Penetrometer Test (CPT) system

The CPT can provide a large quantity of low-cost, repeatable, well-distributed measurements distributed throughout a site. Alternatively, a few relatively undisturbed soil samples may be tested in laboratory, but site variability generally overshadows the benefits gained from a few specialty tests. CPT is becoming the choice in situ exploration tool over the SPT because of the lower cost, repeatability, continuous record, and quantitative nature of the data. The CPT is also easier to interpret because the measurements are more fundamental. However, unlike the SPT, it provides no soil sample.

### *The CPT Measurements*

The two CPT measurements are remarkably unique. The cone resistance is influenced by many geotechnical properties—it varies exponentially, in fact, with soil frictional behavior. For example, the cone resistance can be 200 tons/ft<sup>2</sup> (tsf) (20 MPa) in a sand, and as low as 3 tsf (300 KPa) in clays. The cone resistance can therefore be considered an index of the sand skeleton strength (Douglas and Olsen, 1981). The CPT sleeve friction measurement is a high-strain sliding measurement along a steel cylinder (after the soil has navigated around the cone tip) and is a good indicator of loose or unstable soil structures (Olsen and Farr, 1986). While the cone resistance has been the topic of extensive theoretical and experimental research (too numerous to reference), there has only been limited research on sleeve friction resistance (Olsen, 1984, 1988, Olsen and Farr, 1986, and Masood, 1990).

### *Developing CPT Prediction Relationships for Geotechnical Properties*

There are numerous means for establishing correlations of CPT measurements with geotechnical properties. Laboratory chamber testing, while very useful, has historically been done only on clean sands (silty sands have recently been tested in

laboratory chambers (Rahardjo, 1989)). Also, the results of CPT chamber tests are sensitive to chamber boundary conditions. Theoretical formulations are typically derived only for a particular soil type and must always be thoroughly verified with laboratory and/or field test data. Laboratory-based correlations, while attractive for pure sands and pure clays may be of limited usefulness in evaluating soils composed of mixtures of these materials.

Historically, quantitative CPT correlations with geotechnical properties have been based only on the cone resistance. CPT sleeve friction resistance was used only for soil classification (Douglas and Olsen, 1981, Robertson and Campanella, 1984). Researchers have typically compared CPT cone resistance ( $q_c$ ) and laboratory strength test results (or field strength measurement results) in an X-Y scatter plot to develop best fit correlations. CPT prediction of geotechnical properties should be based on combination of the two basic CPT measurements ( $q_c$  and  $f_s$ ) because these measurements are always performed and each reflects different aspects of geotechnical behavior.

### *Stratigraphic Influences on CPT Correlations*

Using field data to correlate CPT results with geotechnical properties is an attractive approach, however there are limitations. Stratigraphic variation of soil types and geotechnical properties between a CPT sounding and a nearby borehole can introduce major errors into a correlation. The use of uniform sites only would significantly reduce correlation error, however, there are only a limited number of well-documented uniform sites in the world. These uniform sites also do not represent all soil types, and most importantly do not represent a wide range of strengths (e.g. relative density for sand) for each soil type. It is therefore preferable to represent many soil types and relative strength levels by using sites with less than perfect soil uniformity. Site stratigraphy (i.e. uniformity) must still be accounted for

when developing CPT correlations. A subjective quality index can be assigned to each CPT-to-boring comparison and used as an index for quantifying bias error potential (e.g. a CPT encounters a clay layer but the nearby borehole encounters a sand at the same elevation).

### *Accounting for Factors that Influence Geotechnical Properties*

Many factors influence geotechnical properties and should be accounted for when developing CPT-based correlations. The three factors of strongest influence are: 1) soil type, 2) soil state, and 3) confining stress level. Soil type and confining stress are self explanatory. The soil state (i.e. void ratio at a standard confining stress level) can be defined as the normalized geotechnical property level (e.g. Standard Penetration Test (SPT) normalized blow count,  $N_1$ ). Therefore, a CPT technique for predicting geotechnical properties must directly or indirectly account for all three of these influencing factors.

### *Using CPT based Soil Classification*

Soil type reflects the bulk soil composition in terms of sand and silt grain types and sizes (if present) together with the clay type (if present). The CPT soil characterization chart (Douglas and Olsen, 1981, Olsen, 1984, Olsen and Farr, 1986, Olsen, 1988) can *approximately* predict soil type, primarily based on the observation that the cone resistance is exponentially influenced by sand grain frictional behavior and is therefore an index of the soil structure. The Olsen (1988) CPT soil characterization chart, shown in Figure 1.2, represents the state-of-the-art for CPT prediction of soil type from knowledge of the cone resistance (log scale) and friction ratio (which is defined as the sleeve friction resistance as a percent of the cone resistance level).

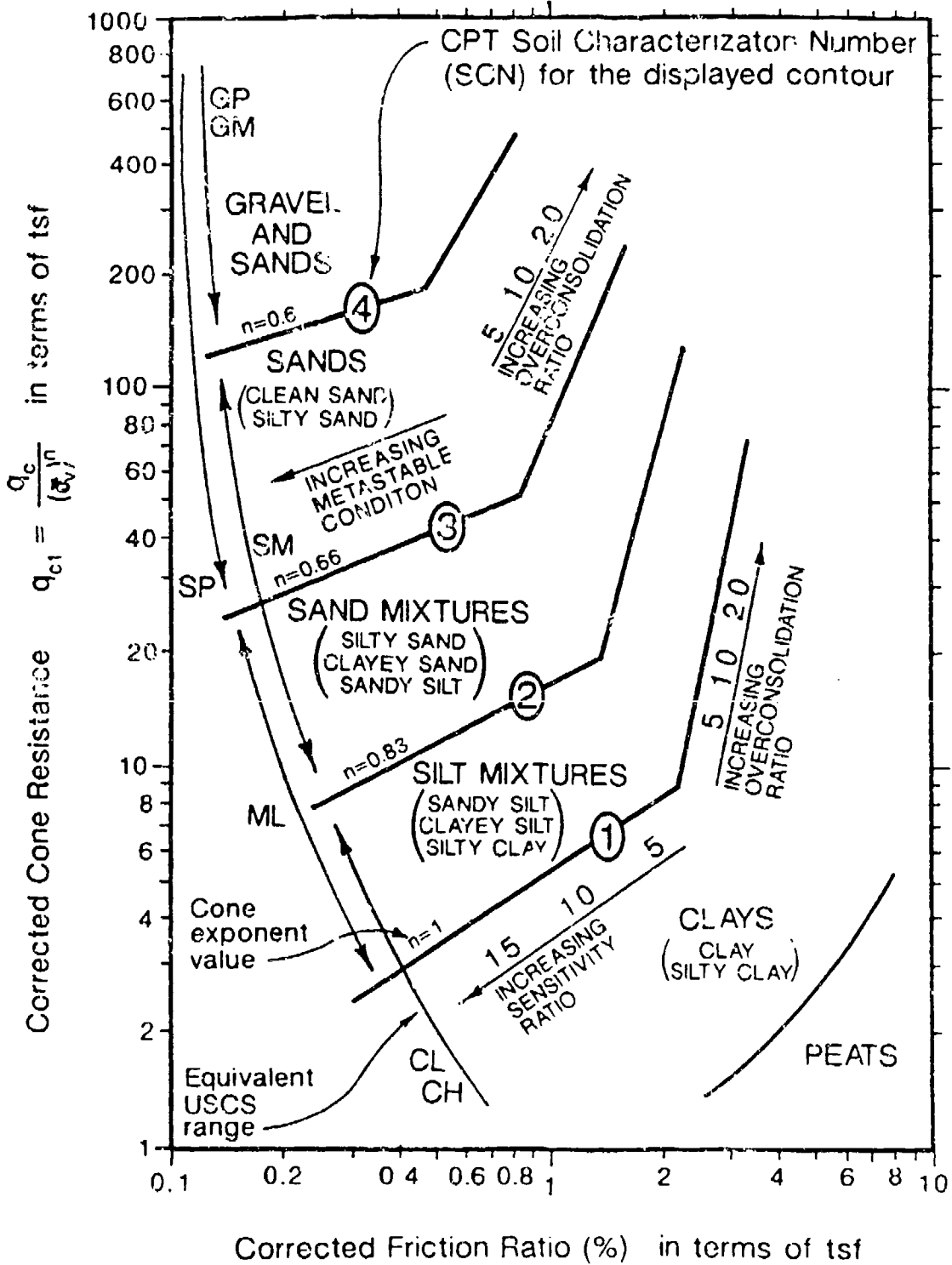


Figure 1.2 The CPT soil characterization (Olsen, 1988)

### *Accounting for Stress Effects in CPT Correlations*

Confining stress influences CPT measurements and geotechnical properties differently. It will be shown that confining stress influences are dependent on soil type and relative strength. The influence of confining stress must be properly accounted for when developing correlations of CPT to geotechnical properties. These confining stress influences are also important during prediction of geotechnical properties using field CPT data. If stress influences are not properly considered, geotechnical properties for shallow (e.g. 5 feet) or deep (e.g. 200 feet) situations may be over- or under-predicted by 50% or more. CPT prediction of normalized geotechnical properties accounts for confining stress influences on properties.

The process of using stress normalization to predict geotechnical properties is illustrated in Figure 1.3. CPT data are initially normalized to an equivalent value at standard vertical effective stress (i.e. atmospheric pressure) using stress exponent techniques. The normalized geotechnical property is then predicted using the normalized CPT values. Finally, the in situ property is determined using stress exponent concepts. The stress normalization technique for CPT measurements and two geotechnical properties (i.e. SPT-N value and shear wave velocity) are fully examined in this dissertation. Normalized geotechnical properties will be derived based on the CPT soil characterization chart.



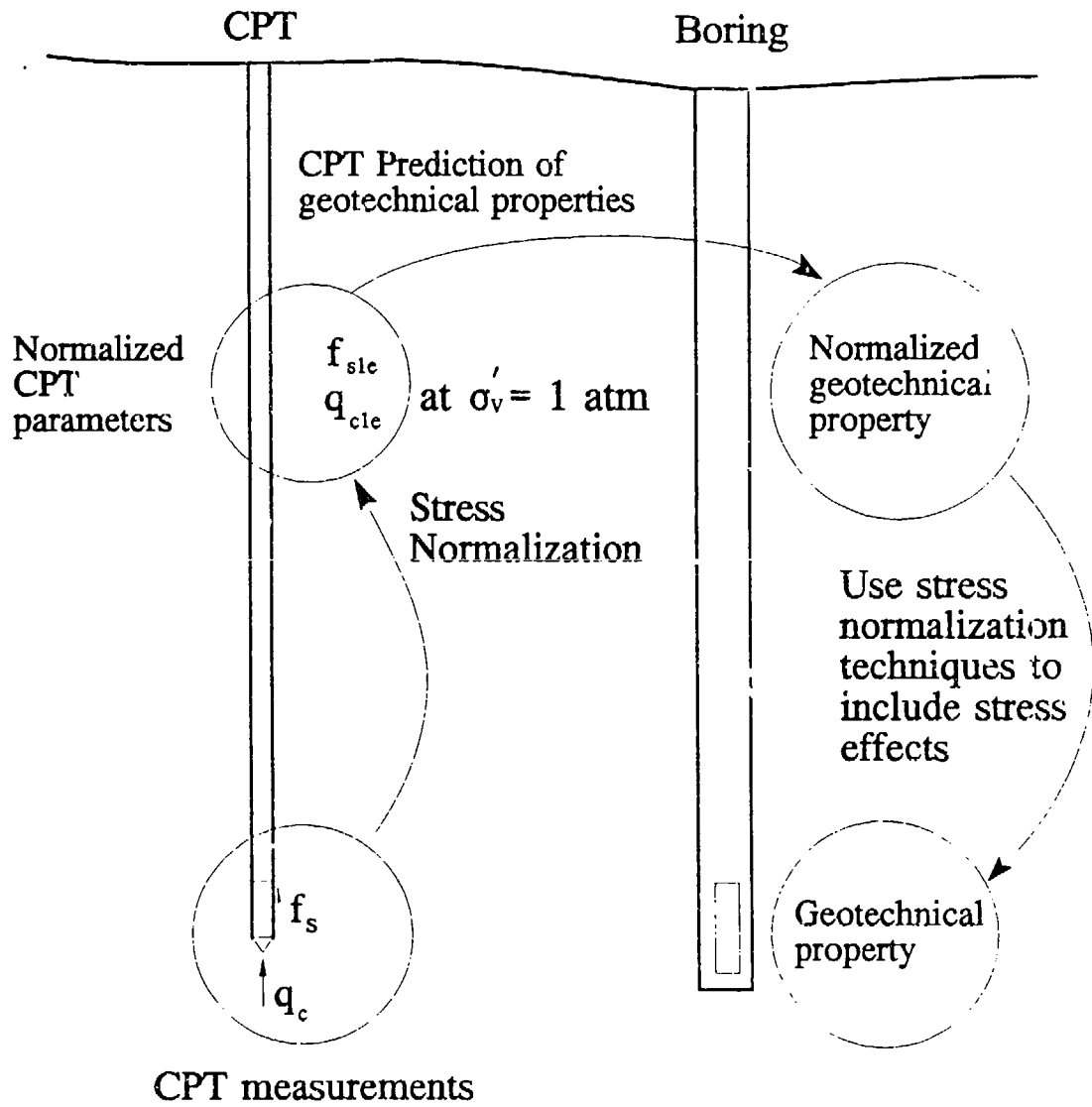


**Figure 1.3** Using  $\sigma'_v$  stress normalization for CPT prediction of geotechnical properties

## Outline of Dissertation

High pressure triaxial testing of sands and the effect of confining stress level on Mohr envelope curvature are reviewed in Chapter 2, because for a given relative density, the friction angle decreases with increasing confining stress. It will be shown that this friction angle decrease continues until a specific confining stress is achieved, namely the Stress Focus (corresponding to an approximate depth of a few thousand feet). Specimens of all initial relative densities for a particular sand type will have approximately the same strength (and density) at the Stress Focus, which corresponds to a uncemented sedimentary rock strength. It will also be shown that the decrease of friction angle with increasing vertical effective stress can be explained in terms of dilation effects, grain crushing, and grain-to-grain rolling influences.

The basic stress exponent concept required for stress normalization and determination of the Stress Focus is described in Chapter 3. Stress normalization is achieved using a stress exponent on the vertical effective stress.

CPT cone resistance normalization formulation for all soil types based on limit equilibrium and cavity expansion theories is developed in Chapter 4. This formulation also accounts for the observed exponential relationship between cone resistance and vertical effective stress.

CPT laboratory chamber test data are evaluated in Chapter 5. This evaluation supports the contention that cone resistance can be represented by stress exponents and the Stress Focus. Standard Penetration Test (SPT) chamber test data are also used to show that the Stress Focus location is dependent on the sand classification.

CPT data from uniform in situ soil layers are used in Chapter 6 to establish a technique for CPT prediction of the stress exponent (required for normalizing CPT data). These data also show that the Stress Focus location depends on soil classification.

New stress normalization techniques for SPT and the shear wave velocity are given in Chapter 7. For the SPT, the constant drilling mud height used for laboratory SPT chamber tests produces stress exponents that are too low. The CPT-determined stress exponent (from Chapter 6) is thus recommended to be used for SPT normalization. Shear wave velocity discussion will emphasize the need for a soil type-dependent stress exponent that can be estimated using the cone resistance stress exponent.

In Chapter 8, correlations are given for normalized CPT parameters with the following normalized geotechnical properties: SPT blow count, undrained cohesive strength based on the unconsolidated undrained triaxial test (TxUU), undrained cohesive strength based on the field vane shear (FVane), and shear wave velocity. These correlations are represented as contours on the CPT soil characterization chart. Each contour was established using an Academic Quality Index (AQI) to subjectively remove bias due to stratigraphic soil type changes between CPT soundings and boreholes. Increasing the inclusionary AQI level increases the data group quality by removing lower quality data.

The dissertation conclusions and recommendations for future research are given in Chapter 9.

# Chapter 2

## Mohr Envelope Curvature and Development of the Stress Focus Concept

### Introduction

Curvature of the Mohr failure envelope (i.e. a gradual decrease in failure envelope slope with increasing effective stress) is well-known. It is incorporated in many nonlinear behavior theories but is rarely used in geotechnical engineering practice. Mohr envelope curvature can be quantified analytically, but there are no comprehensive means for predicting the actual curvature parameters based on soil type and relative strength (e.g. friction angle for sands). At present, these Mohr envelope curvature parameters can only be determined with a series of triaxial tests conducted using a wide range of confining stresses for a given sand type and a given initial relative density. Mohr envelope curvature and the Stress Focus concepts presented in this chapter are the foundation for the CPT stress normalization techniques in this dissertation.

### Baligh Formulation of Curvature Envelope

Baligh (1976) improved precedent cavity expansion theory by incorporating the effects of Mohr failure envelope curvature. Figure 2.1 summarizes the effects of

failure envelope curvature observed by Baligh (1976) in terms of friction angle for several types of sands and relative densities. Baligh (1976) quantified failure envelope curvature and incorporated its effects into cavity expansion theory. He proposed Equation (2.1) to express failure envelope curvature for laboratory triaxial tests.

$$\tau = \sigma \left( \tan \phi_o + \tan \alpha \left( \frac{1}{2.3} - \log_{10} \frac{\sigma}{\sigma_o} \right) \right) \quad (2.1)$$

where

- $\phi_o$  = Reference friction angle at  $\sigma'_v = 1$  ton/ft<sup>2</sup> (tsf)  
 $\alpha$  = Balighs' Mohr failure envelope curvature parameter

The curvature parameter,  $\alpha$ , can be used to modify the reference friction angle,  $\phi_o$ , at the reference stress level,  $\sigma_o$ , as shown in Equation (2.2).

$$\tan \phi_s = \tan \phi_o - \tan \alpha \text{Log}_{10} \sigma'_v \quad (2.2)$$

where

- $\sigma'_v$  = vertical effective stress (tsf)  
 $\phi_s$  = friction angle at  $\sigma'_v$

This curvature parameter ( $\tan \alpha$ ) is simply the semi-log slope for given relative density trend in Figure 2.1. Baligh made no other inference concerning the trends in Figure 2.1 concerning sand type or relative density toward the Mohr envelope curvature parameter,  $\alpha$ .

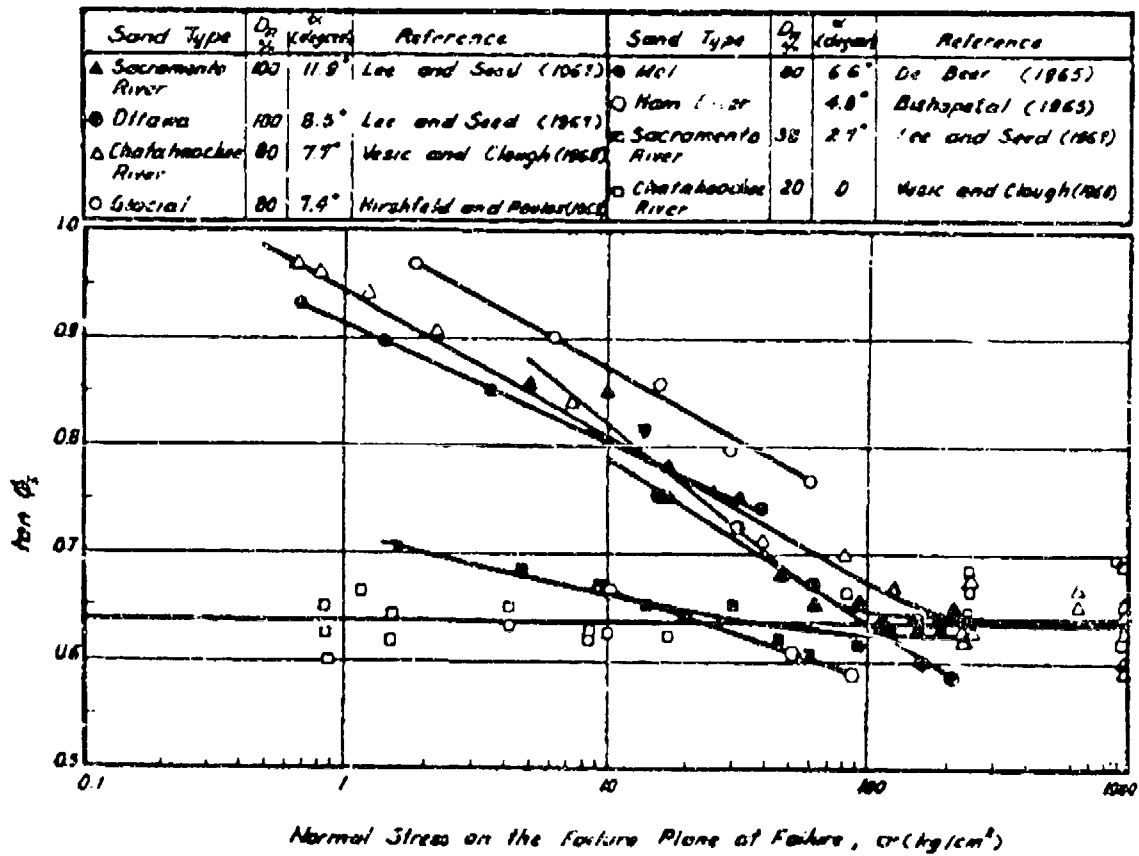


Figure 2.1 Failure envelope curvature effects for different relative densities and sand types (Baligh, 1976)

Yareshenko (1964) proposed an expression for the Mohr failure envelope curvature of the form

$$\tau = (k\sigma)^{1/n} \quad (2.3)$$

Baligh (1976) believed that Equation (2.3) was elegant and convenient for analytical computations, but that it was inadequate for practical applications. He maintained that there were many combinations of  $k$  and  $n$  that could fit experimental results because they were obtained from  $\log \tau$  versus  $\log \sigma$  plots.

## New Strength Normalization Based on Failure Envelope Curvature

A new expression was developed by the author (Equation (2.4)) to describe failure envelope curvature. This "stress normalization" technique will be fully explained in Chapter 3. The normalized shear strength,  $\tau_1$ , in Equation (2.4) is the shear strength at a vertical effective stress of 1 atm. The proposed exponent-based normalization formulation in Equation (2.4) is similar to that of Equation (2.3), except that normalization concepts are used.

$$\tau = \tau_1 (\sigma'_v)_{atm}^t \quad (2.4)$$

where

- $(\sigma'_v)_{atm}$  = Vertical effective stress in units of atm pressure  
(approximately tons/ft<sup>2</sup>)
- $\tau$  = Shear strength at  $\sigma'_v$  in units of atm pressure
- $\tau_1$  = Shear strength at  $\sigma'_v = 1$  atm (i.e.  $\tan(\phi_1)$ )
- $t$  = shear strength stress exponent

This formulation overcomes the limitation stated by Baligh (1976) concerning the Yareshenko (1964) equation, namely that several combinations of  $k$  and  $n$  can fit the same set of data. For loose sands or clays which have little or no failure envelope curvature, the Baligh Mohr envelope curvature parameter,  $\alpha$ , is approximately zero and the stress exponent is approximately 1 (or slightly less). For the dense Ottawa sand in Figure 2.1,  $\alpha$  is approximately  $8^\circ$  and the stress exponent ( $t$ ) is 0.86. Each of the constant relative density trends in Figure 2.1 can be expressed using Equation (2.4) with a constant stress exponent.

## The Stress Focus Concept

It would appear from Figure 2.1 that the only means to determine the stress exponent (e.g. curvature parameter) is with a thorough laboratory strength testing program. However, close examination indicates that all sands have approximately the same friction angle at some high overburden stress: between 70 and 300 atm irrespective of the initial relative density. The overburden stress ( $\sigma_{f\phi}$ ) where specimens of all initial relative densities have the same approximate friction angle ( $\phi_f$ ), is defined as the "Stress Focus". The Stress Focus is therefore a "hinge" to which trends associated with a given soil type and all relative densities converge with increased overburden stress as illustrated in Figure 2.2. This Stress Focus occurs at a confining stress equivalent to a depth of several thousand feet below ground surface.

Data for the Chatahoochee and Sacramento sands in Figure 2.1 were replotted as shown in Figure 2.3 and Figure 2.4, respectively, to illustrate the effects of failure envelope curvature and the resulting Stress Focus. These plots depict vertical effective stress on the vertical axis as a log scale with the values increasing in the downward direction. The dashed least square fit lines are also shown for each initial relative density group. These 30 year old data represent the best quality high stress



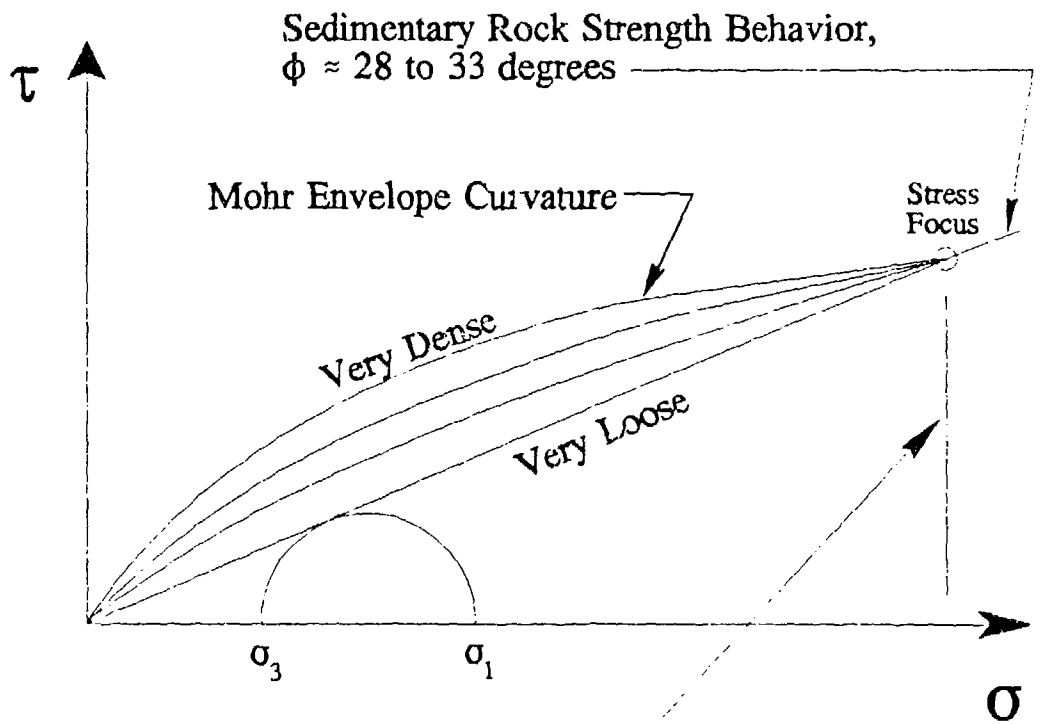


**Figure 2.2** Simplified representation of the Stress Focus using the Mohr envelope curvature

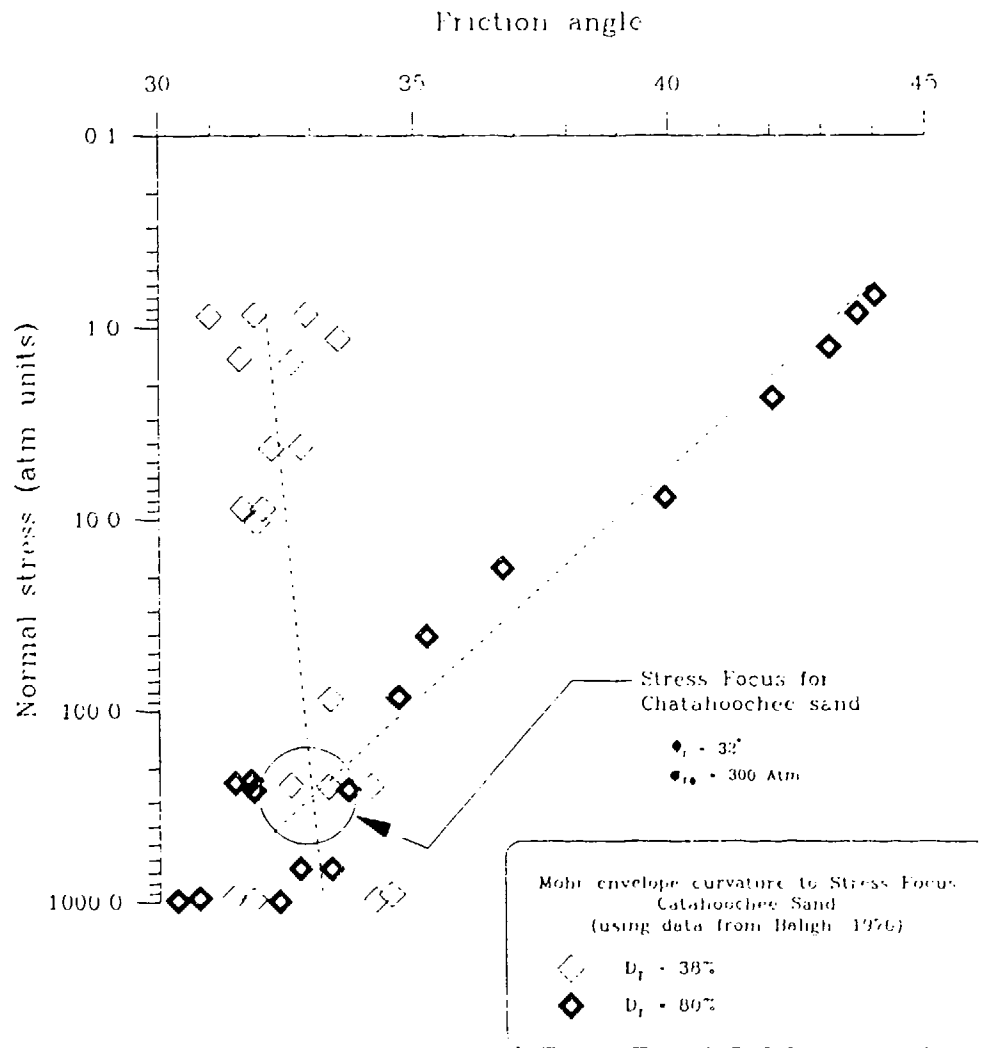
tests available on sand. Other published data do not encompass the range of confining stresses and the number of relative density groups represented in this data set.

Figure 2.3 and Figure 2.4 indicate that at the Stress Focus the friction angle is the same irrespective of the initial relative density from which the samples were consolidated. Dense sands therefore have decreasing friction angle with increasing confining stress until the Stress Focus is reached. At the Stress Focus, initially dense and loose sands have the same friction angle. Loose sands have little Mohr envelope curvature and therefore very little change of friction angle with depth. When the figures are combined (Figure 2.5), the result suggests that the Stress Focus location is dependent on sand type. Stress Focus location dependence on soil type will be further demonstrated in Chapters 4 through 6.

Figure 2.3 and Figure 2.4 are plotted in terms of friction angle whereas Equation (2.4) is expressed in terms of strength. If data for Sacramento sand (from Figure 2.4) is replotted in terms of drained Mohr Coulomb strength (i.e.  $\sigma'_v \cdot \tan(\phi)$ ) versus  $\sigma'_v$ , the result is shown in Figure 2.6. The effect of Mohr envelope curvature in Figure 2.6 is not as obvious as in Figure 2.4, but the stress exponent ( $t$ ) (i.e. slope) and  $t_1$  can be determined directly from this figure and used with Equation (2.4).

## Rock Mechanics and Friction Angle at High Confining Stresses

The Stress Focus (for friction angle) appears to occur at a overburden stress range between 70 and 300 atm. Barton (1976) summarized rock strengths at high stresses (greater than 80 atm) for sedimentary rocks (e.g. sandstone, shale and



**Figure 2.3** Strength Stress Focus described for Chatahoochee sand in terms of friction angle and overburden stress (data from Baligh, 1976)

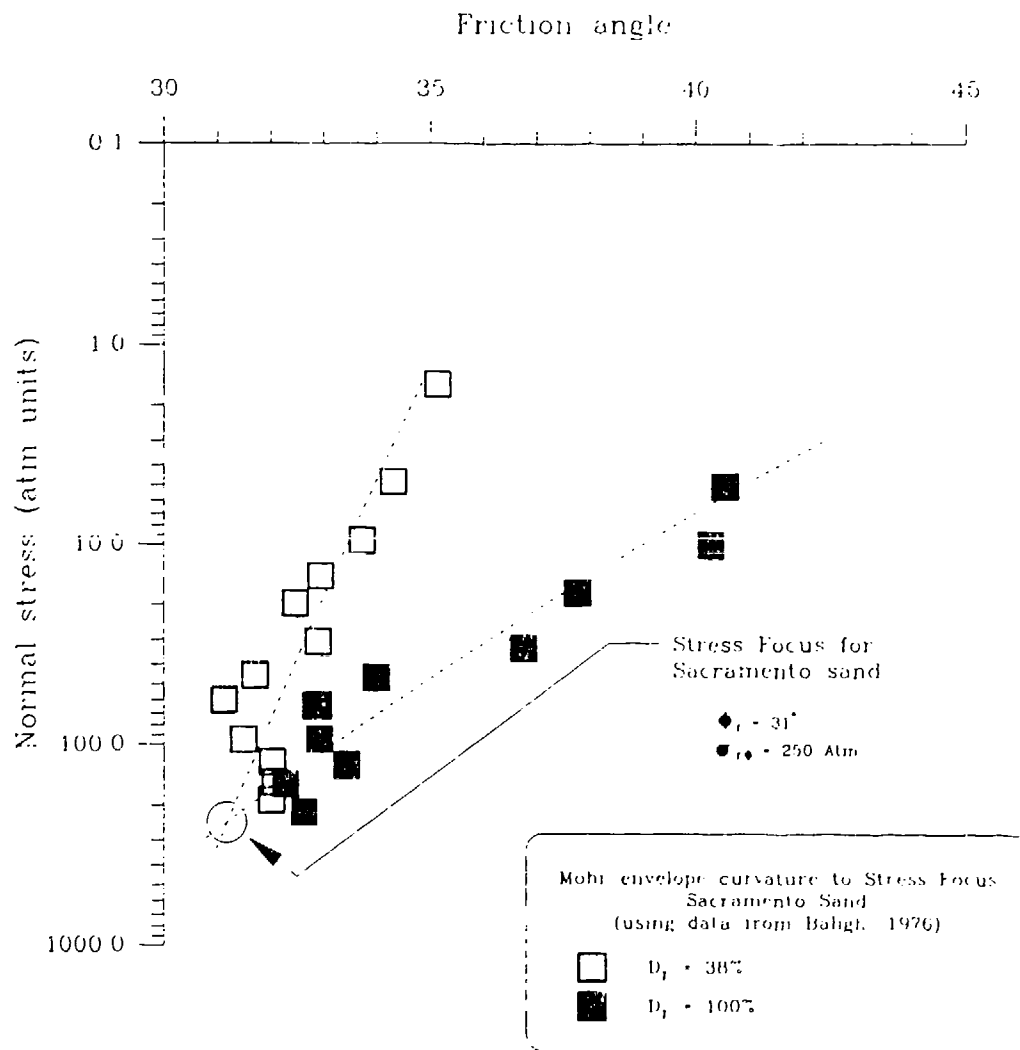


**Figure 2.4** Strength Stress Focus described for Sacramento sand in terms of friction angle and overburden stress (data from Baligh (1976))

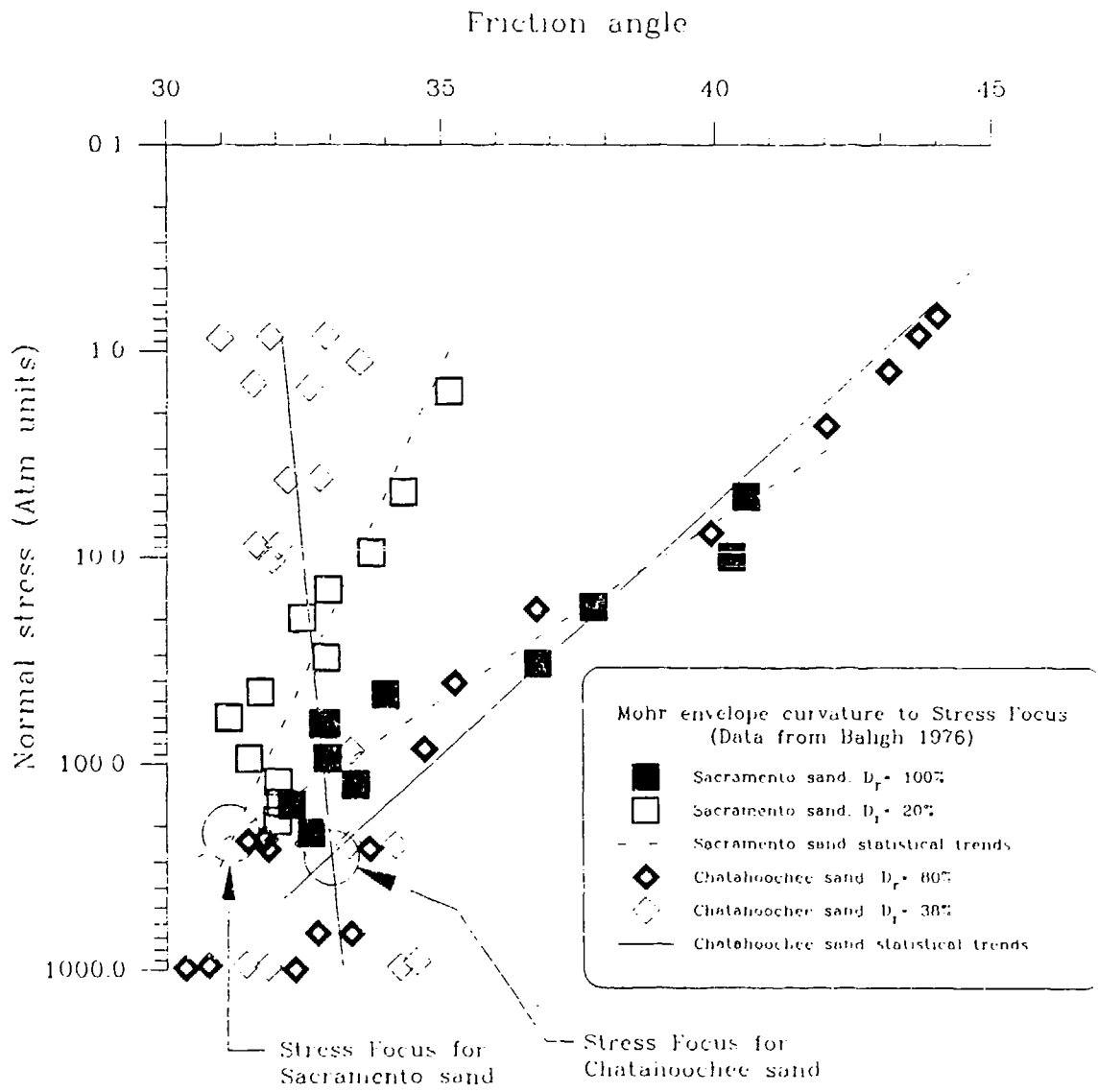


**Figure 2.5** Effect of sand type on Stress Focus location

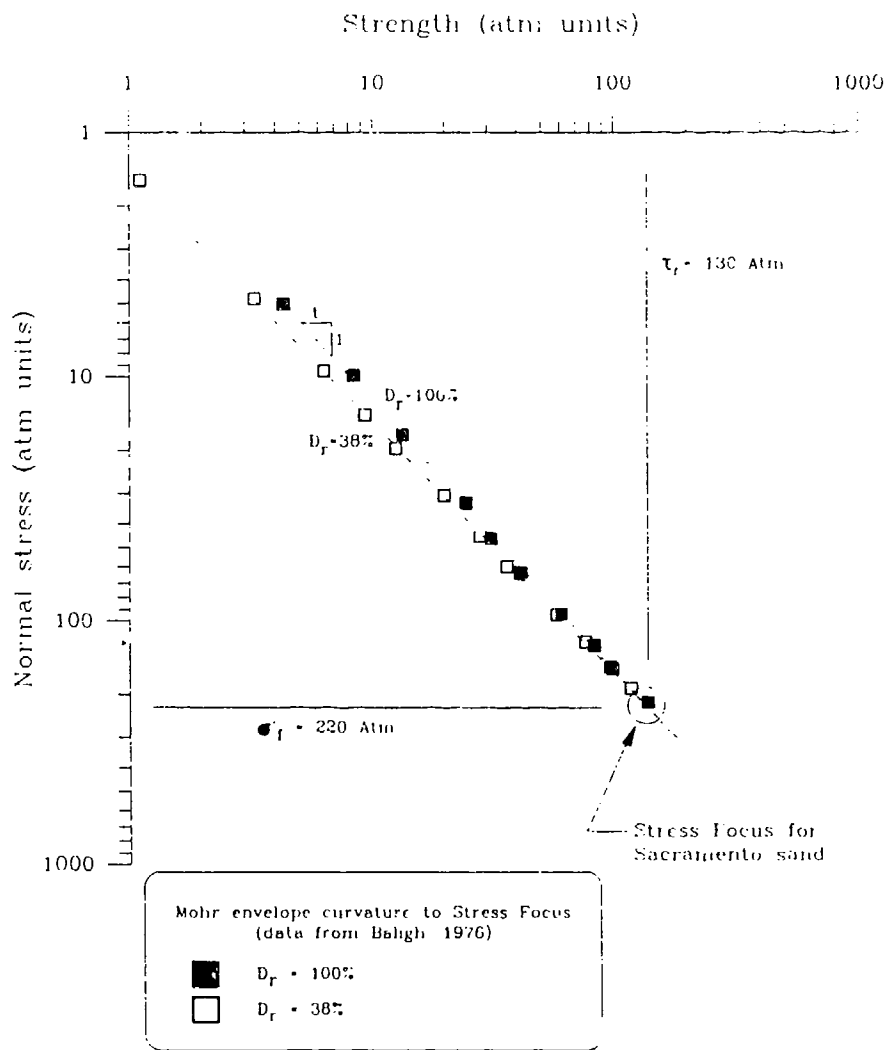


**Figure 2.6** Sacramento sand plotted in terms of strength versus confining stress

siltstone) as shown in Table 2.1. This table indicates that the friction angle (at high confining stress levels) increases from a range between 25° and 30° for clay based sedimentary rock (e.g. chalk, shale, and slate) to a range between 30° and 34° for quartz-based sedimentary rock. The friction angles at the Stress Focus ( $\phi_f$ ) for Chatahoochee and Sacramento sands are approximately 32° and 31°, respectively (from Figure 2.3 and Figure 2.4). This is within the range of 30 to 34° for quartz based sedimentary rock at high confining stress. It therefore appears that sand starts to behave similarly to a sedimentary rock at the Stress Focus.

**Table 2.1** High stress friction angle for sedimentary materials (Barton, 1976)

Material	High pressure friction angle (not having dilative behavior)	Reference
Sandstone	31-34	Coulson, 1972
River sand (normal stress of 30 to 630 atm)	30	Vesic & Barksdale, 1964
Siltstone	27-32 31	Coulson, 1972 Hobbs, 1970
Shale	27 32	Ripley & Lee, 1962 Hobbs, 1970
Chalk	30	Hutchinson, 1972
Mudstone	27	Hobbs, 1970
Slate	25-30	Barton, 1971

Dilation effects in granular materials can explain the friction angle versus confining behavior at stresses less than that at the Stress Focus. Dilation is defined as volume increase with shear. Figure 2.7 shows that the observed friction angle during shear at typical geotechnical confining stress is caused by the accumulative effect of: volume increase effects during shear (i.e., dilation), grain-to-grain

rearrangement and material frictional behavior ( $\phi_\mu$ ). All influences except the material frictional angle ( $\phi_\mu$ ) vary with confining stress level (Mitchell, 1993). This figure illustrates that dense sands have high measured friction angles due to the dilation and frictional effects. On the other hand, very loose sands, at the critical void ratio, exhibit a friction angle due only to grain-to-grain rearrangement and material frictional effects. For dense sands at low confining stresses (e.g. 1 atm), dilation behavior is a major contributing factor toward the strength level. For example, gravel ballast for railroads has a low overburden stress but very high resistance to dilation. Dilation effects therefore increase the apparent friction angle for dense sands.

Initially dense sand appears to have the same strength as initially loose sand at the Stress Focus as shown in Figure 2.5. Very loose sands do not dilate at any confining stress and therefore exhibit no dilation effect at the Stress Focus. Dense sands at the Stress Focus must also have no dilation effect. Dilation effects therefore decrease with increased depth to a minimum (or near zero) level when the Stress Focus is achieved as illustrated in Figure 2.8.

The density for different initial relative densities at the Stress Focus is an important issue. Sand density will increase with increasing consolidation pressure. Initially loose sands will consolidate (i.e. density increase with increasing confining stress level) at a higher rate than initially dense sands. If initially loose sands and initially dense sands have the same strength at the Stress Focus, then the densities may also be equal at the Stress Focus. More likely, the density difference between initially loose and initially dense sands at the Stress Focus are probably evident but minor.

The Stress Focus represents the overburden stress where soil-like behavior becomes (sedimentary) rock-like behavior. It also provides a comprehensive means of relating the initial relative density to confining stress level. The Stress Focus





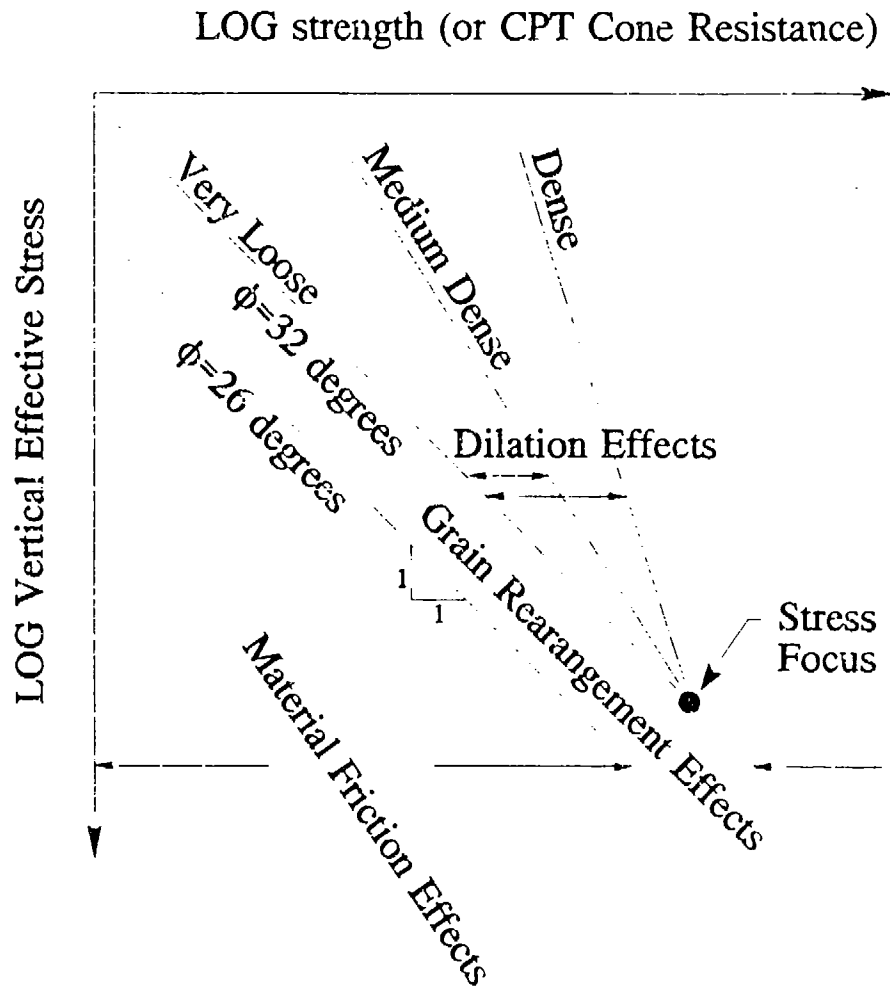


**Figure 2.8** Proposed interaction of friction angle effects and the Stress Focus concept

therefore appears to be a fundamental geotechnical property which can be useful for soil behavior evaluation at all overburden stress conditions.

For confining stresses greater than the Stress Focus, strength is achieved by material friction, grain crushing, and grain rearrangement effects (which can be considered as a minor dilative behavior (Bruce, et.al, 1966). Shear occurs through the grains or at the grain-to-grain contacts because there is little potential for granular rearrangement at high confining stress levels (Vesic and Clough, 1968).

# Chapter 3

## Stress Normalization

### Introduction

Normalization as defined by the Webster's New Collegiate Dictionary (1975) is "to reduce to a norm or standard". In geotechnical engineering, stress normalization allows a variable geotechnical property to be reduced to an equivalent value at a standard confining stress. The easiest obtained standard confining stress for geotechnical stress normalization is the vertical effective stress. It is the only confining stress parameter that can be accurately calculated. The standard confining stress unit should also be atmospheric pressure because English or metric units, are arbitrary stress units.

Stress normalization enables an equation together with correlation curves to cover a wide range of confining stress conditions (analogous to dimensionless analytical solutions). Therefore, normalized CPT measurements can be used to directly predict normalized geotechnical properties even though the confining stress influences on the CPT parameters and on the geotechnical properties may be different.

This chapter will describe the basic stress normalization concept using stress exponents. While the exponent is a basic mathematical concept, a full explanation using geotechnical engineering terminology will simplify the discussion in this

dissertation. The Stress Focus, introduced in Chapter 2, will also be described in terms of the stress exponent.

## The Stress Exponent for Geotechnical Engineering

CPT measurements (in fact, all geotechnical properties) have some degree of nonlinear dependence on increasing vertical effective stress. Curvature of the Mohr envelope was quantified using a stress exponent in Chapter 2. When the behavior of a geotechnical property is represented with an exponent of the vertical effective stress, the representation is referred to as stress exponent-based stress normalization. Linear and exponential behaviors shown at the top of Figure 3.1 become straight lines on a log-log plot as shown at the bottom. Linear behaviors have slopes of one to one and exponential behaviors have slopes which are not one to one. The exponential slope is equal to the horizontal stress exponent ( $e$ ) for a given log unit of vertical overburden stress.

An exponentially curved line in Figure 3.1 becomes a straight line on a log-log plot and can be expressed numerically with the following equation;

$$H = C V^e \quad (3.1)$$

where

H	=	horizontal axis
V	=	vertical axis
e	=	V exponent
C	=	Constant

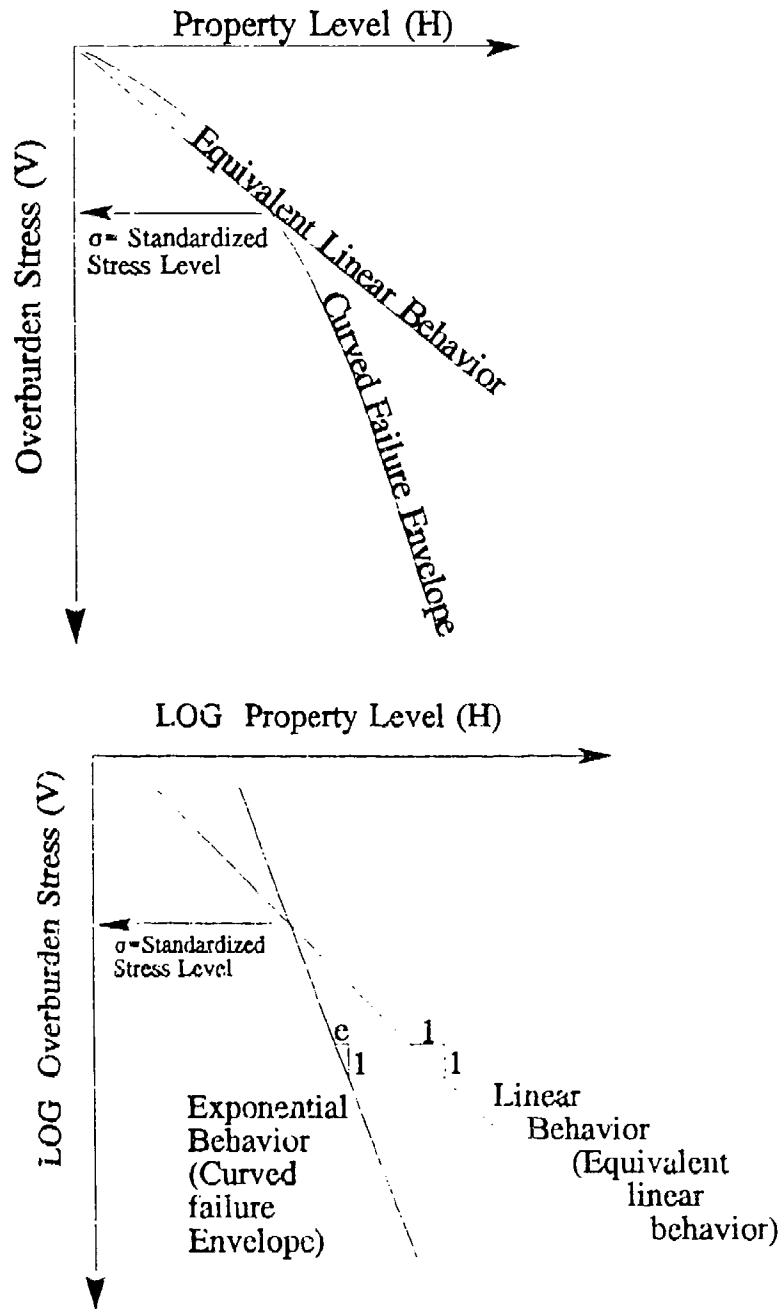


Figure 3.1 Representing geotechnical properties in terms of exponential behavior

This expression can be rewritten to represent the horizontal value when the vertical axis is equal to 1:

$$H_1 = \frac{H}{V^e} \quad (3.2)$$

where

$H_1$  = Horizontal axis value when  $V=1$

The exponent in Equation (3.2) must be specified with a reference such as the "V exponent" because the exponent is applied to V and the slope is equal to the fraction (or multiple) of the  $\log_{10} H$  for one  $\log_{10} V$  cycle. This V exponent (e) is the transformed slope on the log-log chart, namely the distance e for a given V as shown in Figure 3.1. Lines which are nearly vertical have very little V axis dependence and therefore a V exponent of approximately zero. A linear relationship with a 1:1 slope (i.e. 45° line) has a V exponent of 1.

In geotechnical engineering the vertical axis is generally taken to represent vertical effective stress ( $\sigma'_v$ ) and the exponent is referred to as the stress exponent. The stress exponent is thus equal to a fraction or multiple of the  $\Delta \log_{10}(\text{property})$  over one  $\log_{10} \sigma'_v$  cycle. The normalized property value (e.g.  $H_1$  in Equation (3.2)) is simply the H data trend projected from a uniform depth zone to the  $\sigma'_v=1$

horizontal line as shown in Figure 3.2. Stress exponent-based stress normalization for geotechnical engineering is therefore defined as:

$$H_1 = \frac{H}{(\sigma'_v)^e} \quad (3.3)$$

where

- $\sigma'_v$  = vertical effective stress (atmospheric pressure units)
- $H_1$  = The H property at  $\sigma'_v = 1$  atm
- H = The H property at the  $\sigma'_v$  stress level
- e = Stress exponent



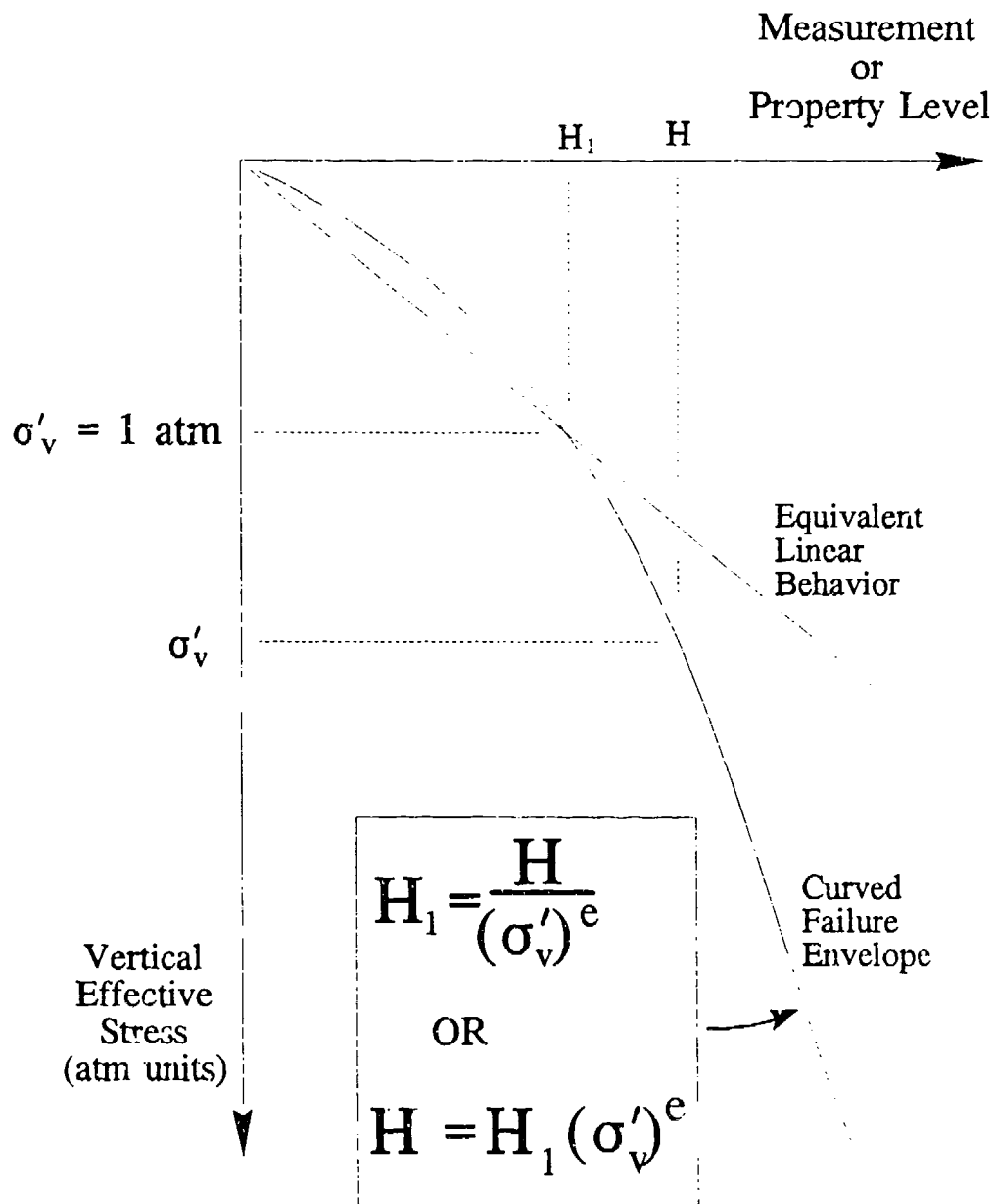


**Figure 3.2** Illustrating the parameters to describe the curvature of the failure envelope for geotechnical engineering

## The Stress Focus and Stress Exponent Interrelationship

The Stress Focus, introduced in Chapter 2, represents the vertical effective stress where all trends of relative density (i.e. curved Mohr envelopes) intersect.

Figure 3.3 is a generalization of the Stress Focus concept with one stress exponent trend shown. Equation (3.4) is a simple representation, in terms of log scales, of the stress exponent line in Figure 3.3 which can be simplified as shown in Equation (3.5).

$$\text{Log } H_1 + (\log \sigma_{FH} - \log(1)) e = \text{Log } H_f \quad (3.4)$$

$$H_f = H_1 (\sigma_{FH})^e \quad (3.5)$$

Equation (3.5) shows that the H level at Stress Focus ( $H_f$ ) is equal to the normalized value (i.e.  $H_1$  at  $\sigma_v = 1$  atm) times the confining stress at the Stress Focus ( $\sigma_{FH}$ ) raised to the  $e$  power. Only three of the four parameters in Equation (3.5) are required to define an expression. For example, if  $H_1$  and  $e$  are known and  $\sigma_{FH}$  can be reasonably estimated, then the H level at the Stress Focus ( $H_f$ ) can be calculated.

## Stress Type and Stress Normalization

Stress normalization using the vertical effective stress will be shown in this section not to introduce error even when a particular geotechnical property is dependent on, for example, lateral stress. CPT measurements and geotechnical properties are controlled by either vertical, mean, octagonal, or lateral stress. This stress type merely reflects a multiple or fraction of vertical effective stress. For example, mean stress is equal to the average of body stresses on the three principle axes as shown in

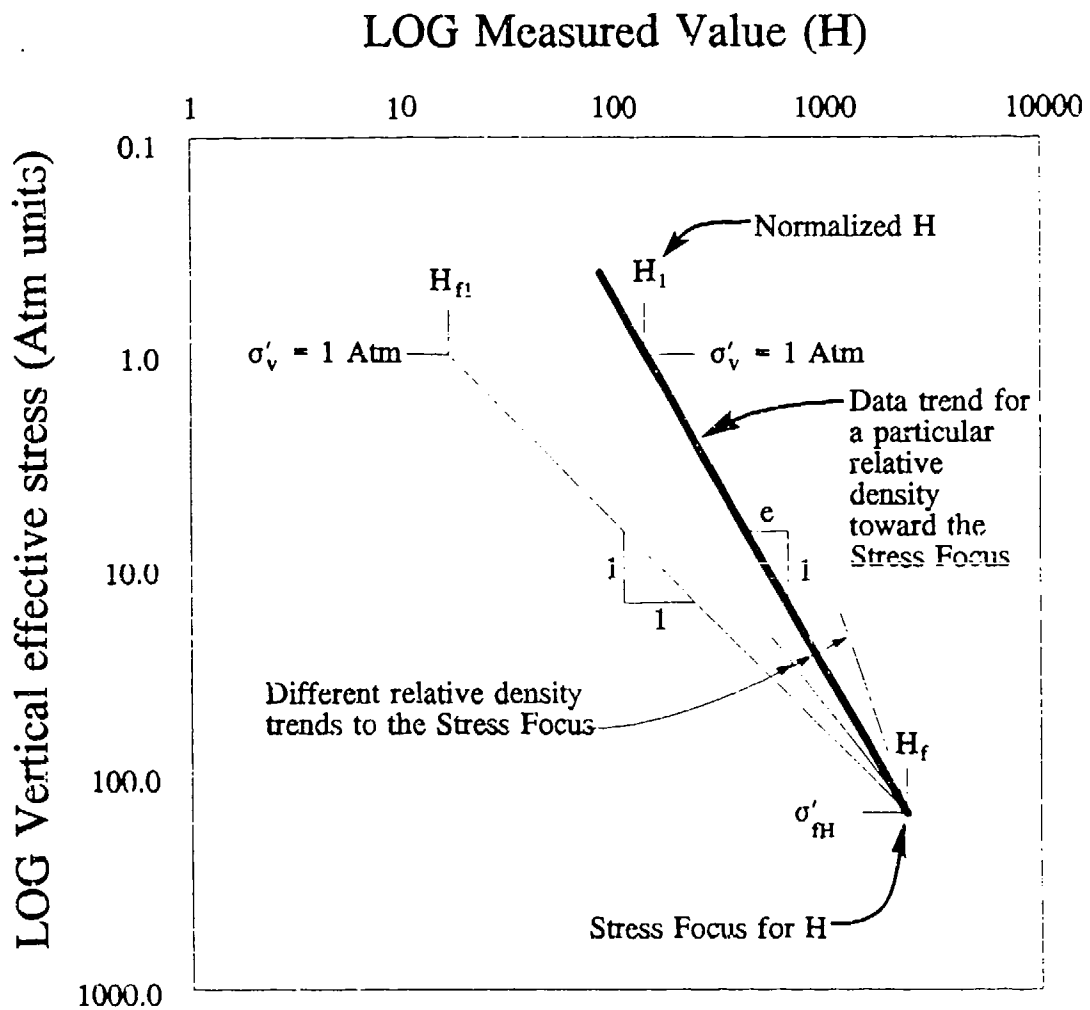


**Figure 3.3** Stress Focus expressed using the stress exponent and normalized value

Equation (3.6);

$$\sigma'_{mean} = \frac{\sigma'_v + \sigma'_h + \sigma'_h}{3} \quad (3.6)$$

All the terms in Equation (3.6) can be defined in terms of vertical effective stress ( $\sigma'_v$ ) as shown by Equation (3.7) and finally by Equation (3.8).

$$\sigma'_{mean} = \sigma'_v \left( \frac{1 + 2K_o}{3} \right) \quad (3.7)$$

$$\sigma'_{mean} = \sigma'_v F_{mean} \quad (3.8)$$

The mean stress in Equation (3.8) is a product of  $\sigma'_v$  and the stress factor,  $F_{mean}$ :

$$F_{mean} = \frac{1 + 2K_o}{3} \quad (3.9)$$

This stress factor can be generalized as  $F_*$  with the \* representing vertical, mean, octagonal, or lateral stress. If  $K_o$  does not change appreciably with confining stress level then  $F_*$  will remain constant for all stress levels. The  $\sigma'_v F_*$  expression can be

substituted into the basic normalized stress equation (Equation (3.3)) with the result shown below;

$$B_1 = \frac{H}{(\sigma'_v F_*)^c} \quad (3.10)$$

which equals;

$$H_1 = \frac{H}{(\sigma'_v)^c} \quad (3.11)$$

where

$$H_1 = B_1 (F_*)^c \quad (3.12)$$

Equation (3.11) is now equal to the basic stress normalization expression (Equation (3.3)) with  $H_1$  in terms of  $F_*$  (Equation (3.12)). If  $K_o$  (i.e.  $F_{\text{mean}}$ ) does not change with vertical effective stress level, then  $H_1$  is a constant (for a given soil type and relative strength). Correlations by Kulhaway and Mayne (1990) have shown that  $K_o$  (e.g.  $F_{\text{mean}}$ ) changes very little with increasing  $\sigma'_v$ . Therefore, the stress type (mean, lateral, etc.) or  $K_o$  are not required for stress normalization as long as the overconsolidation level (or normally consolidation condition) remains constant for all stress levels. As a result,  $\sigma'_v$  can be used as the normalization stress type even if the geotechnical property is controlled by another confining stress factor (e.g. mean or lateral stress).

## The Atmospheric Pressure Standard

Standard atmospheric pressure provides a convenient basis for expressing geotechnical properties. There is only one standard stress level and that is the atmospheric stress—any other stress units such a KPa or psi (pounds/inch<sup>2</sup>) are based on arbitrary units. Atmospheric pressure (atm) is not a usual engineering pressure level but is very close to the English ton/foot<sup>2</sup> (tsf) or one kilogram force per cm<sup>2</sup> (Kgf/cm<sup>2</sup>) or bars units as shown below:

$$1 \text{ atm} = 1.058 \frac{\text{ton}}{\text{ft}^2} = 1.033 \frac{\text{Kg force}}{\text{cm}^2} = 1.013 \text{ bar} = 101.32 \text{ KPa} \quad (3.14)$$

The conventional geotechnical engineering method for expressing normalized parameters is shown in Equation (3.15) with  $P_a$  equal to the atmospheric pressure.

$$\frac{H}{P_a} = \frac{H_1}{\left( \frac{\sigma'_v}{P_a} \right)^\epsilon} \quad (3.15)$$

Equation (3.15) adds an additional factor of complexity to a simple concept. Moreover, if Equation (3.15) expressed in terms of  $H_1$  the following is produced;

$$H_1 = \frac{H}{\left( \frac{(\sigma'_v)^\epsilon}{(P_a)^{1-\epsilon}} \right)} \quad (3.16)$$

This final expression is more complicated than Equation (3.3) for stress normalization because stress units are not atmospheric pressure units. Therefore, atmospheric pressure (atm) is used for stress units throughout this dissertation to keep the stress notation simple and because normalization concepts will become more complex.

# Chapter 4

## Developing the Cone Resistance Normalized Formulation

### Introduction

A cone resistance normalization formulation allows the equivalent cone resistance at  $\sigma'_v = 1$  atm to be determined. Cone resistance normalization is an integral part of the process toward predicting geotechnical properties. If possible, it should have a theoretical background rather than only match the trend of laboratory data. The formulation should be simple and not require elaborate laboratory test-based properties as input to the formulation. It should also account for exponential behavior using the stress exponent concept from the previous chapters.

A CPT cone resistance normalization formulation, based on generalization of bearing capacity formulations, is developed in this chapter. The bearing capacity formulation considers both limit equilibrium techniques (for shallow bearing failures) and cavity expansion theory (for deep bearing failures). The observed non-linearity of cone resistance with vertical effective stress will also be introduced and analyzed further in Chapters 5 and 6.

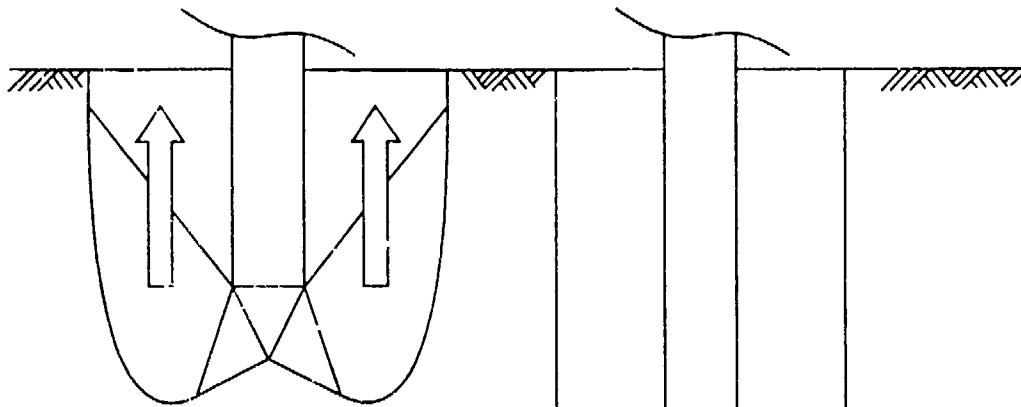
## Comparison of Limit Equilibrium and Cavity Expansion Theories

Most theories for the bearing capacity of both deep foundations (e.g. piles) and penetrometers have severe shortcomings. During the initial half the 20<sup>th</sup> century, bearing failure were evaluated using limit equilibrium (i.e. surface expression) theories. These classical limit equilibrium theories assume soil movement upward to the ground surface using resisting stresses on wedges (Vesic, 1972, Terzaghi, 1943) as shown at the left of Figure 4.1. Limit equilibrium theories are based only on Mohr envelope strength parameters (i.e.  $c$  and  $\phi$ ). In the 1960's and 1970's, cavity expansion theories (Vesic, 1963, 1972) were shown to better describe bearing failure at great depth. Cavity expansion theory assumes a hypothetical spherical or cylindrical expansion of a cavity during intrusion of a penetrometer as shown at the right of Figure 4.1. Cavity expansion theories are based on non-linear strength descriptors and volume change parameters. The cone resistance behavior in laboratory chambers has also been computer modeled using cavity expansion theory together with hyperbolic modeling of the elastic zone (Tseng, 1989).

### Exponential Behavior of the Cone Resistance

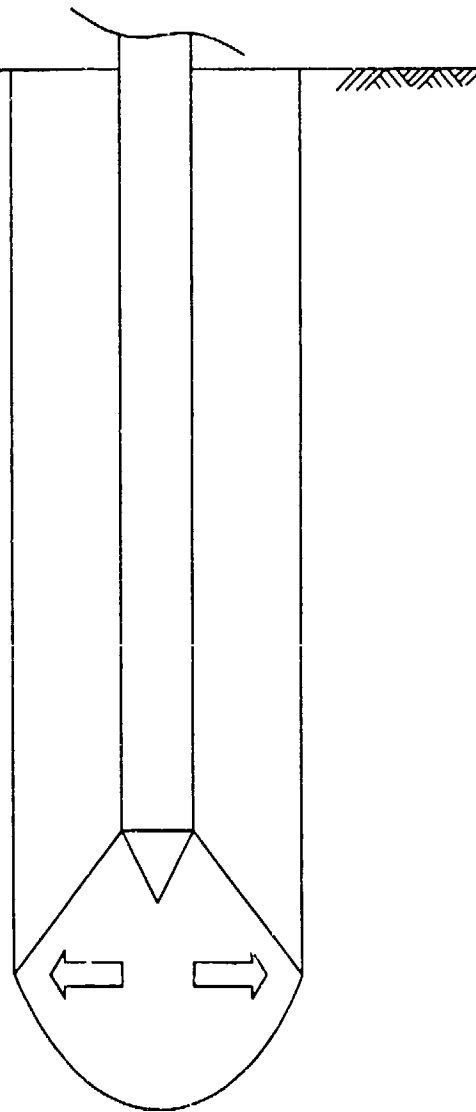
Classical limit equilibrium (surface expression) theories result in bearing stresses which are linearly proportional to vertical effective stress (Terzaghi and Peck, 1967, Durgunoglu and Mitchell, 1973, 1975). Cavity expansion theories, on the other hand, produce a non-linear exponent-based relationship of cone resistance with overburden stress (Vesic, 1972). Cavity expansion theories also show more exponential curvature when soil compressibility and Mohr envelope curvature effects are included (Baligh, 1975).





Limit Equilibrium  
for Shallow depths  
(Soil movement  
toward ground  
surface)

The transition  
between Limit  
Equilibrium and  
Cavity Expansion  
is called the  
Critical Depth



Cavity Expansion  
at depth

**Figure 4.1** Comparison of the Classical Limit Equilibrium based bearing failure to Cavity Expansion bearing failure

Combining a curved Mohr envelope effect with the simplistic limit equilibrium bearing formulation, as illustrated in Figure 4.2, can also create a decreasing, non linear exponential dependence of cone resistance on vertical effective stress. However, the magnitude of curvature is less than observed in laboratory chamber tests. Therefore, the effects of Mohr envelope curvature provide only part of the answer toward defining cone resistance to vertical effective stress behavior.

It will be shown that an exponent of the vertical effective stress (introduced in Chapter 3) can characterize the curved cone resistance behavior observed from chamber tests (in Chapter 5) and from CPT tests in uniform soil layers (in Chapter 6). This stress exponent is based on observed data and accounts for contributing factors such as Mohr envelope curvature, cavity expansion effects, compressibility, grain crushing effects, and others. The cone resistance normalization technique derived in this chapter is the basis for evaluation of chamber and in situ data in later chapters.

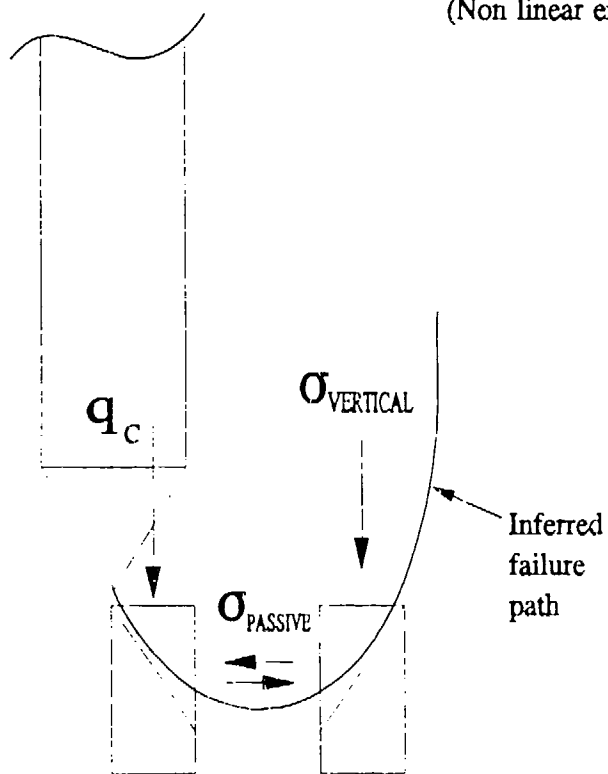
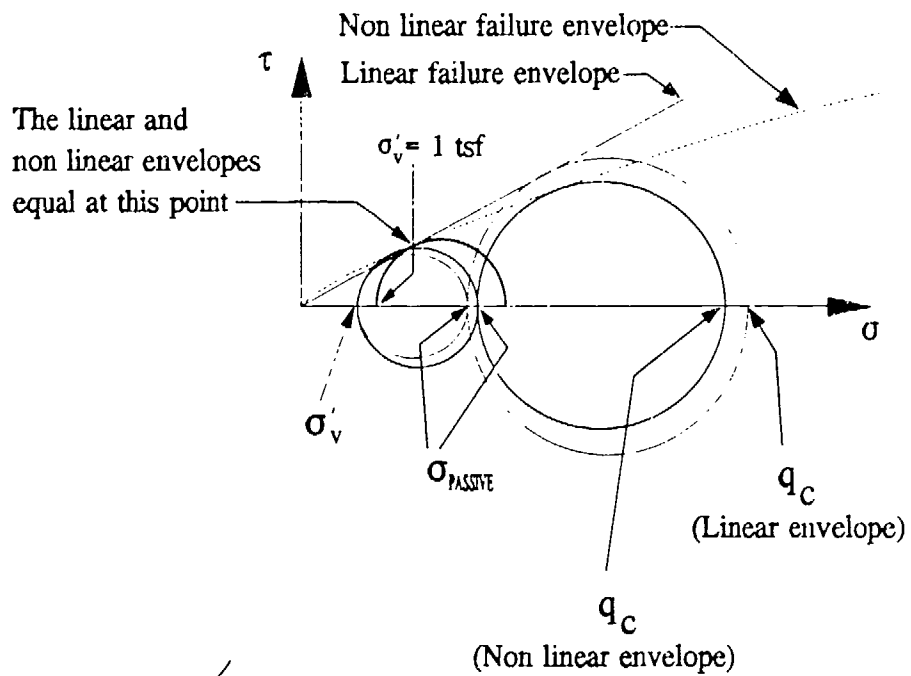


**Figure 4.2** Approximately combining the classical limit equilibrium bearing capacity formulation with non linear Mohr envelope behavior

## Development of the Cone Resistance Normalization Formulation

Limit equilibrium and cavity expansion bearing theories are similar in that they both have cohesive and frictional bearing factor components. The classic limit equilibrium formulation for bearing failure stress is shown in Equation (4.1) (Terzaghi, 1943):

$$q_o = cN_c\zeta_c + \sigma N_q\zeta_q + \frac{1}{2}B\gamma N_\gamma\zeta_\gamma \quad (4.1)$$

where

$q_o$	=	Bearing capacity
$N_c, N_\gamma, N_q$	=	Bearing capacity factors as a function of $\phi$
$\zeta_c, \zeta_q, \zeta_\gamma$	=	Bearing capacity shape factors which depend on the soil angle of internal friction (during shear) and shape of the bearing surface
$c$	=	Cohesion (or shear strength intercept)
$\sigma$	=	Confining stress
$\gamma$	=	Soil unit weight
$B$	=	Strip footing width

The classic spherical cavity expansion formulation is shown in Equation (4.2) (Vesic, 1972).

$$P_L^* = c F_c^* + \sigma_m' F_q^* \quad (4.2)$$

where

$P_L^*$	=	Cavity expansion pressure
$F_c^*$ and $F_q^*$	=	Dimensionless cavity expansion factors
$\sigma_m'$	=	Effective mean normal stress
$c$	=	Soil cohesion
$F_q$	=	$\frac{3(1 + \sin\phi)}{3 - \sin\phi} (I_{rr})^{\frac{4\sin\phi}{3(1 + \sin\phi)}}$
$F_c$	=	$(F_q - 1) \cot\phi$
$I_{rr}$	=	$\frac{I_r}{1 + I_r \Delta}$
$I_r$	=	Rigidity Index = $\left(\frac{G}{S}\right) = \frac{E}{S} \frac{1}{2(1 + \nu)}$
$\Delta$	=	Average compressive volumetric strain in plastic zone
$G$	=	Shear modulus
$E$	=	Young's modulus
$S$	=	Soil shear strength ( $c + \sigma' \tan\phi$ )

The cavity expansion pressure is the pressure required to expand a cavity in situ (i.e. pressure required to expand a balloon at some depth). Cavity expansion pressure is related to bearing pressure because a cavity must be opened for the penetrometer to advance. While cavity expansion is simple in concept, converting it to bearing pressure is not a trivial task. The cavity expansion pressure level is still related to the bearing pressure level, in general.

Both of these formulations can be summarized for penetrometers as shown in Equation (4.3) using the  $Z_c$  and  $Z_\sigma$  bearing factors.

$$q_c = Z_c c + Z_\sigma \sigma \quad (4.3)$$

where

$q_c$	=	bearing stress
$Z_c$	=	cohesive bearing factor
$Z_\sigma$	=	frictional bearing factor
$c$	=	cohesion strength
$\sigma$	=	overburden stress

The bearing stress ( $q_o$ ) or cavity pressure ( $P_L^*$ ) was replaced by  $q_c$  in Equation (4.3) for the cone penetrometer representation. The  $\frac{1}{2}B\gamma N_\gamma \zeta_\gamma$  component in Equation (4.1) can be ignored because the penetrometer width (B) is very small compared to the depth. At any depth the  $Z_c$  and  $Z_\sigma$  can be determined (theory dependent) and the bearing stress,  $q_c$ , may be calculated. The  $Z_\sigma$  and  $Z_c$  bearing factors are dependent on friction angle and cohesive strength for limit equilibrium or on several geotechnical parameters for the cavity expansion theory. The principal difference between the limit equilibrium and cavity expansion theories lies in how the Z bearing factors are determined. The  $Z_\sigma$ , for example, is as simple as the equivalent  $N_q$  factor (Terzaghi, 1943) which is based only on the friction angle, or  $Z_\sigma$  can be based on numerous geotechnical properties which are also influenced by stress level (Vesic, 1972, Baligh, 1976).

The following discussions separately derive a normalized cone resistance expression for clay and sand. Nonlinear exponential effects can then be included using the stress exponent concept. The final step is a normalized cone resistance formulation for all soil types.

## *Development of the Bearing Capacity Formulation for Clay*

The clay based normalized cone resistance can be derived from the generalized bearing capacity formulation in Equation (4.3). Penetration of clay occurs as undrained behavior. Therefore, the bearing stress for quickly loaded saturated clay is not influenced by confining stress. As a result, the  $Z_\sigma$  frictional bearing factor is equal to one (1) (Terzaghi and Peck, 1967)(Vesic, 1972) which reduces Equation (4.3) to:

$$q_c = Z_\sigma S_u + \sigma_{total} \quad (4.4)$$

The cohesive strength ( $c$ ) in Equation (4.3) was replaced with the conventional notation  $S_u$  for undrained shear strength. The next step is to define the net cone resistance. If the clay deposit has zero strength (i.e.  $S_u=0$ ) then Equation (4.3) implies that buoyant total force will act upward on the cone bearing surface:

$$q_c = \sigma_{total} \quad (4.5)$$

The net cone resistance shown in Equation (4.6) is that remaining after removal of buoyancy.

$$(q_c)_{net} = q_c - \sigma_{total} \quad (4.6)$$

Equation (4.4) can now be rearranged as shown using the net cone resistance:

$$(q_c)_{net} = q_c - \sigma_{total} = Z_\sigma S_u \quad (4.7)$$

The net cone resistance,  $(q_c)_{net}$ , is now only dependent on the soil strength. The next step requires dividing both sides of Equation (4.7) by the normalizing vertical effective stress,  $\sigma'_v$ , to produce the following:

$$\frac{q_c - \sigma'_{total}}{\sigma'_v} = Z_c \frac{S_u}{\sigma'_v} \quad (4.8)$$

The normalized clay undrained strength,  $\frac{S_u}{\sigma'_v}$ , in Equation (4.8) is often represented by  $\frac{c}{p}$ , which can also be expressed using normalization terminology as  $S_{u1}$ :

$$\frac{c}{p} = \frac{S_u}{\sigma'_v} = S_{u1} \quad (4.9)$$

Equation (4.8) can now be expressed as the normalized expression for clay as:

$$\frac{q_c - \sigma'_{total}}{\sigma'_v} = [Z_c S_{u1}]_{clay} \quad (4.10)$$

### *Development of the Bearing Capacity Formulation for Sand*

Bearing stress in sands is entirely a function of the effective stress, since sands are frictional materials. Therefore, cohesive undrained strength,  $c$ , is zero and Equation (4.3) simplifies to:

$$q_c = \sigma'_v Z_\sigma \quad (4.11)$$

If a sand has no shear strength (i.e.  $\phi=0$ ), then the frictional bearing factor ( $Z_\sigma$ ) is equal to one (i.e.  $N_q=1$ ) (Terzaghi and Peck, 1967)(Vesic, 1972). Therefore,  $q_c$  equals  $\sigma'_v$  according to Equation (4.11) because  $N_q=1$ . However, for a  $\phi=0$  condition,  $\sigma'_{total}=u$  (hydrostatic stress) which means  $\sigma'_v=0$ , which translates to  $q_c=0$  according to Equation (4.11) which is incorrect (it should instead equal a buoyancy



stress). The  $q_c$  in Equation (4.11) must therefore reflect a net cone resistance similar to that shown in Equation (4.6) for bearing stress of clay. Equation (4.11) can now be rewritten using the net cone resistance as shown below:

$$q_c - \sigma_{total} = \sigma'_v Z_o \quad (4.12)$$

with rearrangement, the normalized expression for sand is:

$$\frac{q_c - \sigma_{total}}{\sigma'_v} = [ Z_o ]_{sand} \quad (4.13)$$

## Modification to the Bearing Formulation for Non-linear Exponential Behavior

The vertical effective stress,  $\sigma'_v$ , in the denominator of Equations (4.10) and (4.13) is the normalizing stress. This  $\sigma'_v$  requires a stress exponent to reflect the observed non-linear behavior of cone resistance with vertical effective stress (concept introduced in Chapter 2 and to be illustrated in Chapter 5). The resulting normalized cone resistance shown in Equation (4.14) is equal to the left side of either Equations (4.10) or (4.13) with a stress exponent ( $c$ ) included. The normalized cone resistance ( $q_{c1e}$ ) subscripts have specific representations: "c" for cone resistance, "1" for normalization to an equivalent value at a vertical effective stress of 1 atm, and "e" to represent that normalization accounts for exponential curvature.

$$q_{c1e} = \frac{q_c - \sigma_{total}}{(\sigma'_v)^c} \quad (4.14)$$

where

c = Cone resistance stress exponent

## Bearing Stress Formulation for All Soil Types

The normalized cone resistance expression for all soil types is the combined effect of the cohesive bearing stress expression from Equation (4.10) and the frictional sand bearing stress expression from Equation (4.13) as shown below:

$$\frac{q_c - \sigma_{total}}{(\sigma'_v)^c} = q_{c1e} = S_{ul} Z_k + Z_q \quad (4.15)$$

This new stress-normalized expression is remarkably similar in appearance to the Terzaghi bearing formulation (expressed for deep penetrations) as shown below:

$$q = c N_c^* + \sigma N_q^* \quad (4.16)$$

Equation (4.15) is expressed in terms of the normalized cone resistance, normalized undrained cohesive strength, and bearing factors. It represents a new technique for cone resistance normalization that will be validated using laboratory chamber data in Chapter 5 and using uniform soil layer data in Chapter 6. It is also the basis for a new technique for prediction of undrained strength of clays in Chapter 8.

It will also be shown, in later chapters, that the bearing factors and the stress exponent in Equation (4.15) are all related to the combination of void ratio and soil type at  $\sigma'_v = 1$  atm. The bearing factors (i.e.  $Z_k$  and  $Z_q$ ) define the mechanical (strength) behavior at a  $\sigma'_v = 1$  atm. And the stress exponent ( $c$ ) defines the exponential stress curvature of cone resistance to vertical effective stress. Therefore, the bearing factors define mechanical strength behavior and the stress exponent defines the curvature of cone resistance to vertical effective stress. Chapters 5 and 6 will specifically show that increasing the initial relative density, of a given sand, creates a higher strength (at  $\sigma'_v = 1$  atm) and a lower stress exponent ( $c$ ).

# Chapter 5

## Cone Resistance Stress Focus— Confirmation Using CPT Chamber Test Data

### Introduction

The Stress focus concept, introduced in Chapter 2, can also be used to describe the relationship of CPT cone resistance with overburden stress. A cone resistance Stress Focus concept can be used to generalize numerous effects such as cavity expansion, Mohr envelope curvature, grain crushing, compressibility, and others. Stress Focus will be confirmed based on cone resistance measurements obtained from CPT laboratory large diameter chamber tests. As additional confirmation of the Stress Focus for in situ penetrometers, the Standard Penetration Test (SPT) chamber test results will also be examined. It will be shown in this chapter that the relationship of cone resistance to vertical effective stress observed in laboratory chamber tests become straight lines when plotted logarithmically indicating a constant stress exponent. It will also be shown that the trends of all relative densities on this logarithmic plot converge to the Stress Focus at great depth as illustrated in Figure 5.1.

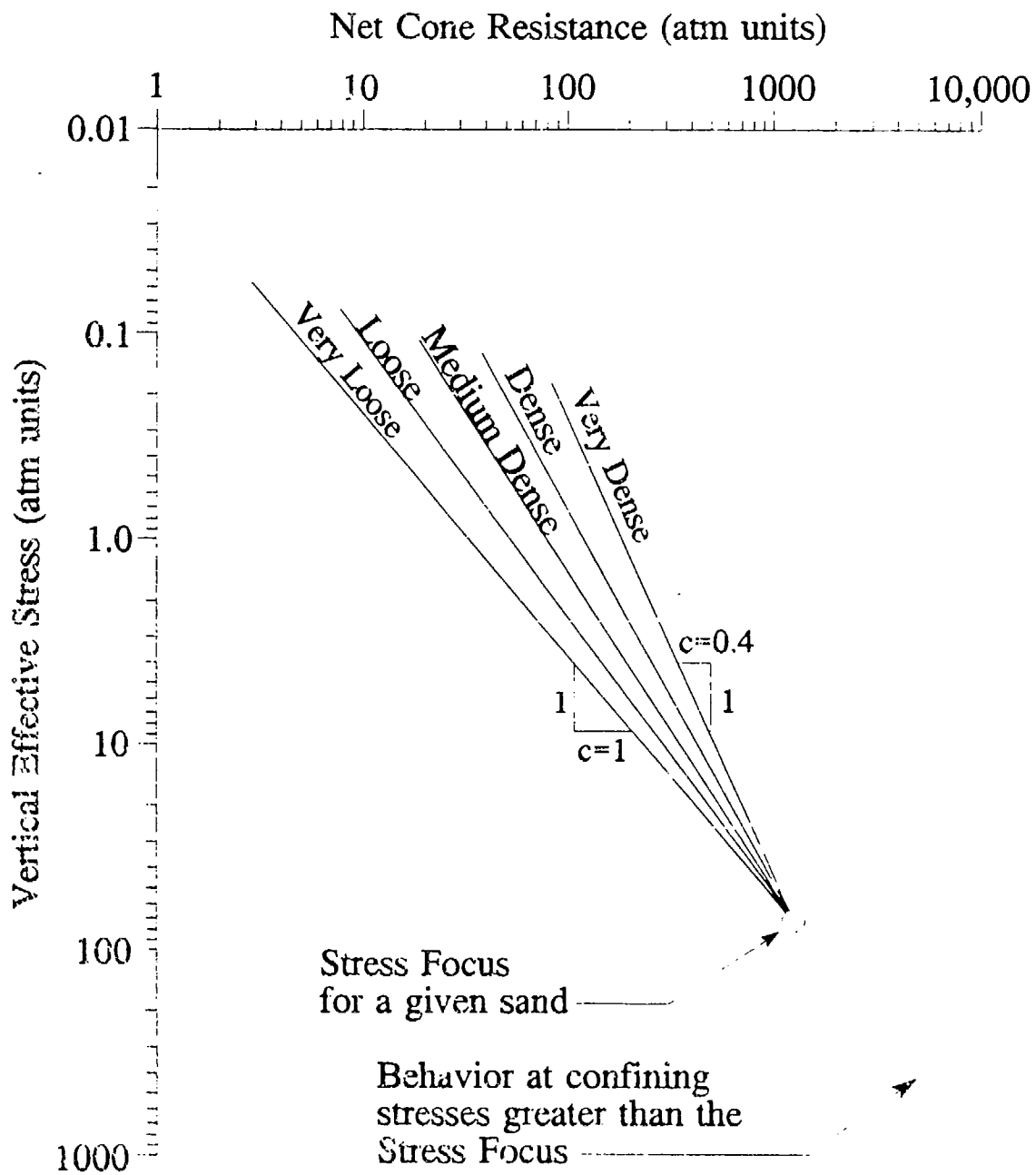


Figure 5.1 Proposed relationship of cone resistance versus vertical effective stress trending for a given sand (or soil) type

It is proposed to show in this chapter that:

- 1) Cone resistance may be expressed as a function of vertical effective stress for a given initial relative density using a constant stress exponent (indicating a straight line on a logarithmic plot)
- 2) The stress exponent decreases with increased initial relative density in sands
- 3) The relationships between cone resistance and vertical effective stress (regardless of initial relative density) converge at great depth (which is defined as the cone resistance Stress Focus)
- 4) Overconsolidation causes a lower stress exponent

## Interpretation of Large Diameter Test Chamber Data

The best means of introducing and defining the components of the cone resistance Stress Focus is with a good example. Figure 5.2 (Baldi, et al., 1981) summarizes relative density contours for Ticino sand derived from a large number of chamber tests at various initial relative densities and confining stress levels. These contours were carefully established by the original researchers for each relative density range. The same contours are replotted in terms of  $\log_{10}$  net cone resistance (e.g.  $(q_c)_{net}$ ) versus  $\log_{10} \sigma'_v$  in Figure 5.3 (net cone resistance is the measured cone resistance minus the vertical total stress as described in Chapter 4). The relationships shown for different initial relative densities in Figure 5.5 all converge to a common Stress Focus for a given sand type. Relative density contours in Figure 5.3 are remarkably straight in spite of the fact that the  $(q_c)_{net}$  versus  $\sigma'_v$  relationship (Figure 5.2) were produced by the original authors from scattered test data without foreknowledge of the Stress Focus concept. These relationships have also been verified by replotting the original data as shown in a later section of this chapter. The lines for all relative densities converge to the Stress Focus because cavity

expansion, Mohr envelope curvature, grain crushing, and compressibility influences are changing. A sand of initially high relative density (dense) will thus have the same cone resistance (and density) as a initially low relative density (loose) sand at the depth of the Stress Focus.

### *Explanation of the Cone Resistance Stress Focus*

The cone resistance at the Stress Focus ( $q_{cf}$ ) in Figure 5.3 is at 2200 atm, and the vertical effective stress at the Stress Focus ( $\sigma_{fc}$ ) is 140 atm. The normalized cone resistance at the Stress Focus ( $q_{cfl}$ ) is 16 as shown in Equation (5.1) and illustrated in Figure 5.4.

$$q_{cfl} = N_q = \frac{2200}{140} = 16 \quad (5.1)$$

The  $q_{cfl}$  represents the bearing factor  $Z_\sigma$  (i.e.  $N_q$ ) for confining stresses greater than the Stress Focus. This  $Z_\sigma$  represents an approximate friction angle between 28 and 31° using the simplistic bearing factors of Janbu and Senneset (1974) (see Figure 5.5) or using cavity expansion techniques (using a low rigidity index) (Vesic, 1972). This friction angle is also within the range (i.e. 30° to 34°) of most granular sedimentary rocks tested at high stresses as was reported in Chapter 2.

Figure 5.4 is an annotated version of Figure 5.3 intended to illustrate all aspects of the stress exponent and Stress Focus concepts. As previously stated, a sand of a given relative density will follow, with increased vertical effective stress, a straight path on a logarithmic plot to the Stress Focus. Dense sands have a low stress exponent, whereas loose sands have the highest stress exponent; the exponent may approach 1 (one). Any point along a given path can be defined by the combination of stress exponent ( $c$ ) and the normalized cone resistance ( $q_{clc}$ ). Alternatively, any point can be defined by the stress exponent ( $c$ ) and the Stress Focus point (that is

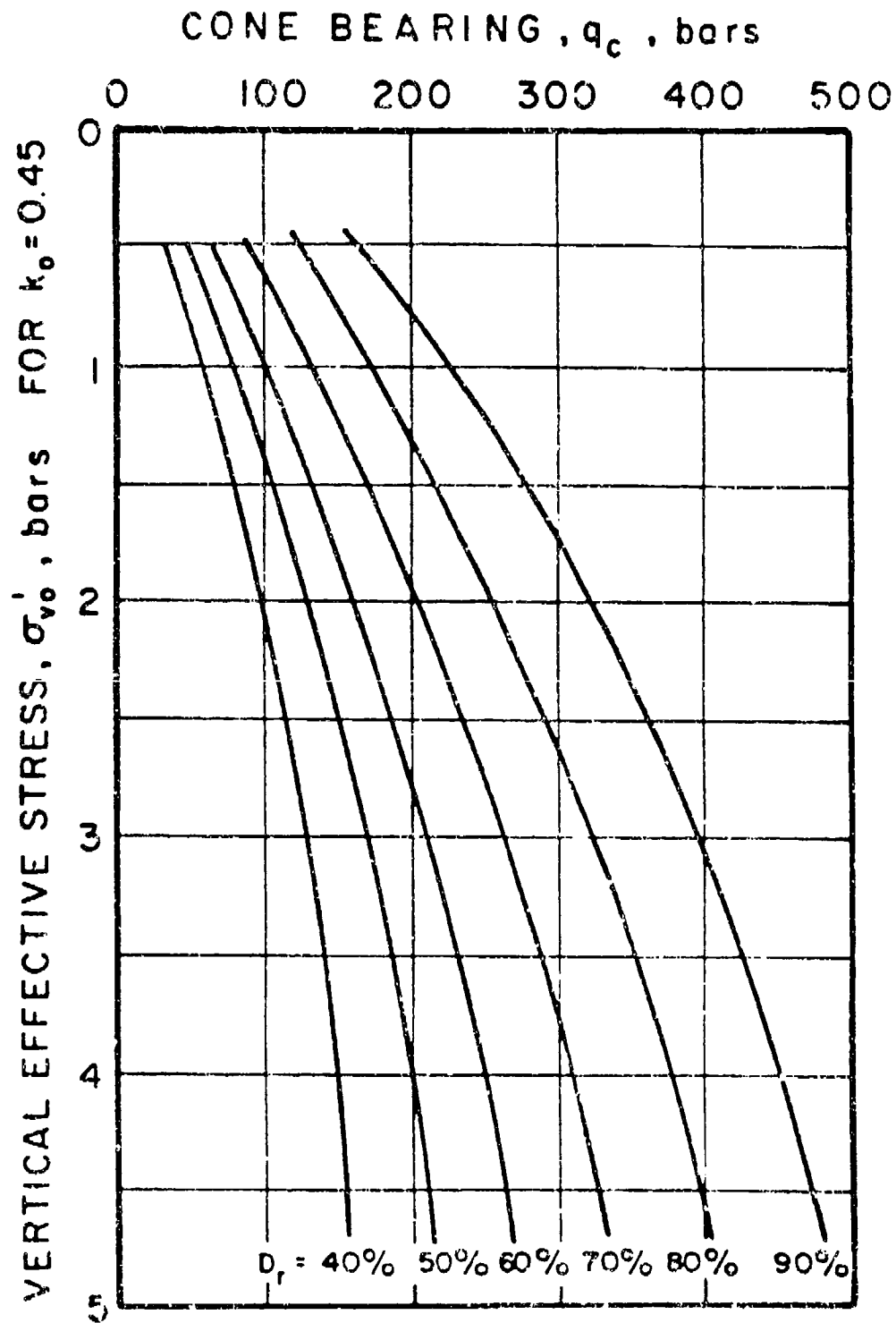
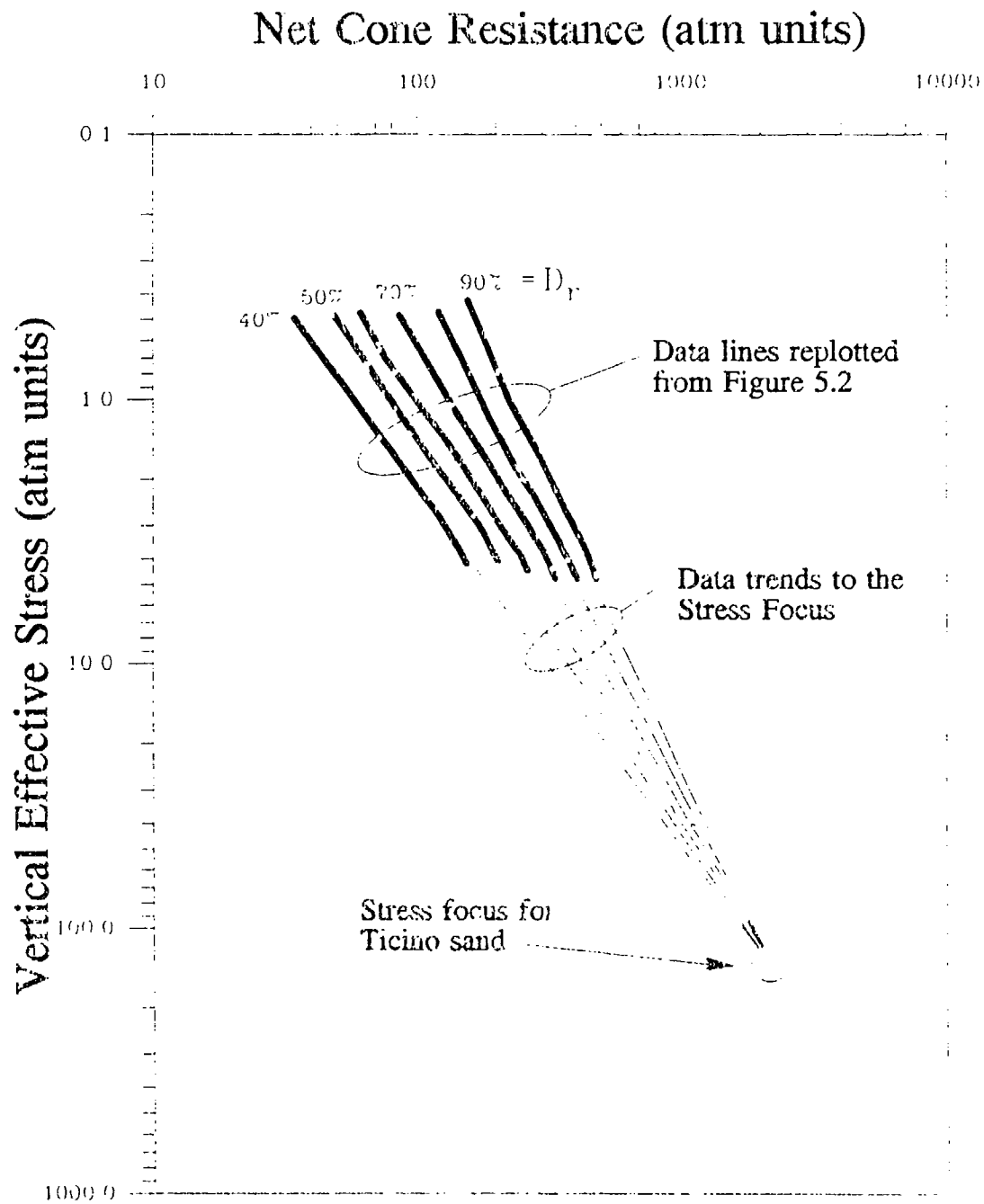


Figure 5.2 Trends of cone resistance versus vertical effective stress for Torino sand (Baldi, et.al., 1981)



**Figure 5.3** Replotting of Baldi, et al., 1981 data curves from Figure 5.2 in terms of  $\text{Log}_{10}$  net cone resistance versus  $\text{Log}_{10}$  vertical effective stress



defined by  $q_{cf}$  and  $\sigma'_{fc}$ ) as described in Chapter 3.

### *Shallow and Deep Bearing Stress in Terms of the Stress Focus*

The bearing stress conditions for shallow and deep conditions may now be better explained as a result of the Stress Focus concept as illustrated in Figure 5.4. Shallow conditions are controlled by vertical expansion based bearing capacity failure (defined by limit equilibrium theories) and deep conditions are controlled by lateral expansion based cavity expansion effects. Shallow bearing stress is associated with a linear relationship between cone resistance and vertical effective stress as reflected by limit equilibrium theories (Terzaghi, 1943, Durgunoglu and Mitchell, 1975) and shown by the transformed linear behavior lines at the top of Figure 5.4. Deep bearing stress conditions are controlled by cavity expansion (Vesic, 1972, Baligh, 1975) and can be expressed exponentially (i.e. transform slope of  $c$ ) as shown at the bottom of this figure.

The transition between vertical (limit equilibrium) and horizontal (cavity expansion) bearing expansion is the "Critical depth" line. Historically, this transition was expressed as the D/B ratio (penetrometer diameter to depth ratio) and is typically 10 to 20. Increasing relative density causes a greater critical depth transition as shown in Figure 5.4 (Ketisel, 1964, Olsen, 1992) for normal penetrometer diameters.

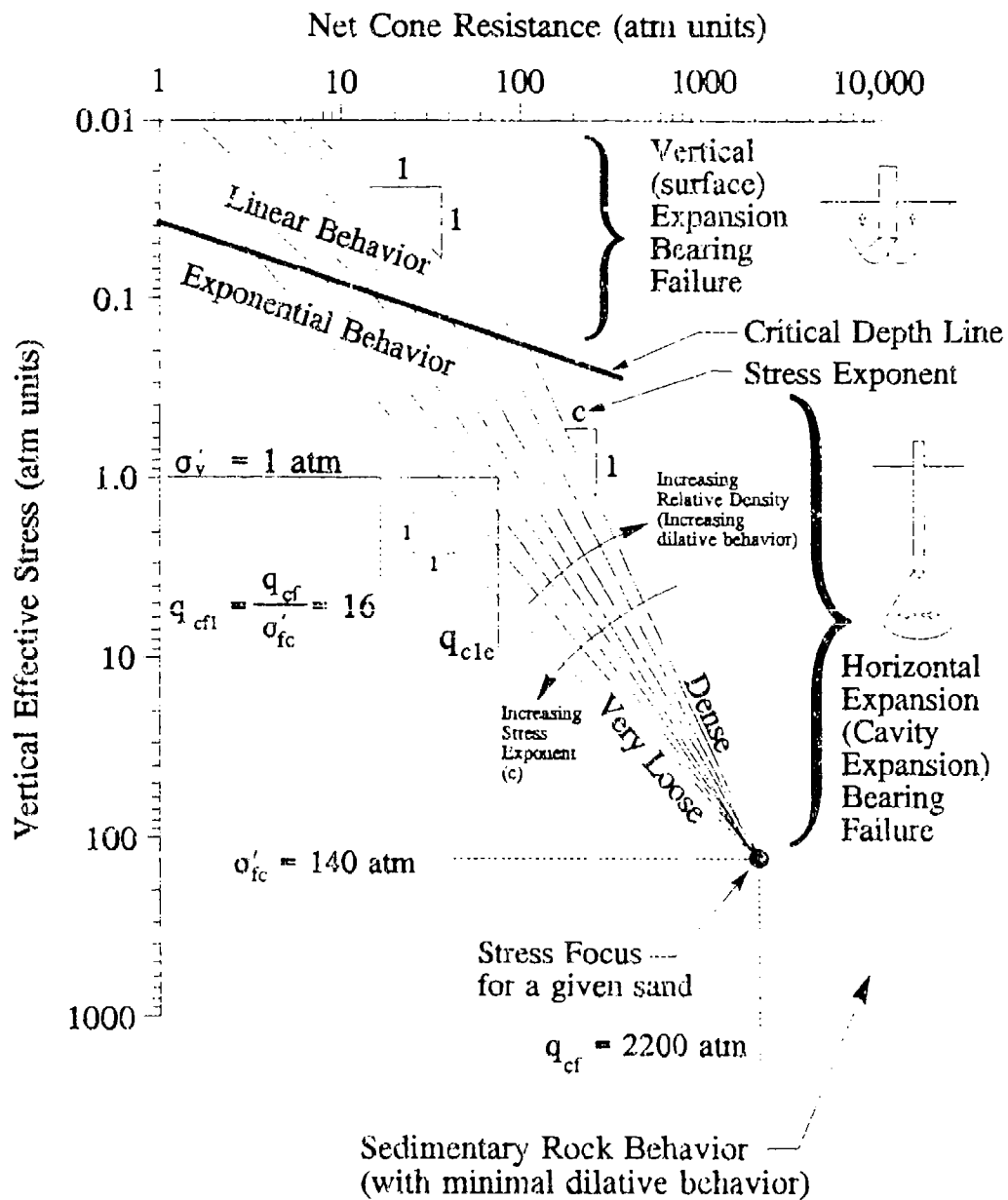


Figure 5.4 Annotated description of the cone resistance Stress Focus together with bearing stress divided into vertical expansion failure and cavity expansion failure

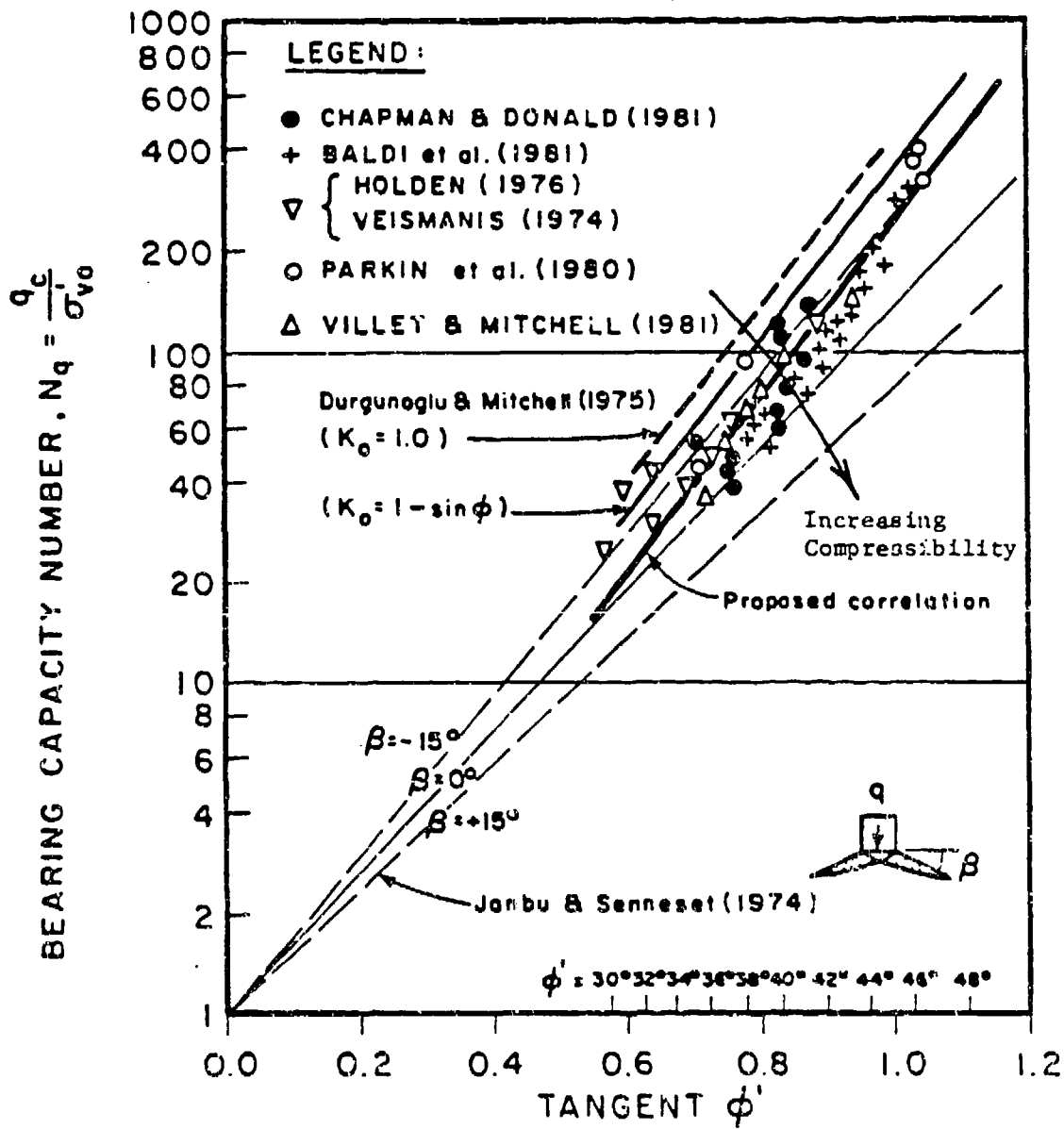


Figure 5.5 Correlations between cone resistance and friction angle based on limit equilibrium theories and laboratory chamber tests (Campanella and Robertson, 1983)

## Using Chamber Data to Establish Trends of Stress Exponent and the Stress Focus

Large diameter chamber tests provide the best experimental means for evaluating stress effects on the cone resistance, because vertical and horizontal stresses can be controlled independently. Numerous researchers over the last 30 years have performed CPT chamber tests using a variety of sands and confining stress conditions. This section will critically examine chamber data toward proving that the cone resistance behavior indeed has a Stress Focus. Standard Penetration Test (SPT) chamber tests results are also examined in a subsequent section because they include data for a large number of well documented sand types. SPT chamber test results verify that the Stress Focus location is sand type dependent.

A computerized database of chamber tests was created based on a data listing provided to the author by Professor M. Jamiolkowski in 1989. This listing represents 410 chamber tests performed by ENEL, ISMES, and NGI over a period of 12 years and represents two sand types, namely Hokksund sand and several variations of Ticino sand.

### *Evaluation of the Chamber Data*

The laboratory chamber data were initially divided according to sand types and further divided into groups representative of normally consolidated and overconsolidated conditions. Each sand type (or batch of a sand) was then divided into groups based on relative density, each having an adequate number of points (e.g. 6 minimum) for statistical evaluation. For each relative density group (of a

given sand type), the individual chamber test data points were plotted as  $\log_{10} (q_c)_{net}$  versus  $\log_{10} \sigma'_v$  as shown in Figure 5.6 through Figure 5.9.

Using statistical least square fit correlations for each relative density group, for the purpose of determining the Stress Focus, was not successful because one or two poor data points will shift the best fit line; statistical correlations are easily biased by poor data at or beyond the limits of data ranges (Taylor, 1990). Therefore a new means was required to determine Stress Focus location. The Stress Focus location can be iteratively varied (in the  $(q_c)_{net}$  and  $\sigma'_v$  directions) until the optimum location is found. For each Stress Focus location, lines are projected from the Stress Focus through each relative density data group. The optimum Stress Focus location has the best data fit for all of the relative density lines.

The Stress Focus locations from the preceding figures are summarized in Figure 5.10. The main observation from these plots is that a cone resistance Stress Focus can be established using CPT chamber test data.

### *CPT Stress Exponent Evaluation*

As shown in the preceding figures, cone resistance for each relative density range is associated with a constant stress exponent relationship (e.g. straight line on a logarithmic plot) to the Stress Focus. The relationship of cone resistance stress exponent ( $c$ ) to relative density for the various sands (i.e. Figure 5.6 to Figure 5.9) is summarized in Figure 5.11. There is an apparent trend of decreasing stress exponent with increasing initial relative density.

Also shown in Figure 5.11 is the cone resistance stress exponent of  $c=0.61$  suggested by the late H. Bolton Seed (Seed, et al., 1981) for relative densities



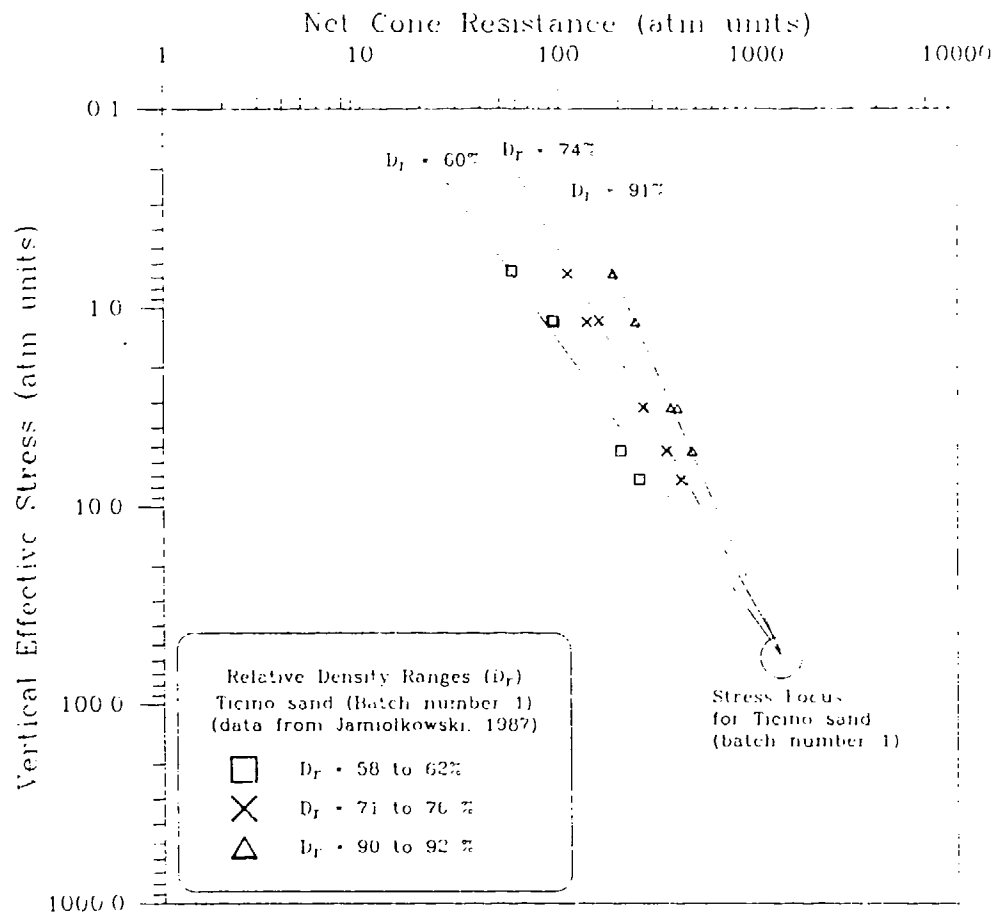


**Figure 5.7** Net cone resistance versus vertical effective stress for Ticino sand (batch #1)

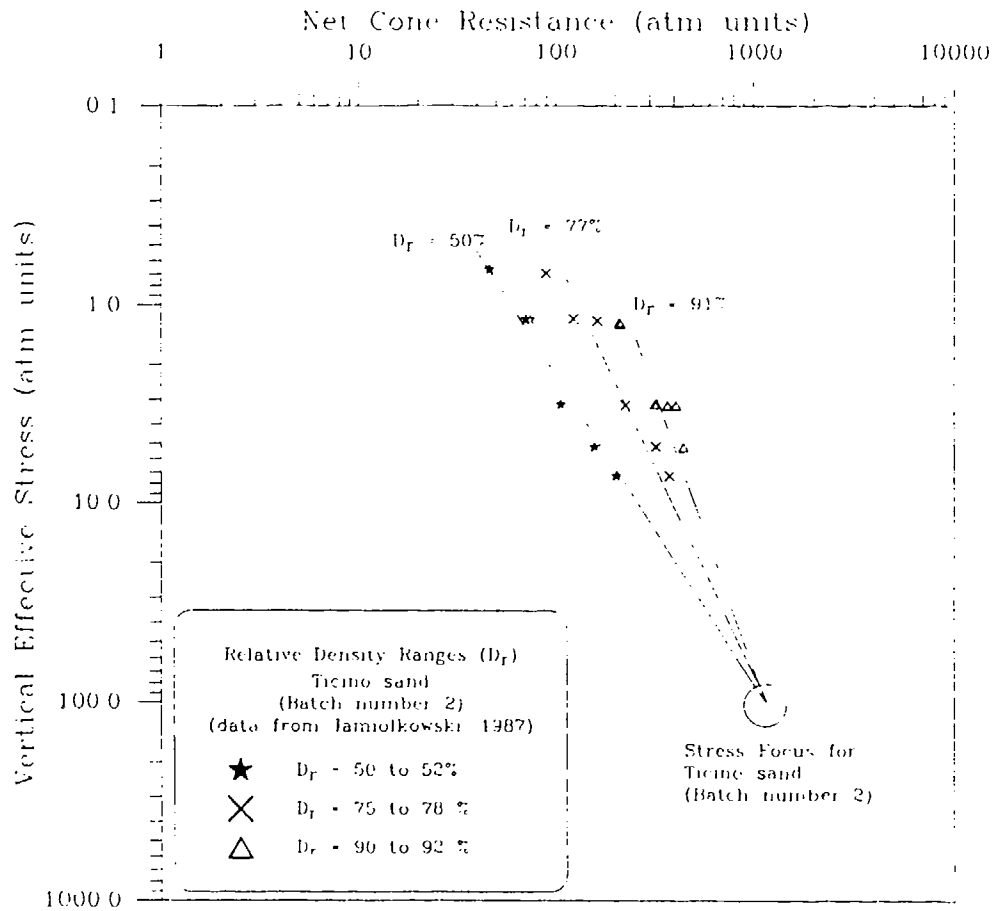


**Figure 5.8** Net cone resistance versus vertical effective stress for Ticino sand (batch #2)



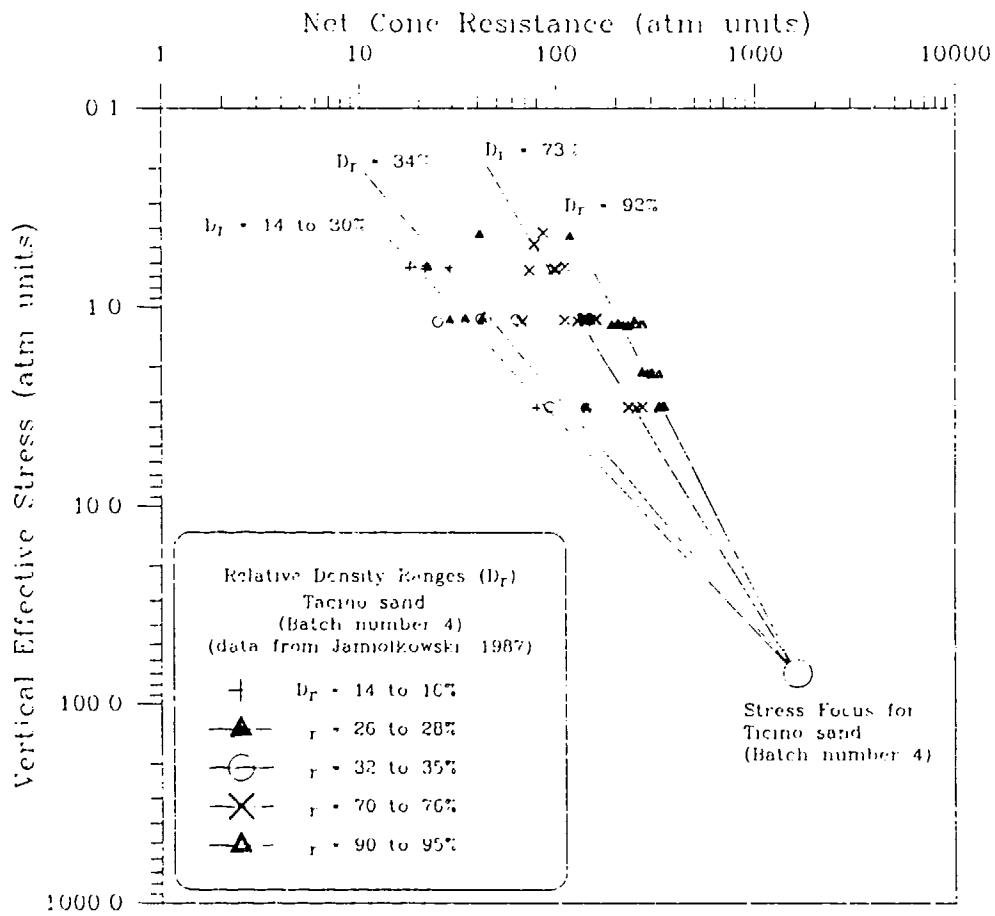


**Figure 5.9** Net cone resistance versus vertical effective stress for Ticino sand (batch #4)

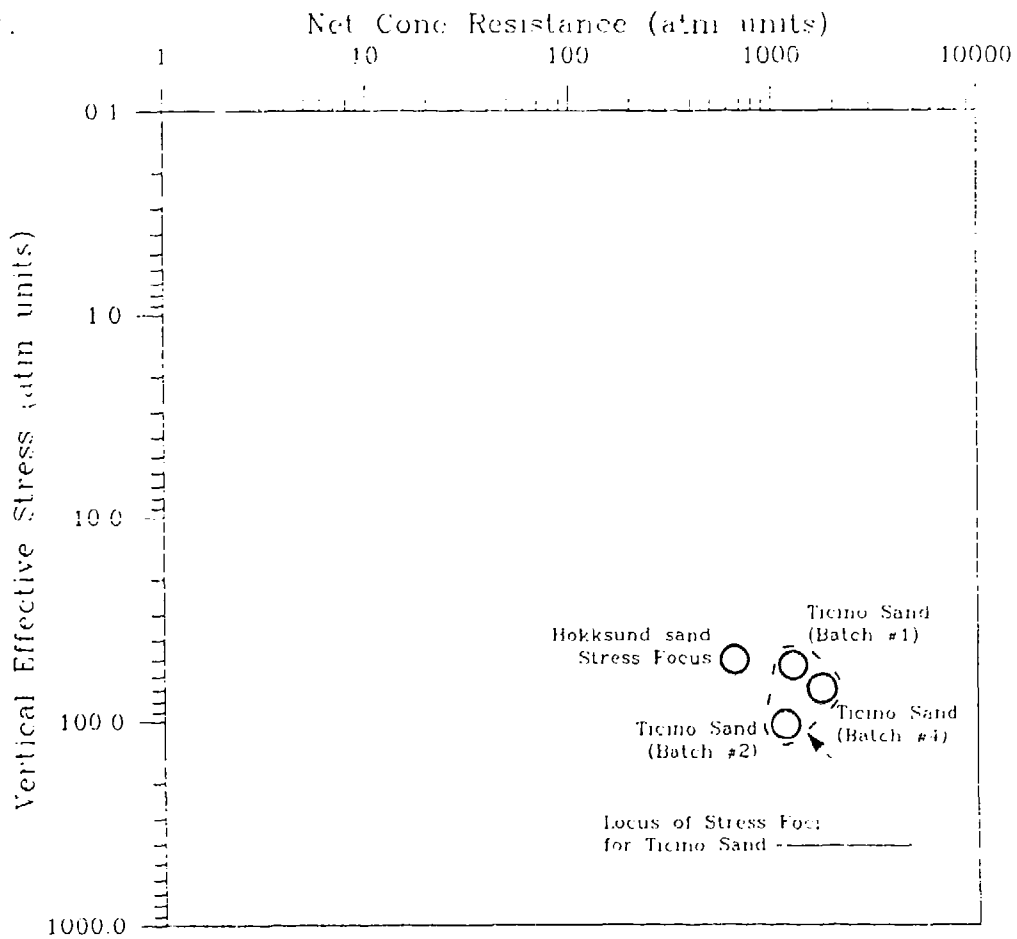


**Figure 5.10** Stress Focus locations for Hokksund and Ticino sands based on evaluation of laboratory chamber tests

between 40% and 80%. The stress exponent is calculated from  $C_p$  using:

$$C_p = \frac{1}{(\sigma'_v)^c} \quad (5.2)$$

The  $C_p$ -based stress exponent was established by Seed, et al., (1981) based on chamber tests performed at the University of Florida. These chamber tests were, at the time, interpreted to have a constant stress exponent for all relative densities (Schmertmann, 1978a). The  $C_p$  based stress exponent of  $c=0.61$  in Figure 5.11 envelops all of the chamber based relative densities from 40% to 80% and specifically represents a relative density of approximately 60%. The overriding conclusion from this figure is that the cone resistance stress exponent is inversely proportional to relative density.

### *Overconsolidation Effects on the Stress Exponent*

There is a consistent observation from chamber test results (and field uniform layer trends discussed in Chapter 6) that overconsolidated soils have low stress exponent values. Figure 5.12 is an example of overconsolidated chamber data having a wide range of relative density levels and numerous overconsolidation levels. The solid lines represent the normally consolidated trend (from Figure 5.9) while the data points and dashed lines represent increasing overconsolidation level. The stress exponents ( $c$ ) for overconsolidation range from 0.06 to 0.24, which also represents the lower range for normally consolidated very dense sand. Overconsolidation at any initial relative density therefore produces low stress exponents. A simple means of explaining overconsolidation effects is to compare the conventional consolidation relationship (e.g. odometer test results) to the cone resistance versus vertical effective stress relationship in Figure 5.13—both have steep slopes associated with overconsolidation. Interestingly, dense sands and overconsolidated conditions are both located in the upper right portion of the CPT soil characterization chart

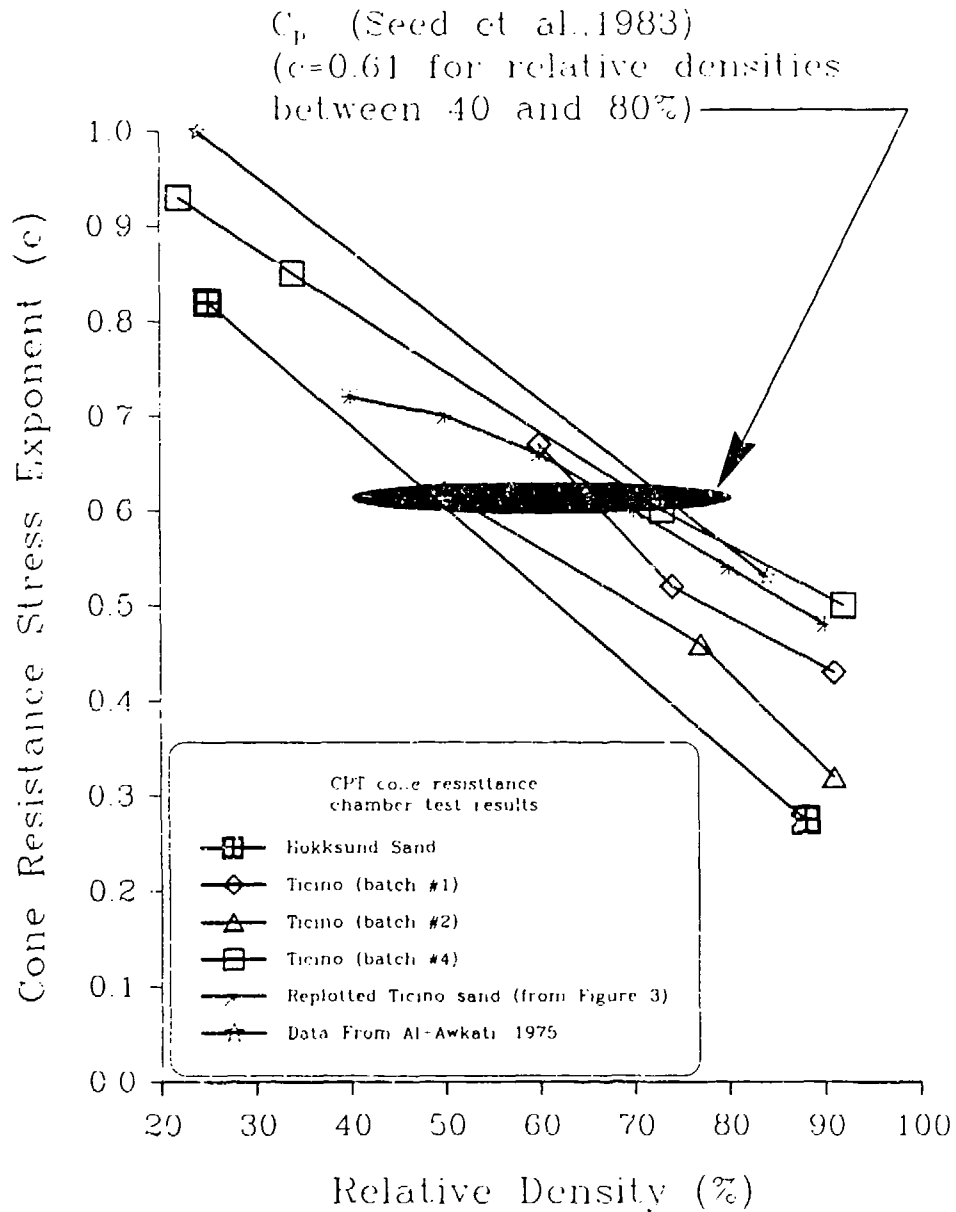


**Figure 5.11** CPT stress exponent range for several sands in terms of the Relative density and CPT cone resistance stress exponent

(Olsen, 1988)(Figure 1.2).

### *Chamber Boundary Effects for Dense Sands*

Chamber size and chamber boundary conditions can affect CPT measurements. Dense sands tested in laboratory (constant stress boundary) chambers produce cone resistances that are lower than measured in situ (Bellotti et al., 1979; Keaveny, 1985). Typical laboratory chambers are too small to accommodate the full cone resistance stress field produced in dense sand by a 3.6 cm diameter probe. Shear stresses that would be generated beyond the radius of a typical chamber do not develop because the pressurized confining water beyond the flexible boundary cannot sustain shear stress or generate elevated lateral pressure. This results in lower measured cone resistance in most chamber tests than are measured in situ for dense sand. Typical chamber correction factors based on the sand type, ratio of chamber diameter to probe diameter, and sand relative density are shown in Figure 5.14. This figure implies that initially very loose, loose and medium dense sands are not influenced by boundary effects with typical chamber diameters (i.e. diameter ratios greater than 40).

The cone resistance Stress Focus concept developed using chamber data in this chapter is valid for very loose to medium dense sands but questionable for dense sands because of chamber boundary effects. Dense to very dense sand must exhibit artificially low measured cone resistances because of chamber boundary effects. However, it appears that cone resistance behavior at all relative densities (for chamber tests on a single sand type) converge to a common Stress Focus (Figure 5.7 to Figure 5.9). This convergence to a Stress Focus and the fact that dense sands must have lower-than-expected cone resistance (e.g. Figure 5.14) must be attributable to chamber-tested dense sands having elevated stress exponents as shown in Figure 5.15. Dense sand tested in chambers and in situ may therefore have the same

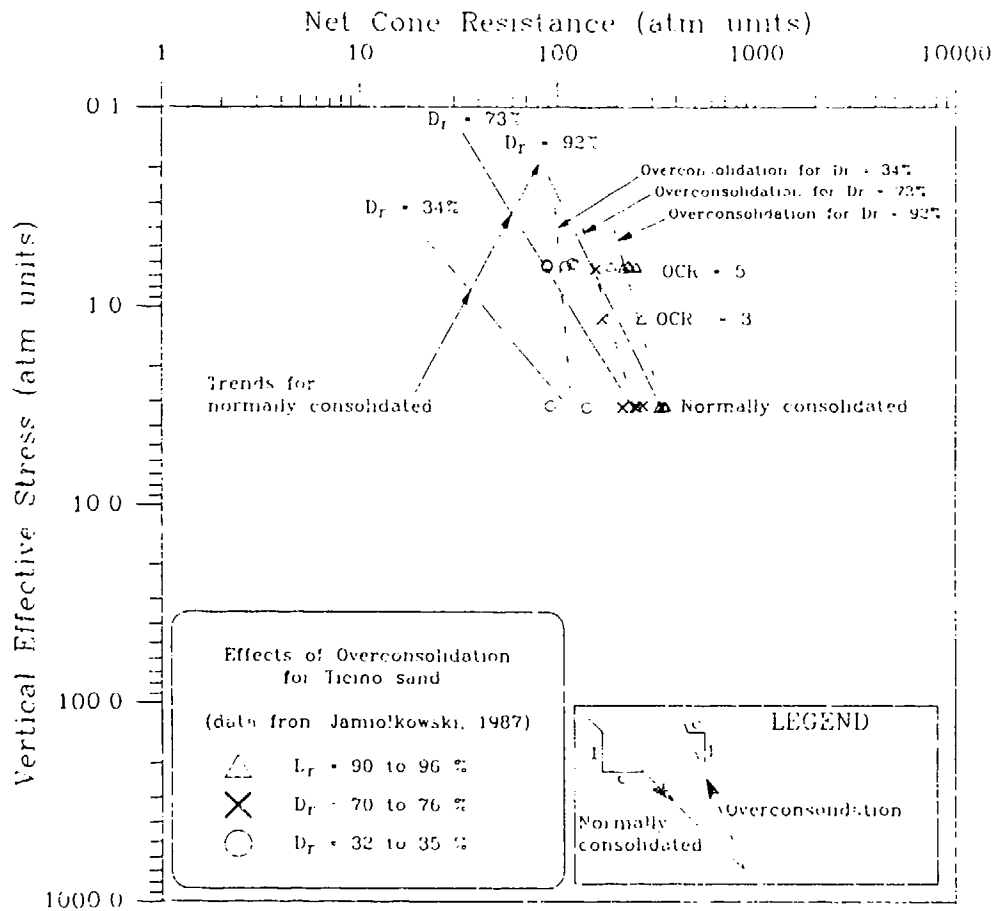


**Figure 5.12** Relationship of the cone resistance stress exponent for overconsolidated sands in chamber tests

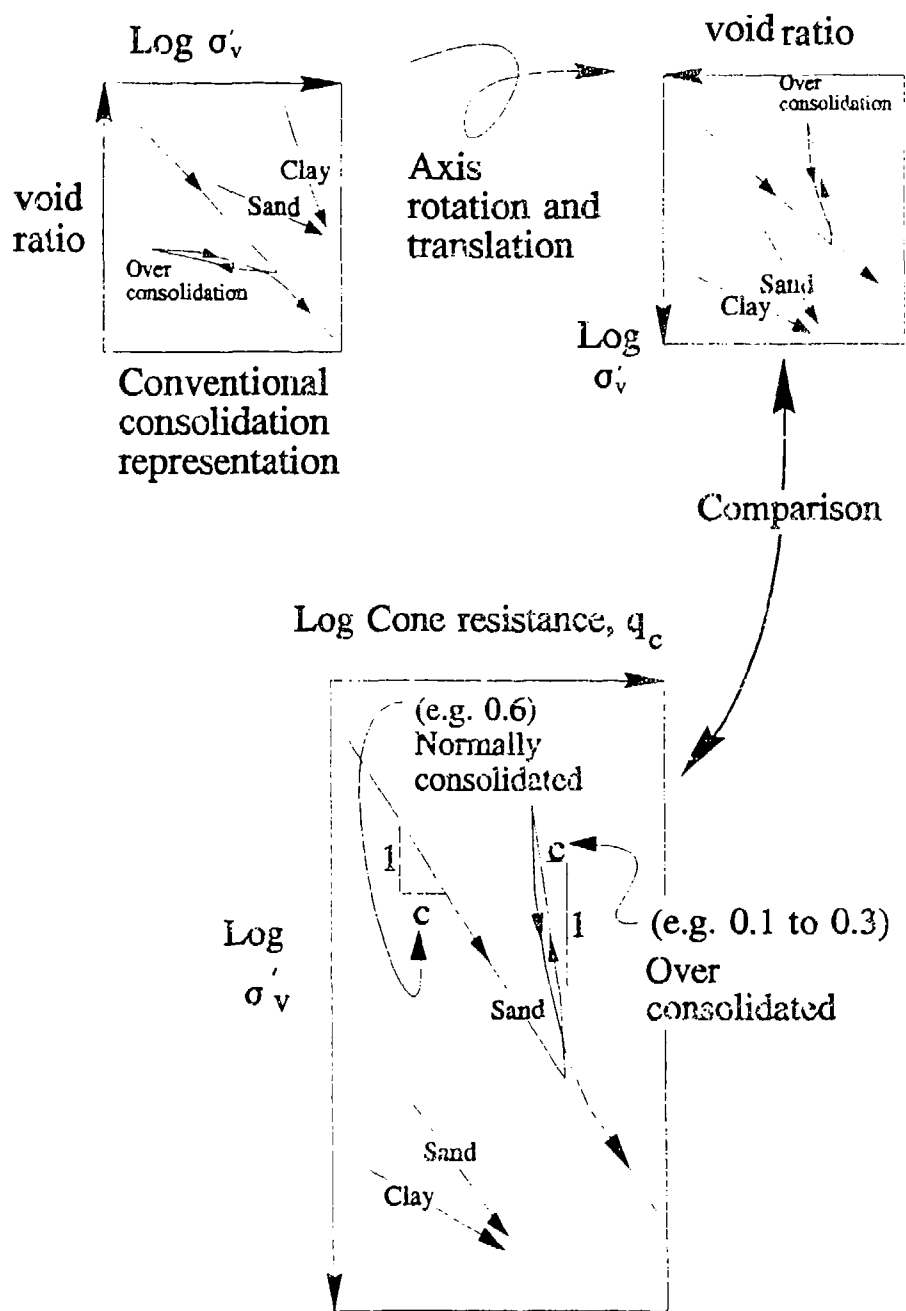


**Figure 5.13** Overconsolidation effects illustrated by comparing the conventional consolidation representation to the observed relationship of cone resistance versus vertical effective stress

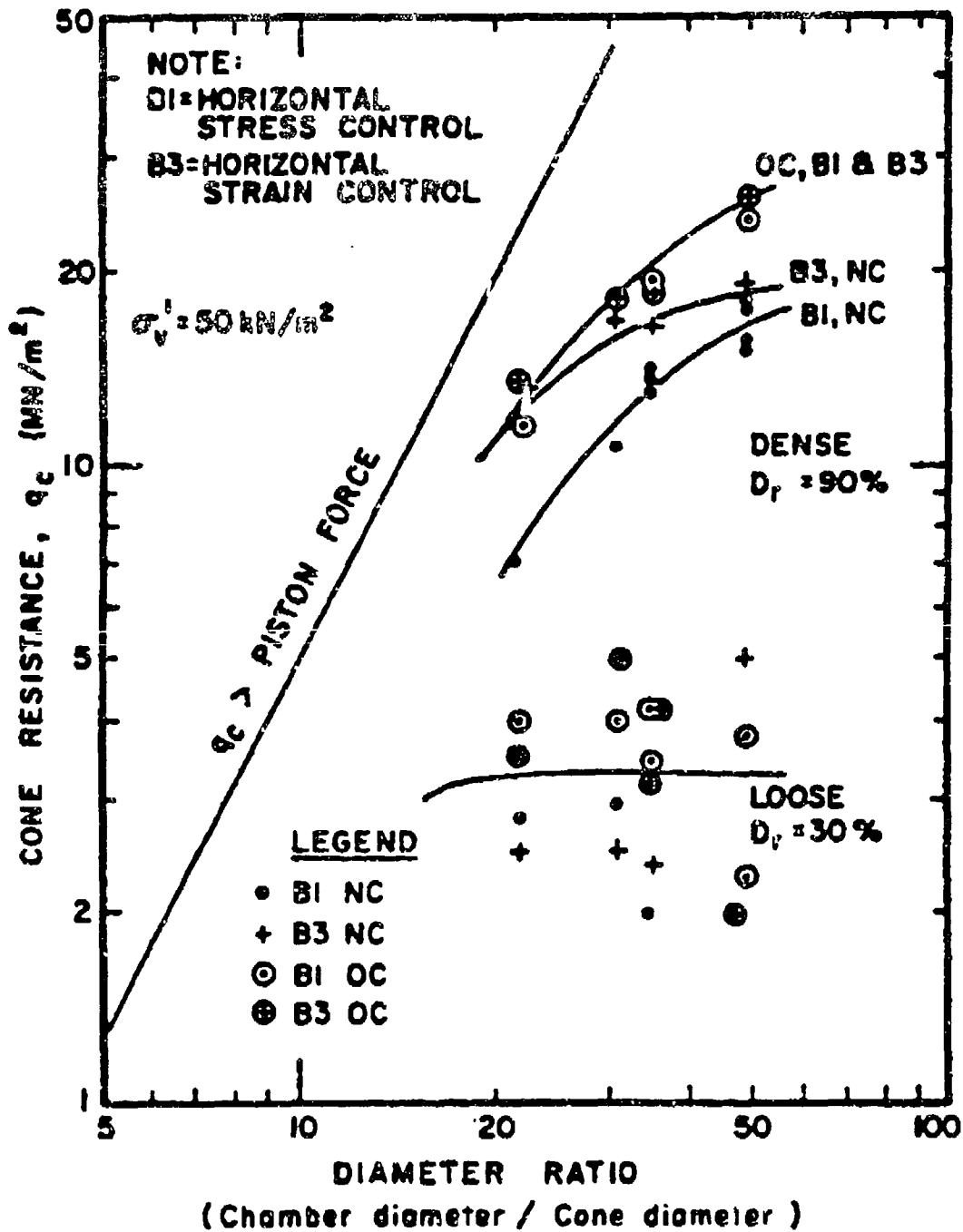
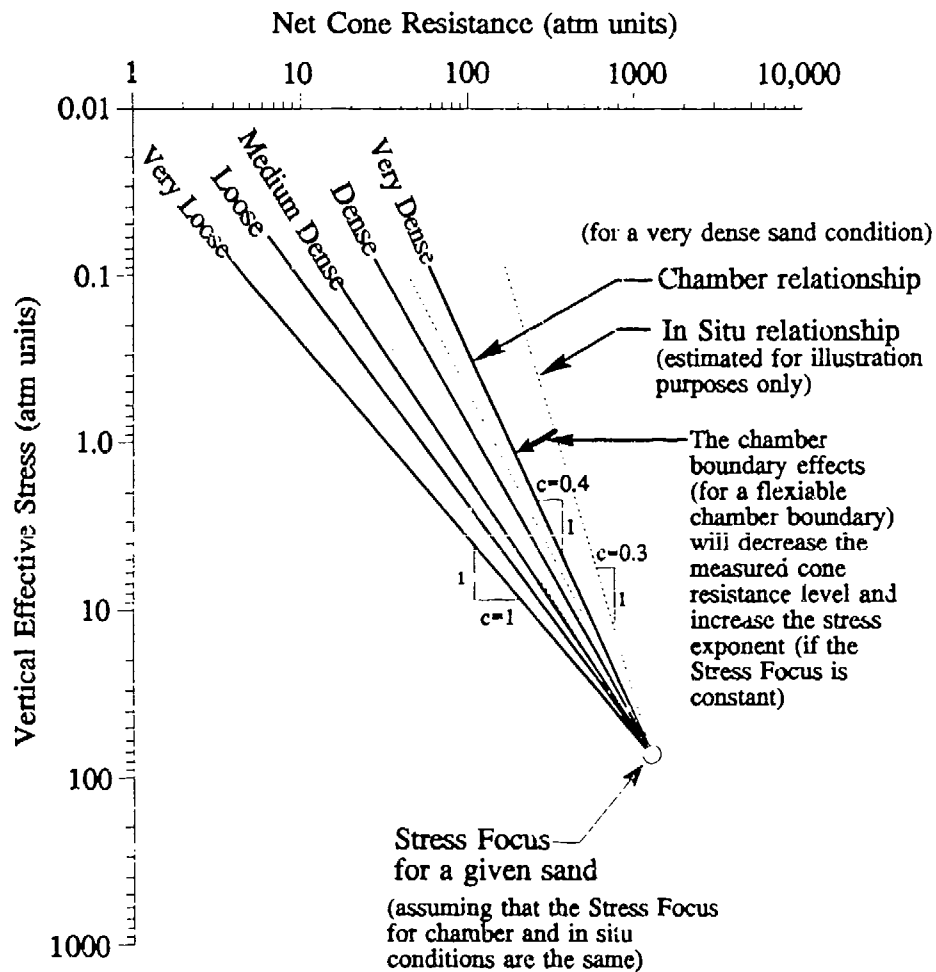


Figure 5.14 Boundary effects on the measured cone resistance level in laboratory chamber test in sand (Parkin and Lunne, 1982)



Stress Focus but different stress exponents. Bulging at the chamber boundary limits the size of the bearing pressure bulb in front of the probe to that developed in a lower relative density sand (i.e. having a higher stress exponent). A sand with an elevated stress exponent is therefore equivalent to a lower relative density sand.

The elevated chamber stress exponent of dense sands in chamber tests can be further illustrated by examining trends of stress exponent versus relative density. Stress exponent versus relative density trends from Figure 5.11 having at least 3 relative density groups were replotted in Figure 5.16. The elevated chamber stress exponents for dense sand are shown by the vertical arrows. This approximated correlation of stress exponent to relative density is more linear than the relationship derived from chamber results.



**Figure 5.15** The reduced cone resistance for dense sands due to "chamber size effects" can be represented with higher stress exponents because all relative densities appear to have a common Stress Focus.

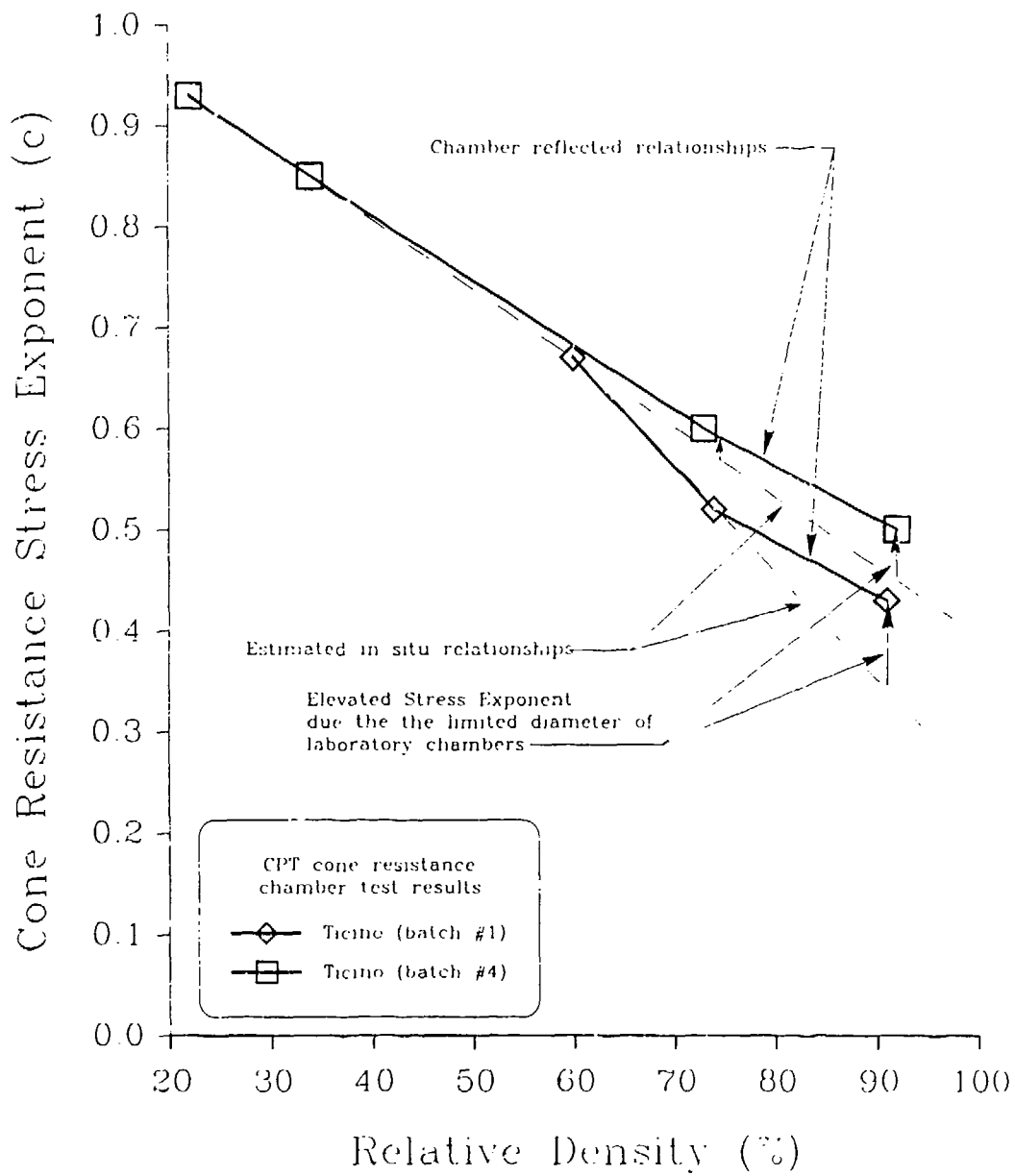


**Figure 5.16** Possible modification of the chamber based stress exponent for dense and very dense sands

## SPT Chamber Evaluation

This section will evaluate SPT chamber test data on sand to show that the Stress Focus location is soil type dependent. These SPT chamber data consisted of tests in 4 well documented sand types and were used to study sand type effects on location of the Stress Focus. Data from SPT Chamber tests were therefore examined for two purposes; 1) to show that SPT data can be expressed with stress exponents and the Stress Focus, and 2) to show that sand composition affects the Stress Focus location. If the Stress Focus is a genuine geotechnical property then SPT chamber tests results should also reflect it.

The Standard Penetration Test (SPT) blow count is defined as the number of blows required to advance a split-spoon SPT soil sampler one foot into the bottom of a borehole using a standardized hammer. The SPT sampler is resisted during penetration by both static and dynamic end bearing and side forces on the sampler (Schmertmann, 1979a, 1979b, Douglas, Olsen, and Martin, 1981, Olsen 1988).

A comprehensive laboratory study of the SPT was performed using large diameter chamber tests at the U.S. Army Waterways Experiment Station (WES) in the mid 1970's by Bieganousky and Marcuson (1976, 1977). SPT chamber tests were performed in a 4-foot diameter chamber very similar in concept to the large diameter chambers used for CPT testing. For an SPT chamber test, a sand specimen is prepared, confining stress applied, a borehole drilled into the sand using rotary wash techniques (and drilling mud), and finally the SPT sampler is driven into the sand beginning at the bottom of the mud-filled borehole. SPT sampler blow counts were obtained from different chamber depths, along the center of the chamber as well as radially out from the chamber center. Only the center test values were used for the current evaluation.

## *SPT Chamber Data Plotting*

The procedures for evaluating WES SPT chamber data are the same as used for CPT cone resistance data in the last section. For Reid Bedford sand, trends related to individual relative density groups are shown in Figure 5.17 to Figure 5.19; all relative density data and trends are combined in Figure 5.20. For Standard Concrete sand, all relative density group trends are shown in Figure 5.21, for Platte River sand, all of the relative density groups trends are shown in Figure 5.22, and finally for Ottawa sand, only one relative density group is available as shown in Figure 5.23 (all data from Bieganousky and Macneason, 1976, 1977). The correlations by Gibbs and Holtz (1957) are shown in Figure 5.24 for comparison.

## *SPT Stress Focus and Sand Type*

The SPT Stress Focus information from the preceding figures are summarized in Figure 5.25 together with trends of mean grain size and material composition in terms of feldspar percentage. Quartz is the primary material type of these sands with feldspar being the secondary material type—increasing feldspar content may reflect a lower overall sand strength. Compared to quartz, feldspar is softer, has lower compressive strength, and has distinct cleavage. In Figure 5.25, as feldspar content increases, the depth for the Stress Focus increases. A deeper Stress Focus (due to feldspar content increase) has a lower calculated normalized cone resistance at the Stress Focus ( $q_{cfl}$ ) (see page 54 for definition) which means that the friction angle at high confining stress is also lower. Chapter 6 will also show that the cone resistance Stress Focus is soil type dependent and exhibit the same general trend as the sand mean grain size in Figure 5.25.

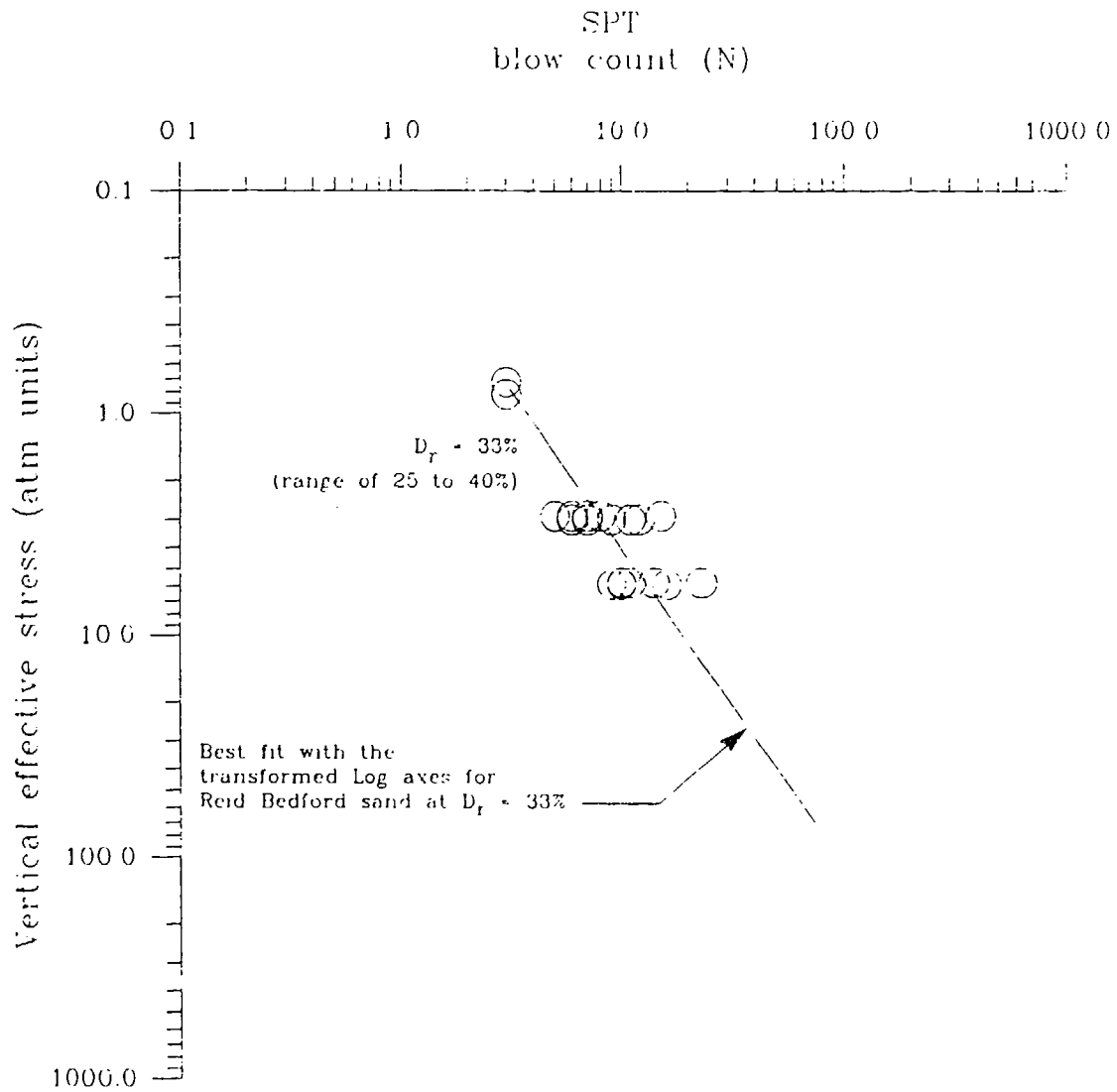


**Figure 5.17** Cone resistance chamber data for a relative density of 33% for Reid Bedford sand

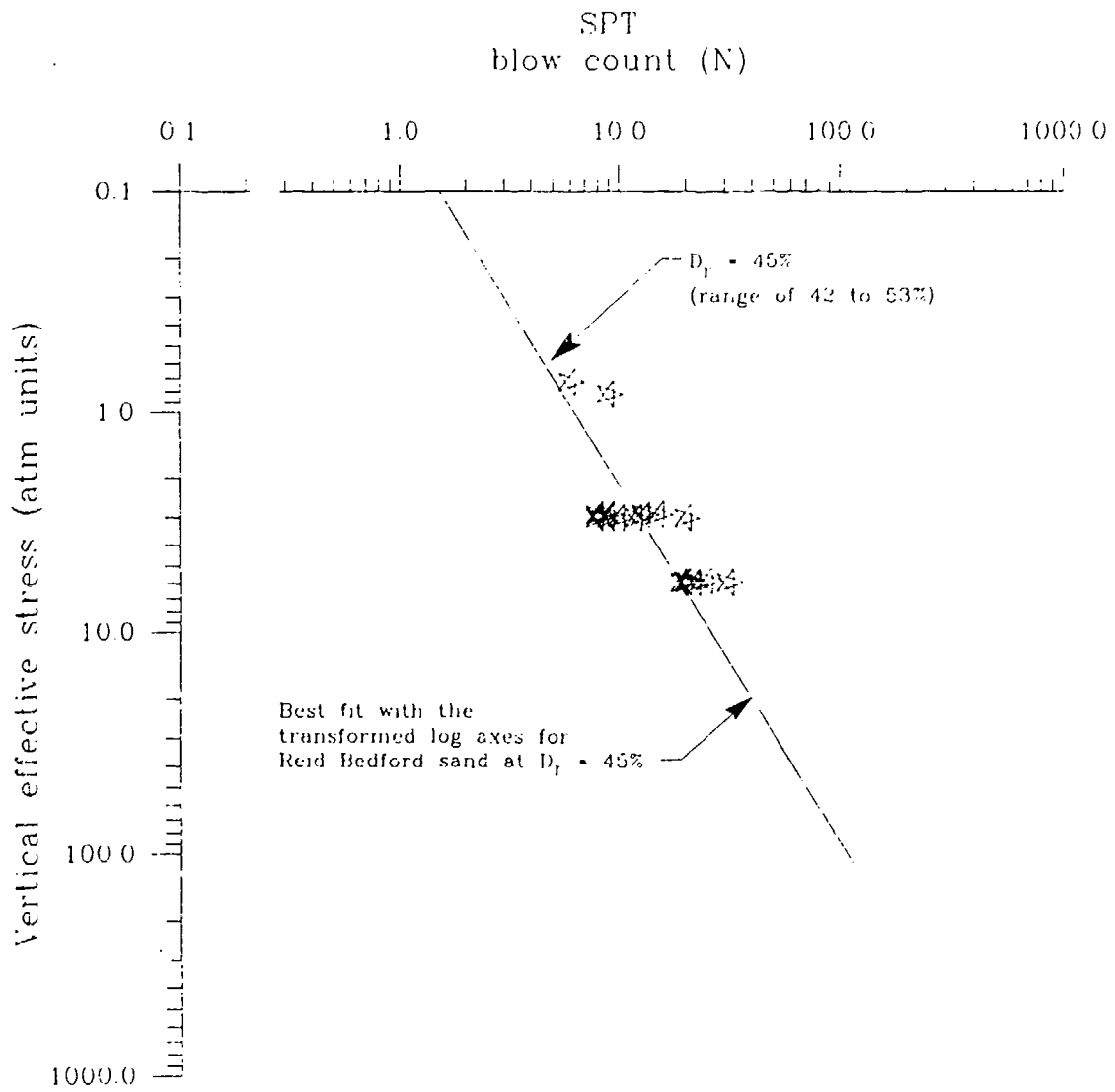


**Figure 5.18** Cone resistance chamber data for a relative density of 45% for Reid Bedford sand

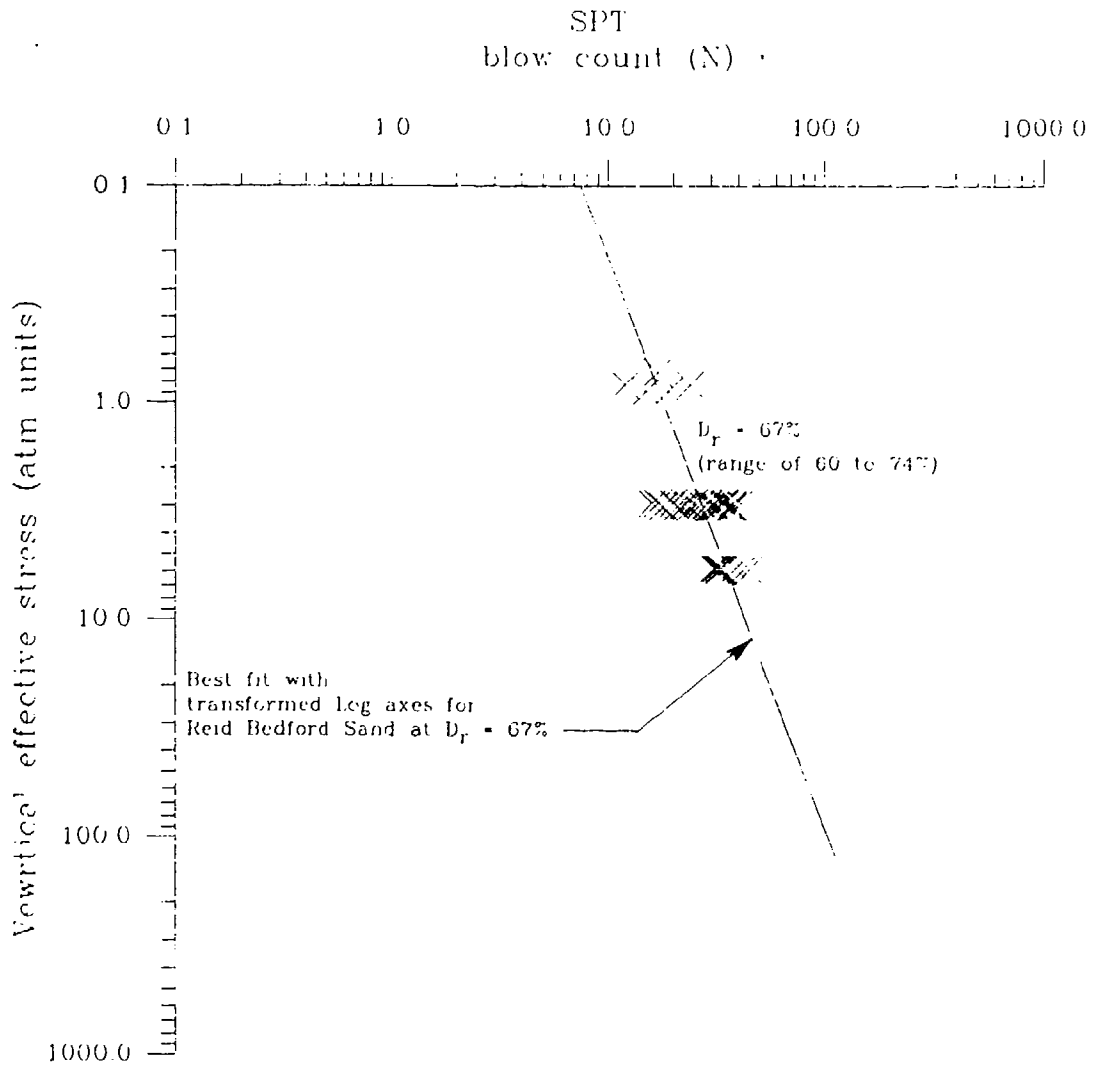


**Figure 5.19** Cone resistance chamber data for a relative density of 67% for Reid Bedford sand



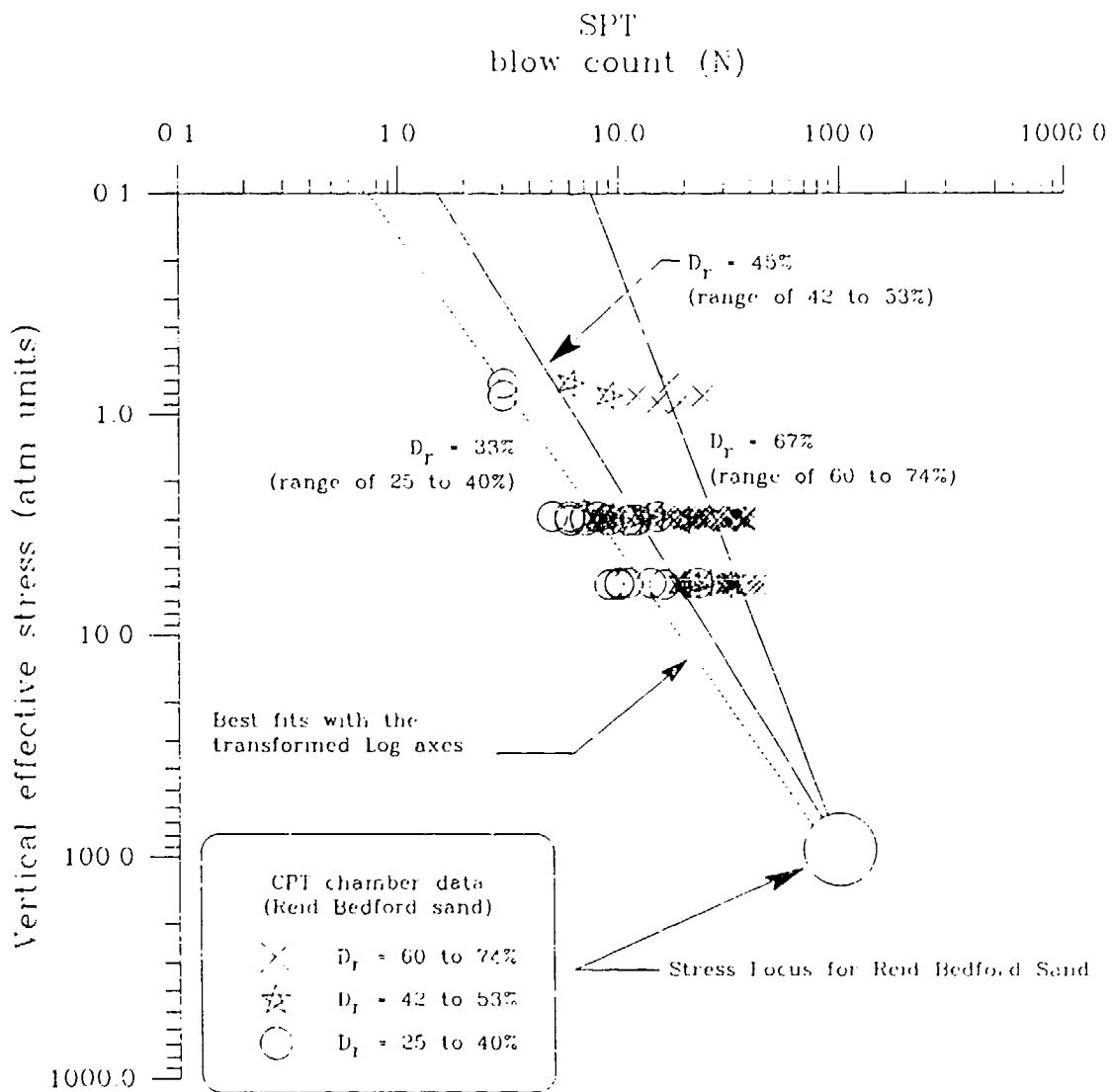


**Figure 5.20** Cone resistance chamber data for all relative densities for Reid Bedford sand together with the Stress Focus

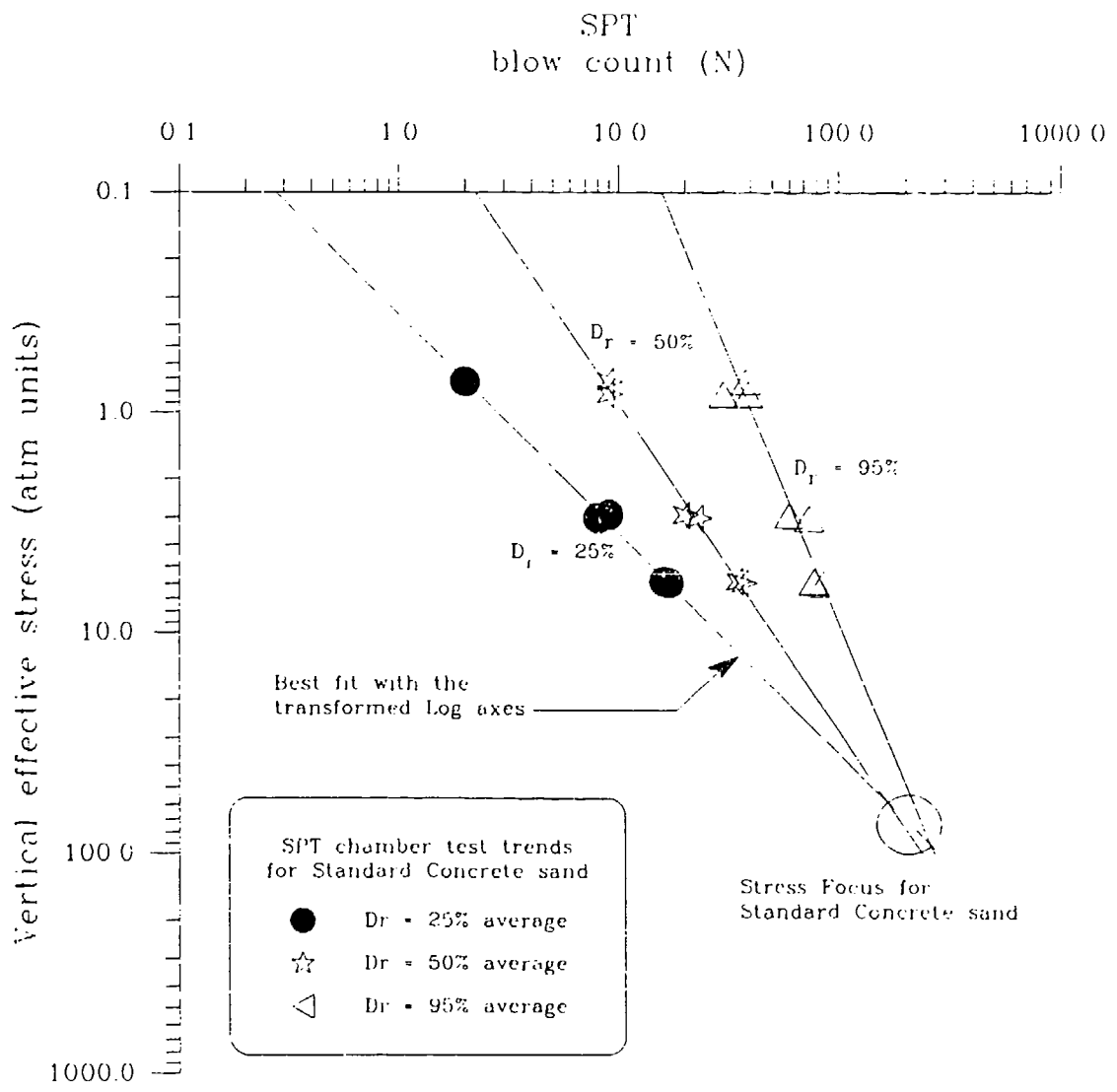


**Figure 5.21** Cone resistance chamber data for Standard Concrete sand together with the corresponding Stress Focus

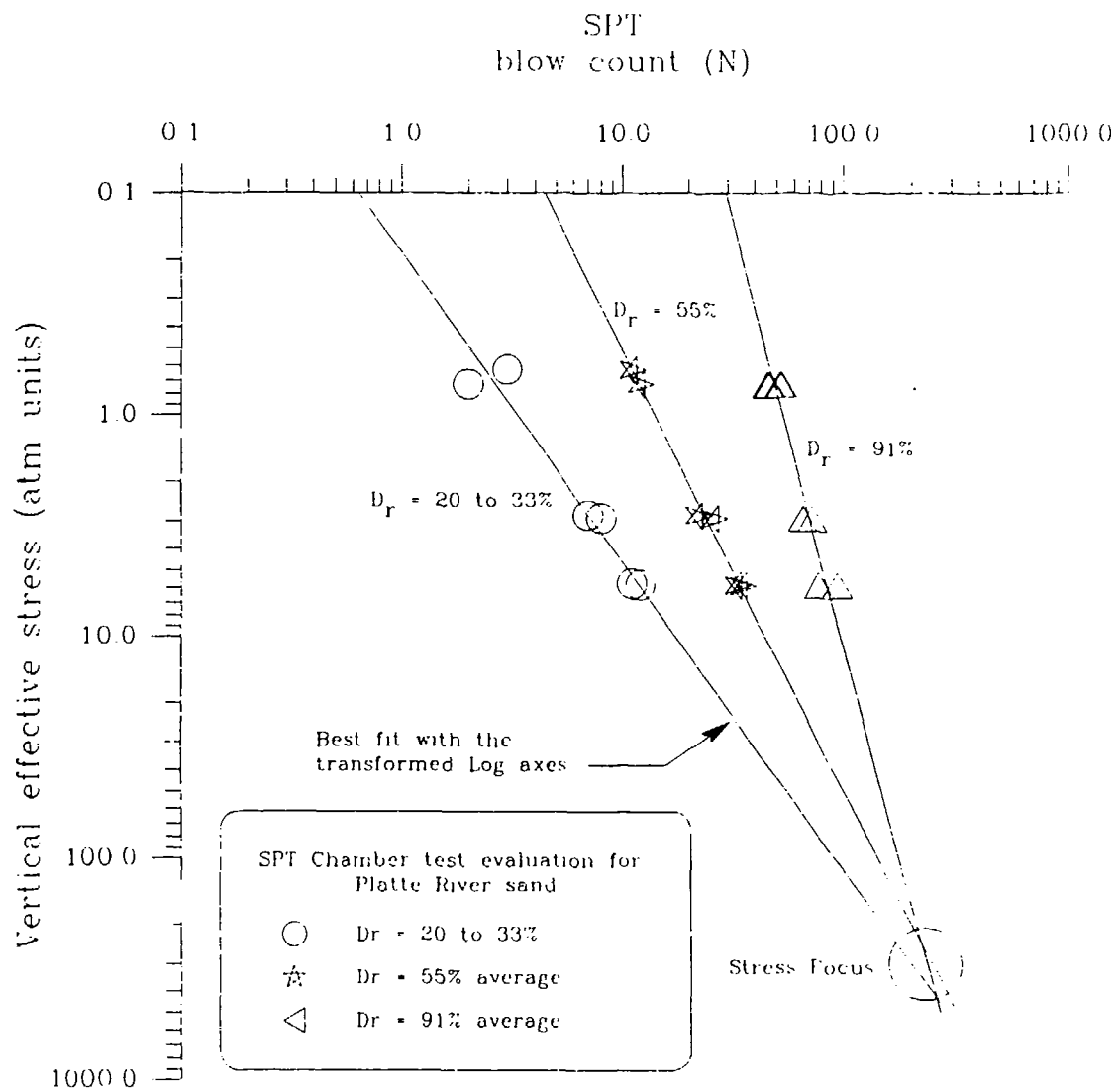


**Figure 5.22** Cone resistance chamber data for Platte River sand together with the corresponding Stress Focus

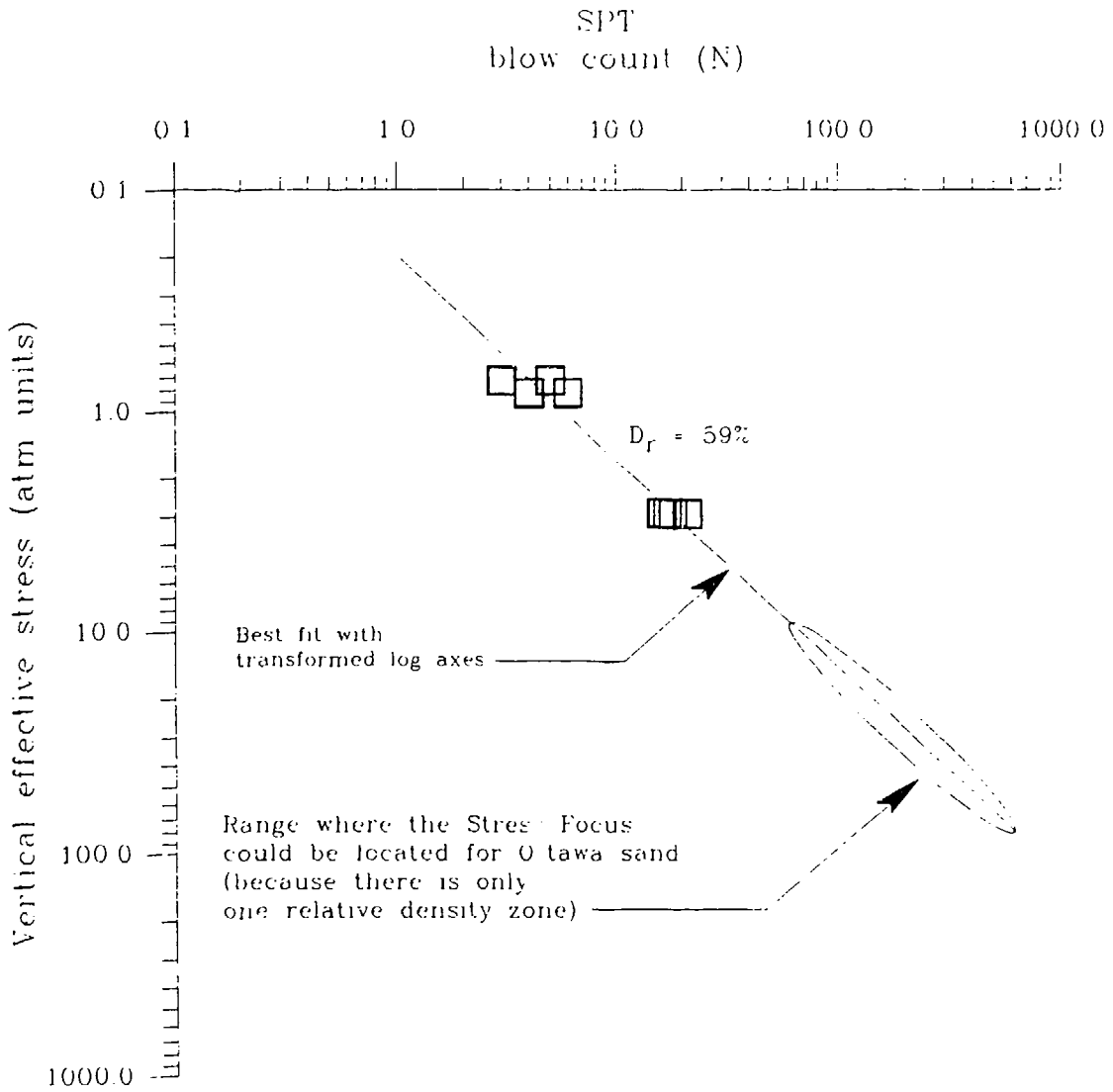


**Figure 5.23** Cone resistance chamber data for one relative density range of Ottawa sand

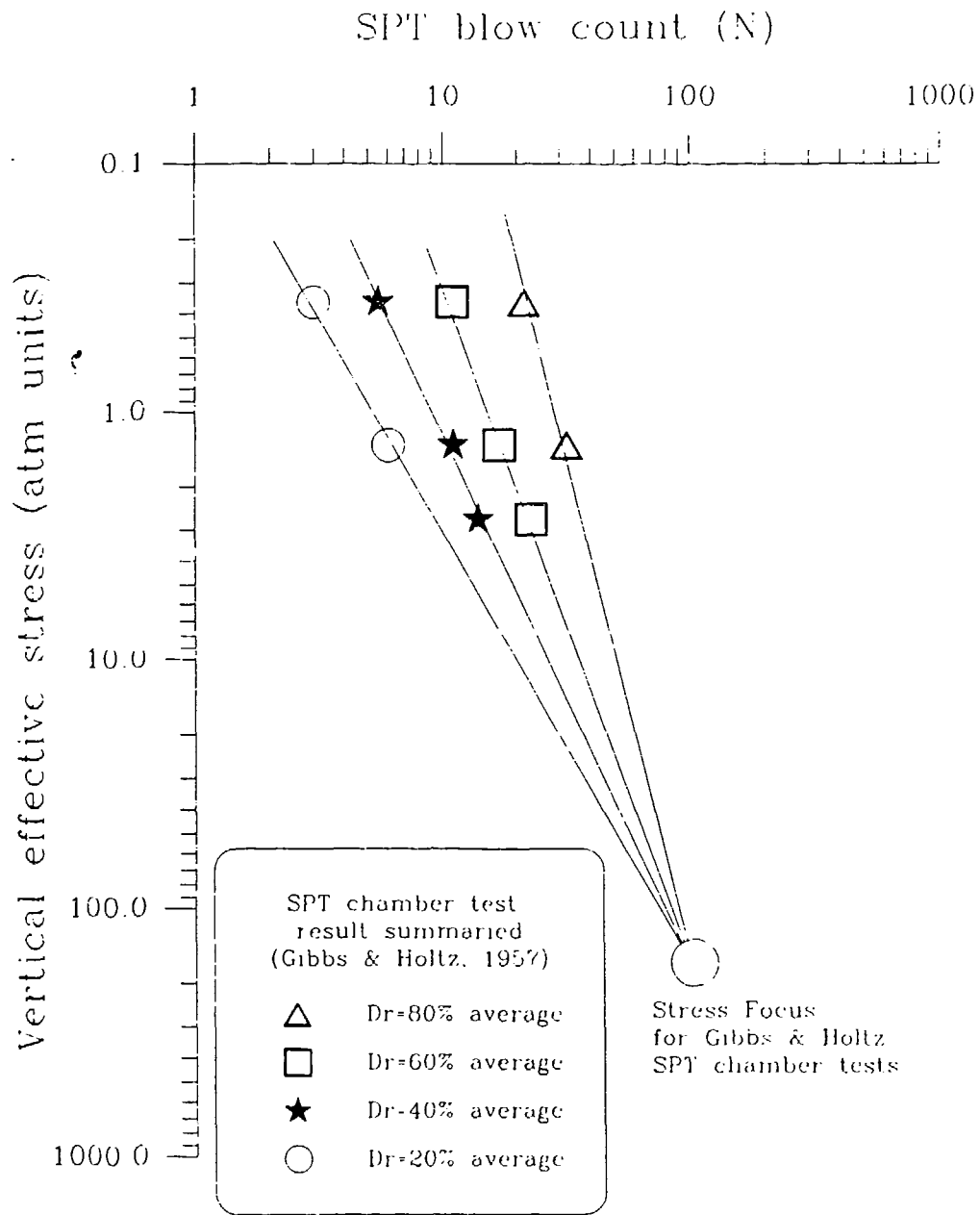


**Figure 5.24** Cone resistance chamber data trends for Gibbs & Holtz data

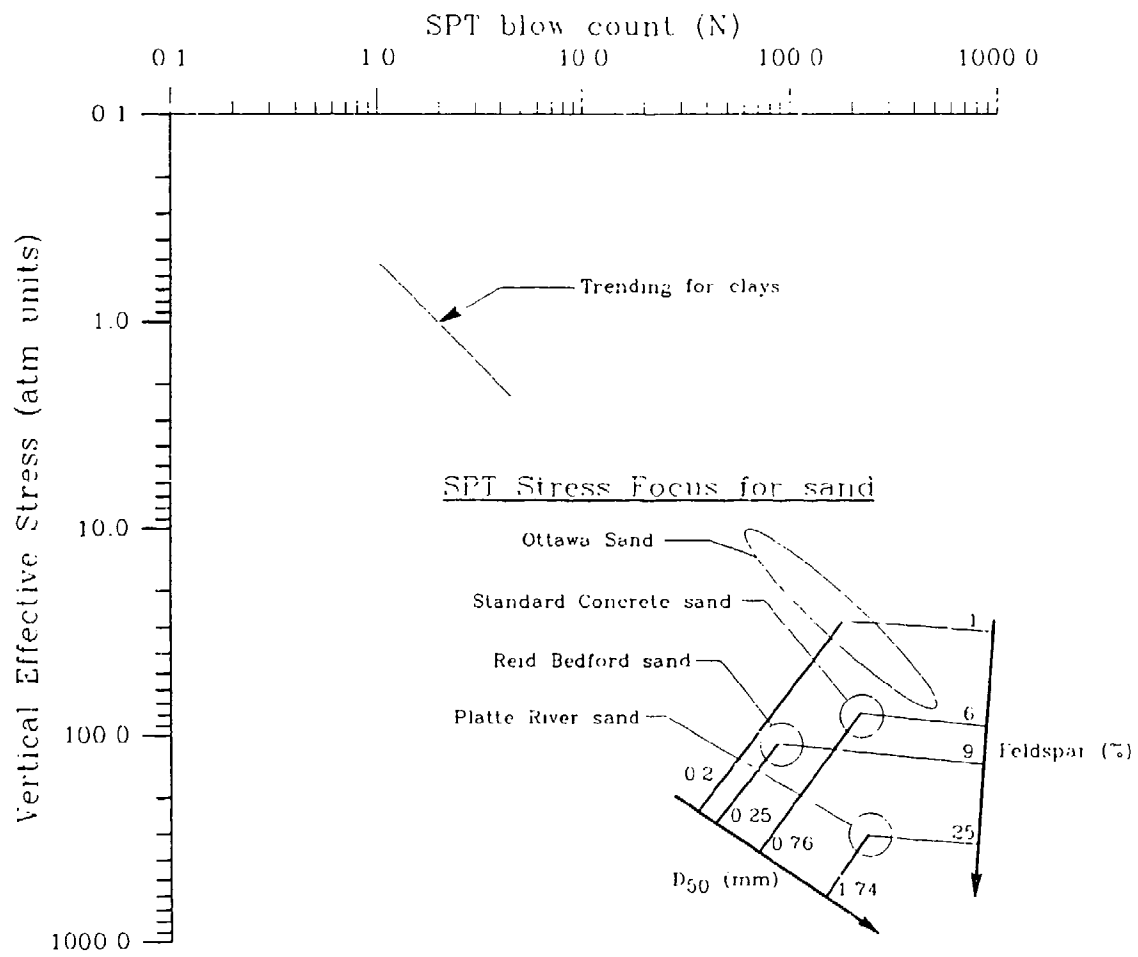


**Figure 5.25** Comparison of SPT Stress Focus locations for different sands to the resulting trends of Feldspar percentage and  $D_{50}$

## *Chamber Test Stress Exponent Discussion*

The SPT stress exponents calculated for data at each relative density (from the proceeding figures on SPT chamber test evaluation) are summarized in Figure 5.26. These SPT stress exponents confirm the general trends based on normalized SPT stress exponent presented by Seed et al. (1981) that are also shown in this figure. However, it is shown in Chapter 7 that the SPT stress exponent should be higher because of mud pressure effects associated with SPT chamber testing.

The stress exponents developed from SPT and CPT chamber evaluations are shown in Figure 5.27 and indicate a difference of approximately 0.18. This figure will also be referenced in Chapter 6 during the introduction of the new SPT normalization technique.

It is also important to note that the distribution of SPT stress exponent for a given relative density in Figure 5.26 may not be due entirely to data scatter. The stress exponent can be related to sand type composition as shown in Figure 5.28 of which is plotted in terms of feldspar content at a relative density of 36% (likely a contractive condition). As previously stated on page 77 and shown in Figure 5.25, increasing feldspar content increases the Stress Focus vertical effective stress. Increasing feldspar content also appears decrease the stress exponent as shown in Figure 5.28. Therefore, conceptually, the combined effects of increasing vertical effective stress and decreasing stress exponent can be illustrated in Figure 5.29. The Stress Focus location and stress exponents therefore appear to be interrelated.

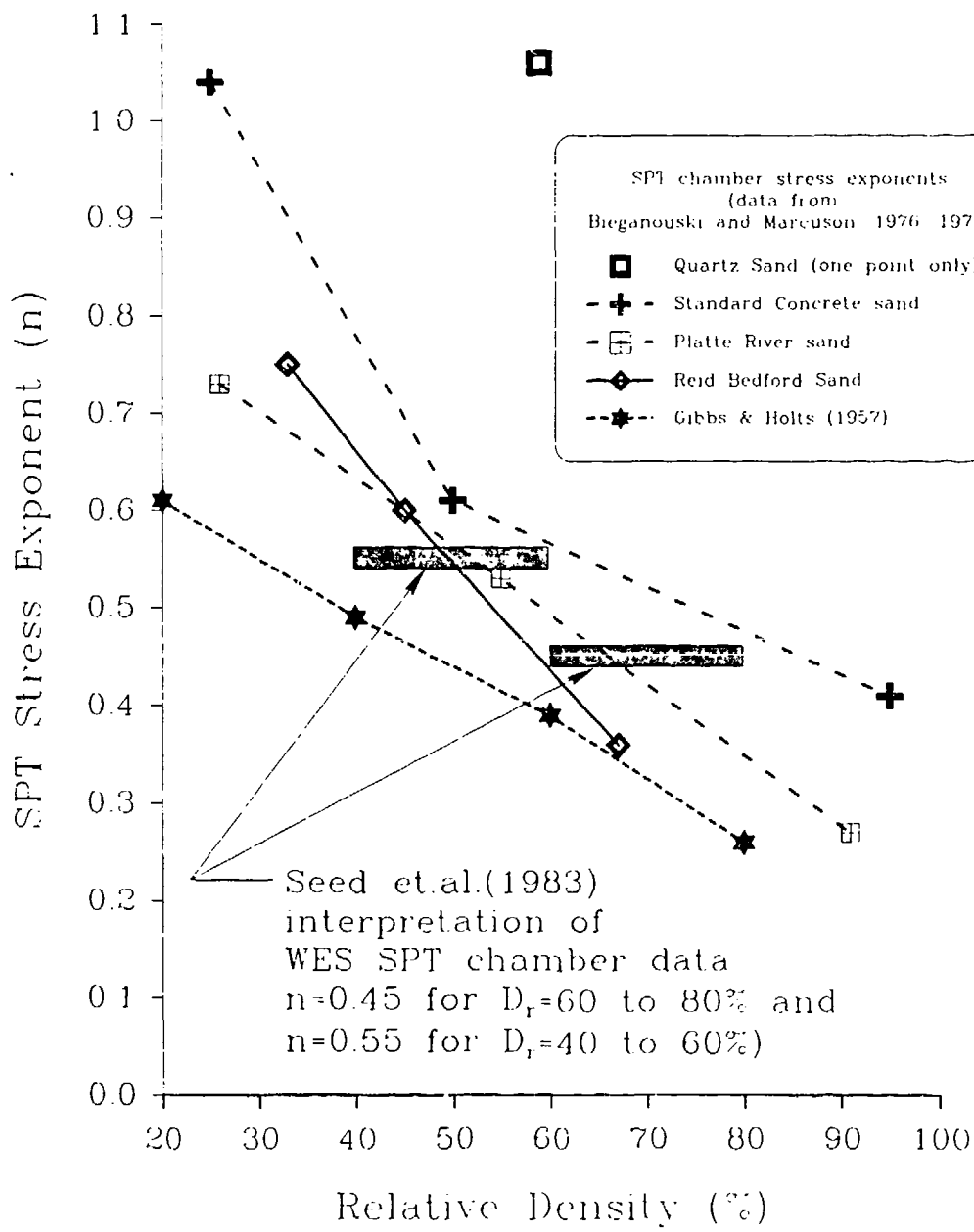


**Figure 5.26** Relationship between relative density and SPT stress exponent for different sands from SPT chamber tests



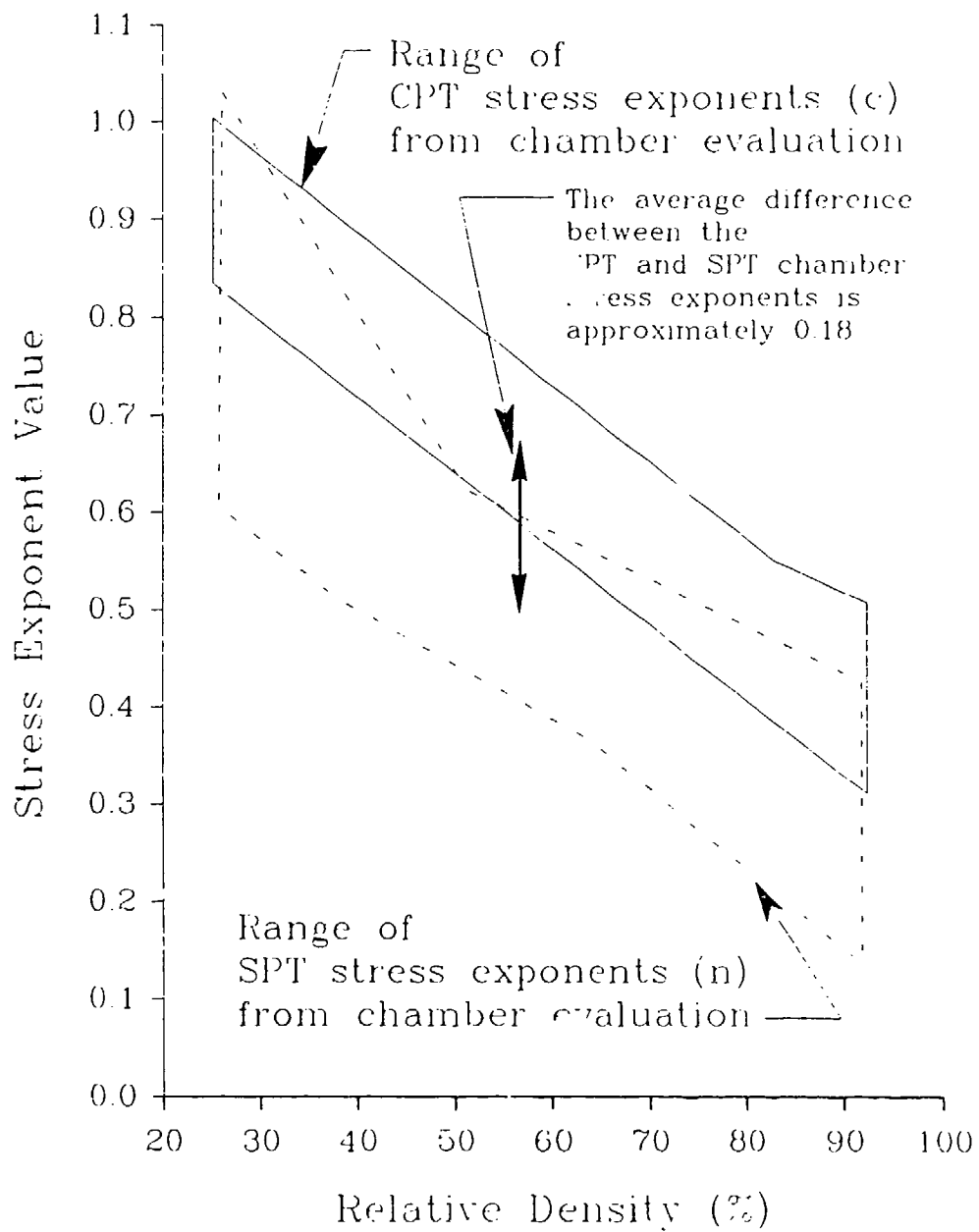


**Figure 5.27** Comparison of the ranges for CPT and SPT stress exponents from evaluation of chamber data

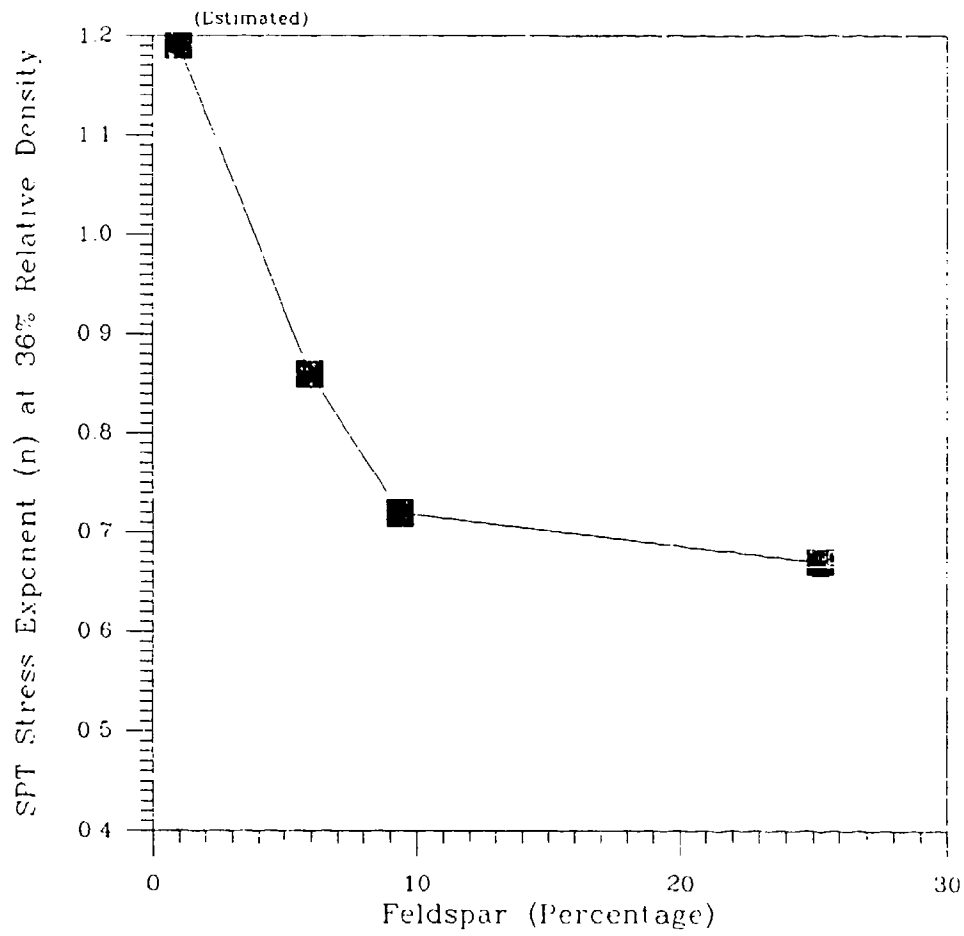


**Figure 5.28** Relationship between SPT stress exponent and Feldspar percentage at a relative density of 36% for chamber tests

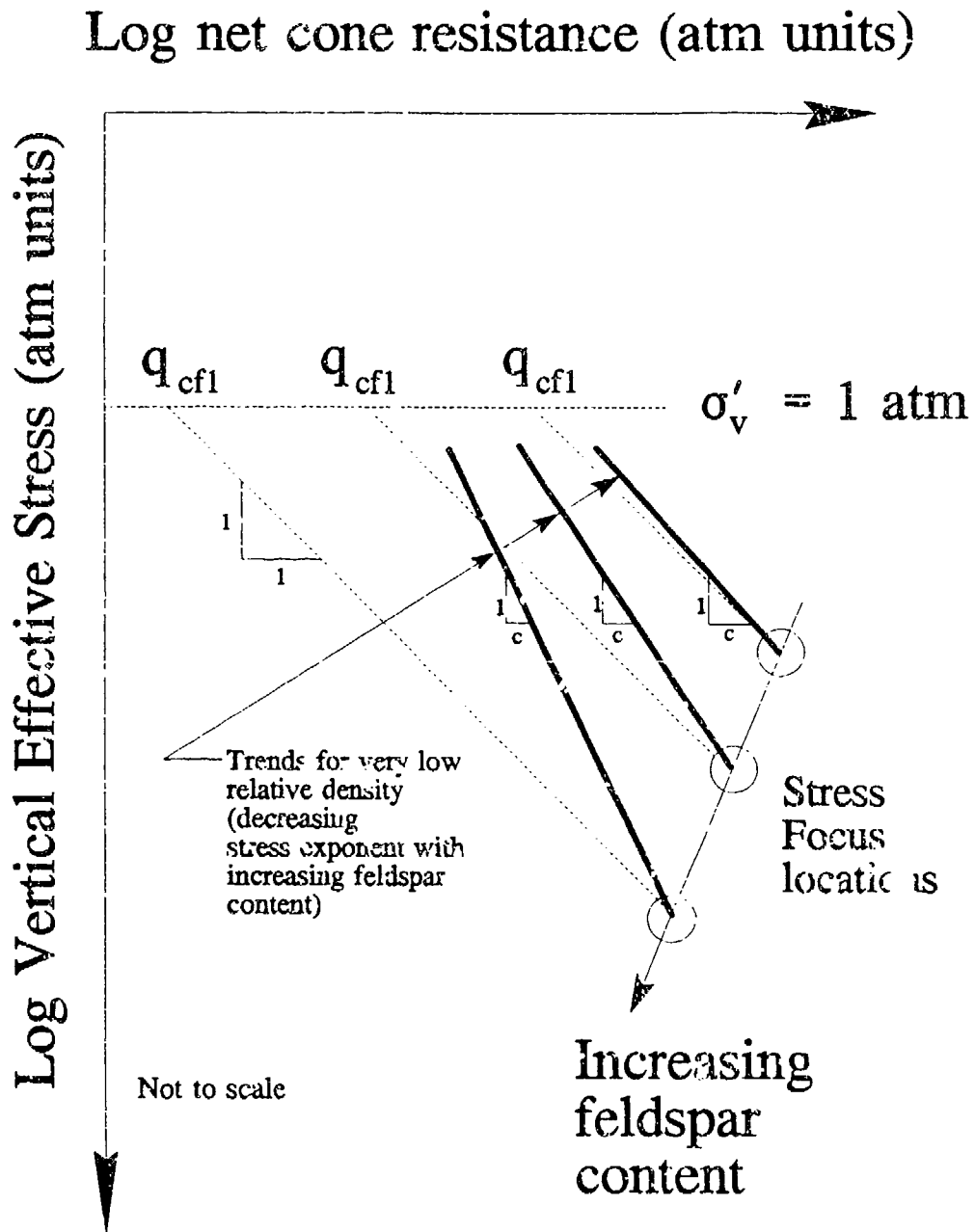


**Figure 5.29** Interrelation of the Stress Focus and the stress exponent (for a very loose sand condition) based on evaluation of CPT cone resistance chamber data for increasing feldspar content

## Conclusion

The CPT cone resistance can be represented with the Stress Focus concept. The cone resistance versus confining stress relationship for different relative densities will converge with increasing vertical effective stress to a Stress Focus that is dependent on sand type. This sand type dependent Stress Focus location appears to be based on gradation effects and material composition. The Stress Focus location appears to occur at a overburden stress ranging from 70 to 300 Atm. Dense sands have the lowest stress exponent and loose sands have a stress exponent of approximately one.

# Chapter 6

## CPT Prediction of CPT Normalization Parameters— Developed using Uniform Soil Layer Data

### Introduction

Stress normalization provides the means to account for confining stress influence on in situ measurements and geotechnical properties. However, to be useful the stress normalization parameters must be predictable using the field CPT measurements without auxiliary information. Data from CPT tests in uniform soil layers can be used to establish correlations for prediction of the CPT cone resistance stress exponent. Specifically, field CPT data from tests in uniform soil layers can be used for several purposes: to show that the Stress Focus exists, the Stress Focus location (i.e. equivalent overburden stress and cone resistance) is dependent on soil type, the cone resistance stress exponent can be estimated using field CPT data, and to prove that the CPT soil characterization chart concepts are valid.

## Limitations and Merits of Using In Situ Data for Stress Normalization

Evaluation of uniform soil layers is more difficult than evaluation of chamber test data. The main difference between in situ uniform layer CPT data and chamber test data is that in situ data can represent all soil types, whereas, to date chamber data can only represent clean sands (and in some cases sand with fines) of low to medium relative density. On the other hand, the initial relative density and confining stress levels can accurately be varied in chamber test programs. The principal merit of in situ uniform soil layer data is that it can represent the full spectrum of soil types and thus that it can be used to determine the Stress Foci for all soil types. However, when a very uniform soil layer is found, it represents only one relative strength level; e.g. a sand with a 70% relative density or a clay with an undrained normally consolidated strength ratio ( $c/p$ ) of 0.32.

A single uniform soil layer has a constant trend of log net cone resistance versus  $\log \sigma'_v$  that can be represented with a constant exponent slope. To establish the Stress Focus for a single soil type requires numerous uniform layers of varying relative strength consistency levels. A database representing uniform soil layers must therefore be large enough for the purpose of establishing the Stress Focus for numerous soil types.

## Establishing In Situ Uniform Layer Trends

A uniform soil layer is defined as a constant soil type at a constant initial relative strength (e.g. friction angle for sand or  $\frac{c}{p}$  for clay). A plot of  $\text{Log}(q_c)_{\text{net}}$  versus  $\text{Log}(\sigma'_v)$  (and  $\text{Log}(f_s)$  versus  $\text{Log}(\sigma'_v)$ ) will follow a straight path over the uniform soil layer interval as illustrated in Figure 6.1. These net cone resistance relationships can be projected to the normalizing stress of  $\sigma'_v = 1$  atm to determine the normalized cone resistance,  $q_{c1c}$ . The log-log slope is the cone resistance stress exponent ( $c$ ). Soil samples are not required for this technique, although proper soil classification is useful for indexing purposes.

Logarithmic plotting emphasizes the lower stresses, therefore special care was exercised while identifying uniform soil layers—For example, a depth interval of 3 to 8 ft has approximately the same  $\text{log}(\sigma'_v)$  differential (i.e. 0.3) as the depth range from 30 to 60 ft. Shallow uniform soil depth zones are artificially emphasized. It would be easy to use a simple  $\Delta \text{log}_{10}(\sigma'_v)$  criterion such as 0.2 to represent a minimum uniform depth zone. However, it was important to examine deep layers for small  $\Delta \text{Log}_{10}(\sigma'_v)$ , such as 0.08, that could represent a uniform 12 foot layer at  $\sigma'_v = 2$  atm.

Approximately 600 field CPT soundings were examined for depth zones having a constant relative strength. This was accomplished by plotting all CPT soundings using the  $\text{Log}_{10}(\text{net } q_c)$  versus  $\text{Log}_{10}(\sigma'_v)$  and then examining the traces for any

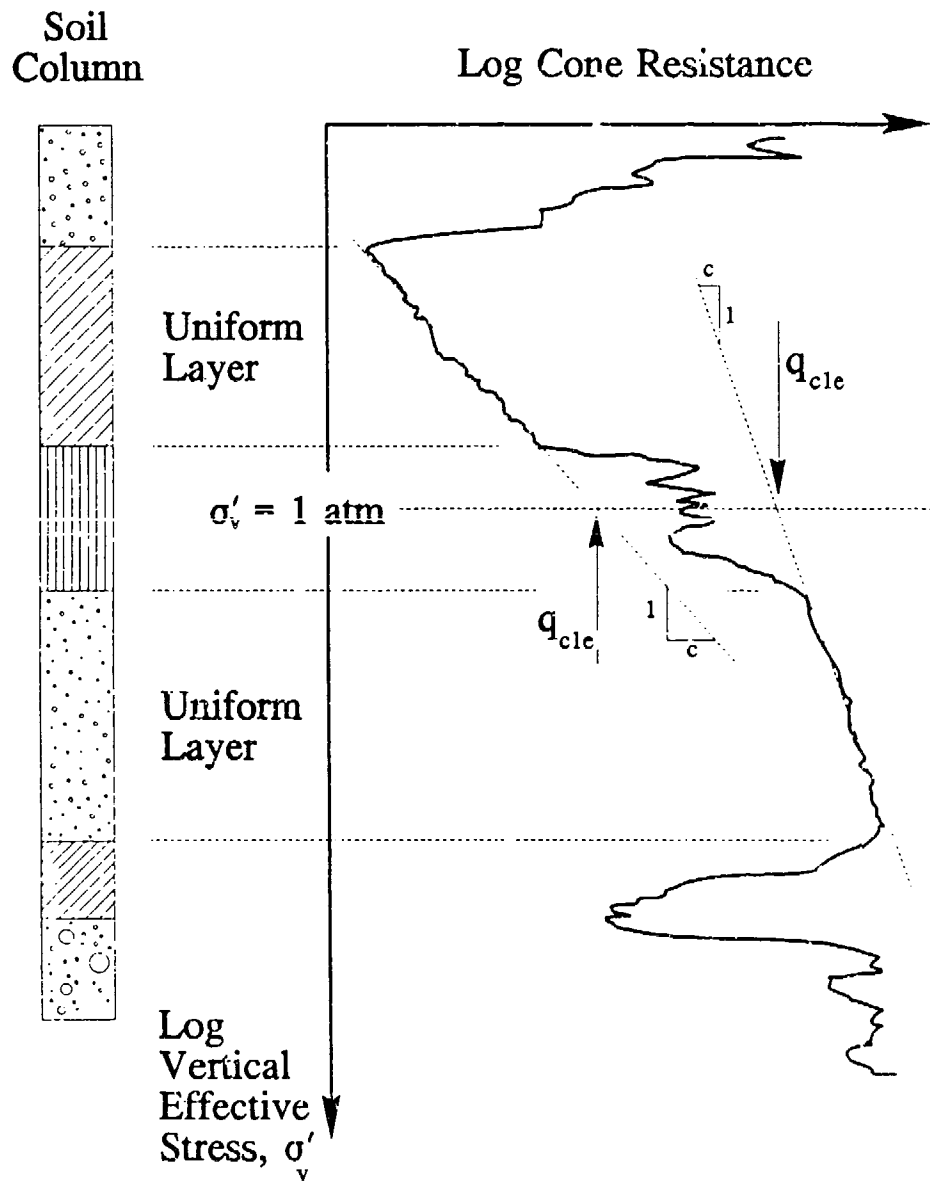


**Figure 6.1** Determining the cone resistance normalization value ( $q_{cle}$ ) and corresponding stress exponent ( $c$ ) using uniform soil layers



depth zone having constant slope (indicating a uniform relative strength level). Identifying uniform soil layers using CPT data was a developed skill that improved as more data was evaluated. Only 78 uniform soil layers were extractable from the 600 CPT soundings. An example of a uniform soil layer is shown in Figure 6.2 with the soil layer limits and normalized parameters shown by computer-plotted lines based on the data from the database. For each uniform soil layer, the following information was extracted;

- 1) normalized cone resistance,  $q_{c1e}$  (e.g. equivalent  $(q_c)_{net}$  at  $\sigma'_v = 1$  atm)
- 2)  $q_c$  log-log stress exponent (c)
- 3) Normalized sleeve friction resistance,  $f_{s1e}$   
(e.g. the equivalent  $f_s$  at  $\sigma'_v = 1$  atm)
- 4)  $f_s$  log-log stress exponent (s)
- 5) Calculated normalized friction ratio,  $R_{r1e}$ , based on  $f_{s1e}$  and  $q_{c1e}$
- 6) Soil type if there is a nearby boring or the deposit type if known
- 7) The Academic Quality Index (AQI) which is based on soil layer uniformity potential and quality of the cone and sleeve friction resistance measurements-(see Chapter 8 for description). The AQI is a subjective quality index based on the academic grading scale; 75% is average, 85% is good and 95% is excellent.
- 8) Top and bottom  $\sigma'_v$  limits of the soil layer.

## Establishing Cone Resistance Stress Exponents using the CPT Soil Characterization Chart

The CPT soil characterization chart was used to develop predictive contours for the cone resistance stress exponents using data from uniform soil layers. As illustrated in Figure 6.3, uniform soil layers are identified (Step #1), normalized CPT parameters are calculated (Step #2 & #3), the results are assigned to a point on the

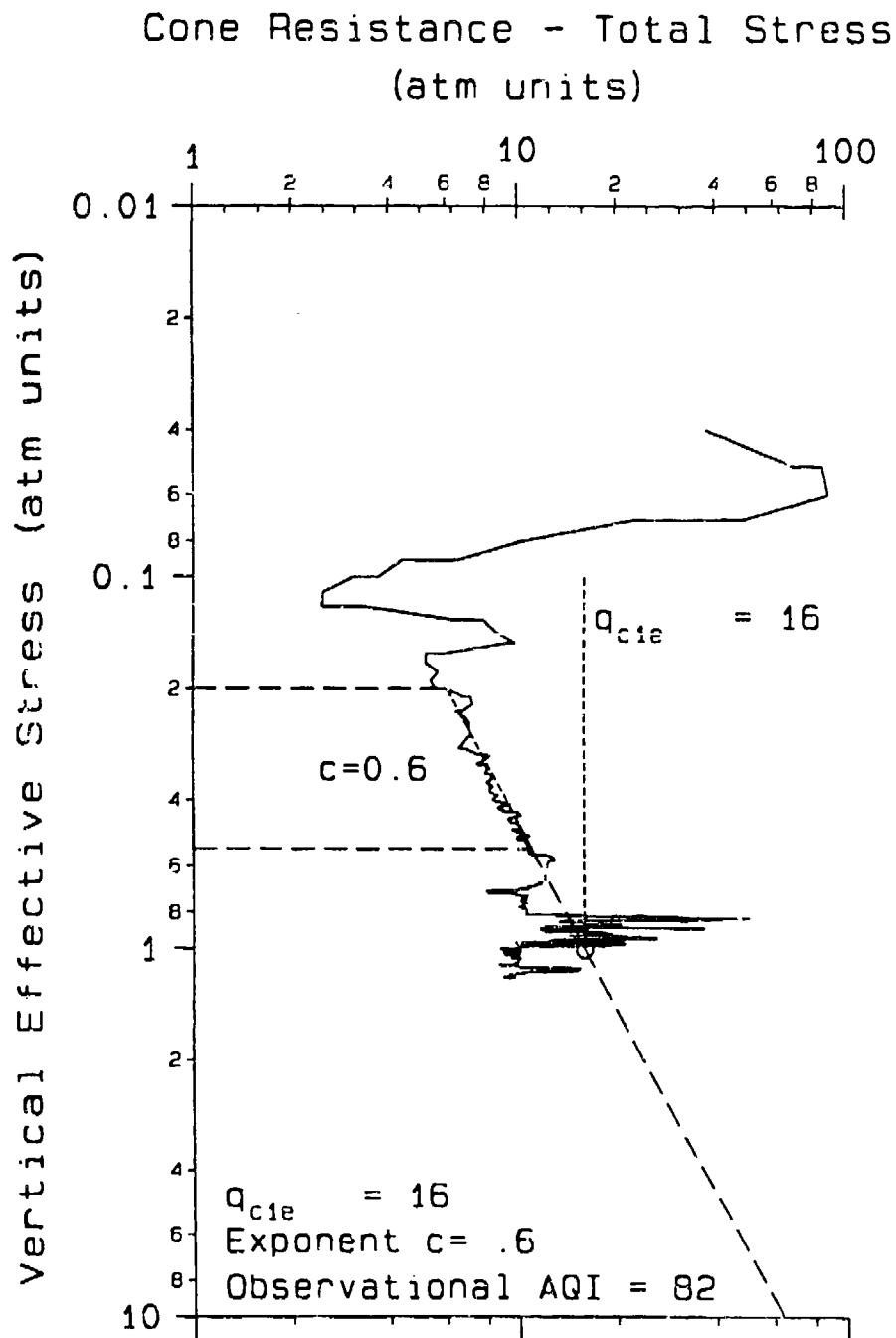


**Figure 6.2** Example of in situ cone resistance data having a uniform soil layer with the stress exponent,  $c$ , and normalized cone resistance,  $q_{c1e}$ , defined

CPT soil characterization chart (Step #4), and the point is assigned the cone resistance stress exponent (c) (Step #5). This point represents one uniform soil layer. Figure 6.4 to Figure 6.13 represent a few interpreted uniform soil layers for different soil types and relative strengths. Also shown at the bottom left corner of each figure is a representation of the CPT soil classification chart (logarithmic 3 cycles by 2 cycles) and the normalized point that represents the uniform soil layer. All available data from uniform soil layers are plotted in Figure 6.14 using the techniques illustrated in Figure 6.3. The estimated contours of cone resistance stress exponent based on the trends of plotted data points are also shown in Figure 6.14.

### *Discussion of Cone Resistance Stress Exponent on the CPT Soil Characterization Chart*

Figure 6.15 is a replot of Figure 6.14 with the soil type of each uniform soil layer data point indicated. Also shown in this figure are CPT soil classification lines from Olsen (1988). The soil classifications of the uniform soil layers approximately match the CPT soil classifications. Figure 6.16 is an annotated version of Figure 6.14 that also describe various soil characterization zones. Note the lack of uniform soil data for soil mixtures and silt in the middle of Figure 6.14; Thick layers of a soil mixture or silt are seldom found in nature because the required deposition dynamics are difficult to maintain over large soil depths.

The contours of cone resistance stress exponent in Figure 6.16 reveal important information about the estimated cone resistance contours. Loose sands typically have low friction ratios (Masood, 1990) because the  $N_q$  bearing factor is low. Loose sands should also exhibit little Mohr envelope curvature and, therefore have a stress exponent very close to one as described in Chapter 2. The stress exponent contour of one approaches the annotated loose sand zone on the CPT soil characterization chart, as expected. Also, normally consolidated clays should have stress exponents



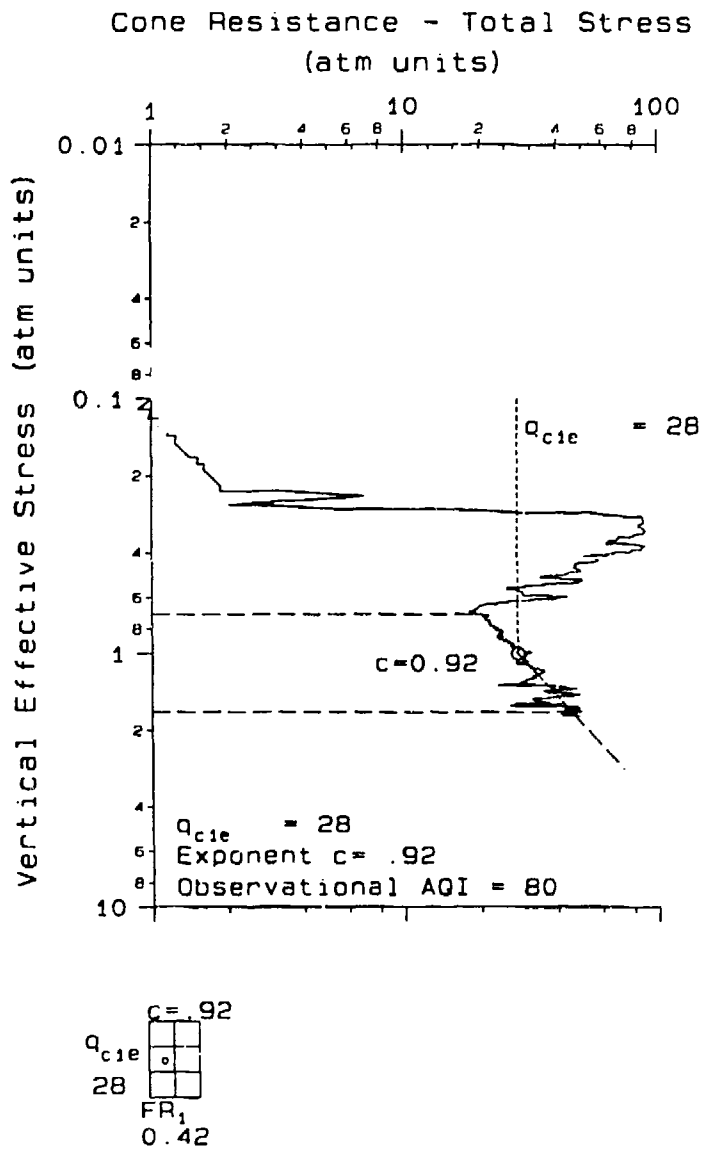


**Figure 6.4** Uniform sand layer at the Holmen, Norway (NGI research site)

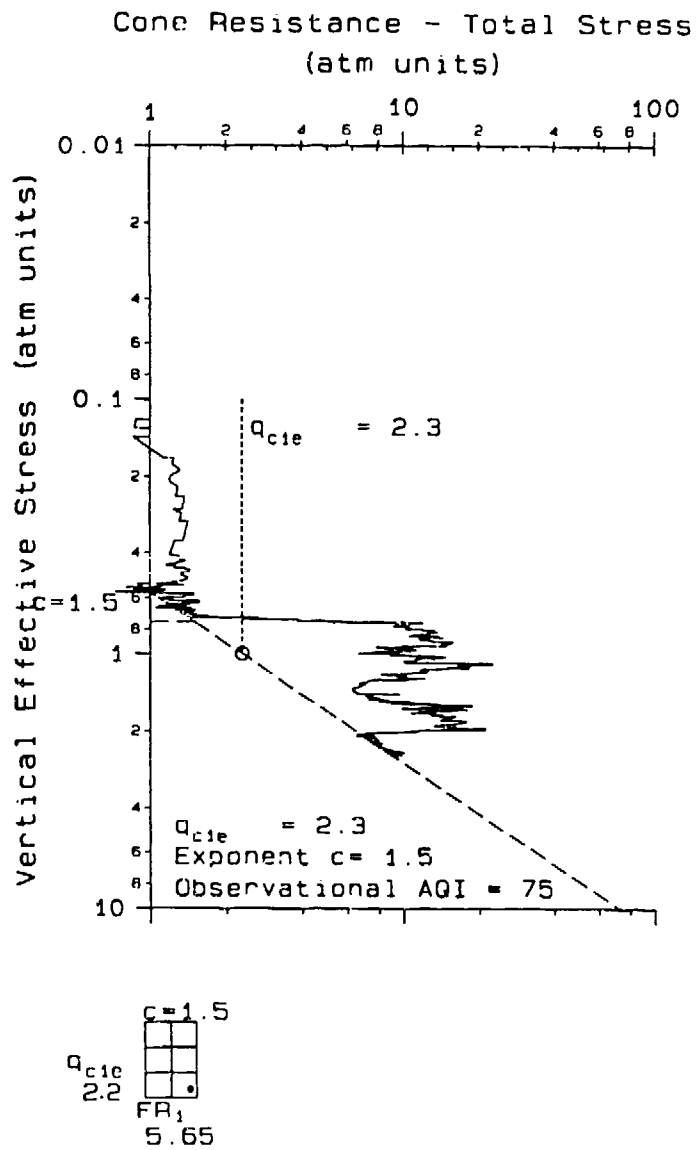


**Figure 6.5** Uniform unstable silty clay layers for a Hong Kong Bay deposit (airport replacement project)

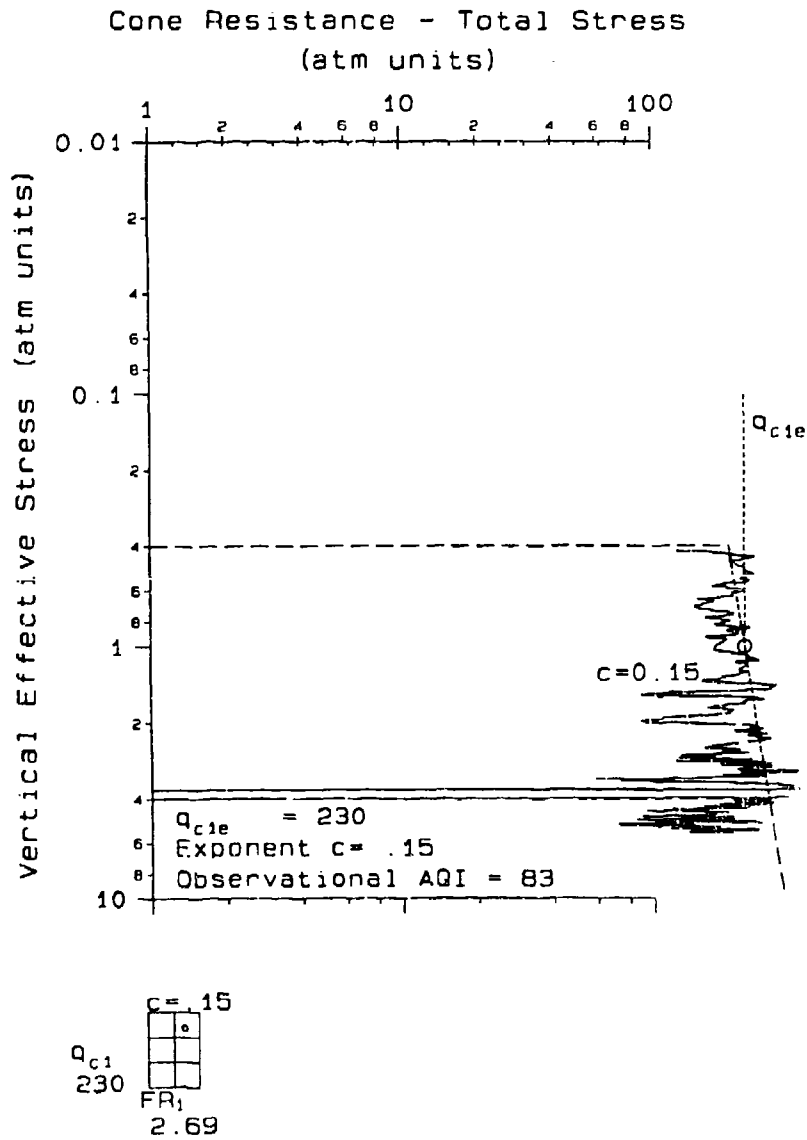


**Figure 6.6** Uniform sandy silt layer in the core of Ririe dam (Corps of Engineers)

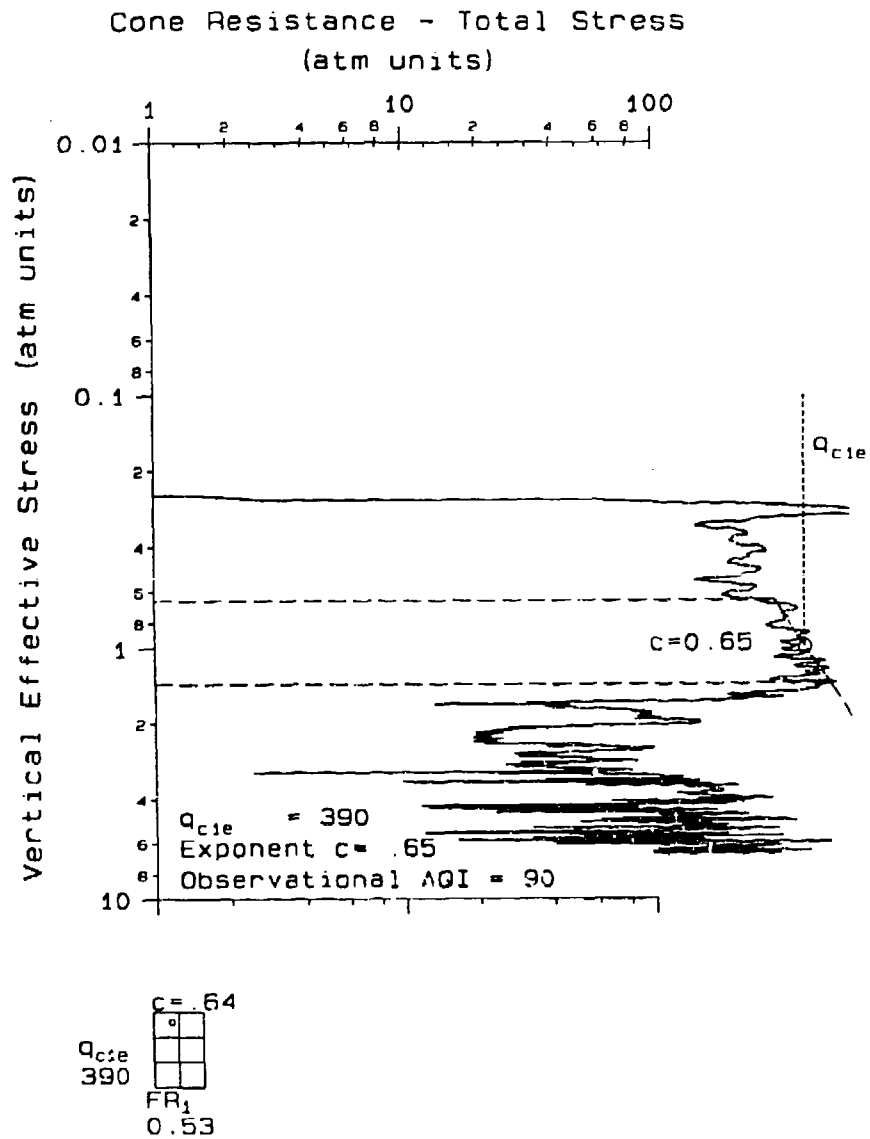


Figure 6.7 Uniform sand layer for project code DE-S-R



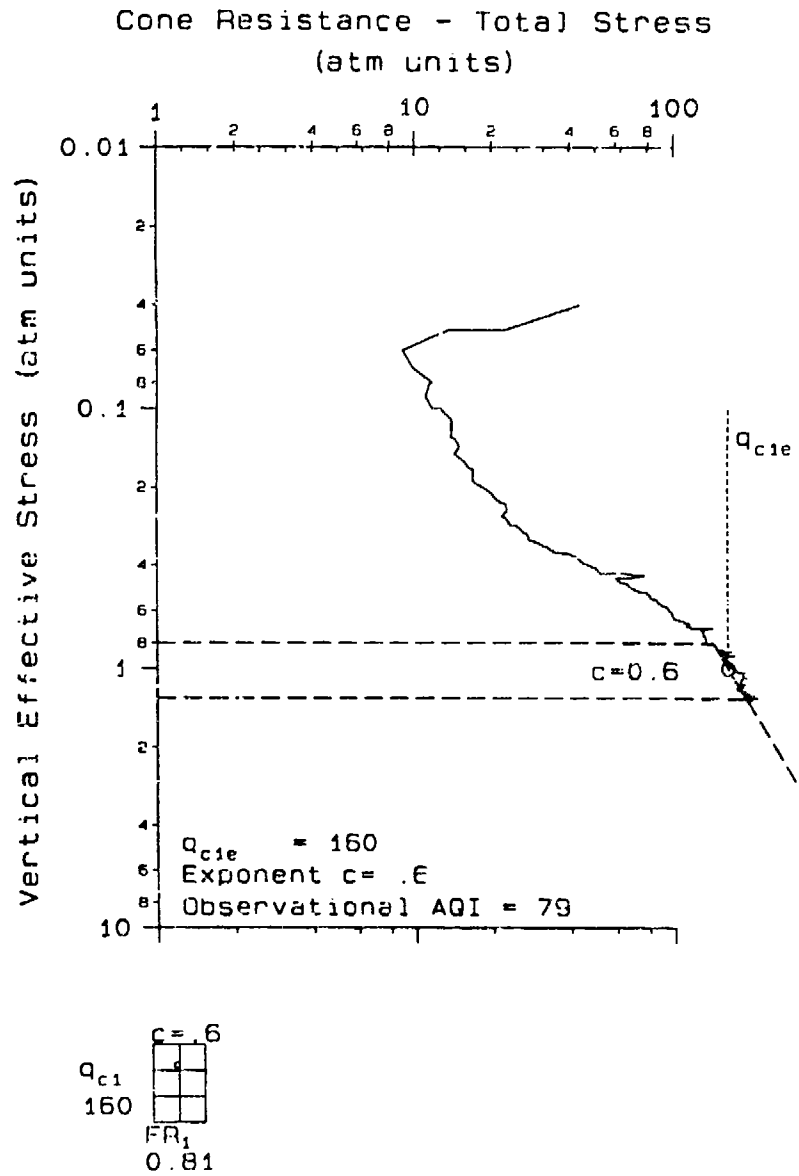


Figure 6.8 Uniform silty sand layer in the Atchafalaya River (dredging study)

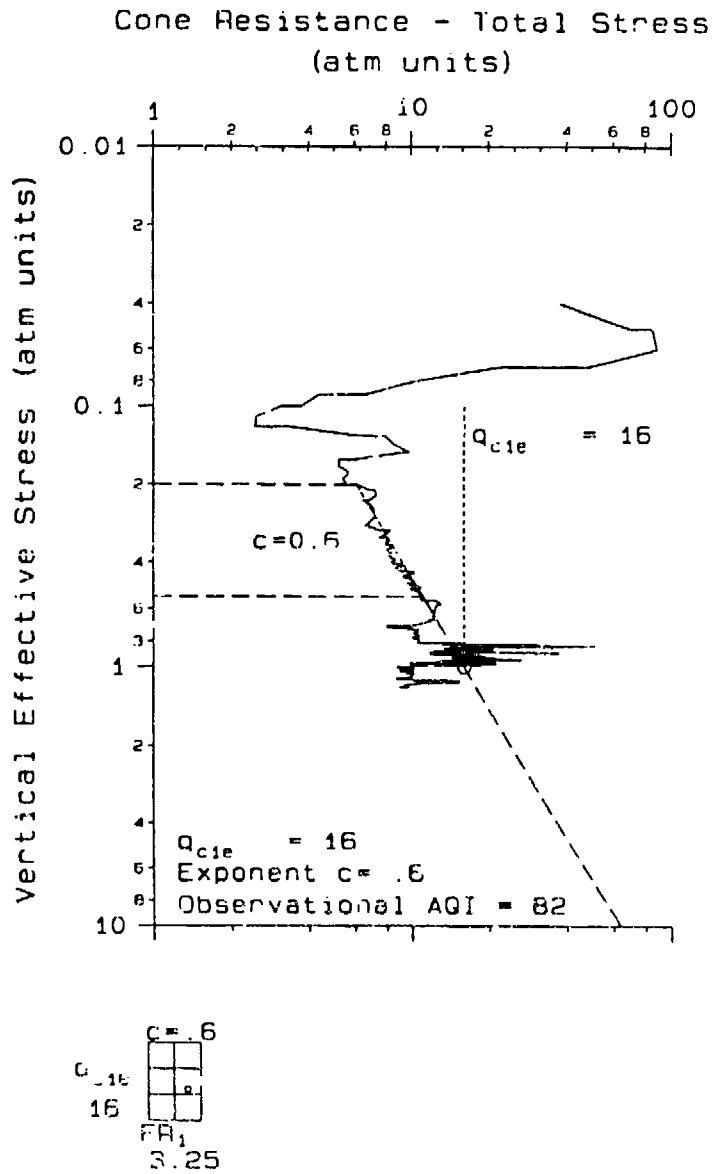
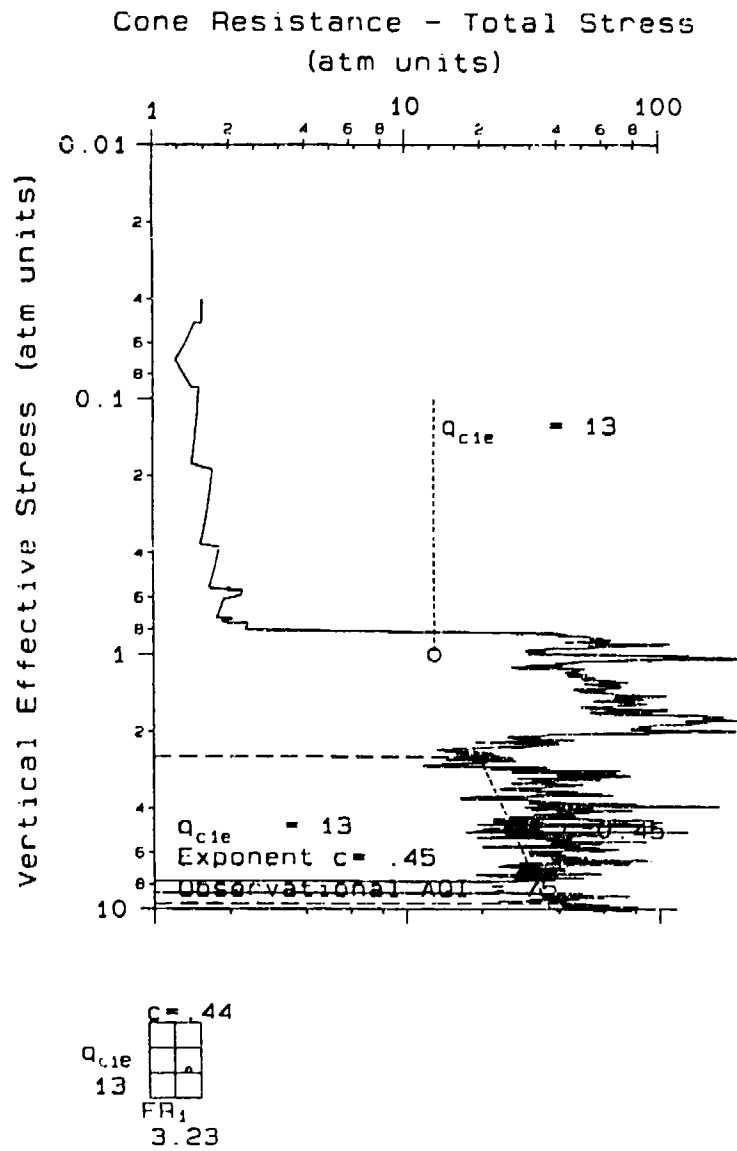
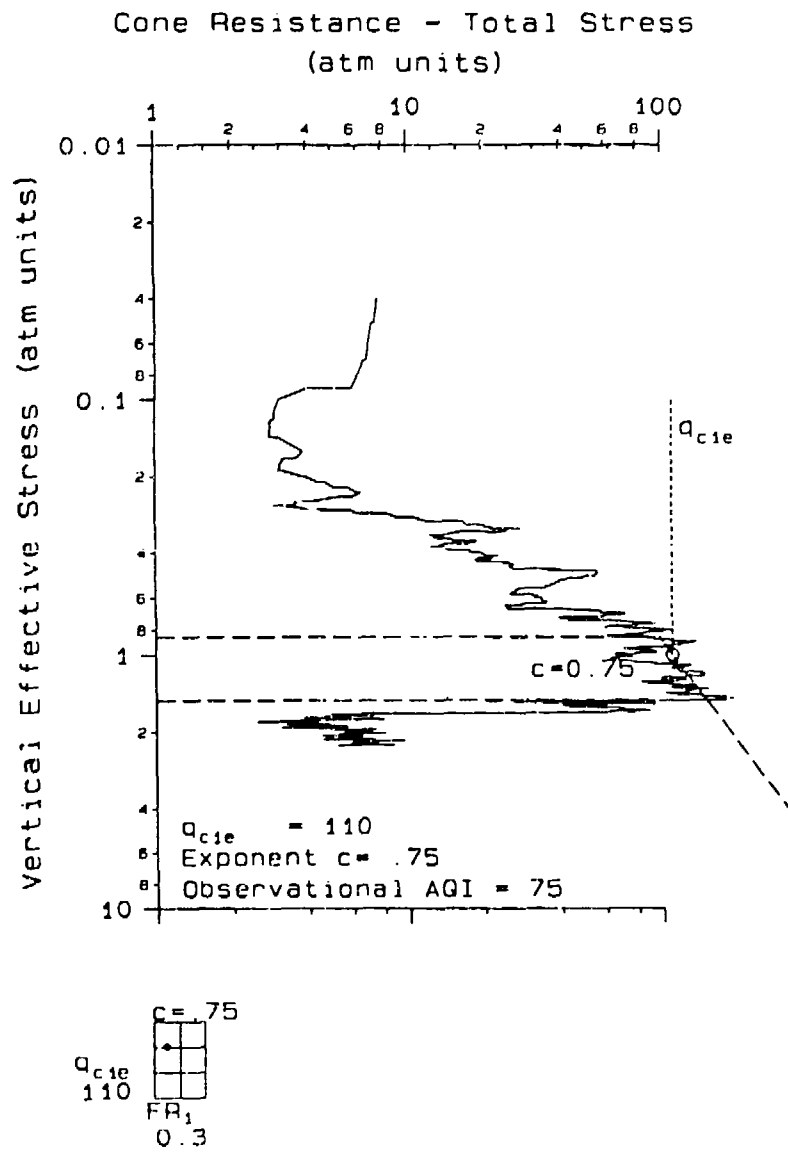


Figure 6.9 Uniform silty clay layer in the Anchafalaya River (Dredging study)



**Figure 6.10** Uniform silty clay layers of the foundation for Lucky Peak Dam (Corps of Engineers)



**Figure 6.11** Uniform sand layer segment at the McDonalds Farm, Sea Island, Canada

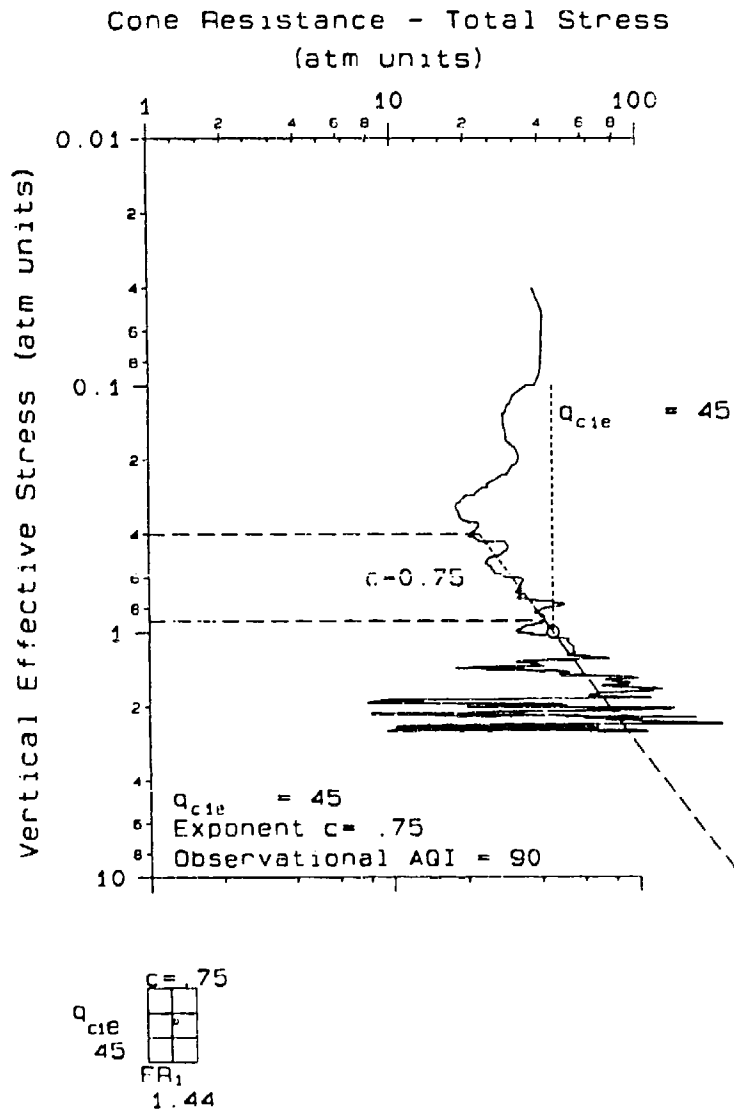


Figure 6.12 Uniform silty sand layer at Salinas (Old Hilltown), California (USGS research project)

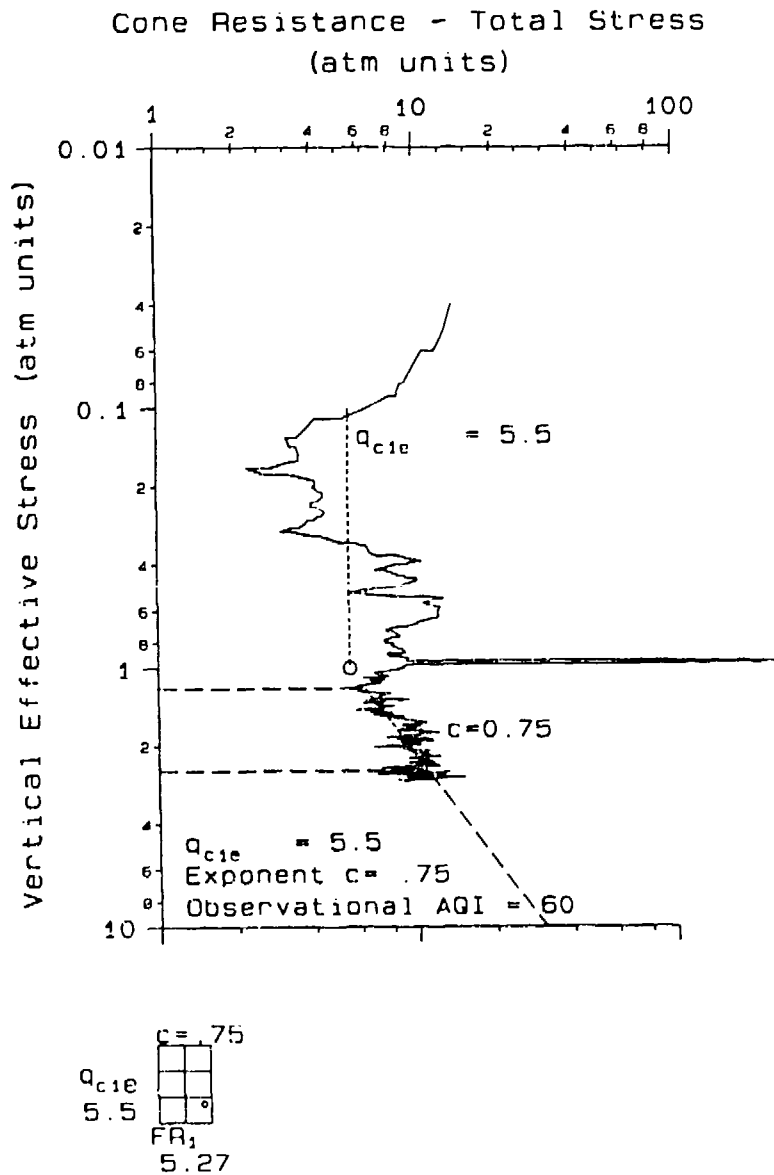
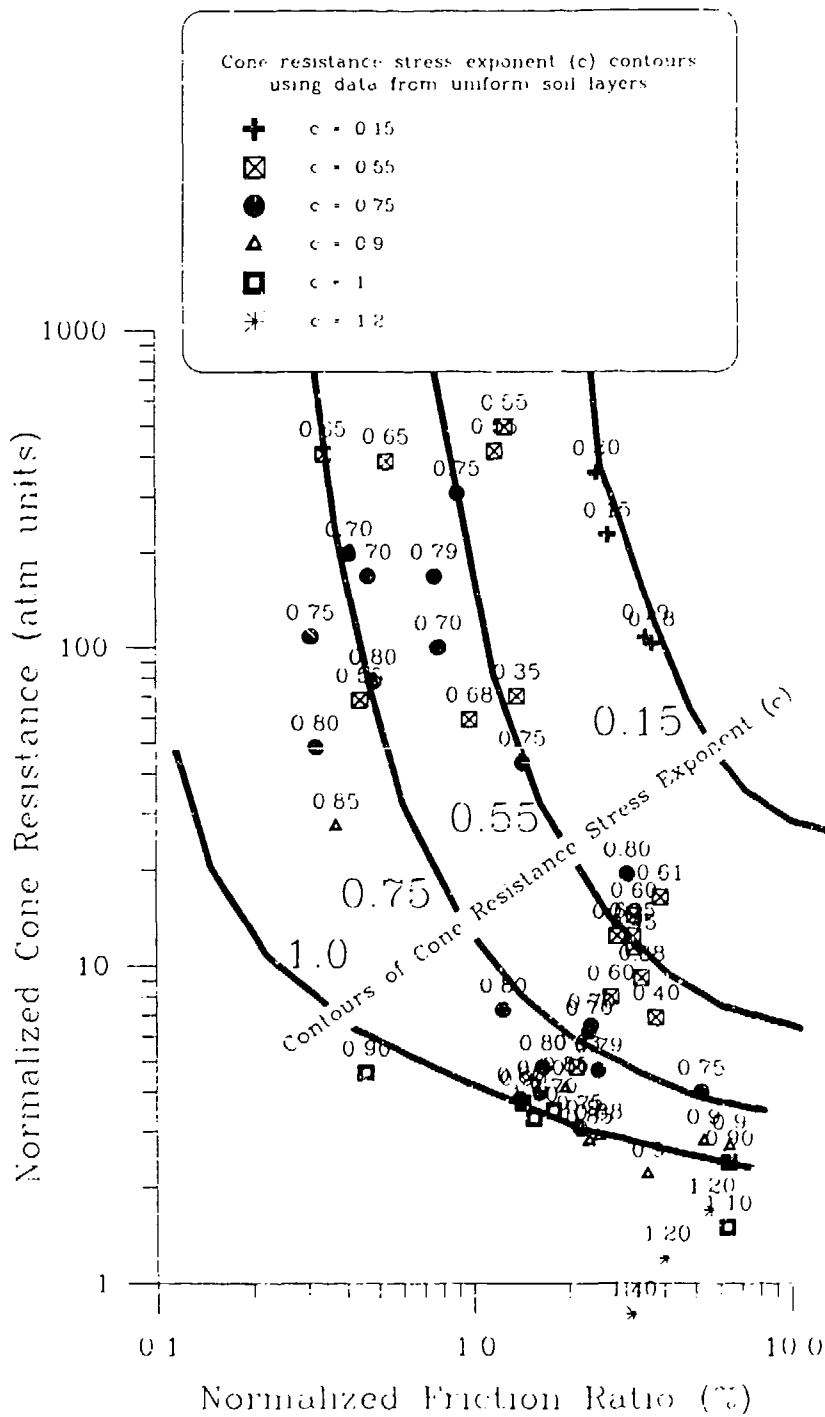
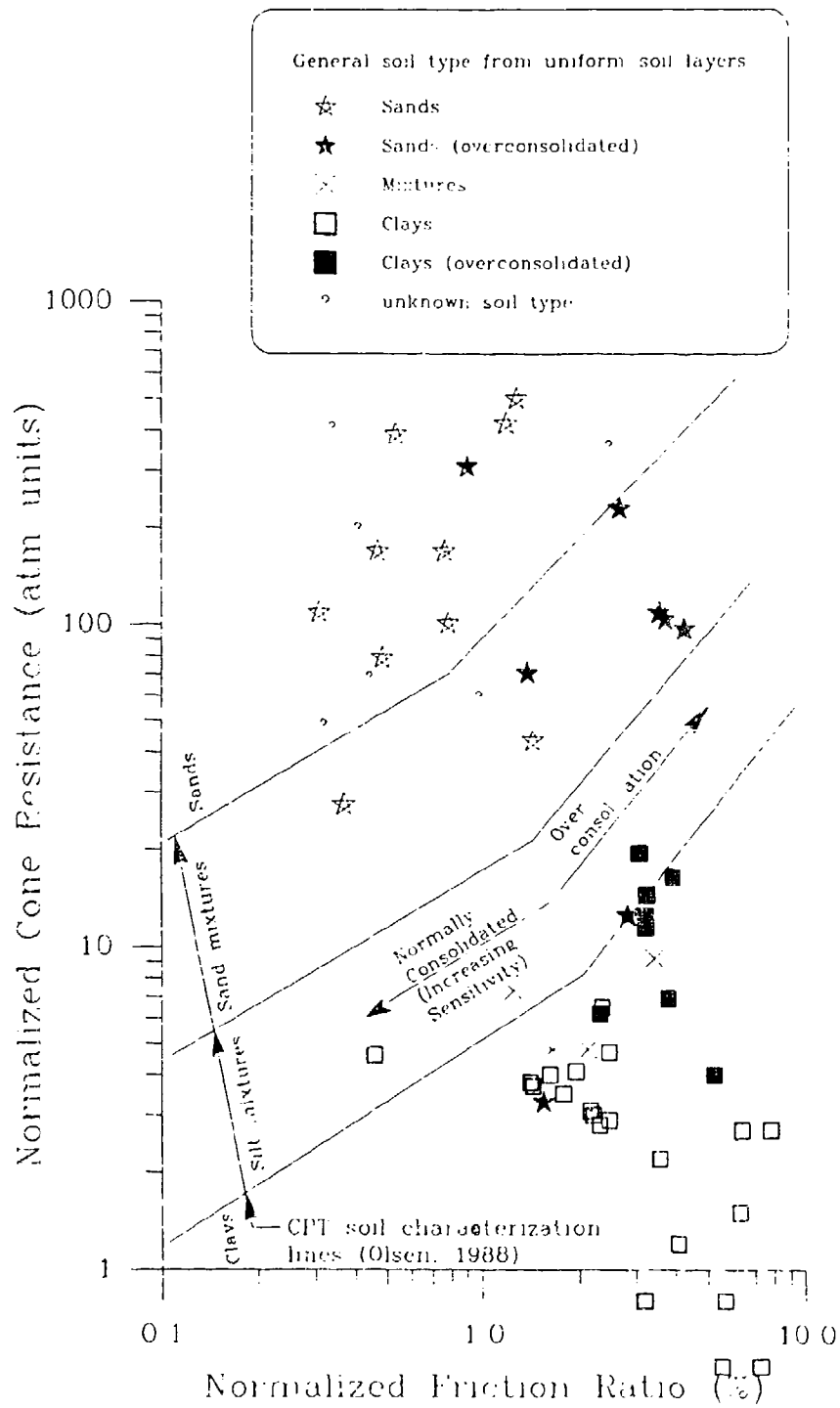


Figure 6.13 Uniform foundation clay layer (Levee failure investigation)



**Figure 6.14** Establishing contours of cone resistance stress exponent using CPT data from in situ uniform soil layers with constant relative strength



**Figure 6.15** Comparing soil types from uniform soil layers to the CPT soil classification line (from Olsen, 1988)



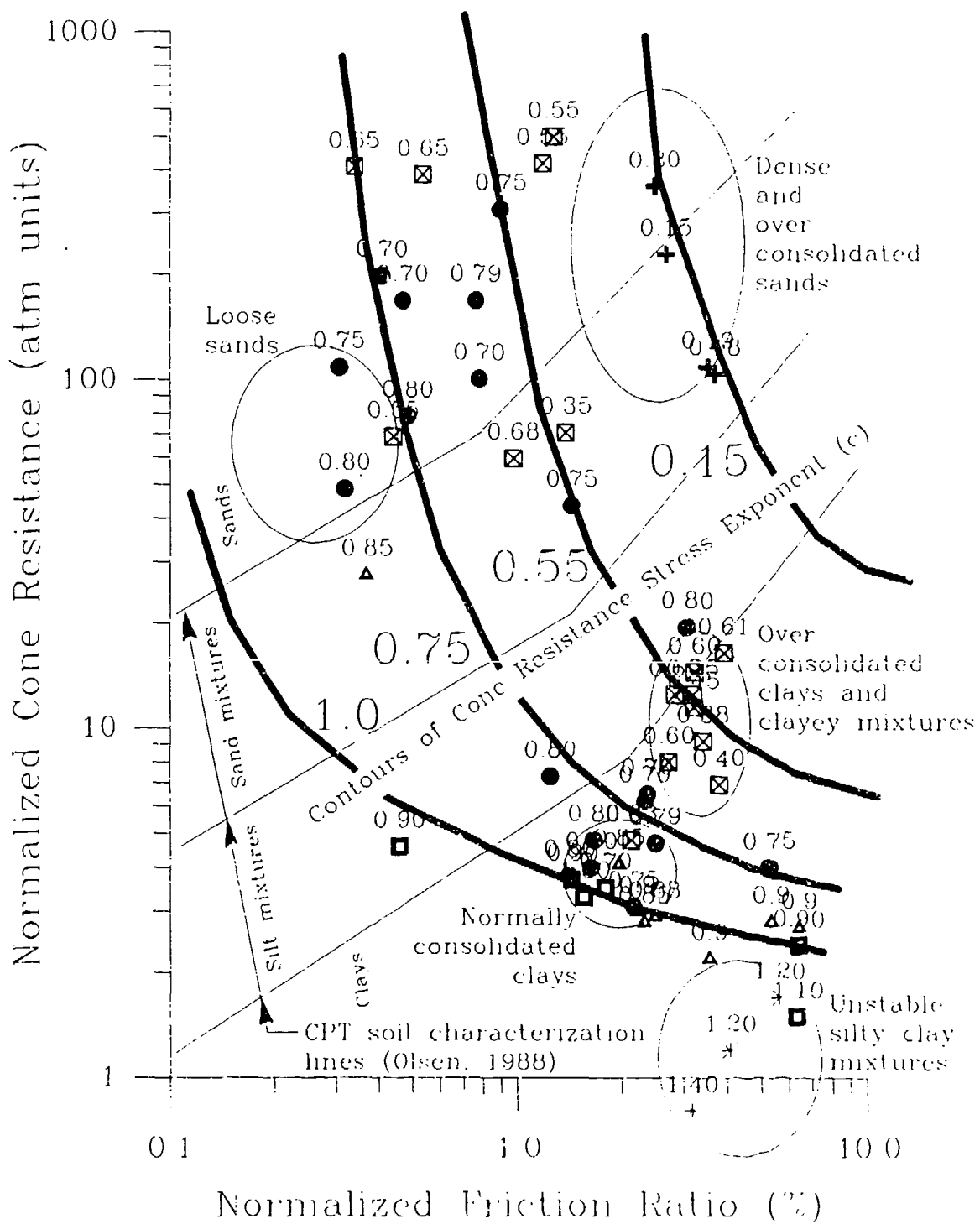


**Figure 6.16** Annotated version of the cone resistance stress exponent chart showing soil zones (and strength character) together with CPT soil characterization line

of one or slightly less; the stress exponent contour for normally consolidated clay is between 0.8 and 1, as expected. Dense and overconsolidated sands have stress exponents contours between 0.15 and 0.55, as expected. Overconsolidated clays are shown to have stress exponent contours between 0.55 and 0.75, also as expected. Unstable silty clay (i.e. silt structure with underconsolidated clay matrix) have stress exponents of about 1.1 to 1.5 and are located at the bottom right of the CPT soil characterization chart, which is a new finding.

The cone resistance stress exponent contours displayed in Figure 6.16 are approximately perpendicular to the CPT soil characterization (classification) lines. For a given soil type, increasing the relative strength (e.g. relative density for sand) should move the CPT-based soil characterization (i.e.  $q_{cle}$  and  $FR_{1e}$  point on the chart) along a contour of constant soil type to the upper right (Olsen, 1988, 1984). It was shown in Chapter 2 that as relative strength increases, the stress exponent decreases. Soil type and relative strength should be independent of each other because they define different aspects of a soil; i.e. what it is and the state that it's in. For a given soil type, a relative strength increase can be represented on the CPT soil characterization chart as a decreasing stress exponent contour level (i.e. increasing relative strength) along a given soil type contour as shown in Figure 6.16. The CPT soil characterization chart is therefore, verified in part, therefore, because the soil classification contours are approximately perpendicular to the stress exponent contours.

## Establishment of the Sleeve Friction Resistance Stress Exponent

The CPT sleeve friction resistance is obtained through a high-strain strength measurement where the confining stress on the sleeve is equal to the cylindrical cavity expansion pressure (Masood, 1990). Sleeve friction resistance is also influenced by many of the same geotechnical properties as the cone resistance. However, the sleeve friction is a high strain strength measurement; whereas the cone resistance is a bearing stress (many times higher than confining stress) that is dependent on both small and large strains. Therefore, the sleeve friction stress exponent should not be equal to the cone resistance stress exponent.

### *Direct Correlation of Sleeve and Cone Stress Exponents*

The first attempt toward developing a correlation between sleeve friction stress exponent and cone resistance stress exponent using uniform soil layer data was simply a scatter plot of sleeve resistance stress exponent ( $s$ ) versus cone resistance stress exponent ( $c$ ) as shown in Figure 6.17. This figure shows a large data scatter but suggests that both stress exponents are approximately equal without considering soil type or relative strength consistency contributions. The large scatter does indicate that other factors are influencing the relationship between the two exponents.

The sleeve friction is more difficult to measure accurately than the cone resistance because of mechanical constraints such as strain-gauge accuracy, thermal effects, and dirt clogging the joints (Olsen, 1994). As a result, it was not possible to establish contours of the sleeve friction stress exponent ( $s$ ) or the ratio of  $s/c$  on the CPT soil characterization chart. A reliable  $s/c$  ratio would allow the less accurate

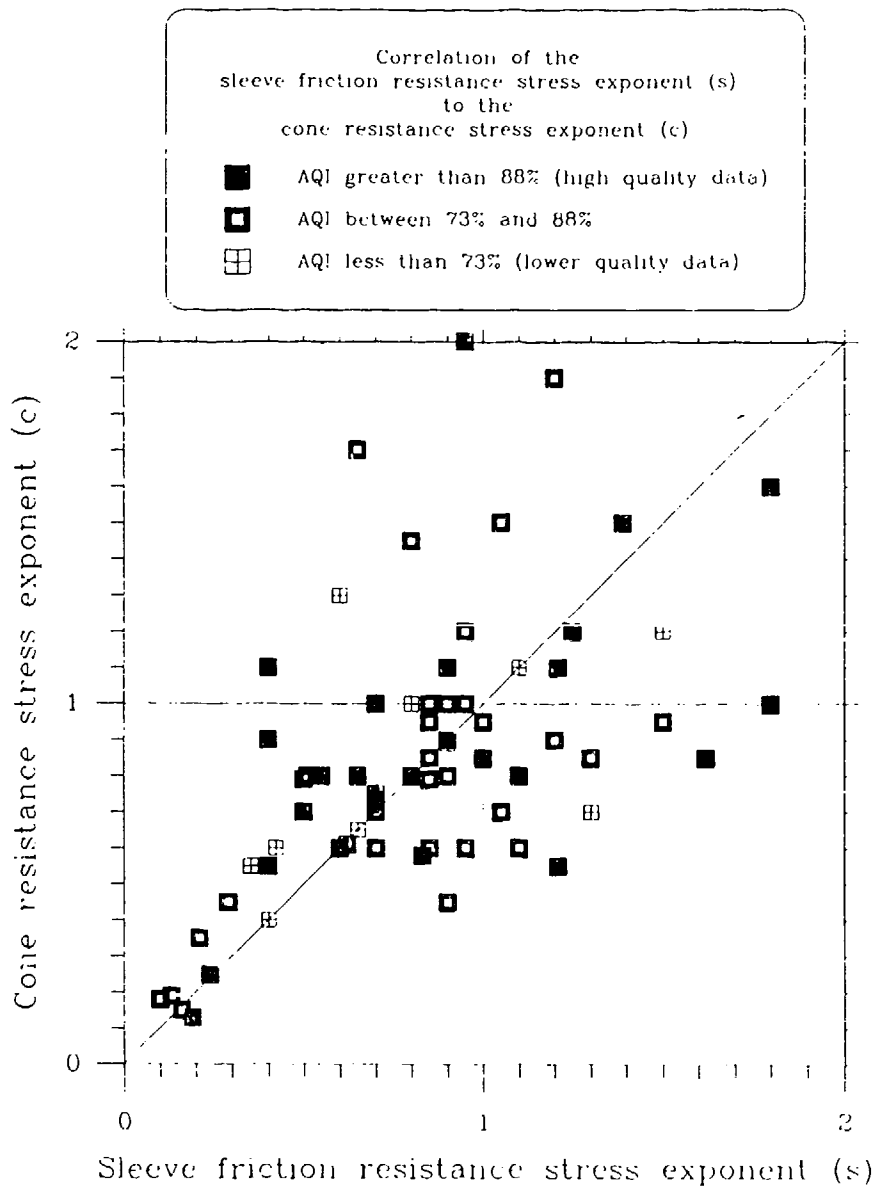


**Figure 6.17** Relationship of sleeve friction resistance stress exponent (s) to the cone resistance stress exponent (c) using uniform soil layer data

sleeve resistance stress exponent (s) to be indexed to the more accurately determined cone resistance exponent (c). The only correlation that proved satisfactory was that between the s/c ratio and normalized sleeve friction resistance, as shown in Figure 6.18. The s/c ratio is interesting because it is analogous to the ratio of cylindrical expansion pressure (on the sleeve) to the spherical plus cylindrical expansion pressure (for the cone) as illustrated by Equation (6.1). The s/c appears to correlate to the normalized sleeve friction resistance quite well probably because the sleeve measurement is primarily influenced by cylindrical cavity effects.

$$\frac{\text{sleeve stress exponent (s)}}{\text{cone resistance exponent (c)}} \propto \frac{\text{cylindrical pressure}}{\text{cylindrical pressure effects} + \text{spherical pressure}} \quad (6.1)$$

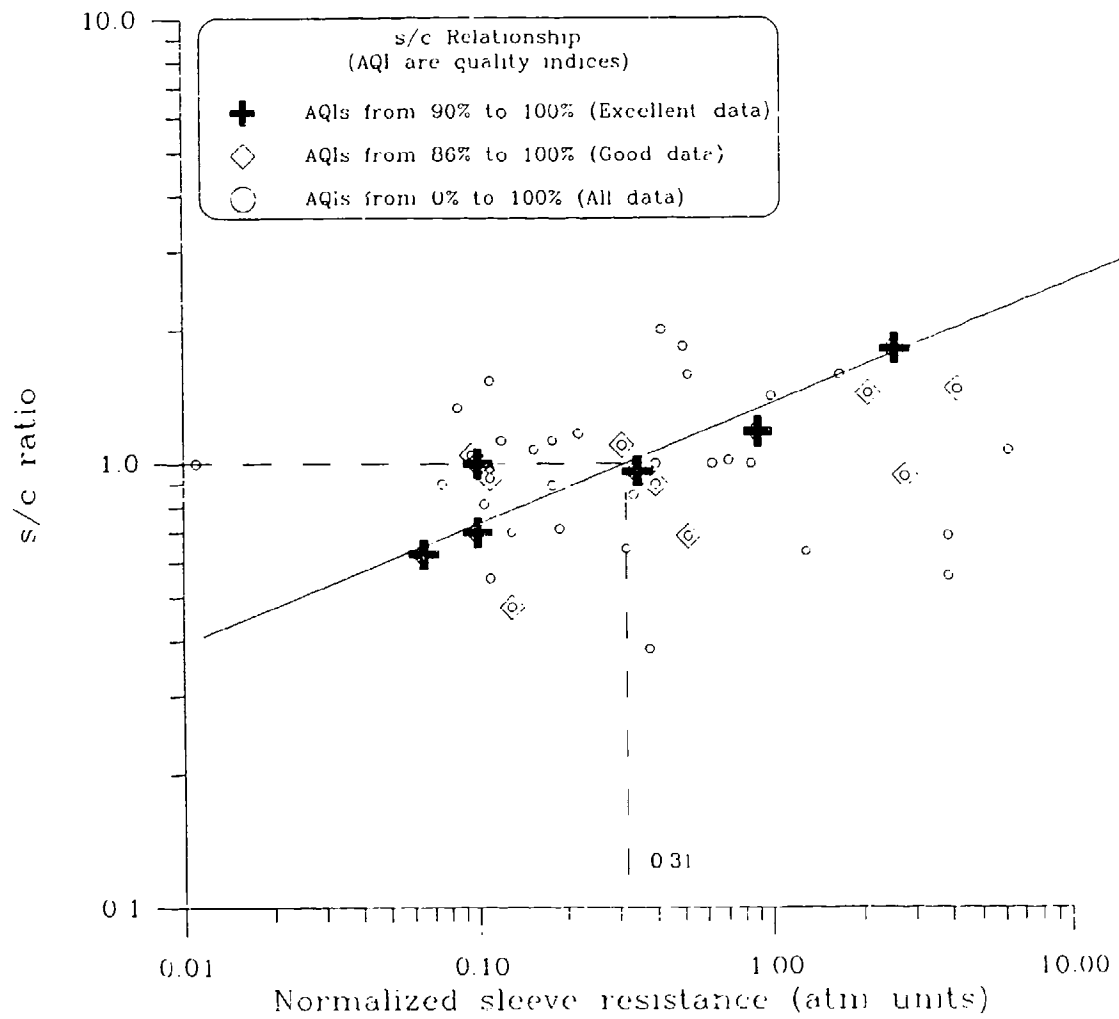


**Figure 6.18** Correlation of the s/c ratio (sleeve to conc stress exponents) to the normalized sleeve friction resistance ( $f_{sle}$ )

## Determining the Soil Type Dependent Stress Focus using Uniform Soil Layer Data

CPT data from tests in uniform soil layers was used to show that the Stress Focus location is soil type dependent. The first step in this process involved dividing the in situ uniform soil layer database into 3 soil classification groups: clays, soil mixtures, and sands. This grouping of data was accomplished based primarily on soil type observed in nearby borings and secondarily on the information about the site geology. Only a small portion of the database was composed of uniform soil mixtures due to the geologic scarcity of such deposits. These soil classification groups were also further distinguished as either normally consolidated or overconsolidated soils. Overconsolidated soils have very low stress exponents (0.1 to 0.3) and do not have a soil type dependent Stress Focus (Chapter 5). Some of the moderately overconsolidated sands probably were classified as normally consolidated dense sands because their behavior is similar to that of a dense sand.

### *Developing the Stress Focus Relationship for Different Soil Types*

All uniform clay layer data collected in this research program are shown in Figure 6.19. The projections for normally consolidated uniform clay layers (using different clay types) produces a Stress Focus at an overburden stress of approximately 9 atm.

A clay Stress Focus can also be observed using Figure 6.20 by plotting the clay and silty clay trends using the stress normalization format from Chapter 3 with the resultant shown in Figure 6.21. The clay trends in Figure 6.21 appear to converge to a Stress Focus at an overburden stress of approximately 5 to 10 atm, that is

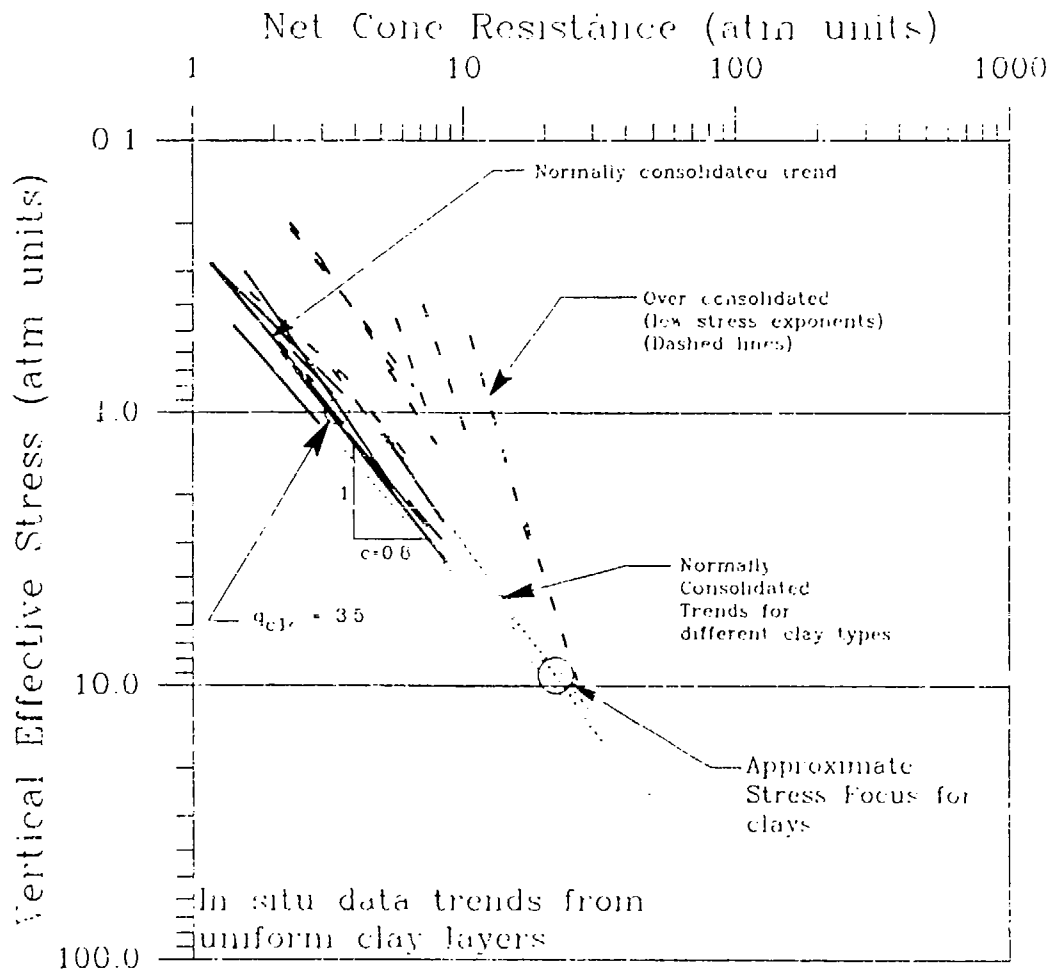


**Figure 6.19** Projections of trends for uniform in situ clay layers in terms of log net cone resistance versus log vertical effective stress



approximately the same as 9 atm from Figure 6.19.

The data in Figure 6.19 indicate that normally consolidated clays have a stress exponent ( $c$ ) of about 0.8 to 1.0 and a normalized cone resistance ( $q_{c1c}$ ) of about 3.5 atm. A cone resistance stress exponent of 0.8 (also shown in Figure 6.16) is significant because prior geotechnical property formulations (e.g. prediction of  $S_u$  for clay) have historically implied a stress exponent of one. The stress exponent of 0.8 to 1 results because net cone resistance rather than the raw cone resistance was used to establish the trend—soil strength level is more proportional to the net cone resistance than the raw cone resistance (Chapter 4).

The Stress Focus for clay occurs at a vertical effective stress of approximately 9 atm. The undrained strength at the clay Stress Focus, assuming a  $c/p$  of 0.31, is approximately 5600 psf (280 KPa). A clay strength of 4000 psf (200 KPa) has a strength descriptor of hard (Peck, et al., 1974) and is at the lower boundary for classification as a compaction shale. It is therefore reasonable to assume that a shale like behavior starts at the Stress Focus for clay deposition.

Overconsolidated clays were observed to have a higher  $q_{c1c}$  and lower stress exponents than for a normally consolidation condition. The overconsolidated stress exponents typically ranged from 0.4 to 0.6, whereas normally consolidated clay stress exponents range from 0.8 to 1. The clay stress exponent due to overconsolidation is therefore approximately 50% to 60% of that associated with the normally consolidated condition.

All uniform sand layer projections are shown in Figure 6.22. The uniform sand layer trends are shown to project to a general Stress Focus because different sand types can not be distinguished. Overconsolidated sands have low observed stress exponents, as expected.

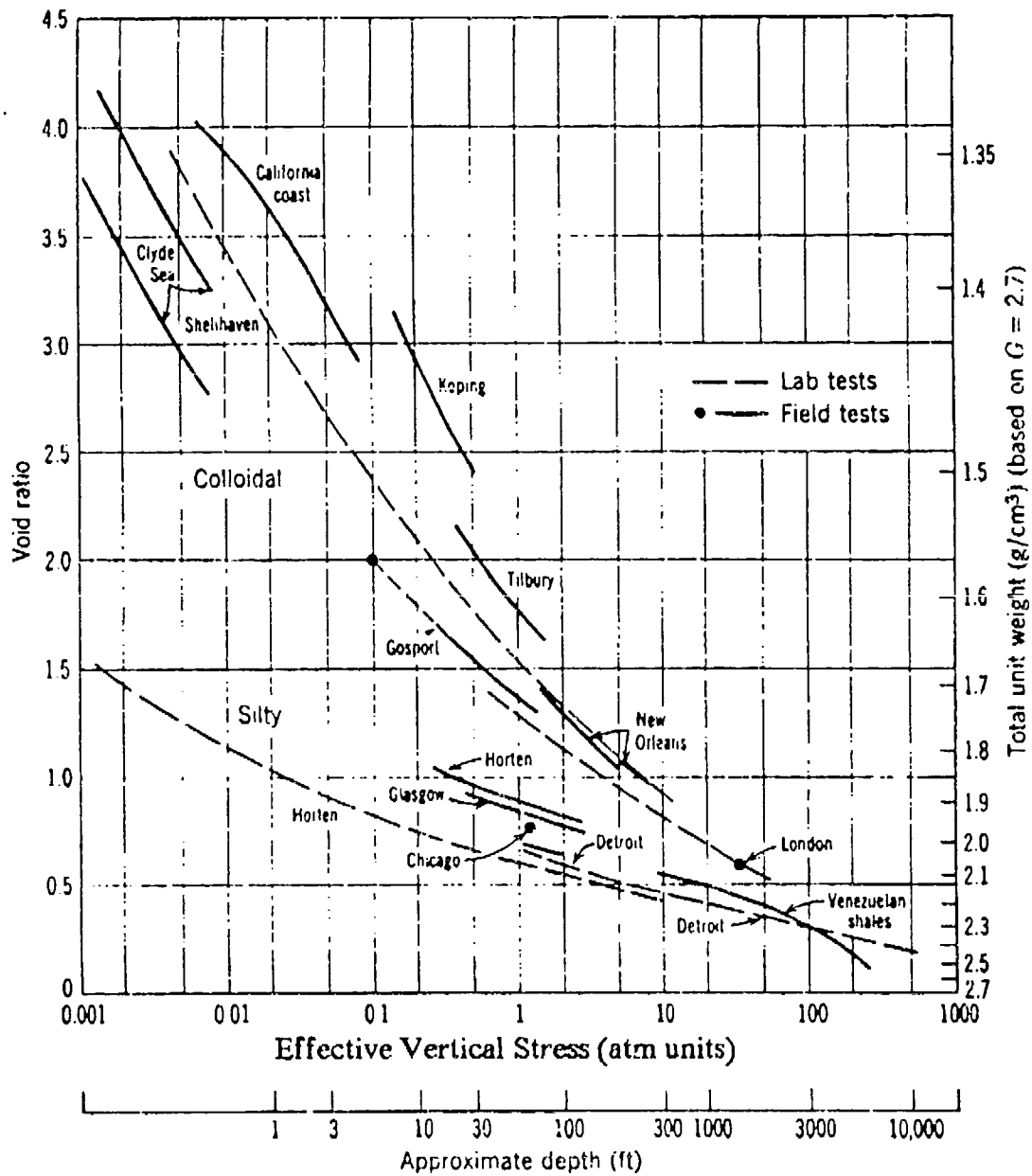


**Figure 6.20** Compression curves for several clays and silty clays  
(from Mitchell, 1993; Lambe & Whitman, 1969)

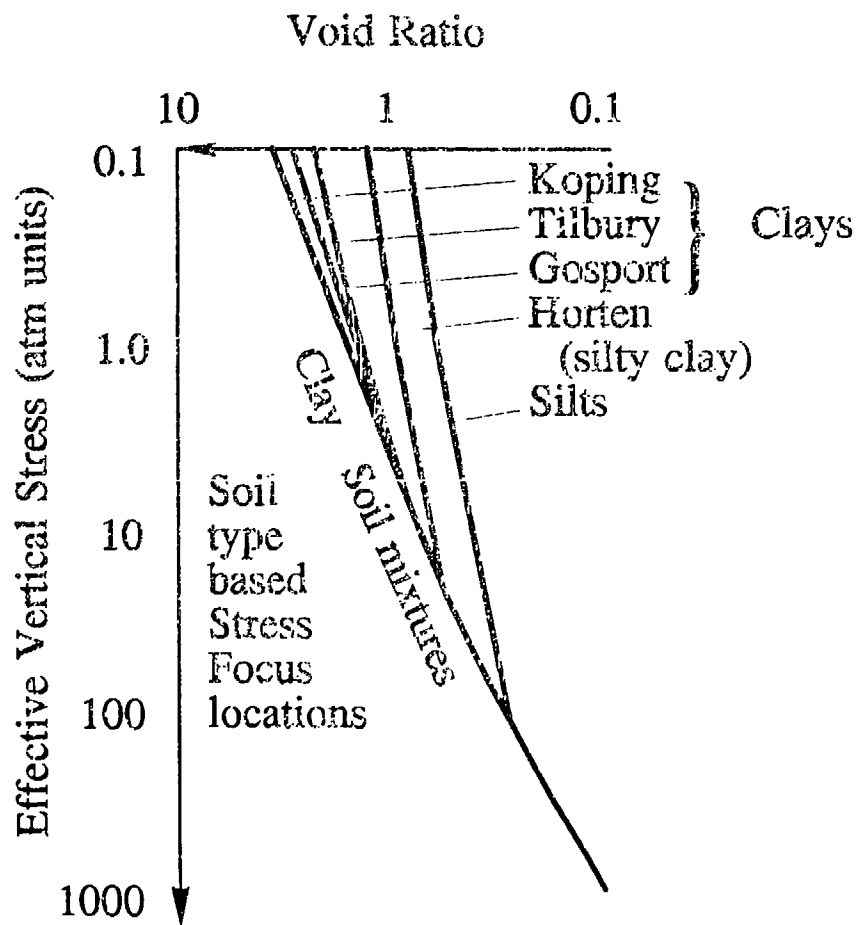


**Figure 6.21** Replot of selected soil types from Figure 6.20 in using stress normalization format to show that clays have an approximate Stress Focus

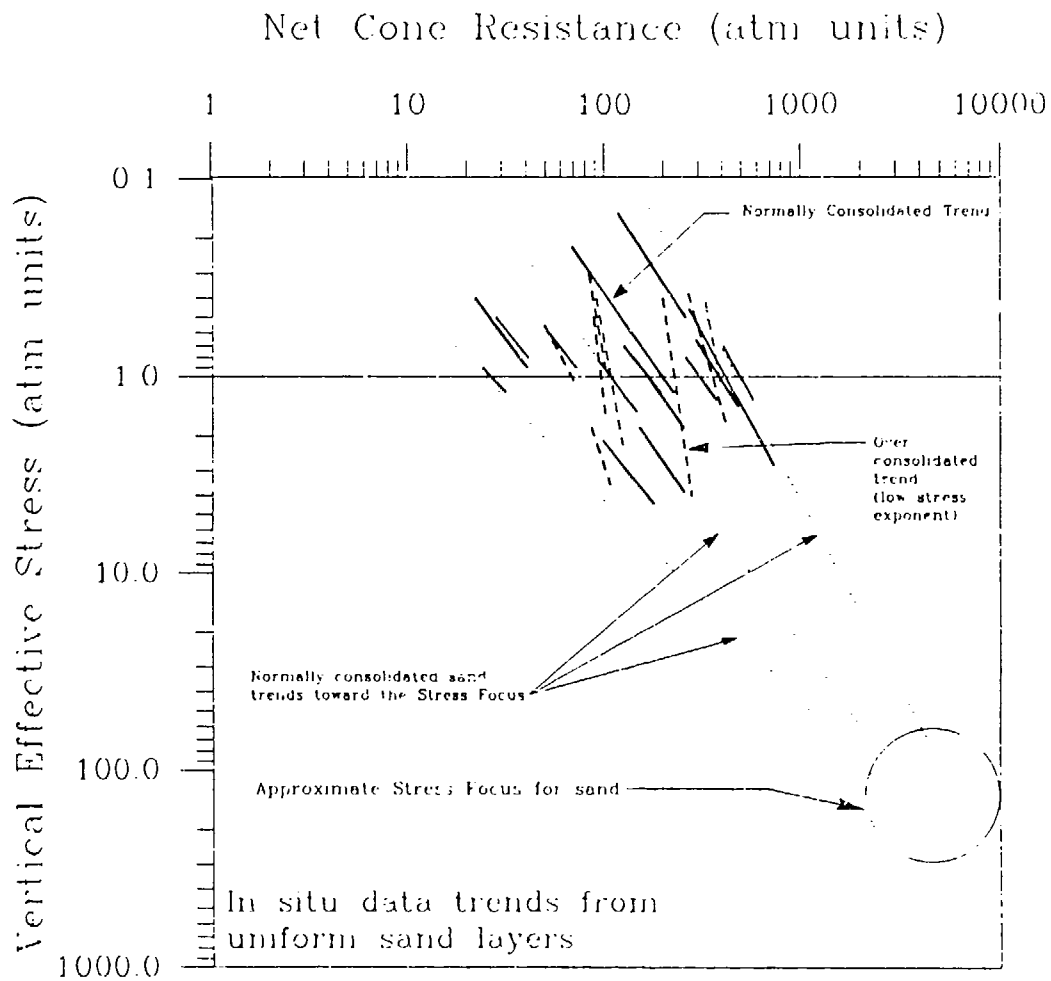


**Figure 6.22** Projections of trends for uniform sand layers in terms of log net cone resistance versus log vertical effective stress

All uniform soil mixture layer projections are shown in Figure 6.23. Soil mixtures are more complex and cover a wider range of conditions than do clays or sands. As a result, the soil mixture layers projections are more complicated than for clay or sand. For example, dense silty sand can be stronger than a dense clean sand and a honeycombed silty clay may have a moderately high sensitivity much like salt-leached clay. The locus of Stress Focus trends in Figure 6.23 represents the zone projection for all soil mixture classifications. Clayey soil mixtures project to the upper left of the elliptical locus and stronger sandy silts with higher  $q_{c1e}$  are project to the lower right of the elliptical locus. Unstable soil mixtures are also depicted and project into the soil mixture Stress Focus to the upper left of the elliptical locus.

### *Soil Type Dependent Trend of the Stress Focus*

There is enough information at this point to support establishment of a soil type-dependent Stress Focus that will be called the "Stress Focus boundary". Shown in Figure 6.24 are the Stress Foci for clay (from Figure 6.19), soil mixtures (from Figure 6.23), and sands (from Figure 6.22). Also shown are the Stress focus locations for Hokksund and Ticino sands from laboratory chamber test evaluations (from Chapter 5). The soil type dependent Stress Focus boundary is shown as a thick dashed line that passes through all of the Stress Foci. This boundary is curved and represents an increasing normalized Stress Focus ( $q_{cfn}$ ) (see Chapter 5 for definition) as the soil classification changes from clay to sand. Conceptually, the Stress Focus boundary represents the boundary between a soil-like and (sedimentary) rock-like mechanical behavior.

The soil type dependent Stress Focus boundary is depicted again in Figure 6.25 to show behavior at confining stresses lower and higher than the Stress Focus. For confining stress less than the Stress Focus, a few example soil types are depicted

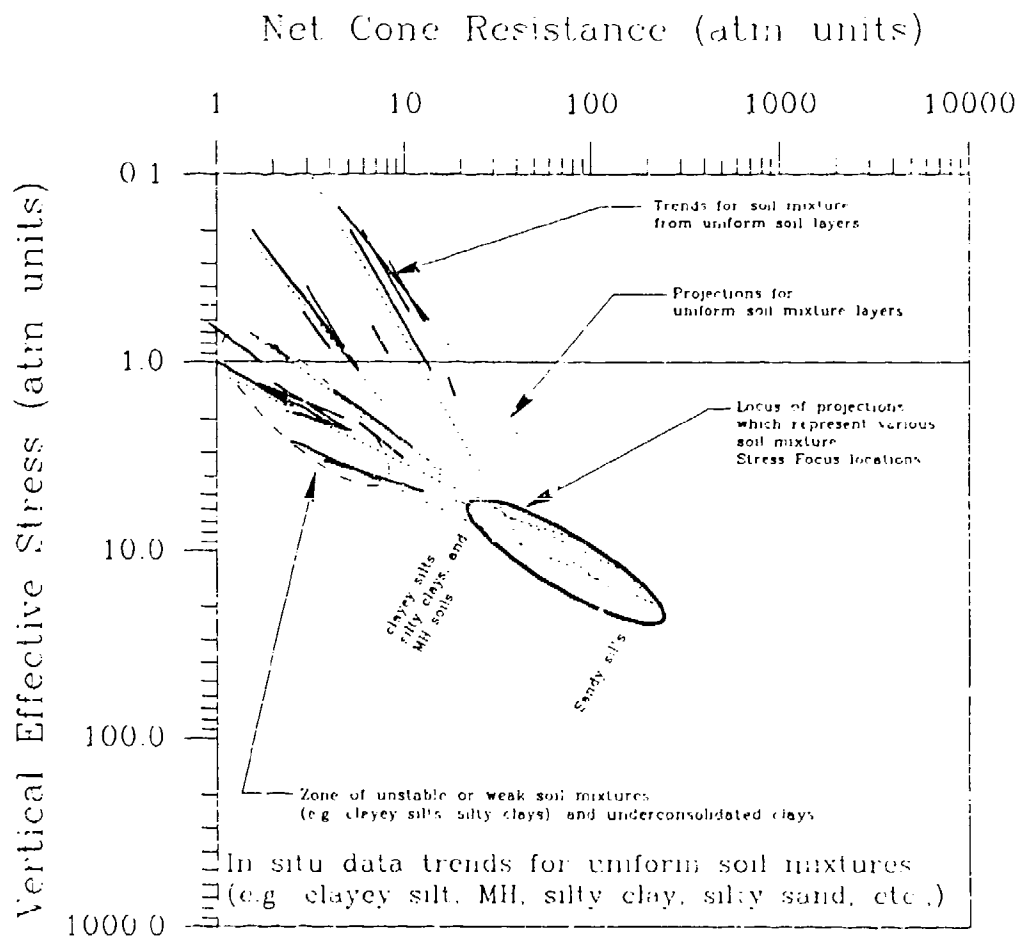


**Figure 6.23** Projections of trends for uniform soil mixture layers in terms of Log cone resistance versus Log vertical effective stress

together with different relative strength trends. Also shown is the probable behavior for all soil types at confining stresses beyond the Stress Focus; this behavior is likely at a stress exponent of one and in a domain where strength behavior is (sedimentary) rock-like.

## Conclusions

The main requirement for normalizing the CPT measurements is the stress exponent. Figure 6.16 can be used to determine the cone resistance stress exponent using field CPT data. The sleeve friction resistance stress exponent is estimated using Figure 6.18 in conjunction with Figure 6.16. Cone resistance stress exponent contours are approximately perpendicular to soil classification lines in the CPT soil characterization chart; representing indirect support for the validity of the chart. Finally, in situ uniform soil layer data and chamber test data were used to establish the soil type dependent Stress Focus boundary.

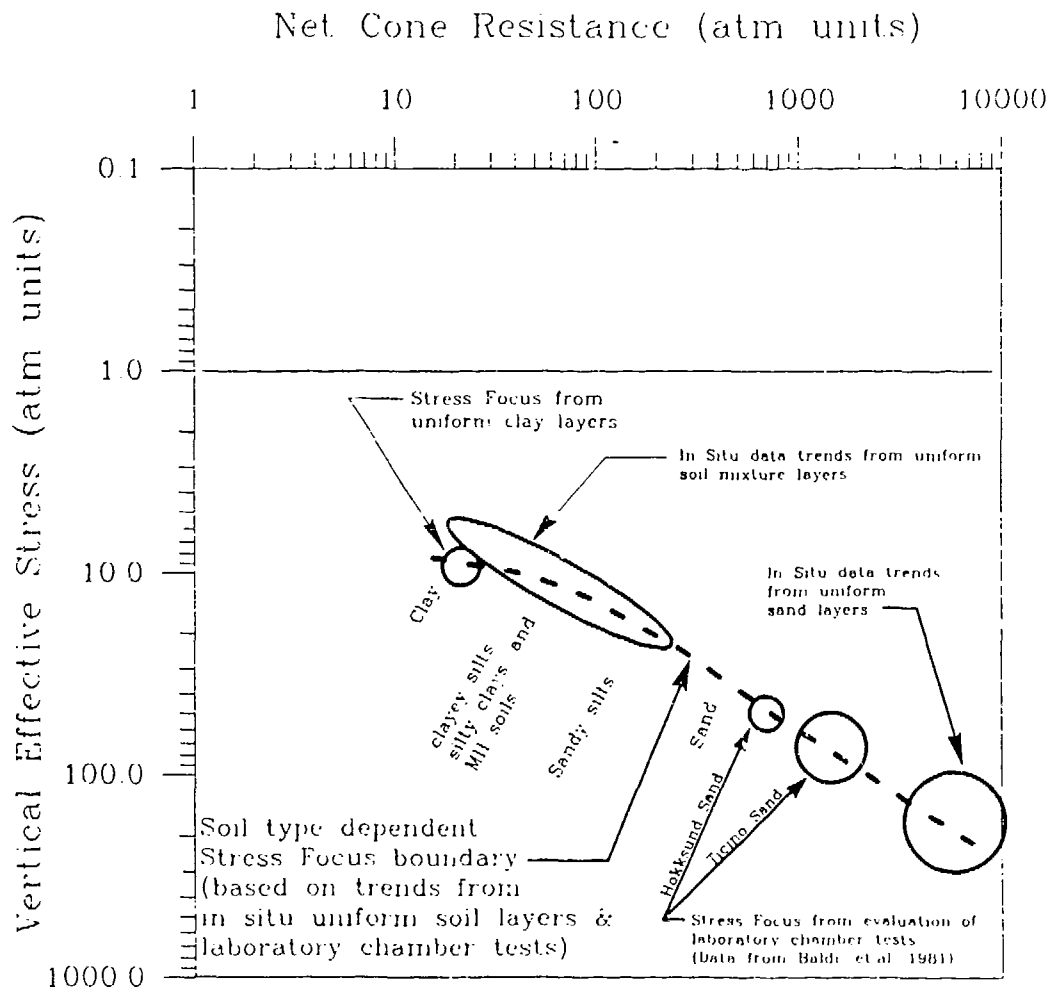


**Figure 6.24** The soil type dependency trend for the Stress Focus based on uniform soil layer and laboratory chamber test evaluation



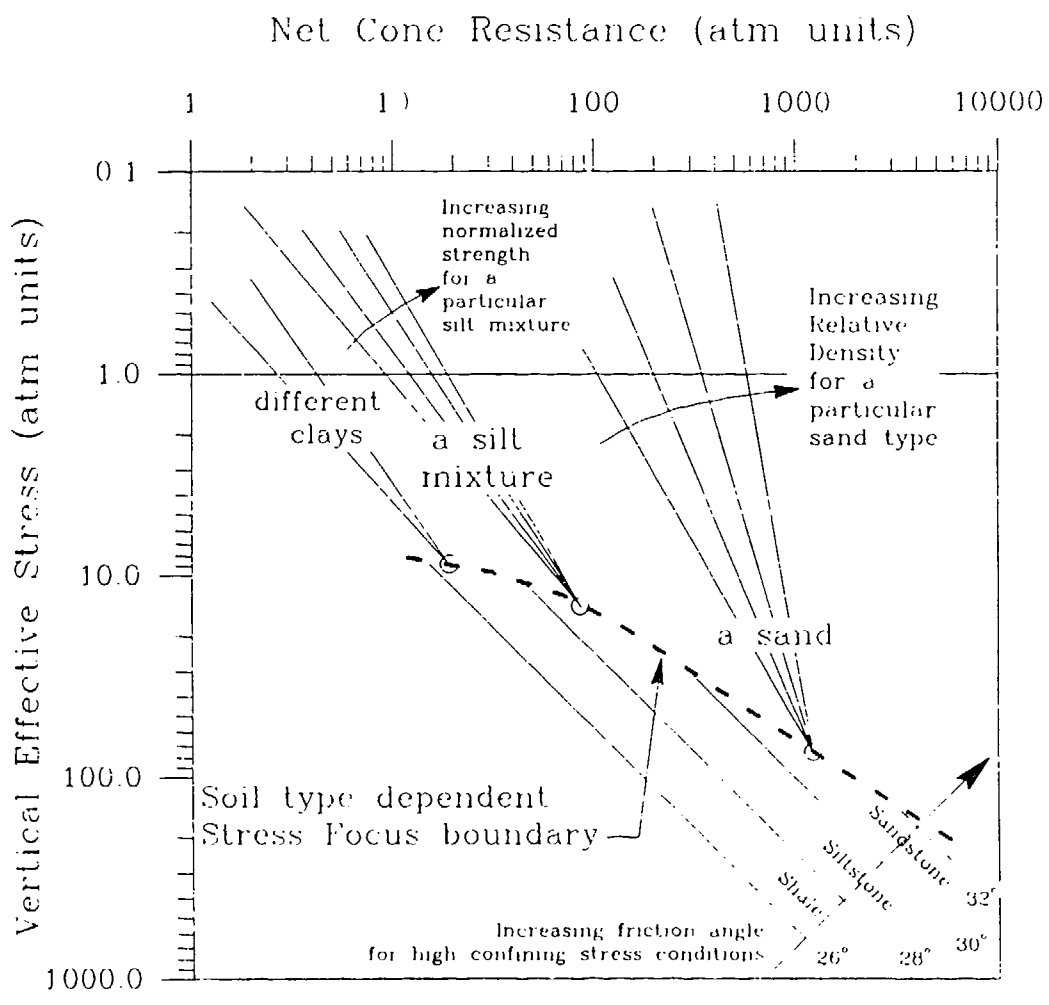


**Figure 6.25** Inferences concerning the soil type dependent Stress Focus

# Chapter 7

## Normalization of Selected Geotechnical Properties

### Introduction

Geotechnical property normalization is vital toward development of CPT-based prediction correlations and prediction of in situ geotechnical properties. CPT prediction of geotechnical properties requires accurate stress normalization; otherwise, for very shallow or very deep conditions, the stress normalization will itself induce errors into the predictive process. This chapter will describe new normalization techniques for the Standard Penetration Test (SPT) blow count and the shear wave velocity.

### Standard Penetration Test (SPT) Normalization

Normalization is required to convert the measured SPT blow count,  $N$ , to a representative value that would be measured when vertical effective stress equals 1 tsf (e.g. approximately 1 atm). This normalized SPT blow count can then be used to predict a variety of normalized geotechnical properties, such as liquefaction resistance and friction angle. A new observation will be introduced that results from the fact that SPT laboratory chamber tests are subject to a stress relief

associated with the constant mud pressure in the chamber borehole. During a SPT laboratory chamber test, the borehole mud height is always the same (approximately 6 feet), regardless of the chamber confining stress level. Quantifying this pressure relief will show that the SPT chamber-derived stress exponents are too low. It will also be shown that the correct SPT-based stress exponent for field applications is equal to the CPT-based stress exponent.

### *Historical SPT Blow Count Normalization*

The state-of-the-practice for Standard Penetration Test (SPT) blowcount normalization for the last 12 years was developed by Seed et al. (1983) and later confirmed by Skempton (1986). This SPT normalization technique uses an exponent of the vertical effective stress for two relative density ranges. Seed et al. (1983) used data from the Bieganousky and Marcuson (1976, 1977) study to develop the SPT  $C_N$  normalization parameter shown in Figure 7.1. The SPT blow count,  $N_{60}$ , (i.e., measured using equipment that delivers 60% of theoretical maximum free-fall hammer impact energy or adjusted to simulate same) is converted to a stress-normalized value,  $(N_1)_{60}$ , at an equivalent vertical effective stress of 1 ton/ft<sup>2</sup>

using the following equation:

$$(N_1)_{60} = N_{60} C_N = N_{60} \frac{1}{(\sigma'_v)^n} \quad (7.1)$$

where

- $(N_1)_{60}$  = Normalized SPT blow count, equivalent SPT at a vertical effective stress of 1 ton/ft<sup>2</sup> (approximate atmospheric pressure)
- $N_{60}$  = SPT measured blow count at 60% of theoretical maximum free-fall energy which is the US approximate average achieved in practice
- $\sigma'_v$  = Vertical effective stress in tons/ft<sup>2</sup> (e.g. approximately 1 atm, 100 KPa, 0.1 MPa, etc.,)
- $n$  = SPT overburden stress exponent  
( $n \approx 0.55$  for relative densities from 40 to 60% and  $n \approx 0.45$  for relative densities from 60 to 80%)
- $C_N$  = SPT normalization factor (See Figure 7.1)

A range of  $C_N$  values back-calculated from field and laboratory chamber test results is shown in Figure 7.2 (Skempton, 1986) in terms of overburden stress. Overburden stress is always represented in terms of tons/ft<sup>2</sup> (approximately 1 atm) and  $C_N$  is equal to 1 when the vertical effective stress is 1 tsf (i.e. approximately 1 atm). For the last 12 years, equivalent SPT stress exponents of 0.45 for relative densities from 60 to 80% and 0.55 for relative densities between 40 to 60% as shown Figure 7.1 have been widely used. The CPT chamber-based stress exponents are typically 0.6 to 0.7 (Schmertmann, 1979a), with 0.61 commonly used for relative densities between 40 and 80% (Seed, et al., 1983). Therefore different stress exponents for CPT and SPT normalization have been inferred from chamber test.

There appear to have been no theories developed to explain why the stress exponents for Equation (7.1) decrease with increased relative density or why there is a difference between CPT and SPT chamber derived stress exponents.

### *SPT Blow Count Normalization*

As background, SPT chamber data were evaluated in Chapter 5 and show that the SPT Stress Focus location is sand type dependent. Also shown were correlations of SPT chamber derived stress exponent versus relative density. The SPT chamber testing procedures used by Waterways Experiment Station (WES) were also described in that chapter.

### *Stresses at the SPT Sampler*

Distinguishing the stress states developed during penetration at and nearby the SPT sampler is important for the discussions to follow. These stresses are illustrated in Figure 7.3. The SPT blow count reflects a complex combination of static and dynamic forces acting at the end and along the side of an SPT sampler. The combination of all these forces on the SPT sampler determines the SPT blow count. The SPT blow count is also dependent on confining stress as reflected in the  $C_n$  normalization technique. Therefore, because the SPT blow count is proportional to the confining stress, the stresses influencing the SPT sampler ( $\sigma_{si}$ ) are dependent on the confining stress ( $\sigma_{sc}$ ) adjacent to the SPT sampler. If the mud pressure influences the confining stress next to the SPT sampler ( $\sigma_{sc}$ ) then the stresses that influence the SPT blow count ( $\sigma_{si}$ ) will be affected.

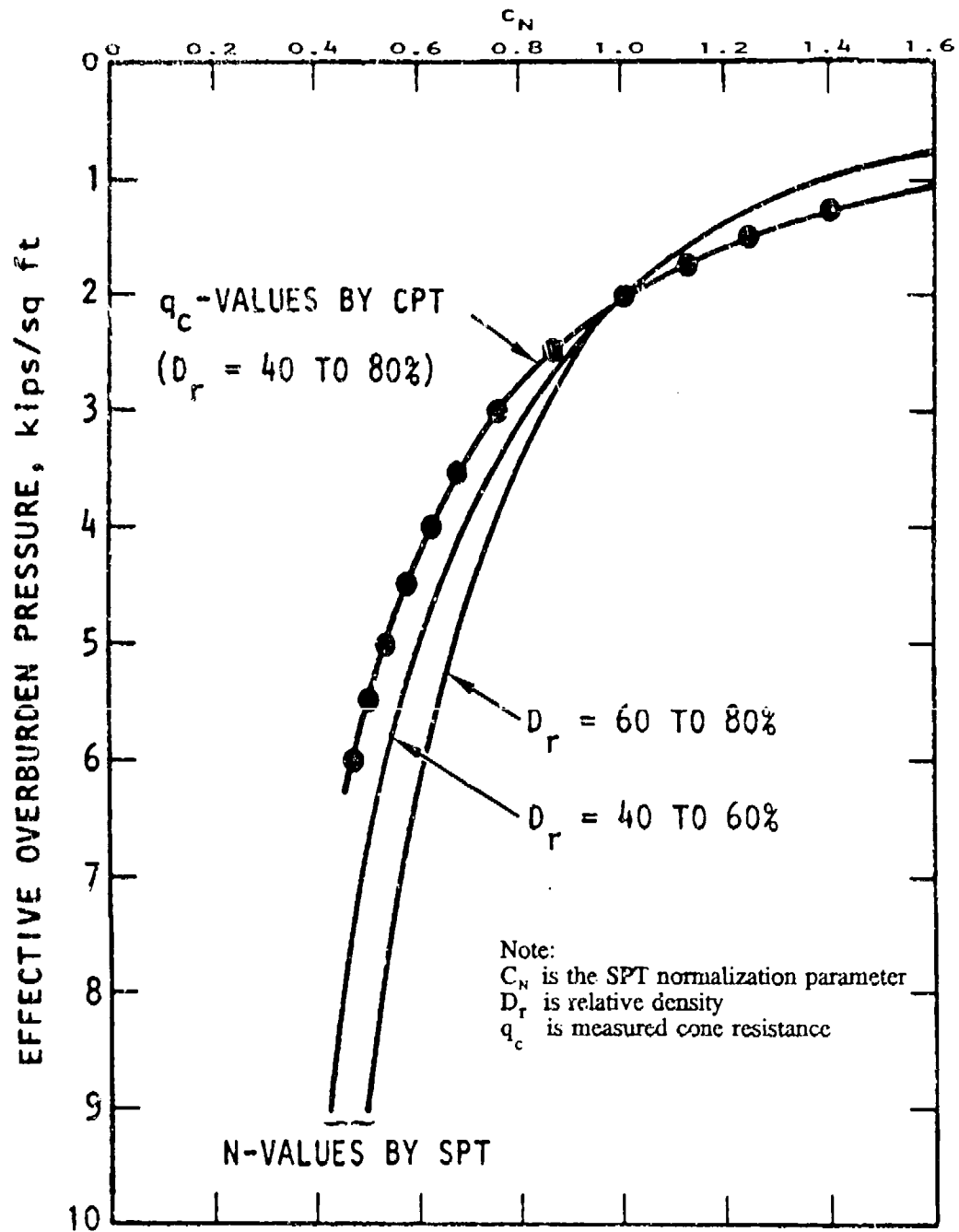


**Figure 7.1**  $C_N$  versus vertical effective stress (Kips/ft<sup>2</sup>) relationship developed by Seed et al. 1983 (Note: 2 Kips/ft<sup>2</sup> = 1 atm)

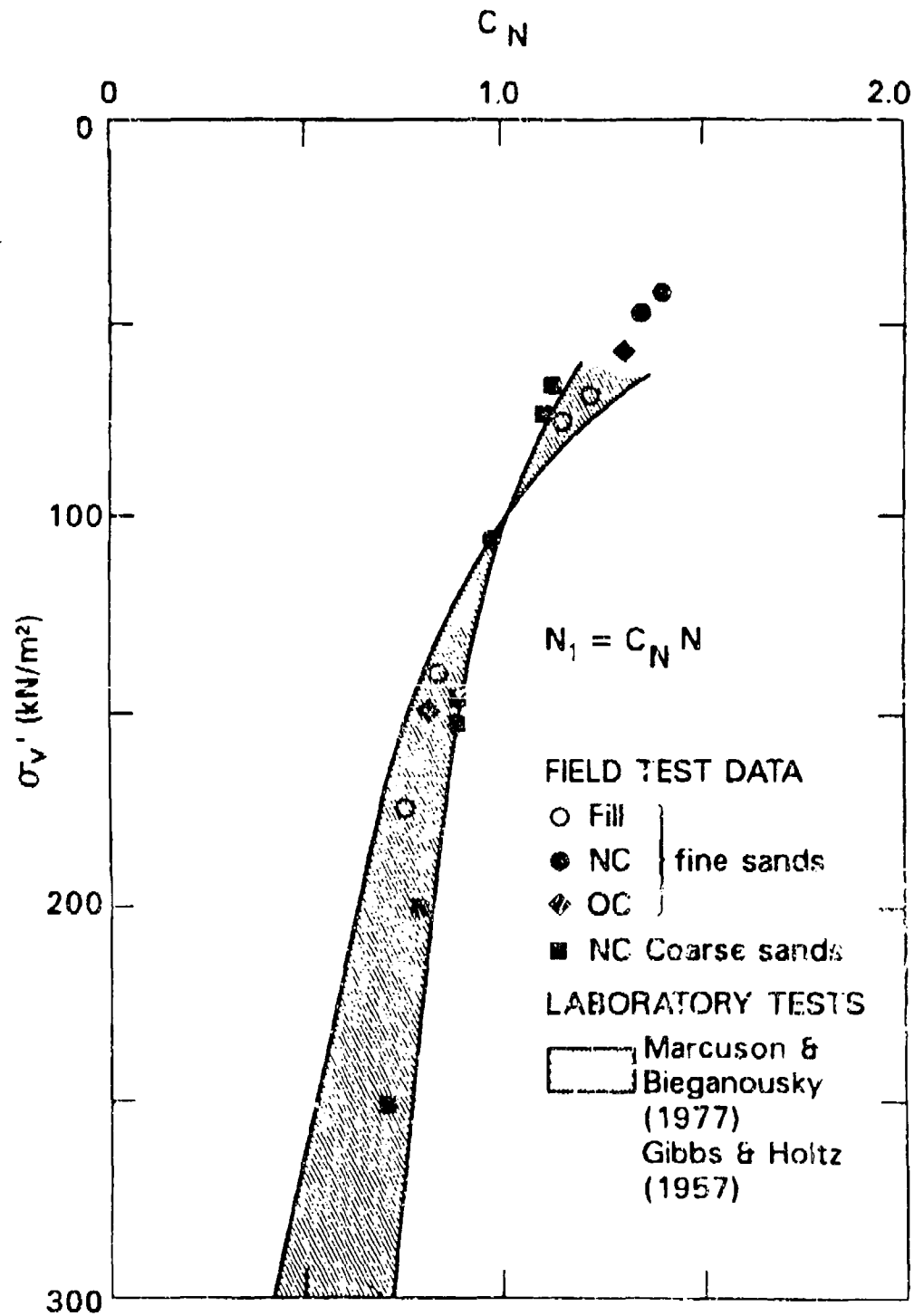


Figure 7.2 Back-calculated SPT  $C_N$  parameters from field and laboratory chamber test (Skempton, 1936)

## *Mud Stress Influence at the SPT Sampler*

In the field, the borehole mud pressure is approximately equal to the soil vertical effective stress. If the borehole mud pressure is low (which is true in chamber testing) in comparison to the soil vertical effective stress, then the confining stress ( $\sigma_{sc}$ ) next to the SPT sampler will be reduced. It is outside the scope of this dissertation to determine analytically the exact reduced stress level at the sampler due to reduced mud pressure effects; however, an approximation will be examined. At the bottom of the chamber borehole, the reduced mud pressure decreases the effects of the in situ vertical effective stress around the SPT sampler. The typical 5-inch diameter borehole bottom can be thought of as an equivalent "reversed" circular footing exerting an upward stress equal to the difference between the in situ vertical effective stress and the mud pressure as shown in Figure 7.3. At a SPT sampler penetration of 18 inches (1½ feet), the ratio of equivalent footing diameter to depth is 3½; this results in a "reversed footing" stress transmission of approximately 5% based on the simplistic Boussinesq stress distribution theory (Lambe and Whitman, 1969). However, the SPT blow count is determined by advancing the SPT sampler from 6 to 18 inches below the bottom of the borehole. At a depth of 6 inches, the ratio of equivalent footing diameter to the depth is 1.1 which corresponds to a "reverse footing" stress transmission of approximately 30%. Therefore, the mud pressure effects on the SPT sampler end bearing forces during penetration starts at a transmission of 30% and reduces to 5% at the end of penetration.

The side frictional forces generated during 18 inches of SPT sampler penetration are also affected by the mud pressure effects. The SPT sampler side friction developed from 0 to 6 inches below the bottom of the borehole dominates the sampler side frictional force during sampler penetration from 6 to 18 inches (Schmertmann, 1979a). Moreover, the side friction at 18 inches below the bottom of the borehole will only influence the final blow count. Side friction contributions from the first 6 inches are several times more influential than from the last 6 inches



of penetration. Sampler side friction influence therefore decreases with depth below the bottom of the borehole. As a result, the mud pressure transmission from the equivalent mud pressure "reverse footing" on the SPT side friction is probably greater than 60% because the first 6 inches of side friction is so dominant.

The SPT sampler is resisted during penetration by a combination of end bearing and side frictional forces (Schmertmann, 1979a, and Douglas, et.al, 1981). Reduced mud pressure influences will affect both of these SPT sampler forces. The stresses surrounding the sampler ( $\sigma_{sc}$ ) should therefore be reduced by an amount equal to 10 to 50% of the difference between the in situ vertical effective stress and the mud stress at the bottom of the bore hole (i.e. mud pressure "reverse footing" effect). This 10 to 50% range is based on the 60% value given for side frictional force influence and the 5 to 30% range for end bearing forces. For the immediate discussion to follow, an arbitrary 30% reduction will be assumed. However, other mud pressure reduction factors will also be evaluated at the end of the SPT normalization section.

### *Stresses at the SPT Sampler for Field In Situ conditions*

For a field condition, the mud pressure at the bottom of a bore hole shown as line B in Figure 7.4. The vertical effective stress is shown as line V. The calculated confining stress at the SPT sampler for the field condition,  $(\sigma_{sc})_f$  is shown as line F using the 30% mud pressure influence. The resulting confining stress on the SPT sampler  $(\sigma_{sc})_1$  is linear and very close to the vertical effective stress. Therefore, mud pressure does not significantly influence the SPT sampler for field conditions.

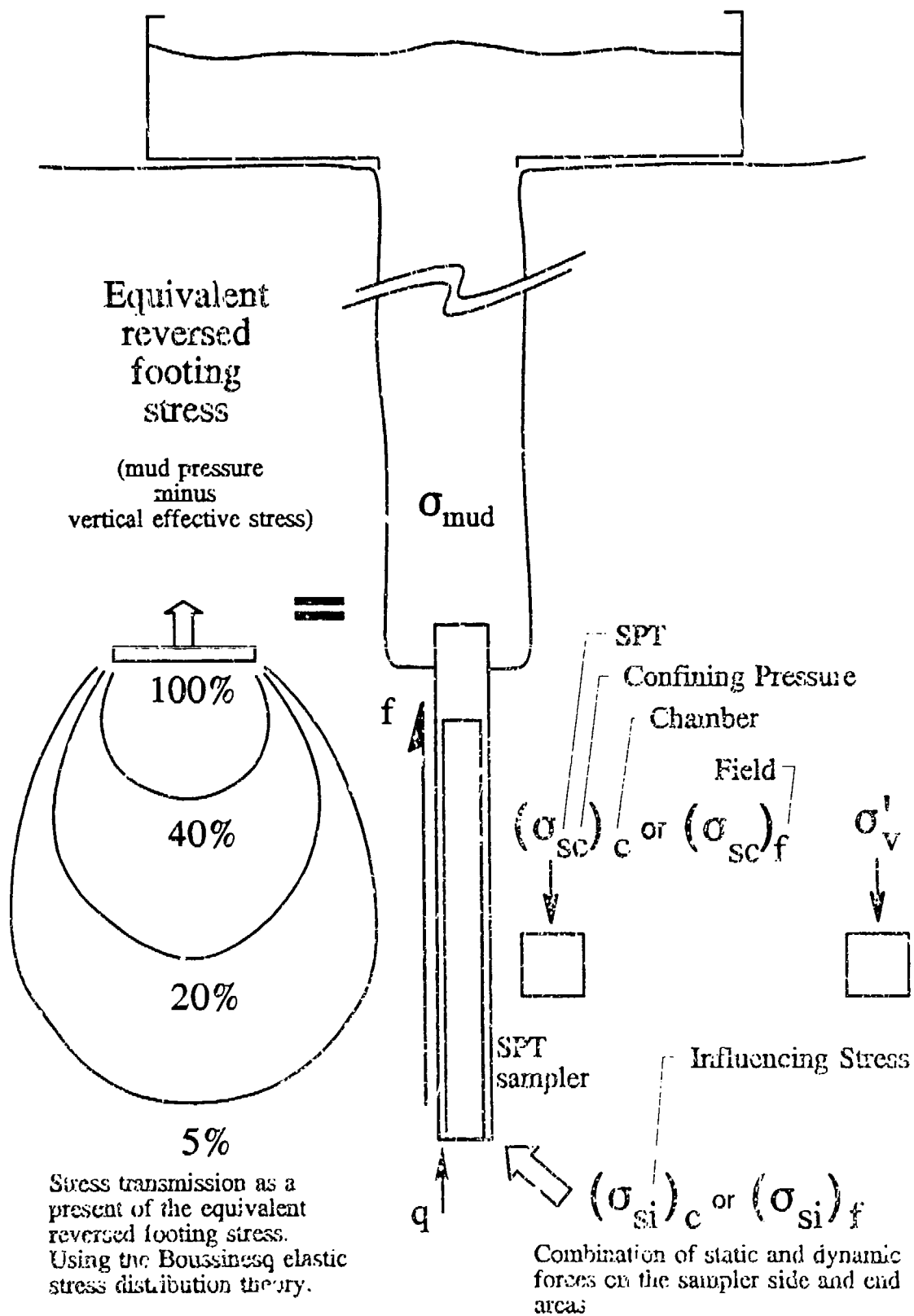


Figure 7.3 Mud pressure effects on the SPT sampler

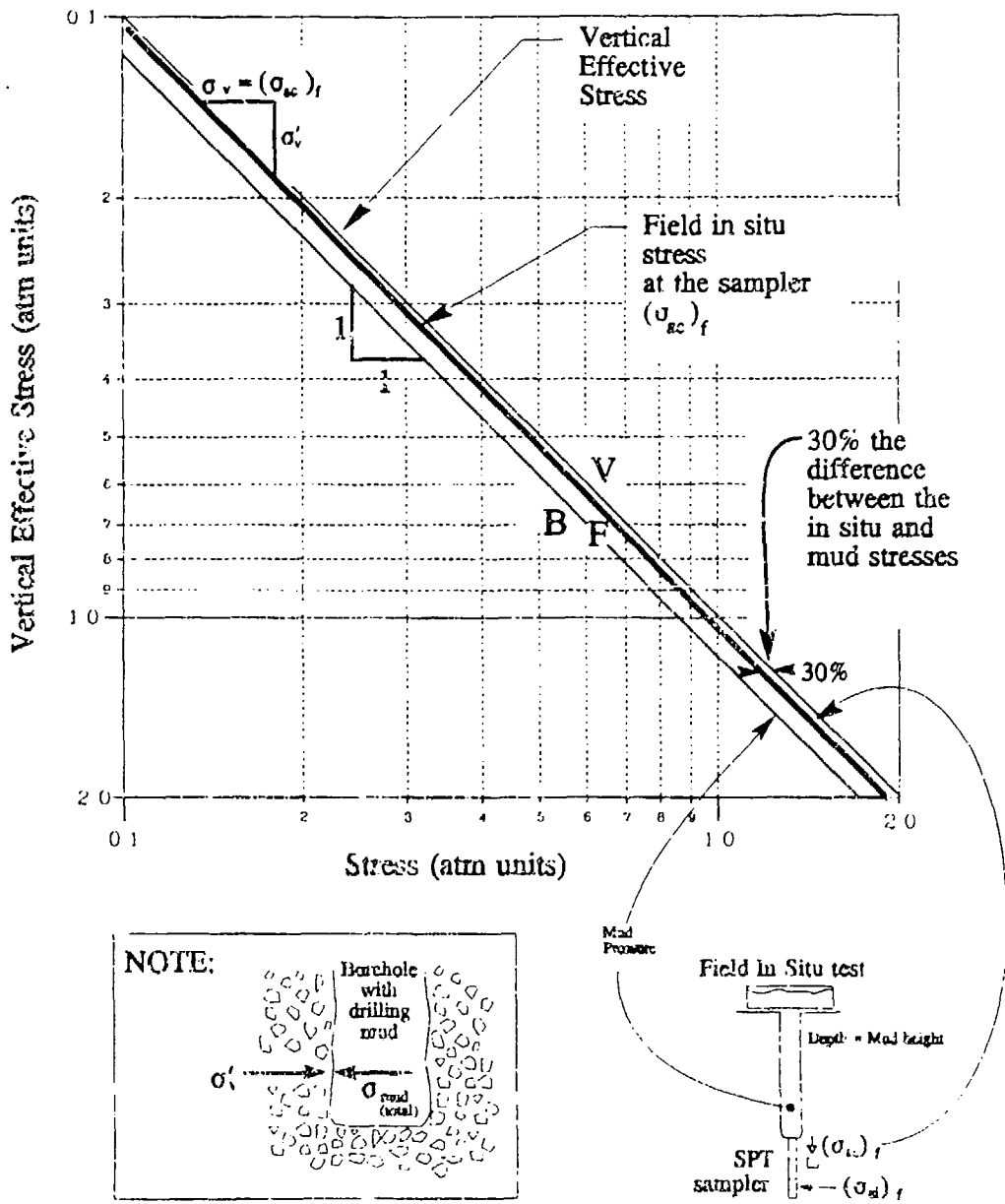


Figure 7.4 Drilling mud pressure effects for the SPT sampler in field boreholes

## *Stresses at the SPT Sampler for Chamber Testing Conditions*

SPT laboratory chamber tests have a constant borehole mud height for all chamber overburden stresses. This mud pressure is always equal to a 4 to 6 feet column of mud having an approximate pressure of 0.16 tsf as shown as Line M in Figure 7.5. The calculated confining stress at the SPT sampler for the chamber condition,  $(\sigma_{sc})_c$ , is shown as line C using the 30% mud pressure influence assumption previously discussed. The slope of Line C on the log log plot in terms of vertical effective stress is 0.70. Line C represents the relationship between confining stress surrounding the sampler (for chamber tests)  $(\sigma_{sc})_c$  and  $\sigma'_v$ .

SPT Chamber tests yield blow count versus  $\sigma'_v$  relationships that are analogous to the stress influencing the SPT sampler  $(\sigma_{si})_c$  versus  $\sigma'_v$ . From historic SPT chamber tests, this relationship between  $(\sigma_{si})_c$  and  $\sigma'_v$  has a SPT stress exponent of approximately 0.50. The 0.50 stress exponent is the average of 0.45 to 0.55 by Seed et al. (1983) or is the average of the range at a relative density of 60% from Chapter 5. A stress exponent is simply the log log slope as shown as Line L in Figure 7.5 for the  $(\sigma_{si})_c$  to  $\sigma'_v$ .

All the stress relationships that influence the SPT sampler have been described and are in terms of  $\sigma'_v$ . Line C (mud pressure influence) describes the reduced confining stress next to the SPT sampler  $(\sigma_{sc})_c$ , and line L (from interpretation of chamber tests) describes the stresses on the SPT sampler that influence the blow

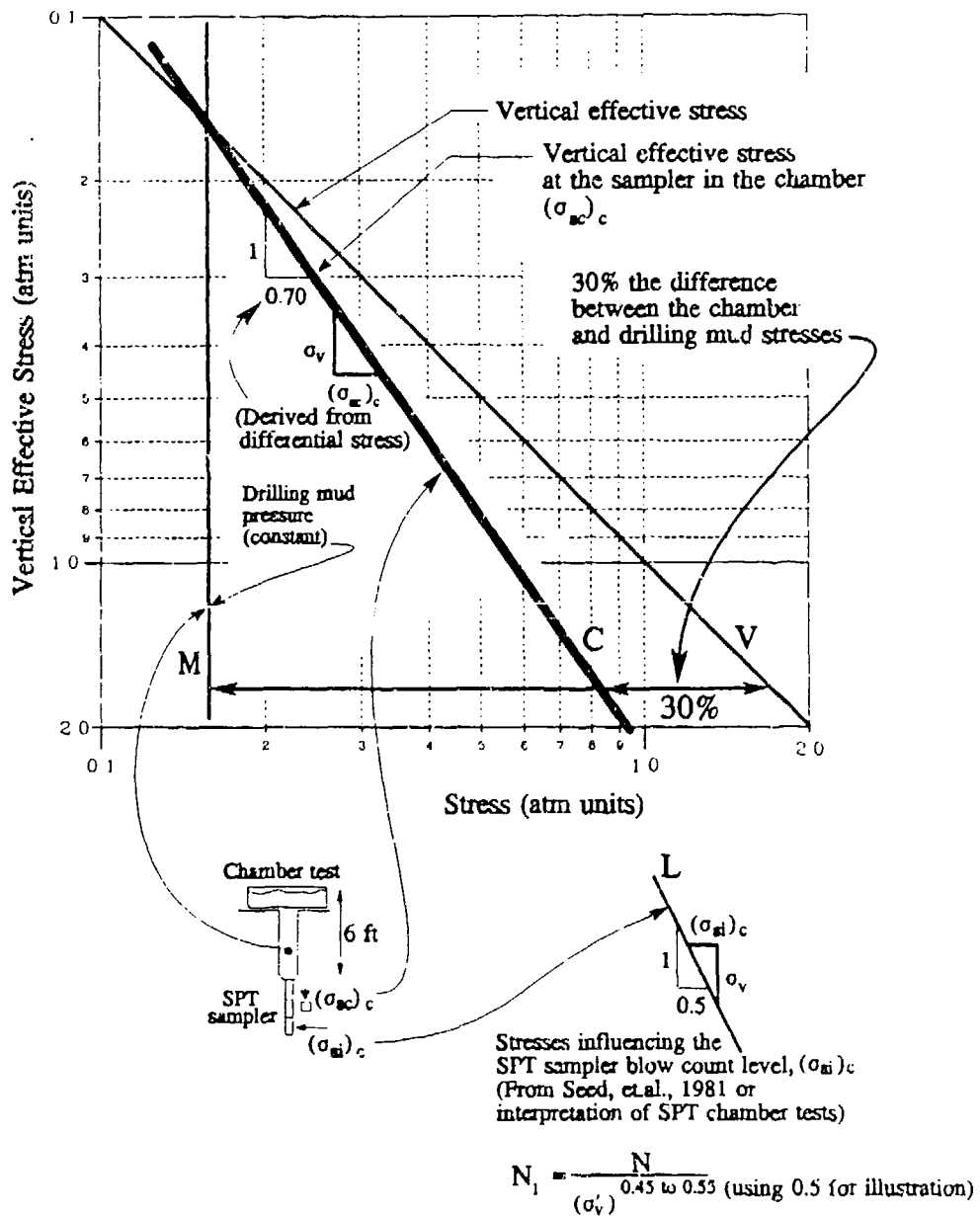


**Figure 7.5** Stress effects on the SPT sampler for historical laboratory chamber tests due to a constant drilling mud stress at differing confining stress levels

count,  $(\sigma_{si})_c$ . Both are in terms of vertical effective stress. Line C can be represented as;

$$C_1 = \frac{(\sigma_{sc})_c}{(\sigma'_v)^{0.70}} \quad (7.2)$$

where

- $(\sigma_{sc})_c$  = SPT sampler confining stress level  
for the chamber condition
- $C_1$  = normalized parameter (equivalent value at 1 Atm)

Likewise, Line L can be represented as:

$$L_1 = \frac{(\sigma_{si})_c}{(\sigma'_v)^{0.50}} \quad (7.3)$$

where

- $(\sigma_{si})_c$  = SPT sampler influencing stresses  
for the chamber condition
- $L_1$  = normalized parameter (equivalent value at 1 Atm)

Equations (7.2) and (7.3) can be combined to determine the ratio of stresses influencing SPT sampler (i.e. blow count) to the confining stress next to the SPT sampler:

$$C_1 = \frac{(\sigma_{sc})_c}{\left( \left( \frac{(\sigma_{si})_c}{L_1} \right)^{\frac{1}{0.50}} \right)^{0.70}} \quad (7.4)$$

with further reduction and condensing:

$$X_1 = \frac{(\sigma_{si})_c}{(\sigma_{sc})_c^{0.71}} \quad (7.5)$$

where

$X_1$  = combined normalized effect

This formulation relates the stresses influencing the SPT blow count,  $(\sigma_{si})_c$ , to the confining stress next to the SPT sampler in the chamber,  $(\sigma_{sc})_c$  with a stress exponent of 0.71. Equation (7.5) therefore relates the SPT blow count (as reflected by  $(\sigma_{si})_c$ ) to the actual confining stresses at the SPT sampler  $(\sigma_{sc})_c$ . For the field SPT condition, the confining stress next to the device is approximately equal to  $\sigma'_v$ . In both cases, SPT blow count is related to the confining stresses surrounding the SPT sampler as shown in Figure 7.6. For the field SPT condition, the confining stress is equal to the vertical effective stress ( $\sigma'_v$ ). However, for chamber SPT tests, the confining stress is equal to the mud pressure reduced confining pressure  $(\sigma_{sc})_c$ . The ultimate goal for field SPT normalization is a relationship of SPT blow count (N) to  $\sigma'_v$ . Equation (7.5) reflect this N to  $\sigma'_v$  relationship because the chamber reduced confining stress  $(\sigma_{sc})_c$  influences the SPT sampler just like the field  $\sigma'_v$  influences the SPT sampler. Therefore, the stress exponent of 0.71 in Equation (7.5)

(rather than 0.5 for Line L in Figure 7.5) is the correct stress exponent for field SPT situations. The next few paragraphs will show that the SPT field condition (i.e. SPT stress exponent) is equal to the CPT chamber conditions (i.e. CPT stress exponent).

A simple means of determining the stress exponent for  $(\sigma_{sc})_c$  based on the mud pressure reduction value and the chamber test stress exponent can be developed based on logarithmic construction with the result shown below:

$$b = \frac{n}{\left(1 - \frac{R_m}{100}\right)} \quad (7.6)$$

for

$$X_1 = \frac{(\sigma_{st})_c}{(\sigma_w)_c^b} \quad (7.7)$$

where

- b = Stress exponent for confining stress adjacent to SPT sampler
- n = Stress exponent determined from SPT chamber tests  
(from historic SPT chamber tests.)
- $R_m$  = Percent reduction of confining stress on the SPT sampler due to the mud pressure

Using the initial example of  $n=0.5$  and  $R_m=30\%$ , the result is  $b=0.71$  using Equation (7.6). For a loose sand, the mud pressure reduction ( $R_m$ ) at the SPT sampler could be 20% (low end of the range of 5 to 50% on page 137), the chamber stress exponent could be  $n=0.6$  (see Chapter 5), and the result is calculated to be  $b=0.75$ . For a dense sand, the reduction factor could be  $R_m=45\%$  (high end of the range of 5 to 50%), the chamber stress exponent could be  $n=0.22$  (see Chapter 5), and the result is calculated to be  $b=0.40$ . The average stress exponent ( $n$ ) for the



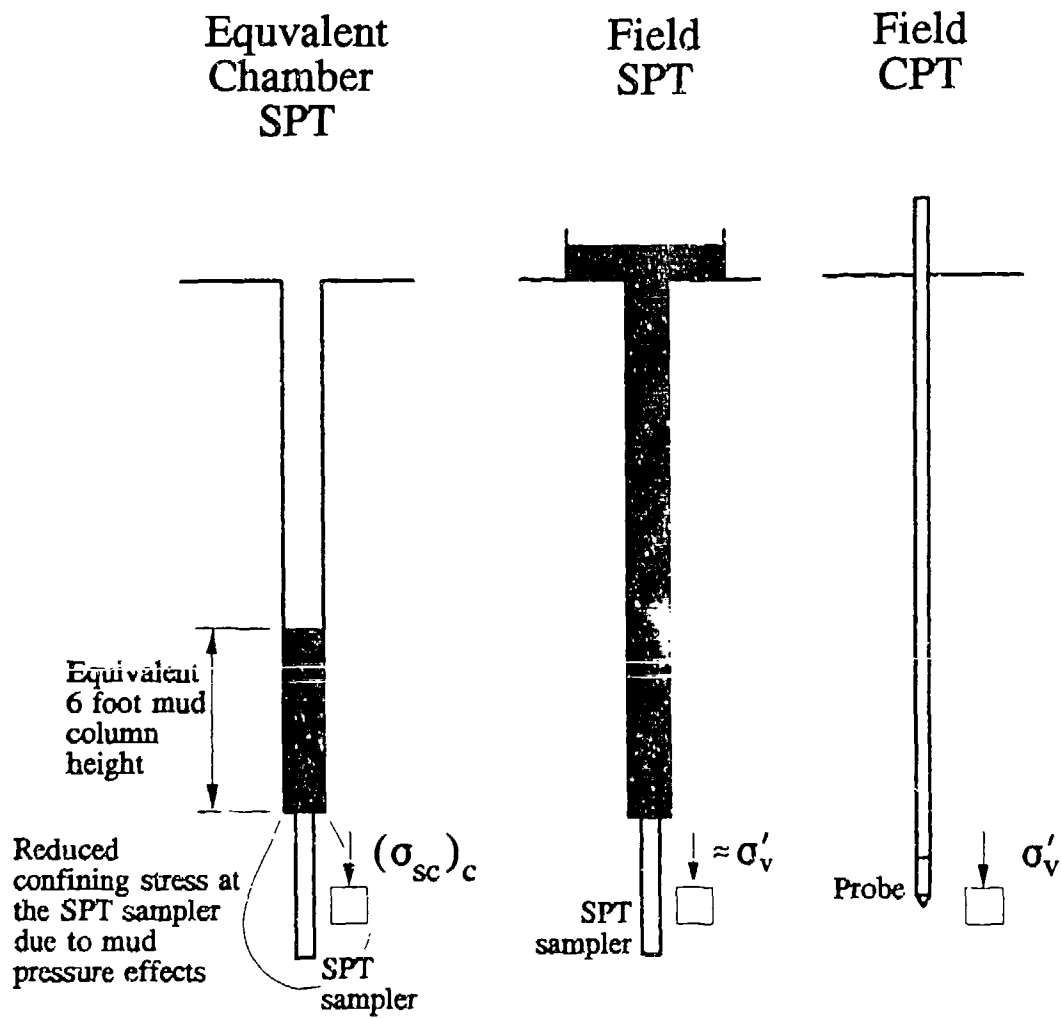


**Figure 7.6** Comparison of confining stress surrounding the SPT sampler (or CPT probe) for chamber and field conditions

SPT chamber stresses influencing the sampler  $((\sigma_{si})_c)$  to  $\sigma'_v$  for these three examples is approximately 0.44; which is at the lower range of the Seed, et al. (1983) range of 0.45 to 0.55. The stress exponent (b) for the SPT field stresses influencing the sampler  $((\sigma_{si})_f)$  to  $\sigma'_v$  for these examples is approximately 0.62; which is within the range of 0.6 to 0.7 from CPT cone resistance chamber tests. For these examples, the difference between stress exponents (n) and (b) are specifically 0.21, 0.15, and 0.18, with an average of 0.18.

The difference between the CPT chamber stress exponents (c) and SPT chamber derived stress exponent (n) are shown in Figure 7.7 (taken from Chapter 6). This stress exponent difference (i.e. c-n) in Figure 7.7 is about 0.18, which is also the approximate difference between the SPT stress exponent (n) and (b) from the previous paragraph. If c-n approximately equals b-n then c=b. Therefore, the cone resistance stress exponent (c) equals the field based SPT stress exponent (b). This is additional evidence that the CPT cone resistance stress exponent (c) is the correct SPT stress exponent for field SPT data normalization.

### *Conclusion*

The Seed SPT stress exponents of 0.45 to 0.55 are in error because of mud pressure influences for chamber tests at high confining stresses. Drilling mud pressures at the SPT sample in chamber tests are too low compared to those that exist in the field. The best stress exponent for SPT normalization is the CPT cone resistance stress exponent. The CPT cone resistance stress exponent also falls within the range of back-calculated  $C_N$  in Figure 7.2. Chapter 6 introduced a technique and chart for determining the CPT cone stress exponents using field CPT data from which the SPT normalization stress exponents can be taken as well. To determine the best stress exponent for SPT stress normalization therefore requires a nearby CPT sounding where CPT stress exponent can be estimated.

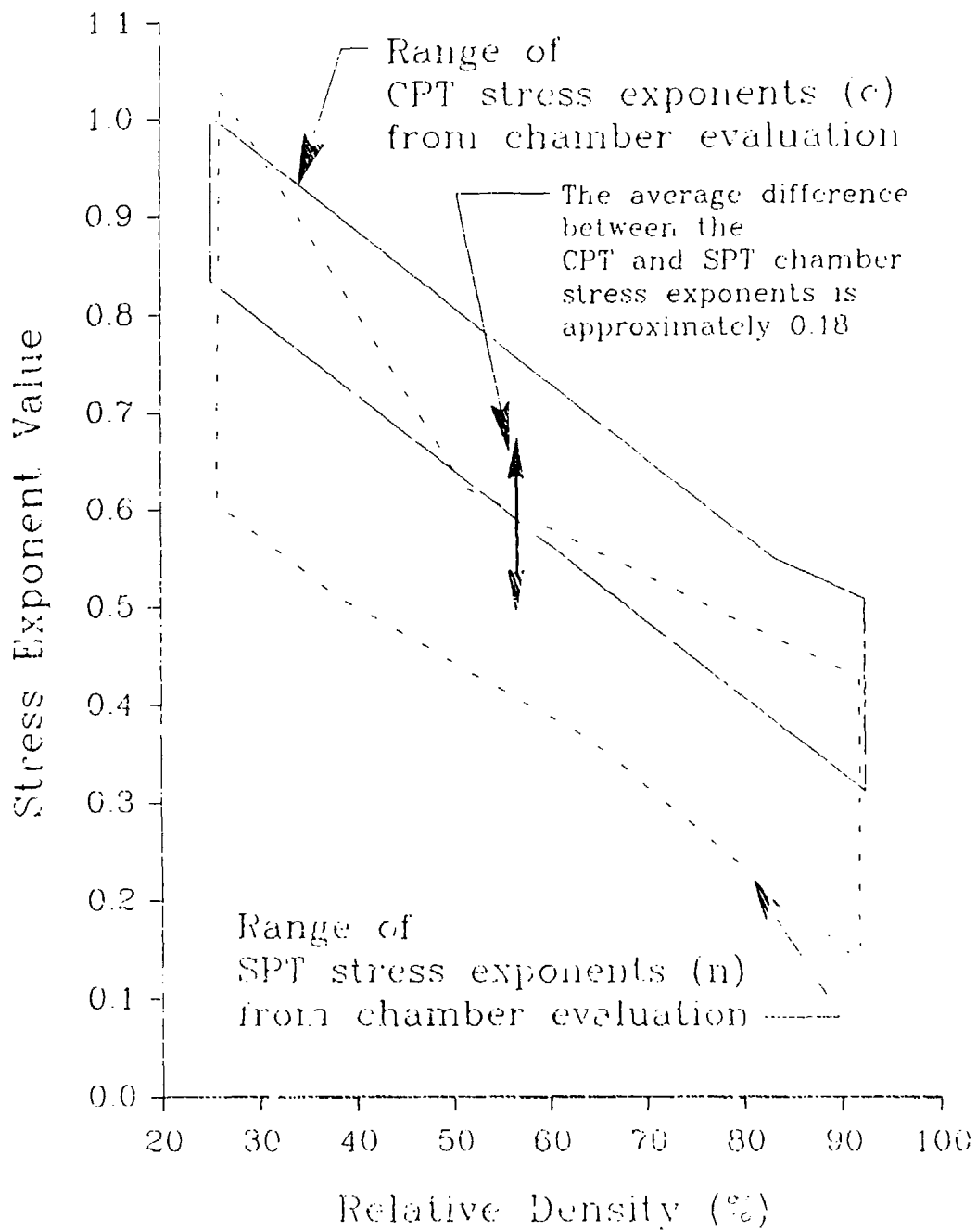


**Figure 7.7** Comparison of the ranges for CPT and SPT stress exponents from evaluation of chamber data

# Normalization of the Shear Wave Velocity

## *Introduction*

CPT prediction of shear wave velocity requires a good technique for normalization of the shear wave velocity—and the shear wave velocity normalization requires a technique for estimating the shear wave velocity stress exponent. Correlations for CPT prediction of shear wave velocity will be developed in Chapter 8. A shear wave velocity normalization formulation must be simple (following the stress normalization concepts from Chapter 3) and be relatable to previously proposed formulations. A variable shear wave velocity stress exponent will be introduced and shown to be dependent on soil type, and predictable using the CPT cone resistance stress exponent.

This shear wave velocity normalization formulation should also be based on the maximum shear modulus formulation because the two are theoretically related. The first step will be to introduce the maximum shear modulus formulation and then show that the historical formulations can be related to it. The next step is converting the normalized maximum shear modulus formulation to the normalized shear wave velocity formulation. The final step is to correlate historical stress exponents for the wave velocity to the stress exponent for the CPT cone resistance.

### *Definition of Normalized Maximum Shear Modulus*

Using the stress normalization concepts in Chapter 3, the normalized maximum shear modulus can be defined as (Olsen, 1988):

$$G_{\max} = (G_{\max})_1 (\sigma_v)_{\text{atm}}^m \quad (7.8)$$

where

- $G_{\max}$  = shear modulus (in Atm units)
- $(G_{\max})_1$  = Normalized shear modulus at an equivalent vertical effective stress of 1 atmospheric pressure
- $m$  = Shear modulus exponent value

This equation requires verification that it does represent a generalized maximum shear modulus formulation. Verification is shown in Table 7.1;  $(G_{\max})_1$  are shown that are derived from historic maximum shear modulus formulations. The next step is converting  $(G_{\max})_1$  to a normalized shear wave velocity ( $V_s$ ) using theoretical relationships.

### *Relating Maximum Shear Modulus to Shear Wave Velocity*

For linear elastic behavior, the maximum shear modulus is theoretically related to shear wave velocity,  $V_s$ , (Telford, et.al., 1976) as shown below:

$$G_{\max} = \rho V_s^2 \quad (7.9)$$

where

- $V_s$  = Shear wave velocity (in units consistent with  $G_{\max}$  and  $\rho$ )
- $\rho$  = Mass density

Table 7.1 Showing the equivalent  $(G_{max})_1$  from historic  $G_{max}$  formulations

Reference	Historic $G_{max}$ formulations	Derived $(G_{max})_1$ for
Hardin & Black (1969)	$G_{max} = 1230 \frac{(2.973 - e)^2}{1 + e} OCR^k (\sigma'_m)^{0.5}$	$(G_{max})_{atm} = (G_{max})_1 (\sigma'_v)^m$ $1230 \frac{(2.973 - e)^2}{1 + e} OCR^k \left( \frac{1 + 2K_0}{3} \right)^{0.5} \left( 14.7 \frac{psf}{atm} \right)^{0.5}$
Hardin & Richard (1963)	$G_{max} = A F(e) (\sigma'_m)^k$	$A F(e) \left( \frac{1 + 2K_0}{3} \right)^k \left( 14.7 \frac{psf}{atm} \right)^{1-k}$
Seed and Idriss (1970)	$G_{max} = 1000 K_2 (\sigma'_m)^{0.5}$	$1000 K_2 \left( \frac{1 + 2K_0}{3} \right)^{0.5} \left( 2116 \frac{psf}{atm} \right)^{-0.5}$

where

- $(G_{max})_1$  = Normalized maximum shear modulus (in atm units)
- $(\sigma'_m)_{psf}$  = mean stress in units of pounds per square foot (psf)
- $(\sigma'_m)_{psi}$  = mean stress in units of pounds per square inch (psi)
- $e$  = Void ratio
- CCR = Overconsolidation ratio
- $F(e)$  = function of the void ratio
- $A$  = soil fabric constant
- $k$  = stress exponent
- $K_2$  = shear modulus coefficient, in psf

This equation can be combined with the normalized shear modulus relationship (Equation (7.8)) to produce the following:

$$(G_{\max})_1 (\sigma'_v)_{atm}^m = \rho V_s^2 \quad (7.11)$$

where

$$(\sigma'_v)_{atm} = \text{Vertical effective stress in terms of Atmospheric pressure}$$

(mean stress ( $\sigma_{mean}$ ) is historically used in this place however  $\sigma_{mean}$  is simply equal to  $F_{mean} (\sigma'_v)$  (See Chapter 2) )

$$m = \text{Stress exponent for } G_{\max}$$

With simple rearrangement, shear wave velocity,  $V_s$ , is equal to:

$$V_s = \sqrt{\frac{(G_{\max})_1}{\rho} (\sigma'_v)_{atm}^{m/2}} \quad (7.12)$$

This is the basis for the normalized shear wave velocity formulation. The normalized shear wave velocity,  $V_{s1}$ , from Equation (7.12) is defined as:

$$V_{s1} = \sqrt{\frac{(G_{\max})_1}{\rho}} \quad (7.13)$$

with the shear wave velocity stress exponent ( $v$ ) equal to  $m/2$ . The normalized shear wave velocity formulation is therefore defined as the following, based on Equation

(7.12) and using Equation (7.13) with  $v=m/2$ :

$$(V_s)_{fps} = (V_{s1})_{fps} (\sigma_v')^v \quad (7.14)$$

where;

$v$  = Shear wave velocity exponent =  $\frac{m}{2}$

$(V_{s1})_{fps}$  = Normalized shear wave velocity in terms of feet/second  
 ( $V_{s1}$  can be defined in any velocity units)

### *Relationships of Shear Wave Velocity Stress Exponent to Soil Type*

Lee and Campbell (1985) presented generalized relationships of shear wave velocity versus depth based on 15 years of project work. This summary of shear wave data obtained for differing site conditions are in terms of log shear wave velocity versus log depth. The publication does not present the actual data; however, it presents the general trends and range based on the data. An example for firm natural soils is shown in Figure 7.8. These shear wave velocity verses depth trends were also represented as shown below;

$$V_s = K (d + c)^n \quad (7.15)$$

where

$V_s$  = Shear wave velocity, in units of ft/second

$d$  = depth, units of feet

$c$  = depth, accounts for the non-linear intersection of shear wave velocity at the ground surface

$n$  = depth exponent

$K$  = constant in terms of  $\text{fps}/\text{ft}^n$



The depth exponent (n) can be related to the shear wave velocity stress exponent (v), because depth is used to calculate the vertical effective stress from the effective unit weight ( $\gamma'$ ) as shown below;

$$(\sigma'_v)^v = (\gamma' H_{depth})^v = (\gamma')^v (H_{depth})^v \quad (7.16)$$

The vertical effective stress and depth parameters in Equation (7.16) both have the same exponent. Therefore the depth exponent (n) in Equation (7.15) is approximately equal to the shear wave velocity stress exponent (v), at least for normalization purposes. Lee and Campbell's (1985) data were summarized for soft natural soils, intermediate firm natural soils, and firm soils as shown in Table 7.2. The depth exponent (i.e. stress exponent) from this table will be related to soil type and the CPT cone resistance stress exponent at the end of this discussion.

**Table 7.2** Shear wave velocity parameters determined from data presented by Lee and Campbell (1985) for differing soil conditions

Soil classification	$V_s$ (ft/sec) at a depth of 20 ft ***	Depth exponent (n) for shear wave velocity ****
Soft natural soils	780	0.46
Intermediate firm natural soils *	950	0.43
Firm soils **	1300	0.1

\* Probably medium dense sands and medium stiff clays

\*\* Probably dense sands

\*\*\* Approximately  $V_{s1}$  at  $\sigma'_v = 1 \text{ Atm}$

\*\*\*\* Approximately equal to the shear wave velocity stress exponent (v)

### *Shear Wave Velocity Stress Exponent trend from a Sand Site*

Baldi, Brazzi, Superbo, Battaglio and Janiolekowski (1988) studied the measured shear wave velocities for Po River sands. These sands have a fines content (in terms

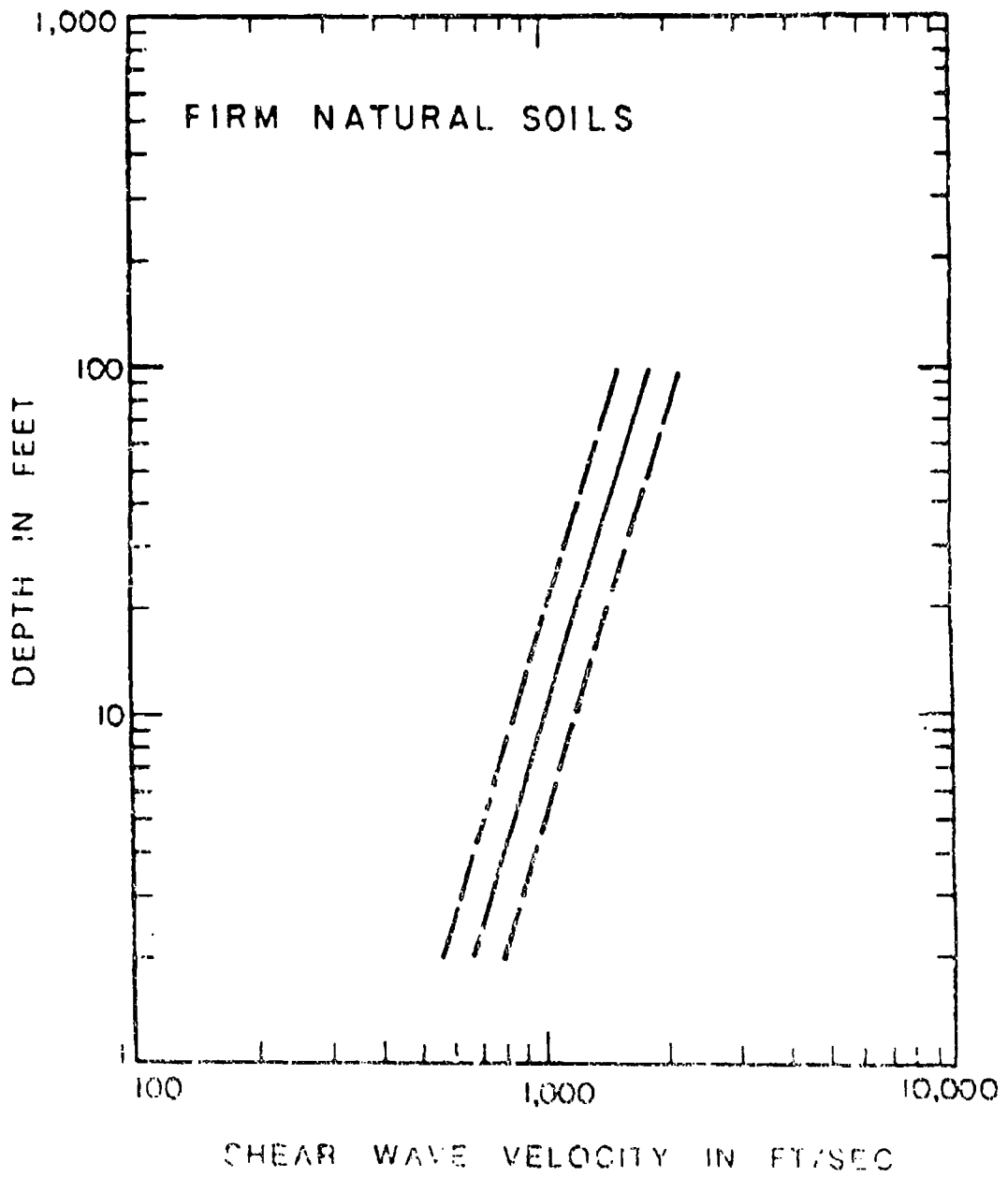


**Figure 7.8** Shear wave velocity versus depth for intermediate and saturated firm natural soils (Lee and Campbell, 1985)

of the percent passing the #200 sieve) ranging from 3 to 9%. They related overburden stress and maximum shear modulus in a form indexable to Equation (7.8) but also related fines content to the stress exponent (m) for the maximum shear modulus as shown below:

$$m = 0.43 + 0.39 \left( \frac{P_{200}}{100} \right) \quad (7.17)$$

where

- m = Stress exponent for the maximum shear modulus  
 P<sub>200</sub> = percent passing the #200 sieve as a percent

This equation can be expressed for the shear wave velocity stress exponent (v) as shown below, because (v) is theoretically equal to half of (m).

$$v = 0.215 + 0.195 \left( \frac{P_{200}}{100} \right) \quad (7.18)$$

For a clean sand (i.e. P<sub>200</sub>=0%) the shear wave velocity stress exponent (v) is 0.21 and for a sand with 10% fines content (P<sub>200</sub>=10%) the stress exponent (v) is 0.24. Therefore for the transition from clean sand to dirty sand, the shear wave velocity stress exponent changes from 0.21 to 0.24.

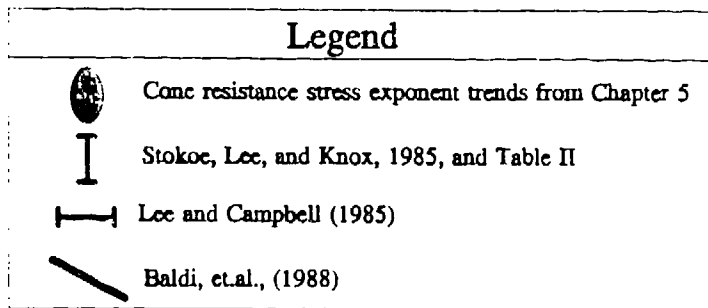
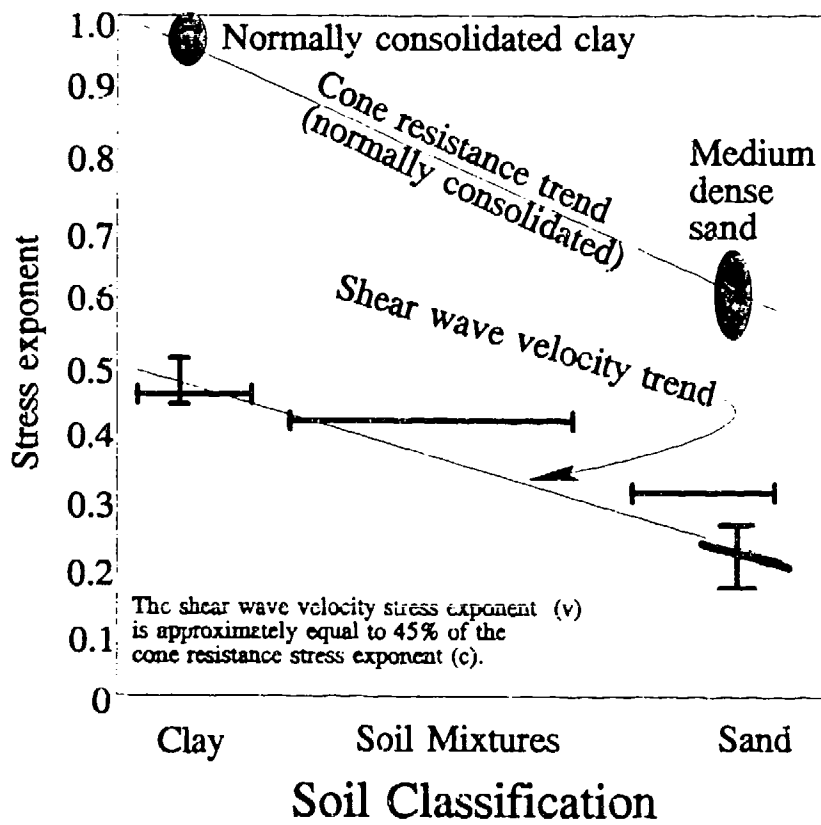
### *Relating Stress Exponents for Shear Wave Velocity & Cone Resistance*

Table 7.3 presents additional data relating the soil type to the shear wave velocity stress exponent from published sources and this research. The table indicates that the shear wave velocity stress exponent for clay ranges between 0.42 to 0.50 and for sands ranges between 0.18 and 0.28. These ranges from Table 7.3 together with the Baldi et al.(1988) and Lee and Campbell (1985) data are summarized in Figure 7.9

in terms of soil type. Also shown in this figure are typical cone resistance stress exponents from Chapter 6 based on soil type. The trends from Figure 7.9 indicate that the shear wave velocity stress exponent ( $\nu$ ) is approximately 45% of the estimated cone resistance stress exponent ( $c$ ). While this stress exponent prediction technique can only be considered an estimate, it represents the best method when there are no uniform layers to support establishment of a stress trend.

**Table 7.3** Published stress exponent for shear wave velocity

Basic soil type	Specific Soil type	$V_{s1}$ (ft/sec)	Stress exponent, $\nu$	Reference
Sand	Review of published dry sands		0.18 to 0.25	Stokoe, Lee & Knox, 1985
	Ottawa sand	equation	0.3	Hardin & Richart (1963)
	Ottawa sand	equation	0.25	Hardin & Richart (1963)
	Fine quartz	782	0.28	Hamilton (1971)
	Fine quartz	846	0.31	Hamilton (1971)
	coarse quartz	941	0.26	Hamilton (1971)
Clays (Normally Consolidated)	Clay		0.5	Hardin and Drnevich (1972)
	Alaskan clays	375	0.42	Singh & Gardner (1979)
Clays (Over Consolidated)	over consolidated Alaskan clay	1400	0.13	Singh & Gardner (1979)
	compacted sandy clay fill	420	0.09	Harding Lawson Assoc (1978)



**Figure 7.9** Comparing the stress exponent ranges for shear wave velocity and cone resistance

## *Conclusions*

The shear wave velocity stress exponent for normalization is related to soil type and can be estimated based on the CPT cone resistance stress exponent. The shear wave velocity ( $V_s$ ) stress exponent ( $\nu$ ) is approximately 45% of estimated cone resistance stress exponent ( $c$ ) (from Chapter 6). This procedure represents a new approach for normalizing shear wave velocity and seems to give good results. To successfully normalize the shear wave velocity, therefore, requires a nearby CPT sounding where the CPT stress exponent can be estimated and then converted to the shear wave velocity stress exponent ( $\nu$ ).

# Chapter 8

## Development of Correlations for CPT Prediction of Geotechnical Properties

### Introduction

One of the ultimate goals of using the CPT as a geotechnical investigation tool is direct prediction of geotechnical properties. Prediction of geotechnical properties using CPT data is illustrated in Figure 8.1; CPT data is normalized, the normalized geotechnical property is predicted, and finally the geotechnical property is calculated for the in situ stress condition.

Historically, research has concentrated on developing relationships between cone resistance and various geotechnical properties. In this chapter, CPT correlations using CPT cone resistance and sleeve friction resistance are developed for prediction of SPT blow count, clay undrained strength, and shear wave velocity. Several important ingredients were required for developing these correlations, namely 1) stress normalization techniques for the CPT (and geotechnical properties), 2) a large database of CPT and soil sample data, and finally, 3) accounting for bias data caused by soil profile differences between CPT soundings and borholes.

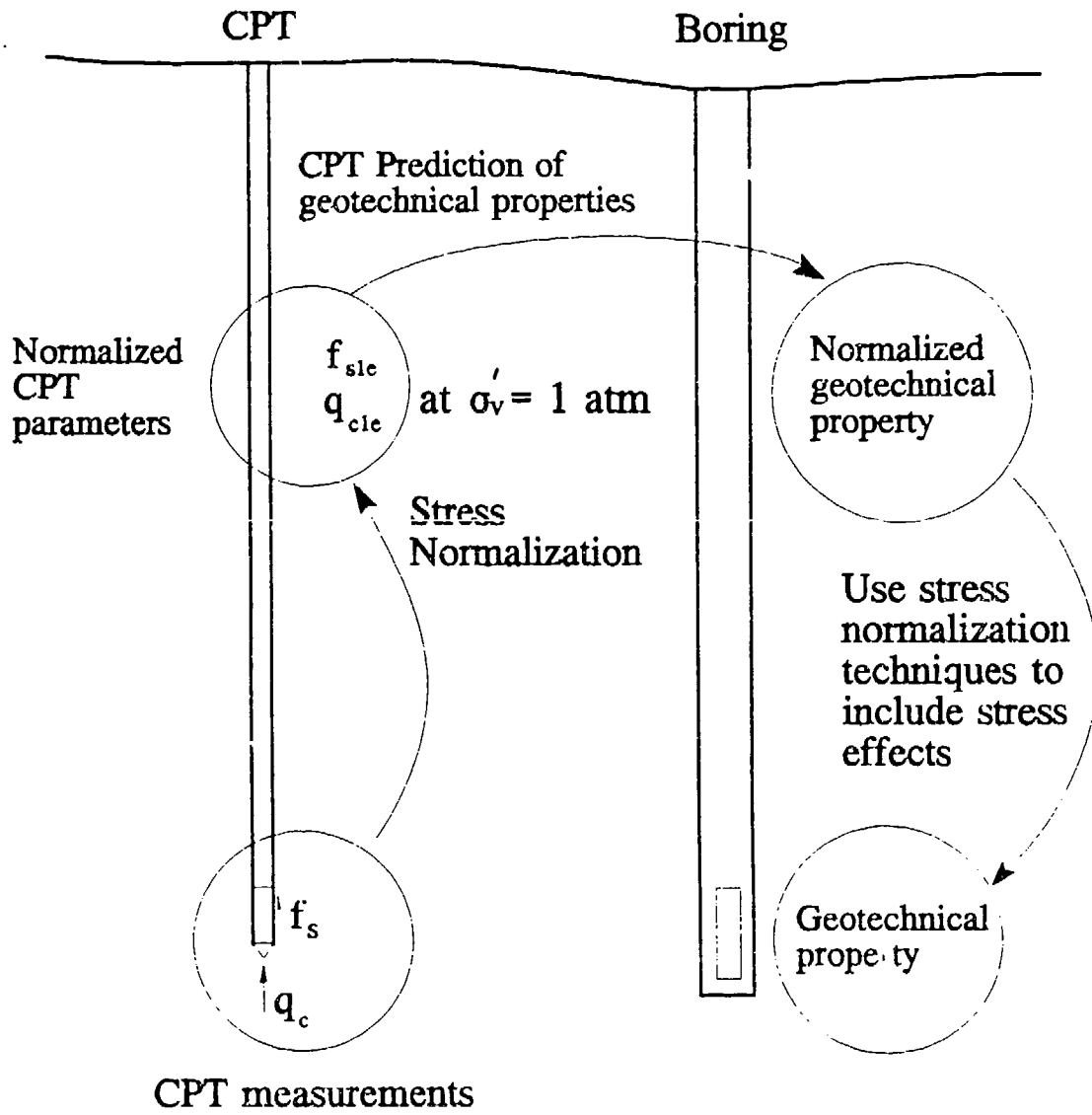


**Figure 8.1** Using CPT measurements to predict geotechnical properties



## The CPT and soil sample database

A large database of CPT and soil sample information that represents soils from around the world is described in the Appendix. This database contains data from approximately 90 projects, 670 CPT soundings, 580 borings, and approximately 8100 laboratory and field test values. The soils include weak clays in San Francisco, Sweden, Hong Kong, (and sensitive clays in Norway), liquefiable soil mixtures from China, stiff clays from South Carolina, and sands from Po River and desert alluvial sands from Nevada (this is only a partial list of the total database).

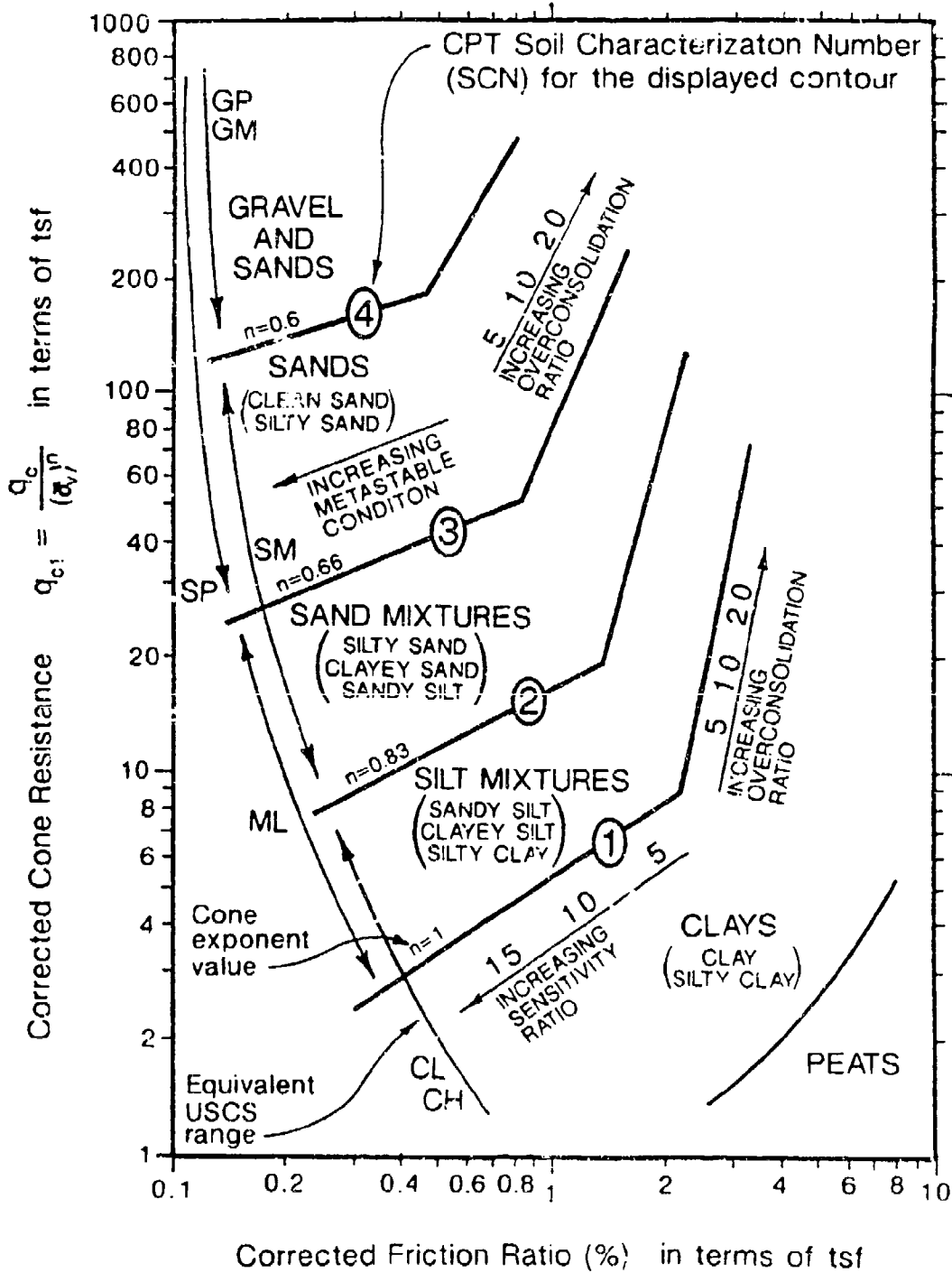
### Using the CPT Soil Characterization Chart to Predict Properties

Two measurements are always better than one when establishing a correlation. Moreover, the CPT provides two measurements which are unique, repeatable, and accurate. The CPT soil characterization chart shown in Figure 8.2 (Olsen, 1988) is based on normalized CPT measurements. This chart provides the means of characterizing soil behavior in terms of soil type and relative strength—the relative strength is in terms of increasing overconsolidation at one extreme and increasing clay sensitivity or a metastable condition in sand at the other extreme. While the underlying normalization technique for this chart was substantially improved as a result of the current research effort, the fundamental aspects of this chart are still valid. This chart therefore provides the two soil behavior indexes based on the normalized CPT measurements, namely soil type and relative strength consistency. The cone resistance stress exponent ( $c$ ) was shown in Chapters 5 and 6 to be inversely related to the relative strength (e.g. relative density for sands). In

Chapter 6, the stress exponent ( $c$ ) contours on the CPT soil characterization chart was demonstrated to be perpendicular to soil classification contours. Soil type and relative strength are independent of each other and this perpendicularity of soil type to stress exponent signifies independence. Consequently, any soil type and relative strength level combination will correspond to a unique point on this chart. Therefore, contours of geotechnical property levels can be established on the CPT soil characterization chart because the chart characterizes soil type and relative strength.

## Statistics and CPT Correlations

Statistical errors can be divided into three categories; systematic (bias) errors, random (variance) errors, and mistakes (Taylor, 1990). Random errors are fluctuation errors about the mean and are statistically characterized by the standard deviation. Bias errors are offset errors from the mean. For CPT data evaluation, bias errors are caused by stratigraphic soil type differences between CPT soundings and nearby boreholes. This type of bias error will be shown to account for most of the statistical error during CPT correlations. However, there is little written about bias errors (Taylor, 1990, Mosteller & Tukey, 1977, Huaslin, Mosteller, and Tukey, 1983). Therefore a subjective quality index and evaluation technique were developed to account for data having bias error. Reducing bias error effects represented the primary statistical evaluation effort used in establishing CPT correlations in this chapter.



$$FR_1 = \frac{f_{s1}}{q_{c1}} 100 = \frac{f_s / \bar{\sigma}_v}{q_c / (\bar{\sigma}_v)^n} 100 = \frac{f_s}{q_c} \frac{1}{(\bar{\sigma}_v)^{(1-n)}} 100$$

**Figure 8.2** CPT Soil Characterization chart in terms of the normalized cone resistance and normalized friction ratio (Olsen, 1988)

## *Bias Error Results from Stratigraphy*

There is always some geological difference between field CPT soundings and nearby boreholes at the same elevation. At a given elevation and for short lateral distances between a CPT sounding and a borehole (such as 10 to 25 feet) the following can be generally assumed; 1) the soil types may be different, 2) the formational environment is generally the same, 3) the vertical effective stress is constant, and 4) the vertical stress history (i.e. overconsolidation level) is generally the same. Soil type changes between CPT soundings and boreholes is therefore more likely the cause of bias error than differences in overburden stress, overconsolidation, or lateral stress. The potential for soil type change for a given elevation interval is dependent on the depositional environment; e.g. a lake or tailings deposit generally has uniform layers and lenses while a rapidly flowing, meandering river produces the most non-uniform deposit.

Stratigraphic soil type change (i.e. geologic change) is a bias error because it shifts the average and increases the variance—other types of random statistical errors only increase the statistical variance level without affecting the average. For example, clay lenses within a sand deposit will move the average downward to the clay trend and away from a sand trend as shown in Figure 8.3. Likewise, silt or sand seams within a clay deposit will create a higher average as also shown in Figure 8.3. Bias error direction is therefore different for clay and sand correlations (or dense/stiff and loose/soft correlations).

## *The Academic Quality Index (AQI)*

The Academic Quality Index (AQI) was developed during this research program as tool for accounting for bias error. It also provides a basis for weighting data from

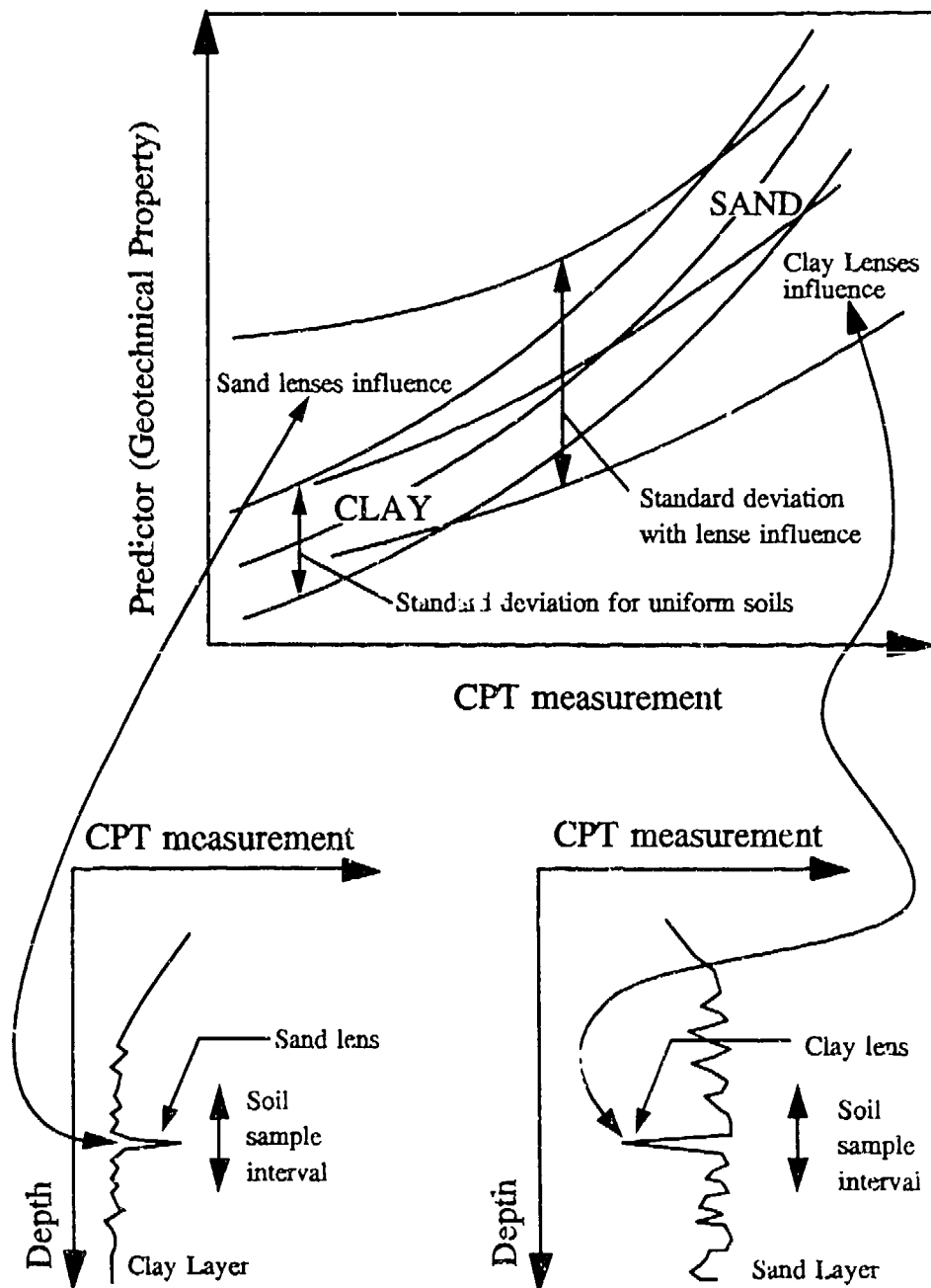


**Figure 8.3** Hypothetical example showing that soil lenses of differing soil type (or strength) can bias correlations

the different sites in the development of CPT to property correlations. This ranking scale is almost a universal scale because it's based on the student academic grading scale understood by all ages and professions. For example, data with average quality has an AQI of 76%, good data has an AQI of 80 to 85% and excellent data has a AQI of 90 to 95%. This index, while subjective, does allow excellent quality data to be isolated from good or poor quality data.

An Academic Quality Index (AQI) can be individually assigned for stratigraphic change potential, CPT work quality, and boring/laboratory quality. The overall CPT AQI is equal to the stratigraphic change potential together with any decreasing influence of measurement quality. The overall CPT AQI therefore reflects the potential for lateral matching of the soil type (and relative strength) between a excellent quality CPT sounding and adjacent quality borehole. Some of the commercial CPT data in the database has poor quality, for example, a high capacity cone used in weak/soft soil where a low capacity, high accuracy cone would have been more appropriate. If the CPT or laboratory testing data quality is not excellent, the overall AQI is less than the stratigraphic AQI. For example, if the stratigraphic continuity is excellent (i.e. AQI of 95%) but the CPT measurements are near the equipment noise level, the overall AQI might only be 80%. If there is little information about site geology or testing quality, then an overall AQI of 76% is assigned. While these are obviously arbitrary distinctions they are easily remembered and useable.

The stratigraphic AQI is based on a simple arbitrary system equal to the estimated percent of soil depth which are continuous between a CPT sounding and nearby borehole. For example, if 76% of the soil layers are continuous between a CPT sounding and borehole then the stratigraphic AQI is 76% as shown in Figure 8.4. This stratigraphic AQI must also account for the CPT-to-borehole distance because AQI will increase as the lateral distance decreases. For example, if the AQI is equal to 76% for a lateral distance of 20 feet, then the AQI might

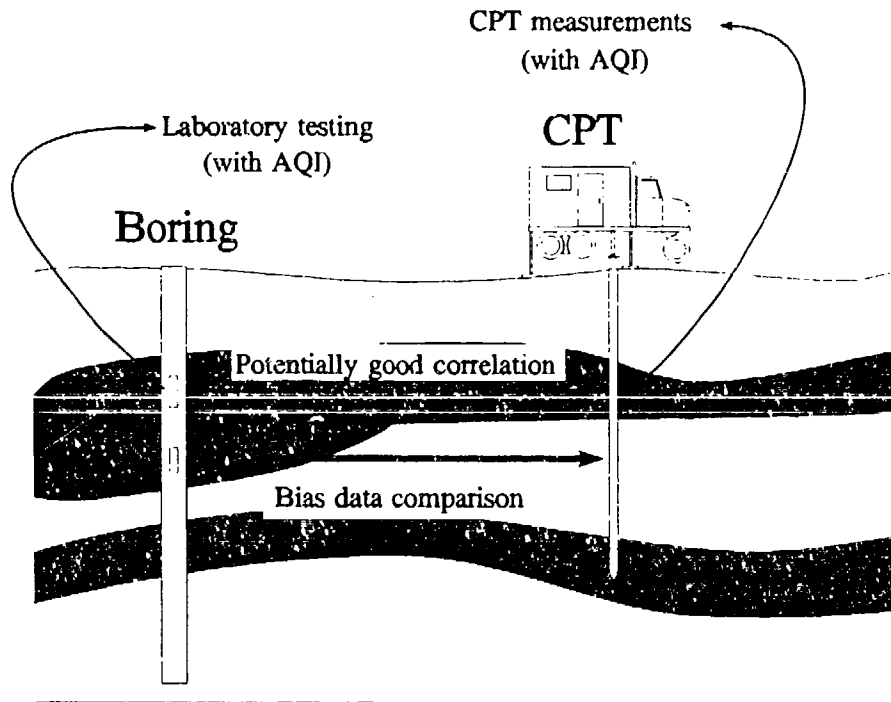


**Figure 8.4** Definition of a stratigraphic AQI of 76% (i.e. 76% of the soil layers are continuous between the boring and CPT sounding)

increase to 85% for a distance of 10 feet. Research sites with thick uniform horizontal deposits can have a stratigraphic AQI of 95% for CPT-to-borehole spacings of 20 feet.

Overall AQI values were assigned for each geotechnical project in database based on the concepts just described. The overall AQI values are shown in the fourth column of table A-1 in the Appendix.

## Developing CPT Predictive Contours

Consider the non-linear response surface based on two dependent parameters as shown in Figure 8.5. The two dependent parameters are the X and Y axis with the contoured (predictive) response surface (or blanket or contours) in the Z direction. This response surface is always non-linear in geotechnical engineering and can be determined by fitting the data points in the 3 dimensional space using gridding techniques (Box and Draper, 1987) if the data noise (i.e. error distribution) is random. Contouring techniques do not account for bias error. The next section will describe a technique using the AQI quality index for establishing the best fit correlation for each contour by excluding biased data. The response surface (i.e. set of contours) is established by separately generating each individual contour and then combining all the contours. Each contour was developed using 2D data scatter plotting software program while also accounting for the shapes of the other contour levels.



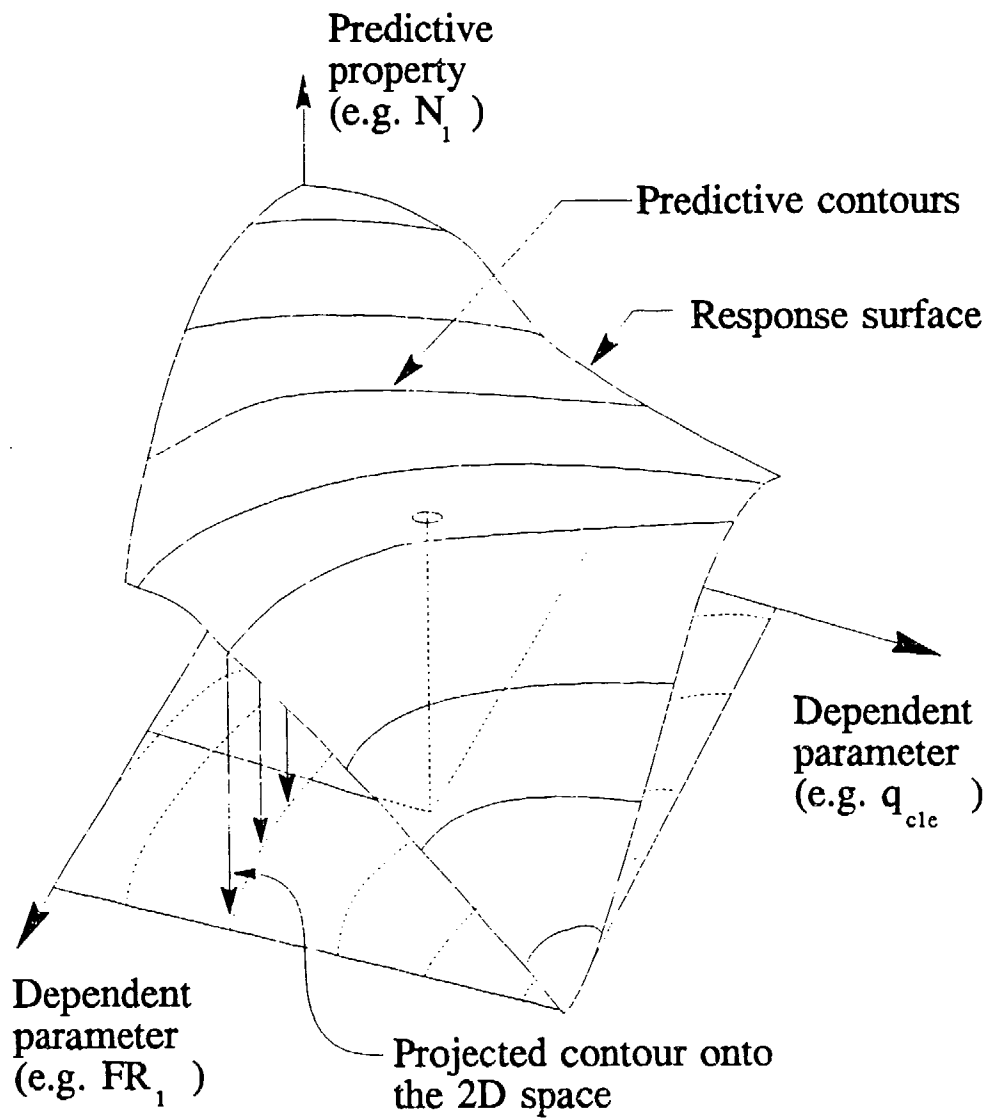


Figure 8.5 Description of a response surface

### *Process for developing CPT Predictive Contours*

Developing contours of geotechnical properties on the CPT soil characterization diagram required numerous steps that are described in this section. All data for a given geotechnical property are extracted from the database and placed into a single sequential computer file list (composed of normalized CPT measurements and corresponding normalized geotechnical properties). Also included in each list are the AQIs for each CPT to geotechnical property comparison. The list is then imported into a spreadsheet for the goal of creating scientific graphics. This spreadsheet data list is initially sorted by the data column having the geotechnical property. The spreadsheet data list is then divided into 6 to 7 geotechnical property level groups (i.e. 100 to 200, 200 to 400, 400 to 800, etc.) for the purpose of establishing CPT based correlations based on data groups. Each of these geotechnical property level groups is then individually sorted based on the AQI column. This final sort differentiates potentially biased data from good data for each geotechnical property level group. To establish a trend for a given geotechnical property level data, all or part of the data within each data group can be plotted. The best correlations (i.e. contours) are established by using the highest quality data which means using the highest AQI level for each data group.

### *Use of the AQI for Developing Predictive Contours*

A low stratigraphic AQI implies a higher likelihood for soil type change between a CPT sounding and borehole. When a group of data having a minimum AQI of, for example, 80% is used for a correlation then this is defined as the "minimum inclusionary AQI" of 80%. If all data is included for a correlation then the minimum inclusionary AQI is zero. By increasing this minimum inclusionary AQI, low quality biased data is excluded and the predictive correlation will shift away from the biased

data. If the minimum AQI is raised too high, there will be insufficient quantity of data to develop a trend. For a particular data set, the optimum AQI might be 85% but if this minimum AQI is increased to 95%, there might only be 2 points which may not be enough data to establish a trend. For a given predictive property the minimum inclusionary AQI must therefore be carefully increased until the optimum trend is established.

An illustrated example will show how the inclusionary AQI concept is used to determine a best fit contour. Consider a hypothetical data range for a normalized shear wave velocity ( $V_{s1}$ ) of 300 to 500 feet/second (fps) (with an average of 400 fps) shown in Figure 8.6-a. The displayed data points represent data having a  $V_{s1}$  between 300 and 500 fps and are plotted in terms of  $q_{c1e}$  versus  $f_{s1e}$ . A  $V_{s1}$  of 400 fps can be considered at the low range typically considered in geotechnical engineering (i.e. 300 to 2000 fps). Therefore, biased data for 400 fps data will tend to skew the average to higher  $q_{c1e}$  and  $f_{s1e}$  levels. The total data in Figure 8.6-a can be divided into two inclusionary AQI ranges (as shown in Figure 8.6-b) in terms of the data range and average for each inclusionary AQI range. With increasing inclusionary AQI ranges, the lower quality data is excluded and the average moves away from the skewed group average. Figure 8.6-c is probability distribution along a cut through the data set in Figure 8.6-b to show how increasing the inclusionary AQI moves the data average by excluding biased data.

The next example is taken from the next section on CPT prediction of the normalized SPT  $N_1$ . All data from the database for SPT  $N_1$  ranging from 1 to 3 (average of 2) are shown in Figure 8.7. For sands, a SPT  $N_1$  of 2 is considered a loose sand and therefore can be biased by dense and medium dense sand layers. When the minimum inclusionary AQI is raised to 89% (shown with solid circles in Figure 8.7), only the best data are included and clearly show a correlation at the lower boundary of the total data scatter.

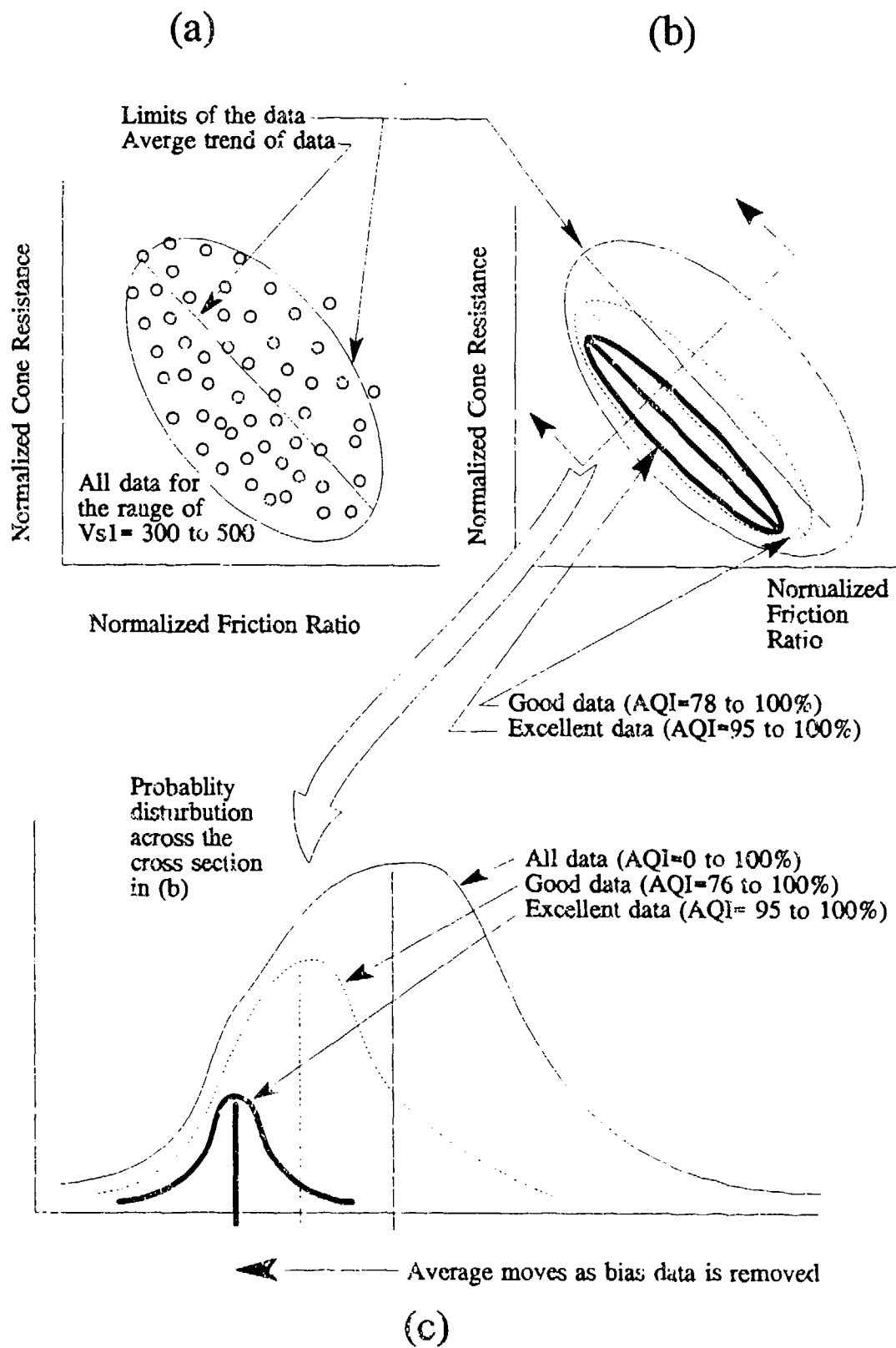


**Figure 8.6** An illustration of the iterative technique for removing bias data using the AQI index

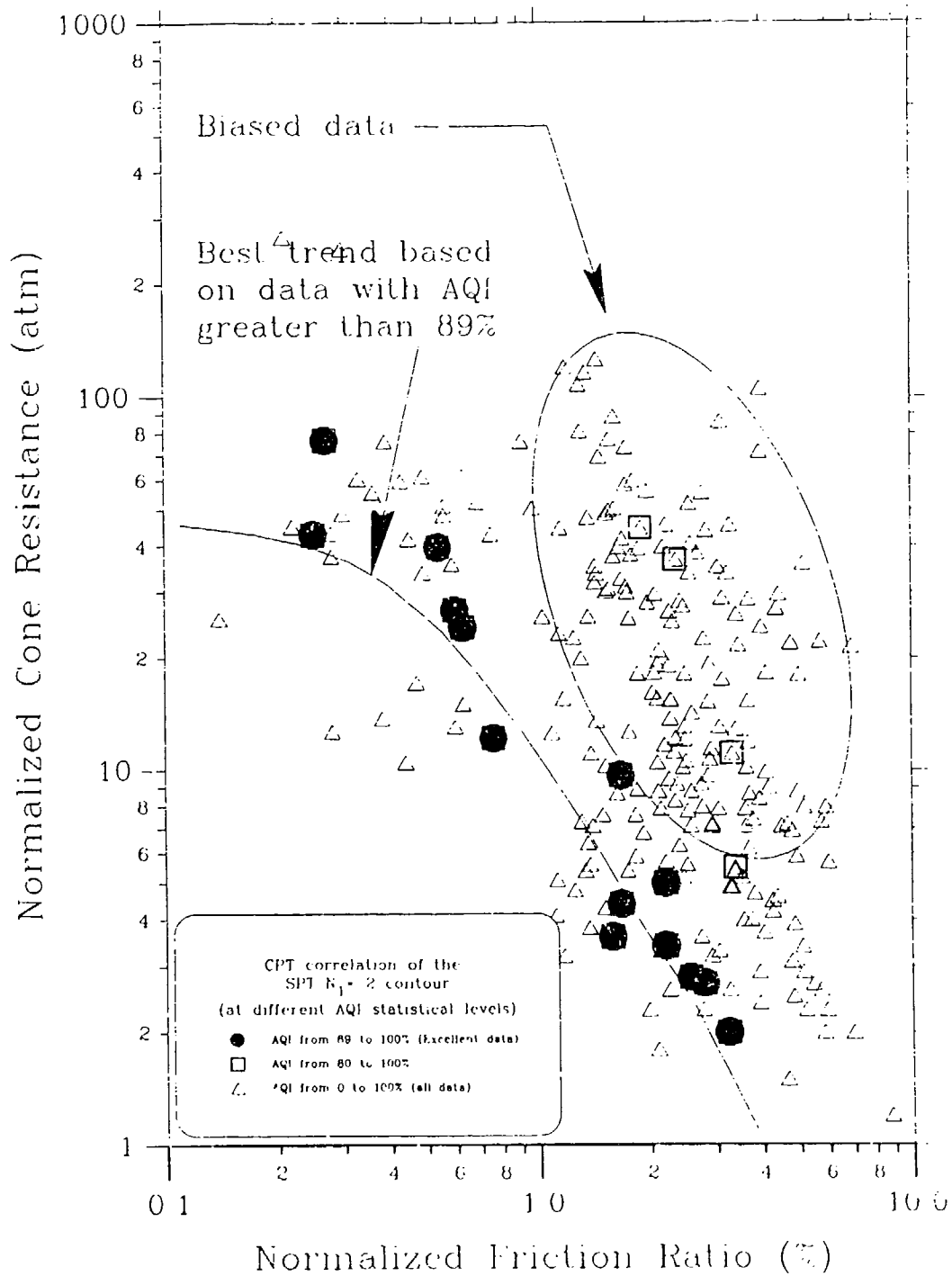


**Figure 8.7** Example using the Academic Quality Index (AQI) toward establishing the best correlation line by excluding biased data

# CPT Prediction of the SPT blow count

## *Introduction*

Prediction of the Standard Penetration Test (SPT) blow count using CPT data is a complex task because the SPT sampler resistance during penetration is dependent on the combination of end bearing and side friction forces which are dependent on soil type and soil strength (Douglas, et.al., 1981). The SPT sampler is resisted by the same types of forces that are measured by the CPT, therefore using both CPT measurements to predict the SPT blow count (Schniertmann, 1979a) is a better approach than using only the ratio of cone resistance to SPT blow count (e.g.  $q_c/N$ ). The forces acting on the SPT sampler are reflected in the final CPT-to-SPT correlation if both CPT measurements are used for the evaluation.

It was shown in Chapter 7 that the historic SPT stress exponents (i.e. 0.45 to 0.55) for normalization are incorrect and the actual values are equal to the CPT cone resistance stress exponents. This also implies that the SPT normalization is dependent on soil type and relative strength consistency as is the CPT normalization (Chapter 6).

Historically, there have been two general techniques for CPT prediction of the SPT blow count; 1) the  $q_c/N$  ratio to predict the SPT  $N$  (Rodin, et.al., 1974, Robertson, et.al., 1983, Seed and De Alba, 1986, Kuehawy and Mayne, 1990), and 2) using both CPT measurements to predict the normalized SPT  $N_1$  (Olsen, 1984, 1986, 1988). What differentiates these two techniques is that the first technique is based on an empirical correlation and the second technique indirectly accounts for the end bearing and side friction forces that act on the SPT sampler.

### *SPT Prediction using Both CPT Measurements*

Research indicates that the resisting stresses on the SPT sampler are analogous to the CPT stresses as shown in Figure 8.8 (Schmertmann, 1979a). McLean, Franklin, and Dahlstrand (1975) developed a computer model of the dynamic forces influencing SPT sampler based on work by Schmertmann (1971). Douglas, Olsen and Martin (1981) also developed a computer model to predict SPT using the CPT measurements based on work by Schmertmann (1979a, 1979b) in terms of the static and dynamic forces on the SPT sampler. This work evolved to a technique of predicting the SPT blow count which uses both CPT measurements (Olsen, 1984) with the most recent published version shown in Figure 8.9 (Olsen, 1988). However, in 1987, there was no realistic means of showing the data that was used to develop the contours of SPT  $N_1$  on the CPT soil characterization chart. Also, the database for this research program is approximately 7 times larger than existed in 1987 for developing SPT  $N_1$  contours.

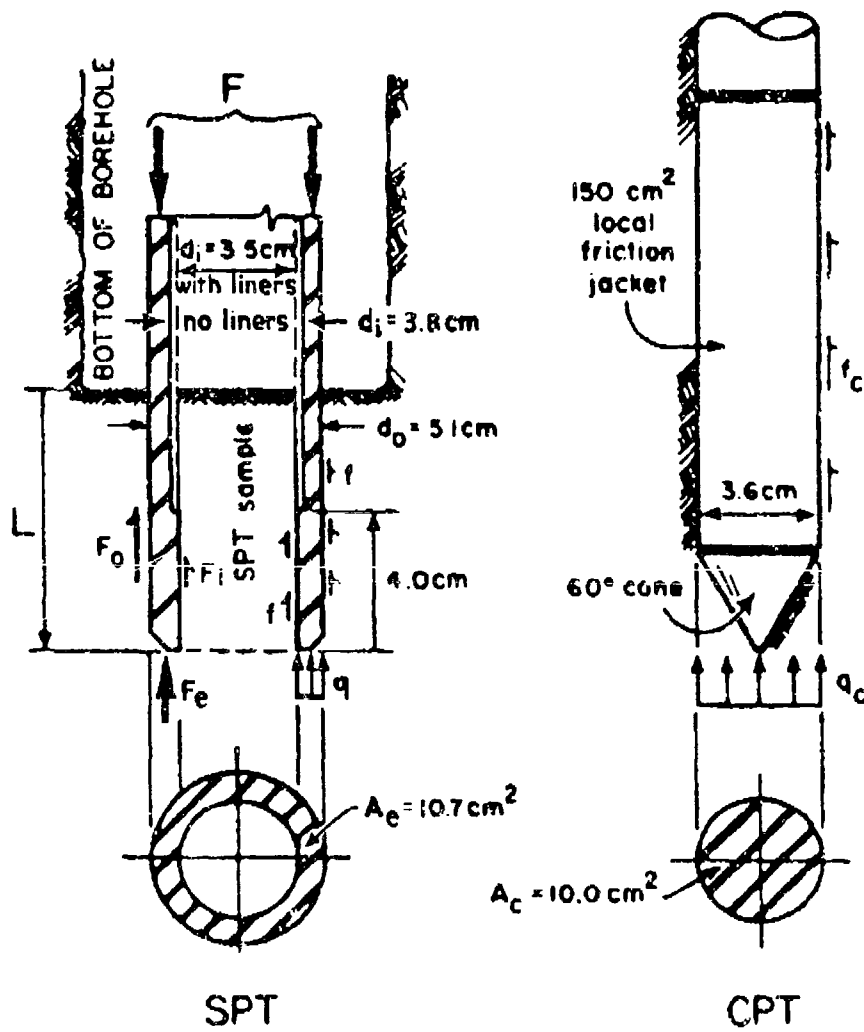


**Figure 8.8** Comparison of forces on the SPT and CPT devices (Schmertmann, 1979a)



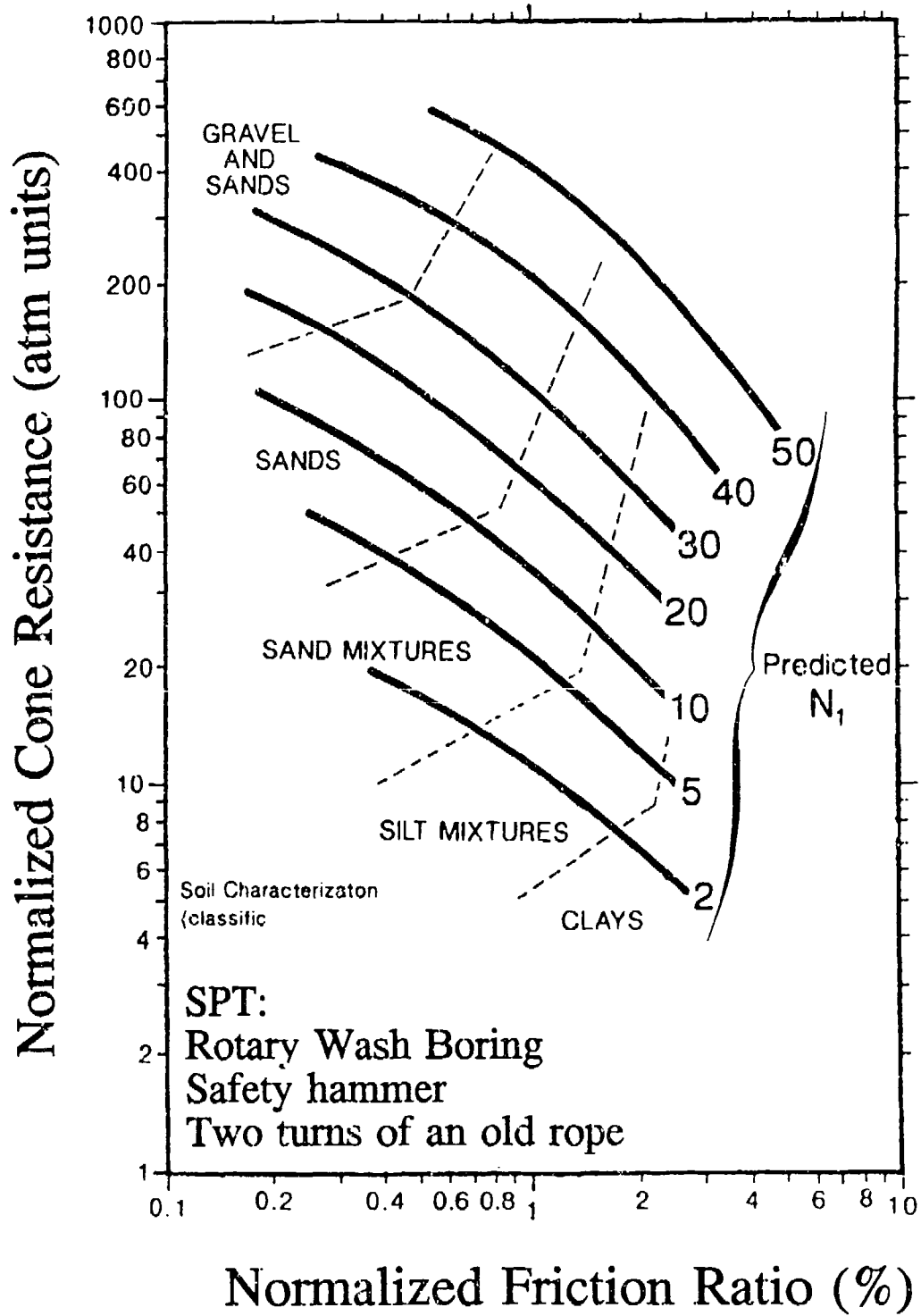


**Figure 8.9** Prediction of the SPT blow count,  $N$ , using both CPT measurements (Olsen, 1988)

### *CPT Prediction of $N_1$ using the CPT Soil Characterization Chart*

Establishing correlations of normalized CPT parameters to SPT  $N_1$  was found to be very dependent on the AQI statistical technique. AQI was used to remove biased data effects thereby allowing the best correlation of CPT to SPT. All SPT data from the database, for all projects, were divided into seven  $N_1$  ranges for the purpose of establishing individual correlation contours on the CPT soil characterization chart. The results of the SPT  $N_1$  correlations are shown in Figure 8.10 to Figure 8.16 for average  $N_1$  levels of 2, 4, 7, 15, 25, 35, and 50. The best fit correlation contour in each figure was based primarily on highest inclusionary AQI but also accounted for the lower quality data together with the shape of the other SPT  $N_1$  contour groups. Figure 8.17 shows all the SPT  $N_1$  predictive contours together with soil classification lines from Olsen (1988).

### *Discussion of CPT Prediction of the SPT Blow Count*

The new contours for predicting normalized SPT blow count (Figure 8.17) in general have more curvature compared to the 1988 version (Figure 8.9); however, for friction ratios less than 0.5%, the contours are parallel to cone resistance, which was not expected. The contour shapes and intervals for the 1988 version are symmetric due to the lack of data; newer version contour shapes and intervals are not in general symmetric. The shape of the contours for the newer version reflect soil type and relative strength contribution. Within the sands area of the chart for friction ratios less than 0.5%, the contour shapes and intervals are symmetric. Within the clay area of the chart (from normally consolidated to overconsolidated), the contour shapes and intervals are also symmetric. However, the contour shapes are changing in the middle of the chart within the soil mixture area (transition between clays and sands).

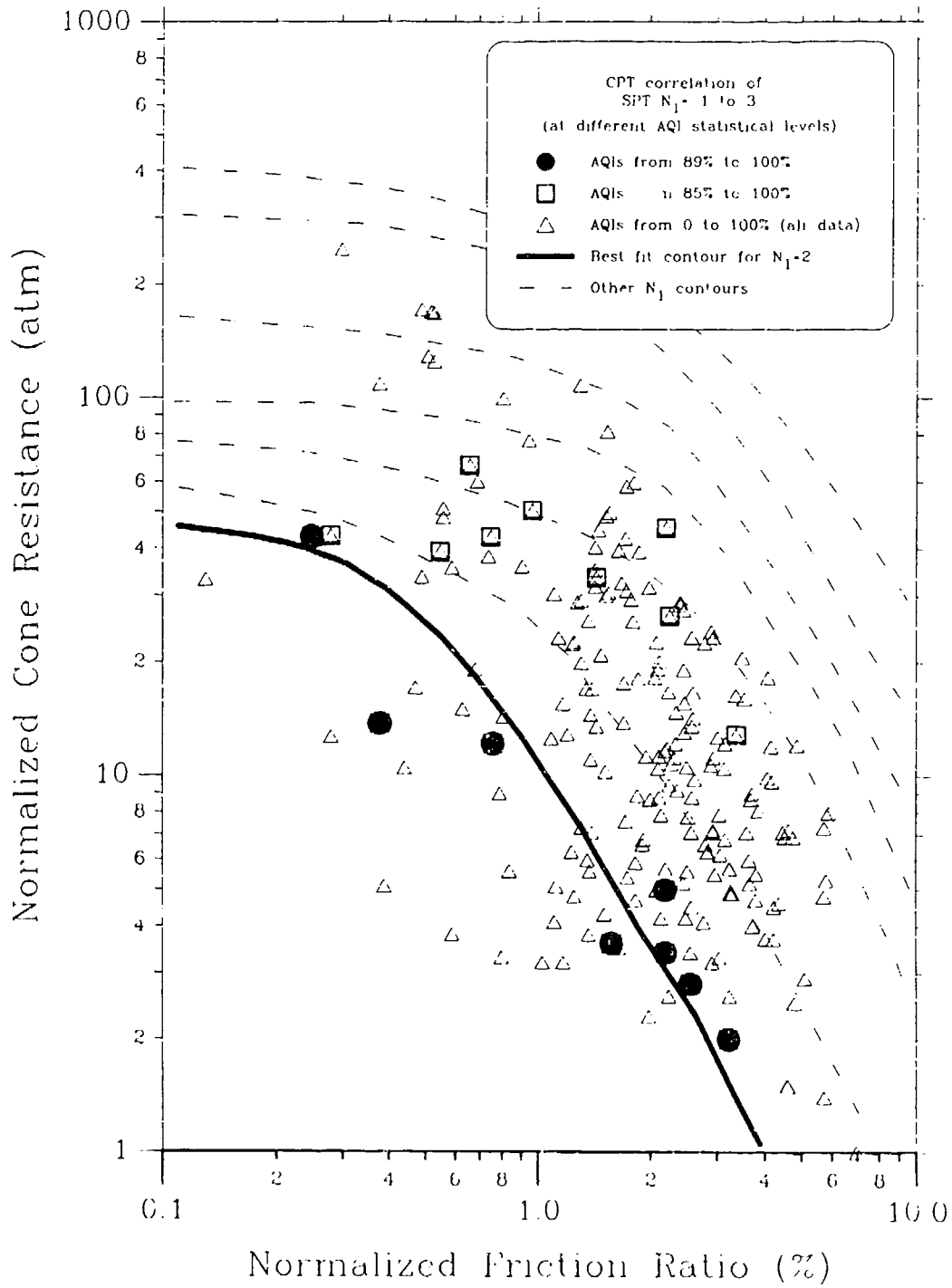


**Figure 8.10** Prediction of the  $N_1=2$  contour on the CPT Soil Characterization Chart

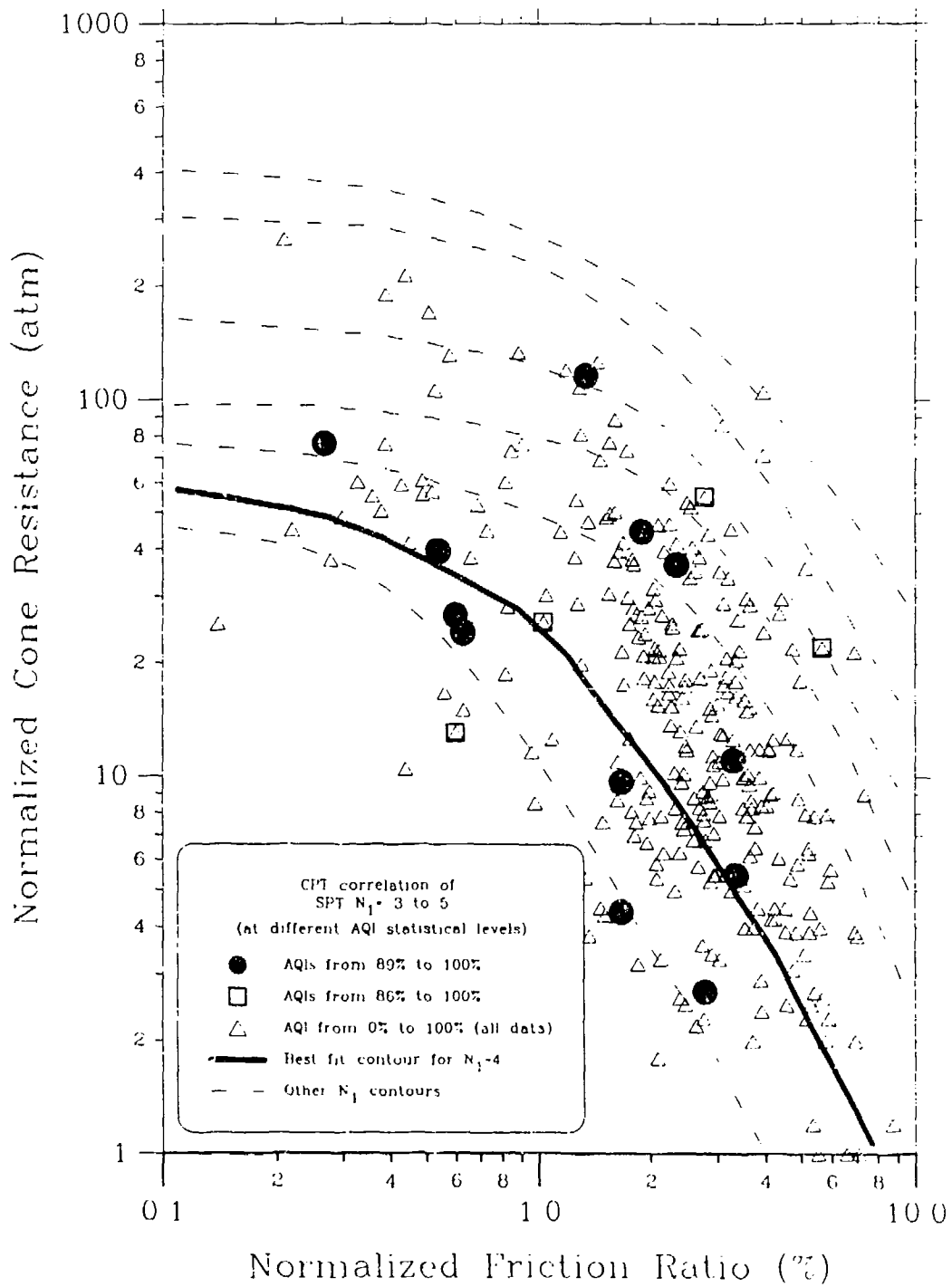
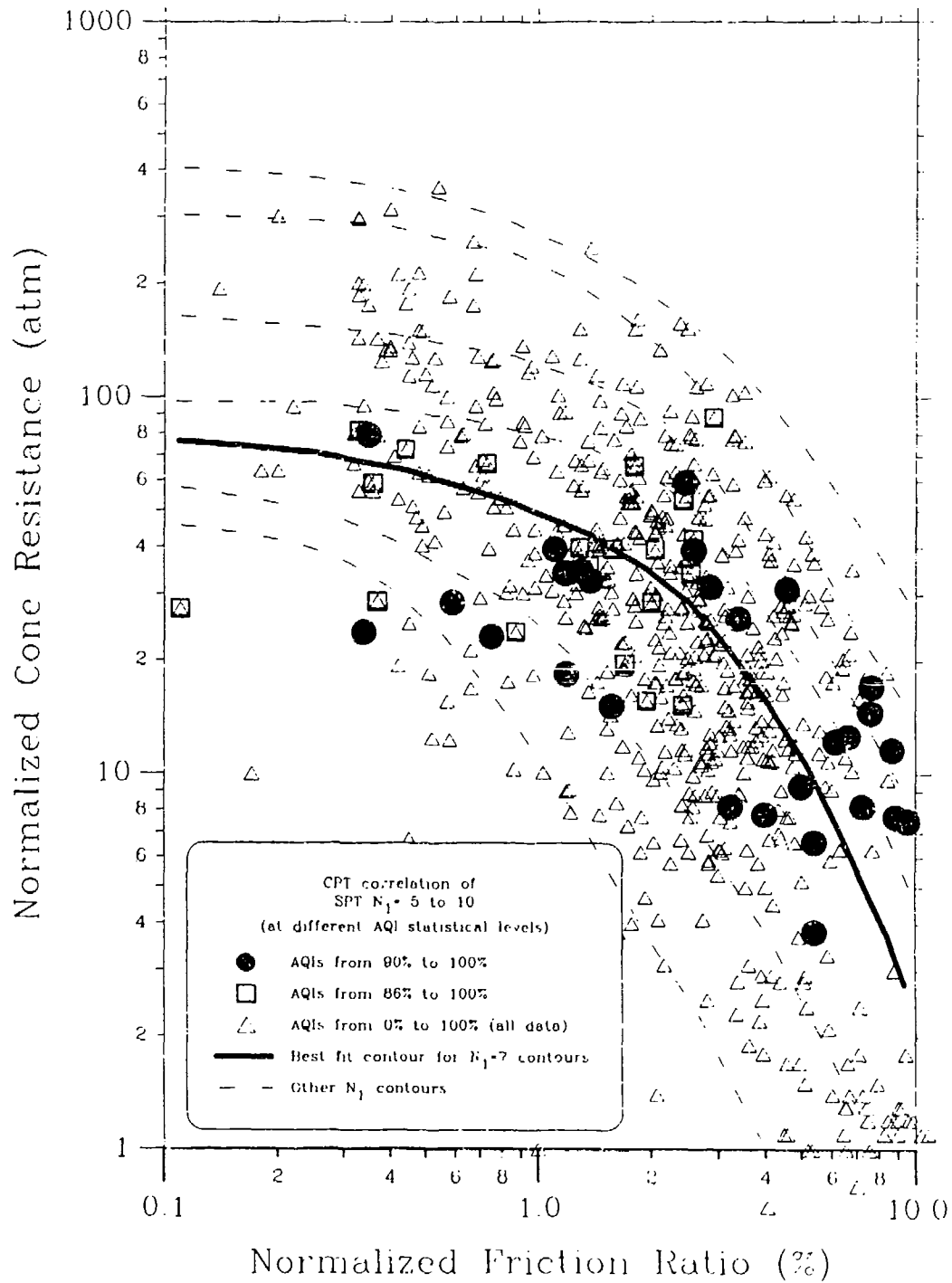
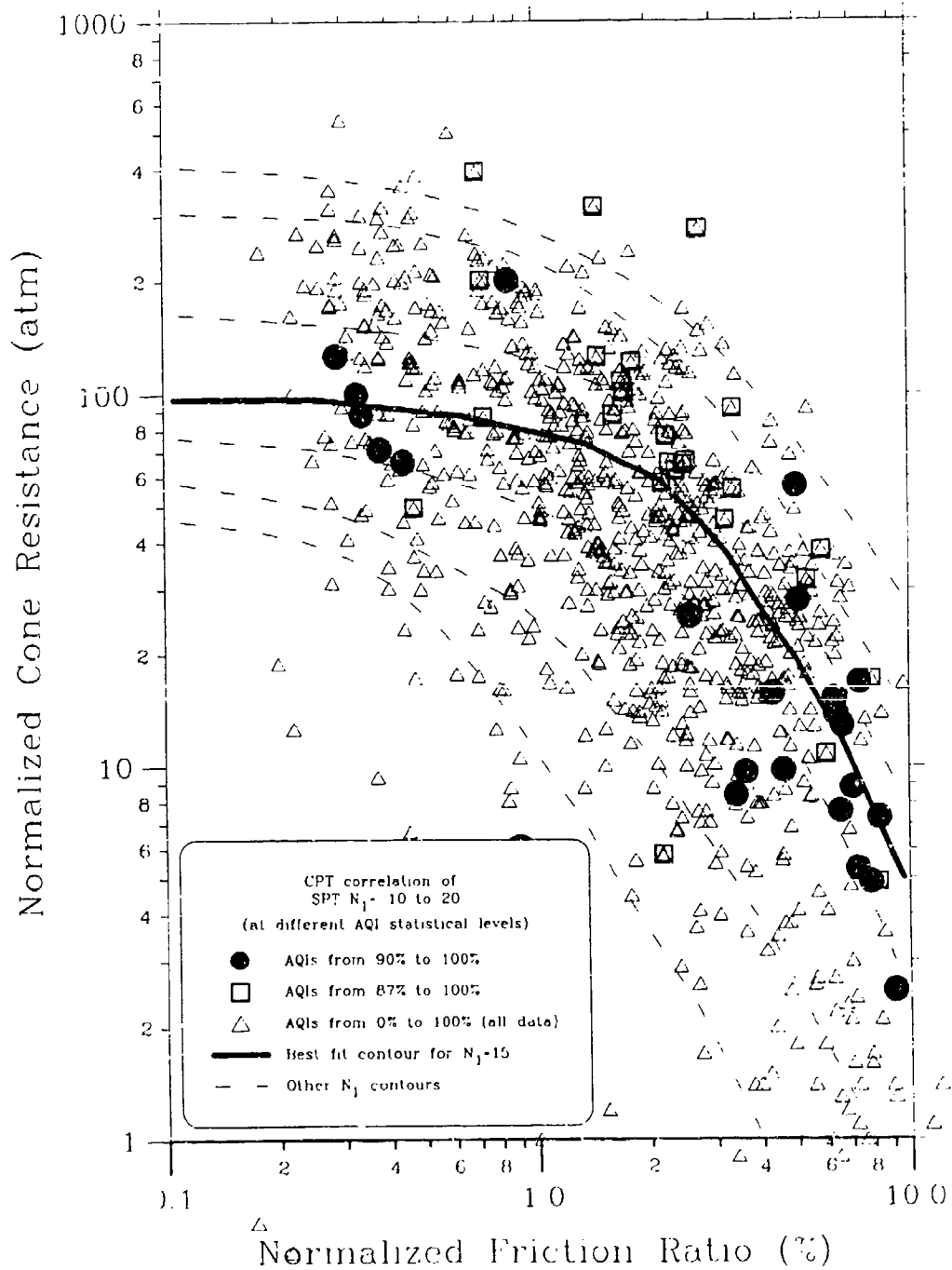


Figure 8.11 Prediction of the  $N_1=4$  contour on the CPT soil characterization chart



**Figure 8.12** Prediction of the  $N_1=7$  contour on the CPT Soil Characterization Chart



**Figure 8.13** Prediction of the  $N_1=15$  contour on the CPT Soil Characterization Chart

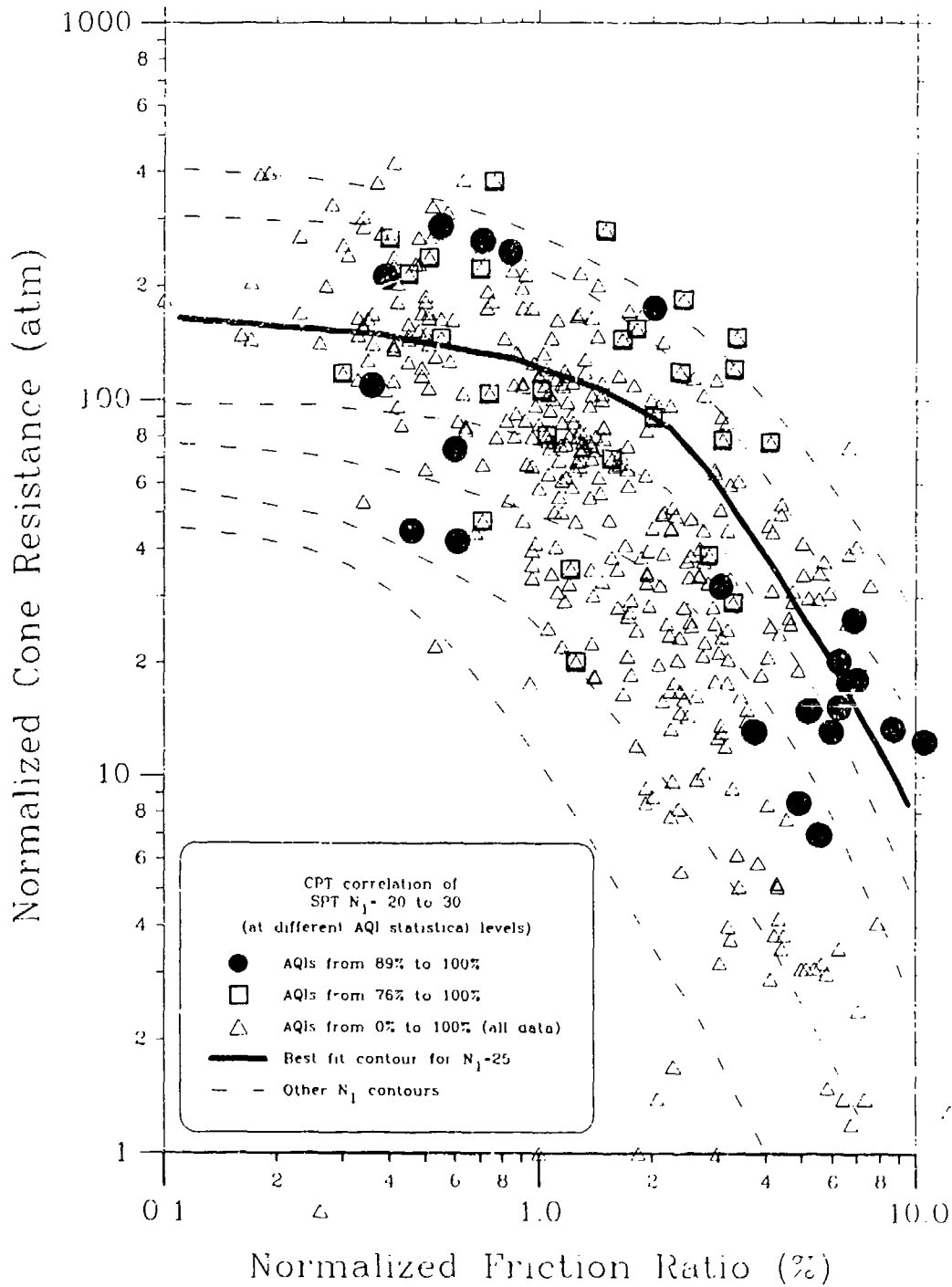


**Figure 8.14** Prediction of the  $N_1 = 25$  contour on the CPT Soil Characterization Chart

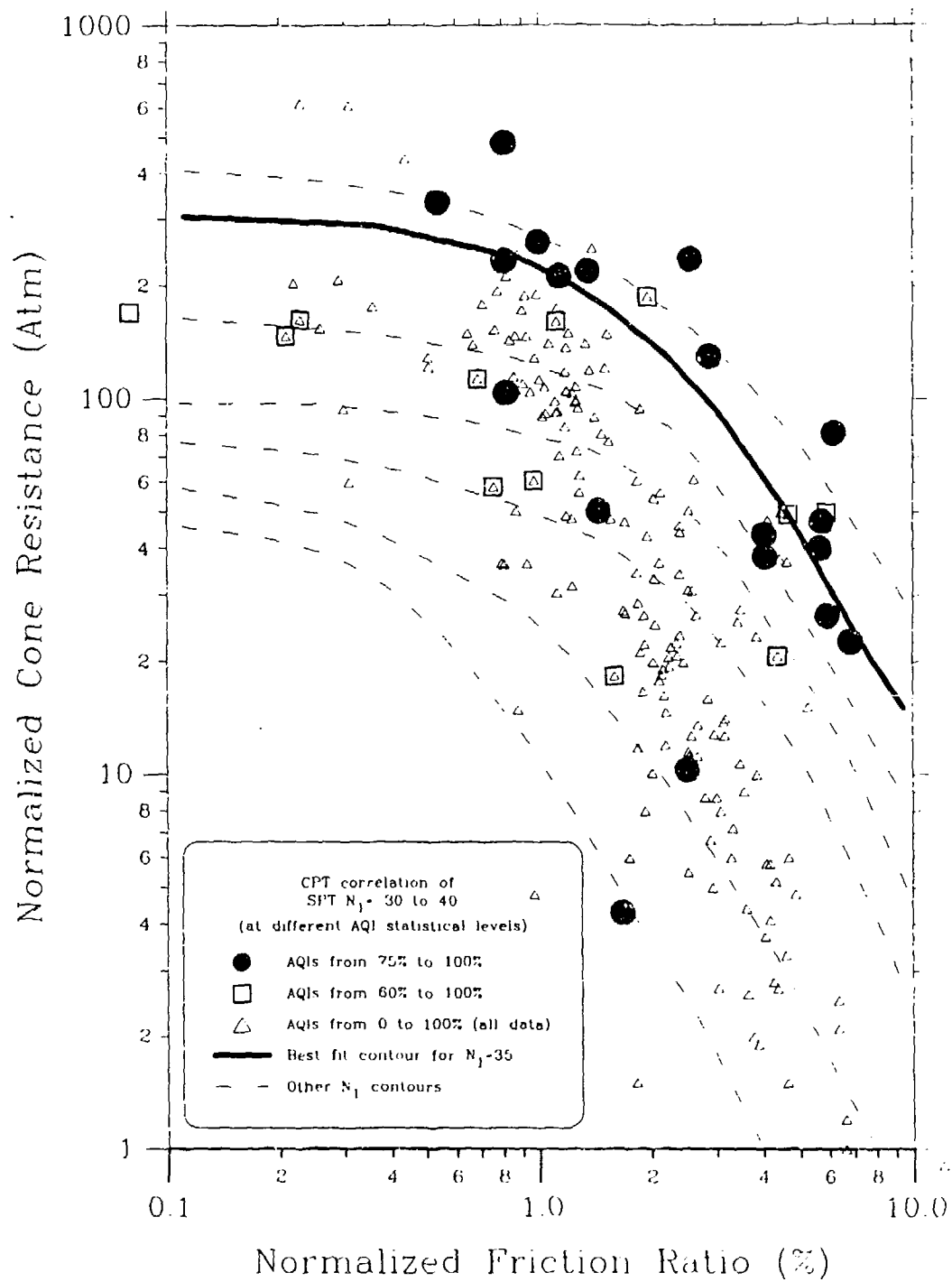


**Figure 8.15** Prediction of the  $N_1=35$  contour on the CPT Soil Characterization Chart



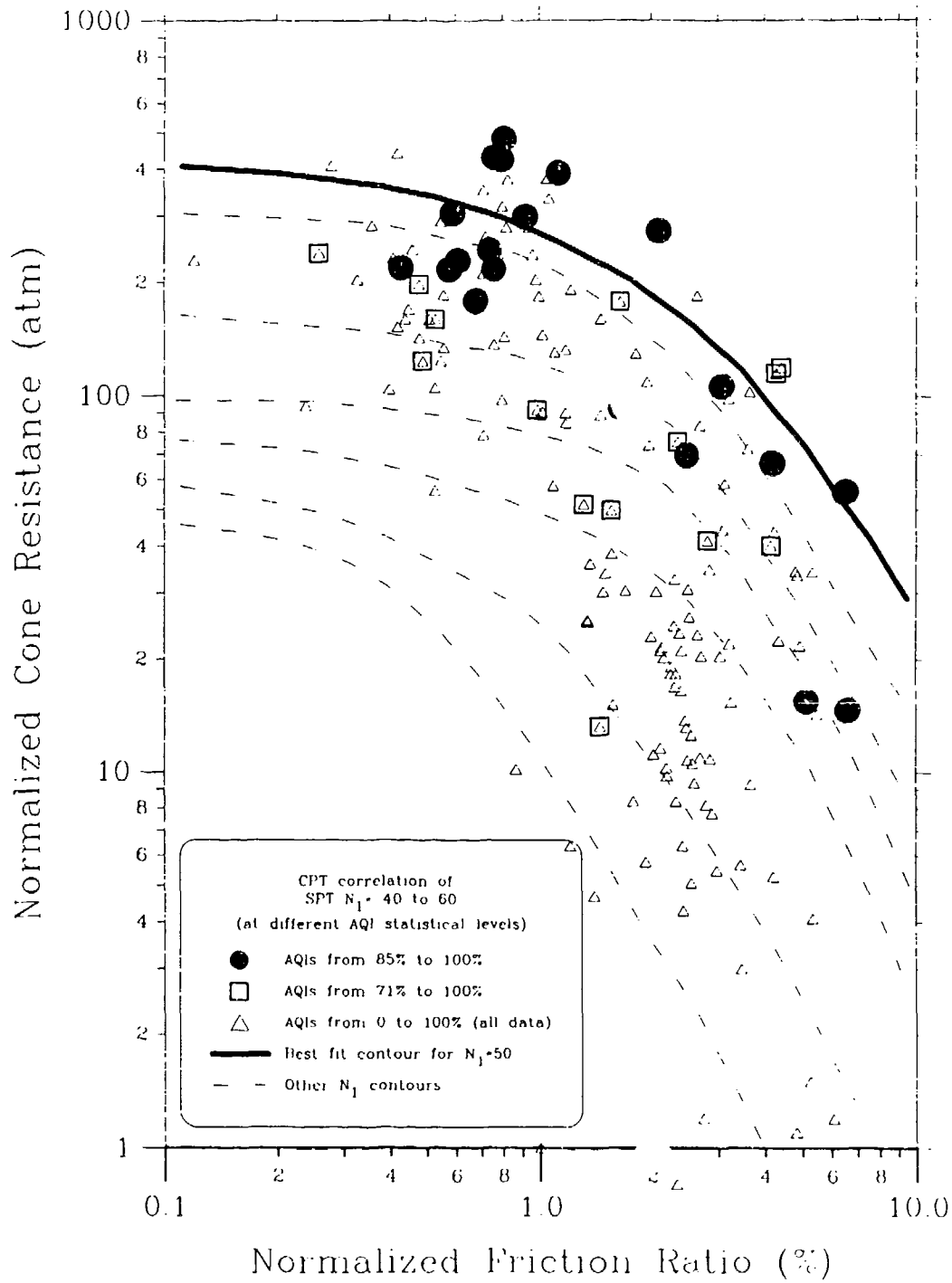


**Figure 8.16** Prediction of the  $N_1=50$  contour on the CPT Soil Characterization Chart

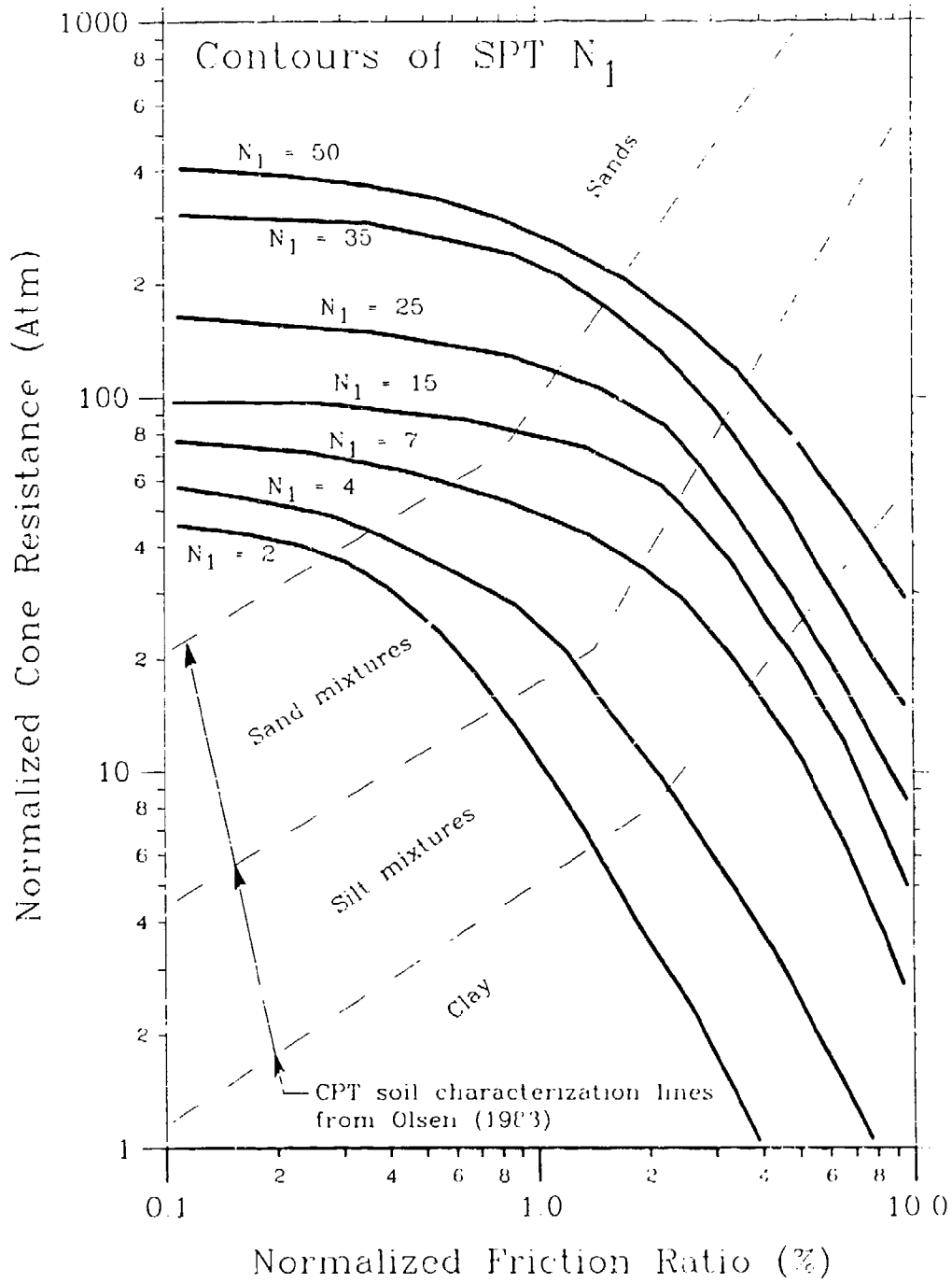


**Figure 8.17** Final plot of the best fit SPT  $N_1$  contours on the CPT Soil Characterization Chart

When the CPT friction ratio is low, such as 0.6%, the contours of predicted SPT  $N_1$  are almost parallel to the normalized cone resistance ( $q_{c1e}$ ) which indicates that the SPT sampler end bearing force dominates the SPT resistance. Therefore, for loose to medium dense sands (which produce low friction ratios, less than 0.6%) (Douglas, 1982) the SPT sampler is resisted primarily by end bearing forces.

For CPT friction ratios greater than 3% in Figure 8.17, the predicted normalized SPT  $N_1$  contours are approximately parallel to the normalized CPT sleeve friction resistance,  $f_{s1e}$  (contours of constant normalized sleeve friction resistance are shown in Figure 8.18). This indicates that the SPT sampler resistance is primarily dependent on the side friction resistance for dense and overconsolidated sands together with all clays. Dense sands and overconsolidated soils also have high lateral stress ratios ( $K_0$ ). For sands, a high lateral stress produces a higher CPT sleeve resistance (Masood, 1990) and therefore would also produce a higher SPT sampler resistance. The relative contribution of SPT side friction forces to SPT end bearing forces can be calculated from the product of factors: the area ratio (i.e. SPT sampler side area to SPT end bearing area) and stress ratio (i.e. the CPT friction ratio). The area ratio is the SPT side friction area to the SPT end bearing area which is equal to 28 at 1½ foot penetration. For clays and overconsolidated sand, the CPT friction ratio is approximately 5% (i.e. stress ratio of 0.05), therefore the SPT side force to end bearing ratio is calculated to be 1.4 (i.e. 28 times 0.05). The SPT side friction force is 1.4 times higher than the end bearing force. However, if side friction forces inside the sampler are included, then the area ratio increases to 44 and the SPT side force to end bearing ratio increases to 2.2.

An example of CPT predicted (using Figure 8.17) versus field measured SPT blow counts is shown in Figure 8.19 together with annotations. Numerous other examples of CPT predicted versus field measured SPT blow counts are shown in Figure 8.20 to Figure 8.27. Prediction of the SPT blow count is difficult as

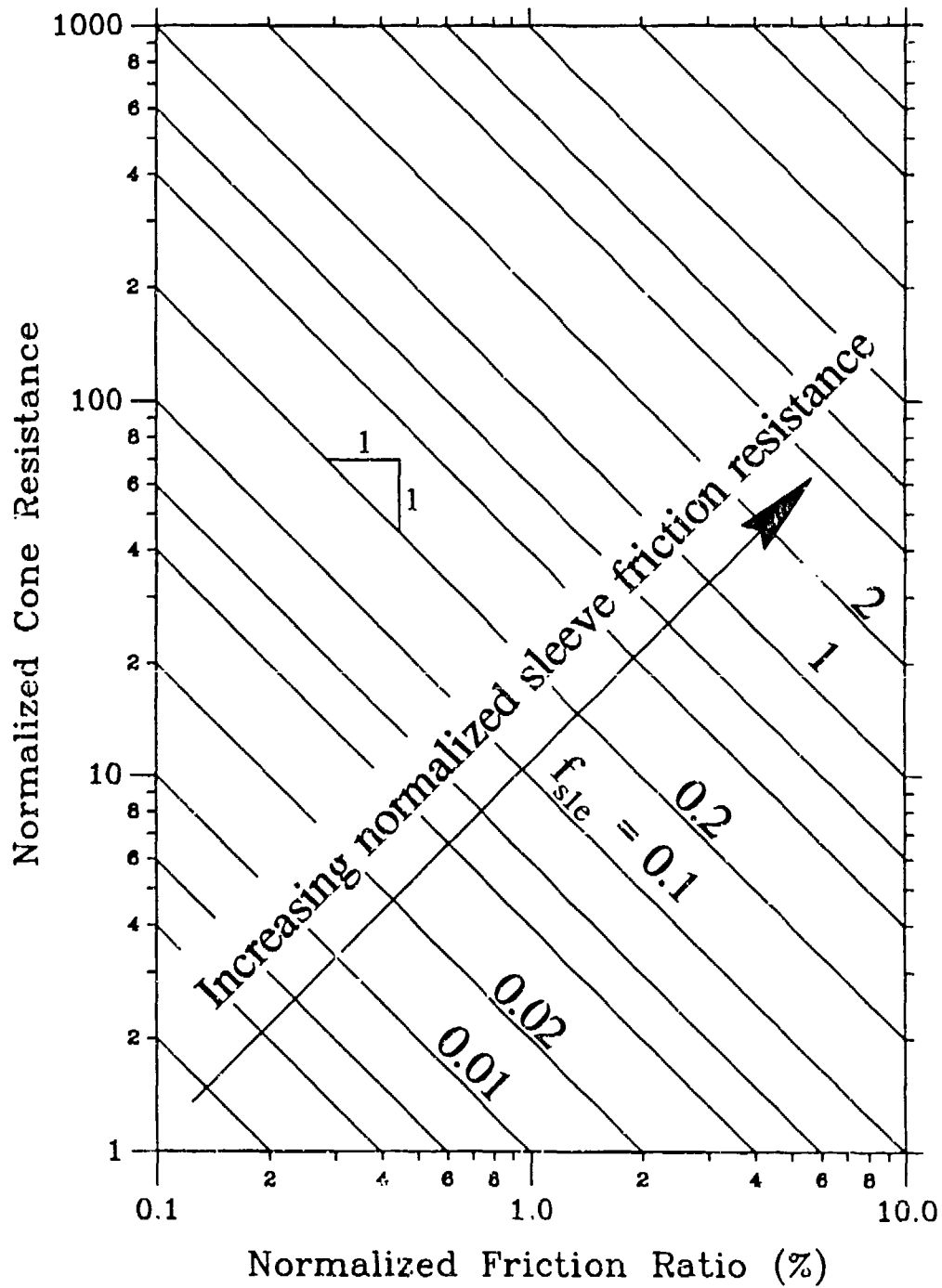


**Figure 8.18** Contours of constant normalized sleeve friction resistance on the CPT soil characterization chart

illustrated by large variance for each predictive SPT blow count contour (for example Figure 8.14). However, as seen from these predicted versus measured examples, the match of predicted versus measure does support this technique of using both CPT measurements to predict the SPT blow count. These figures also show how much detail is missed by having only discontinuous SPT measurement records.

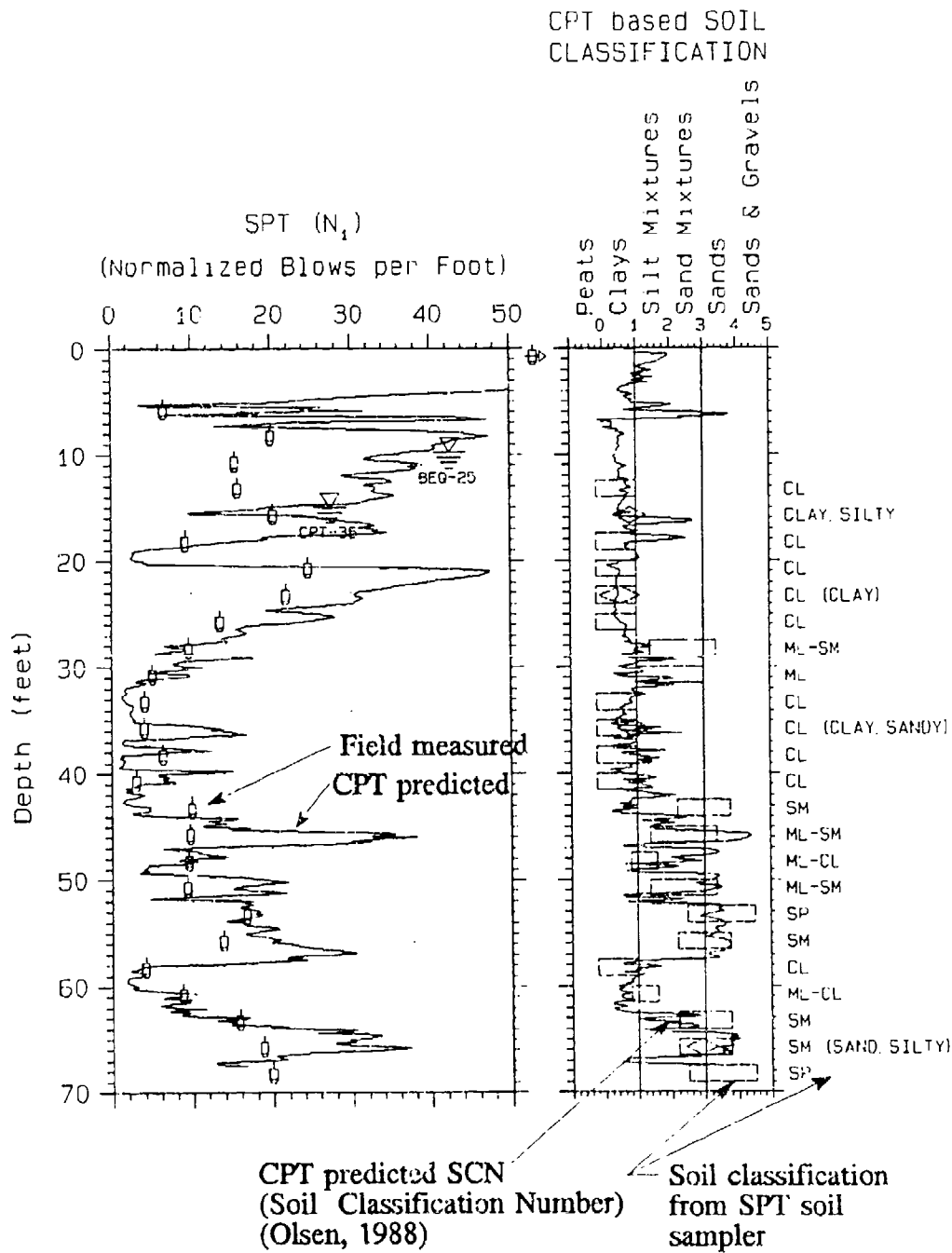


**Figure 8.19** Example of CPT Prediction of SPT blow count with comparison data (Barkley dam seismic evaluation study, data from Olsen, et al, 1989)

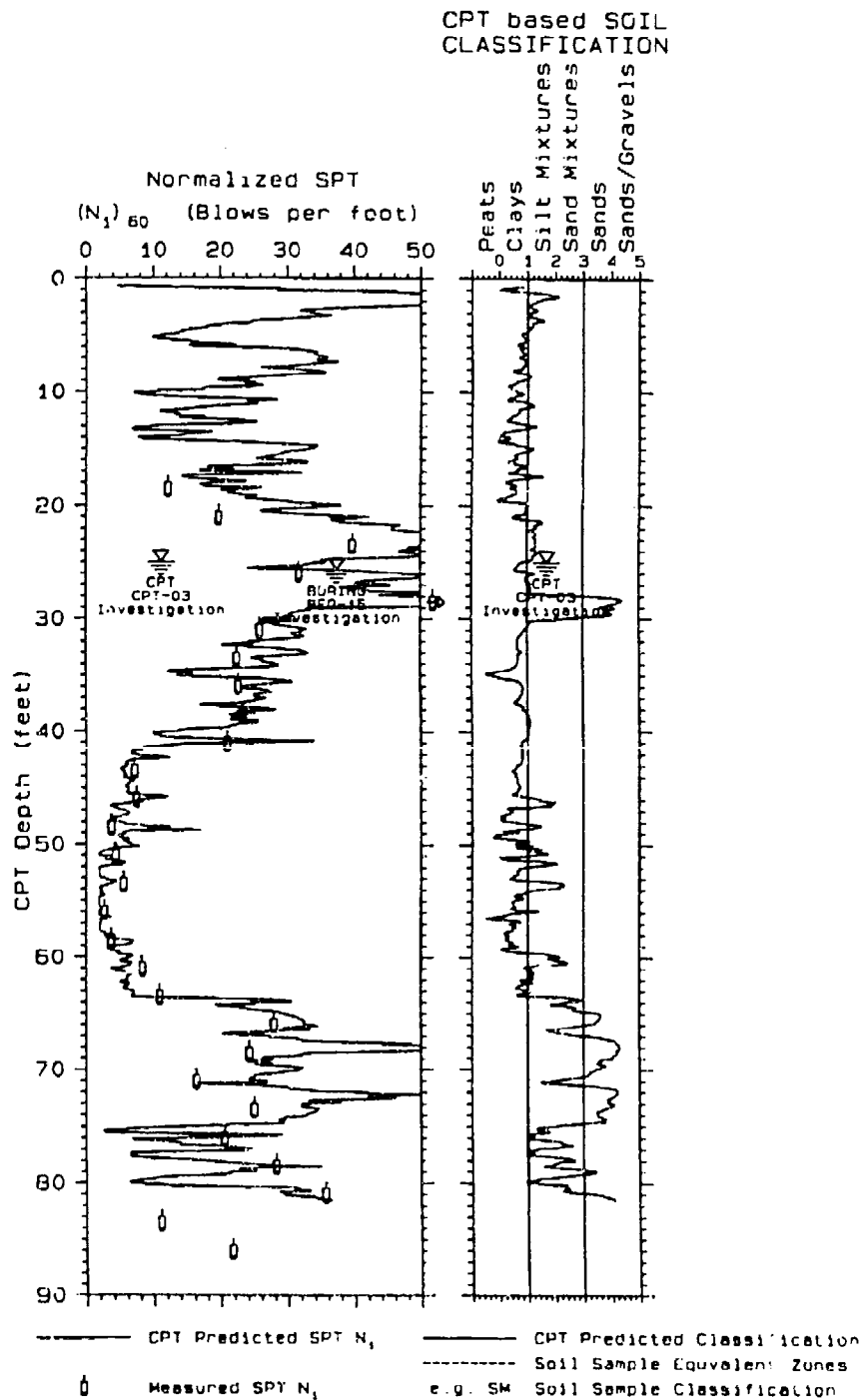


**Figure 8.20** CPT predicted versus measured SPT  $N_1$  for the Barkley dam seismic evaluation study (data from Olsen et al., 1989)

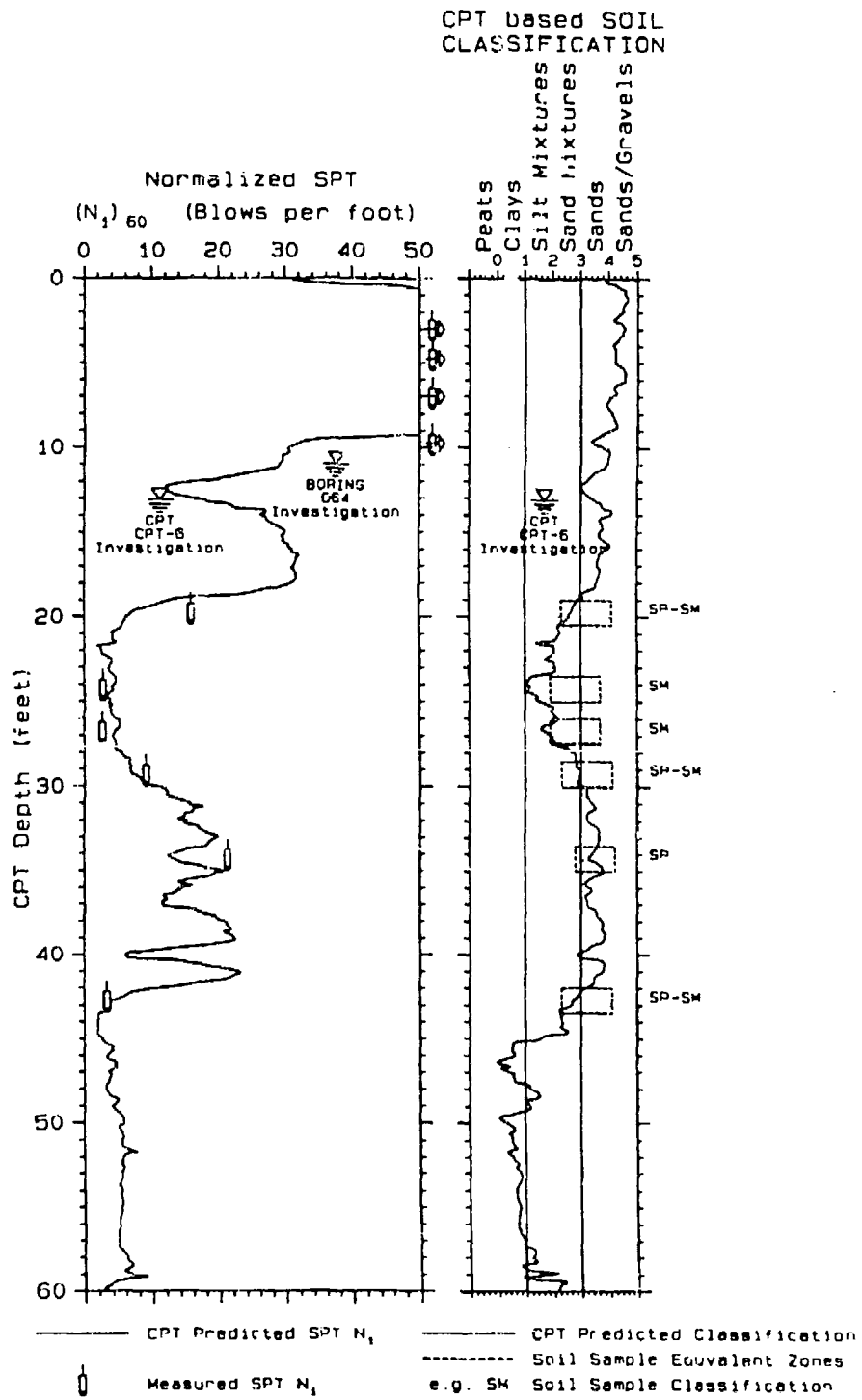


**Figure 8.21** CPT predicted versus measured  $N_1$  for sites on the East coast of the US (data from project code LE-JN)



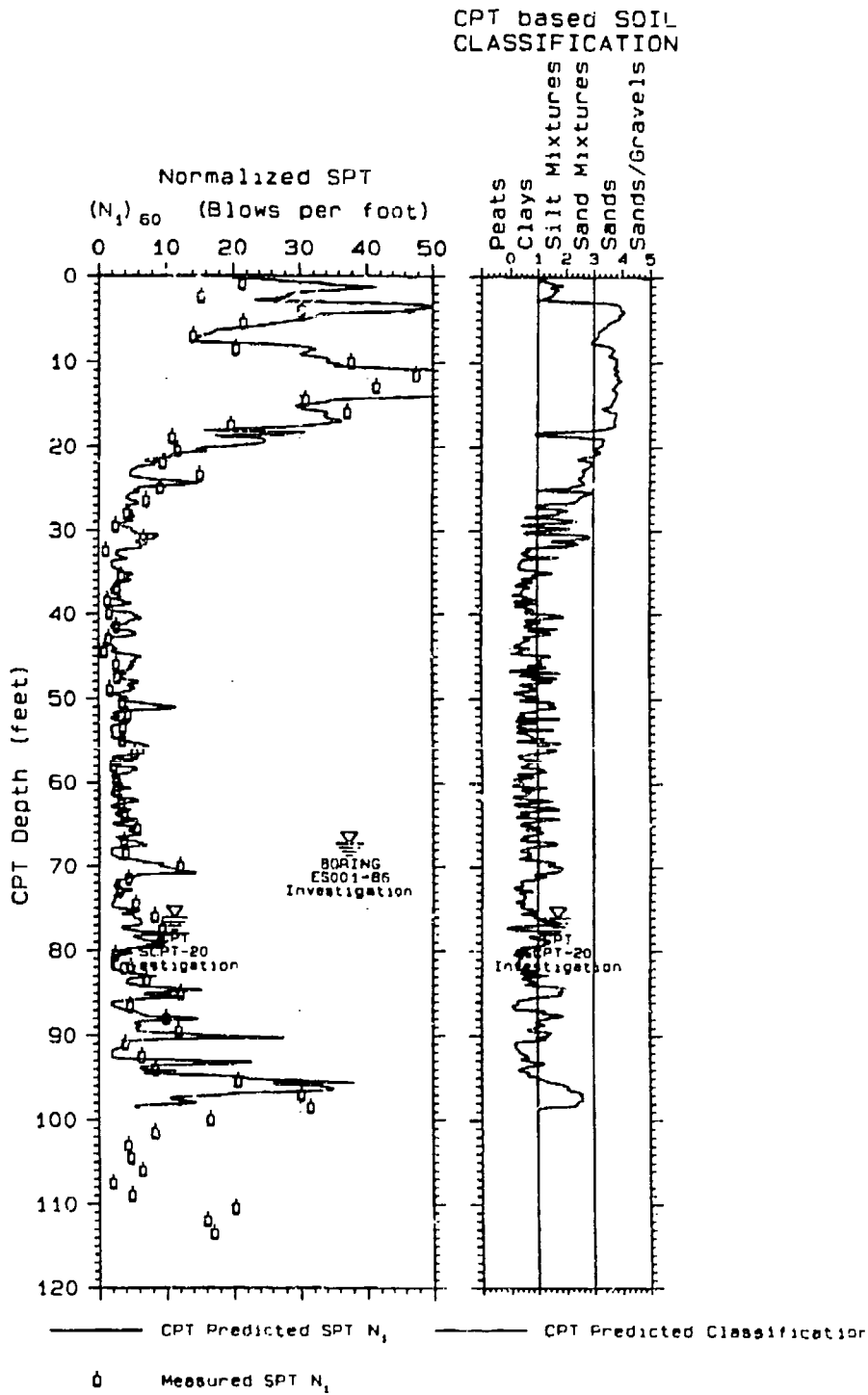


**Figure 8.22** CPT predicted versus measured  $N_1$  for a CPT sounding through the hydraulic core of Sardis dam

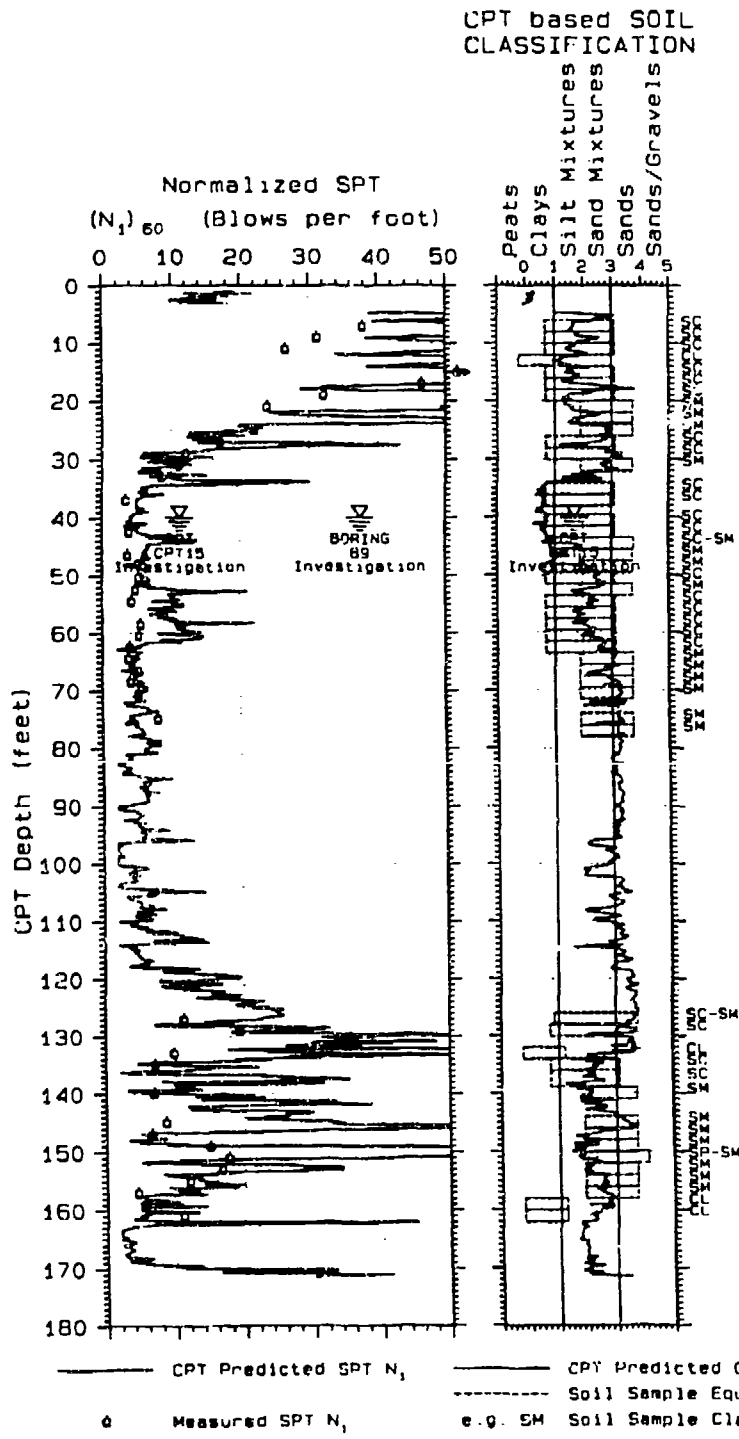


**Figure 8.23** CPT predicted versus measured SPT  $N_1$  for a stiff/dense dirty sand site (project code DE-S-R)

CPT based SOIL CLASSIFICATION

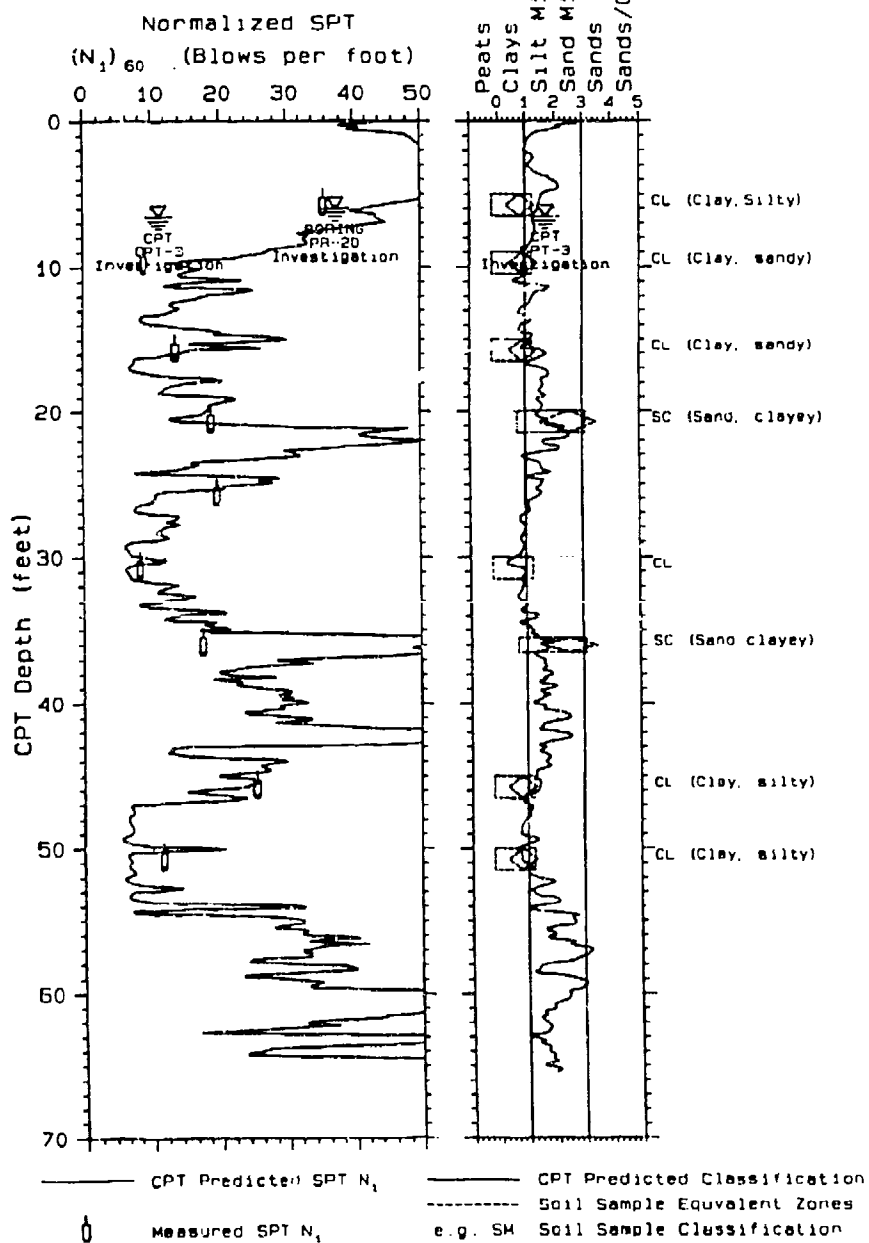
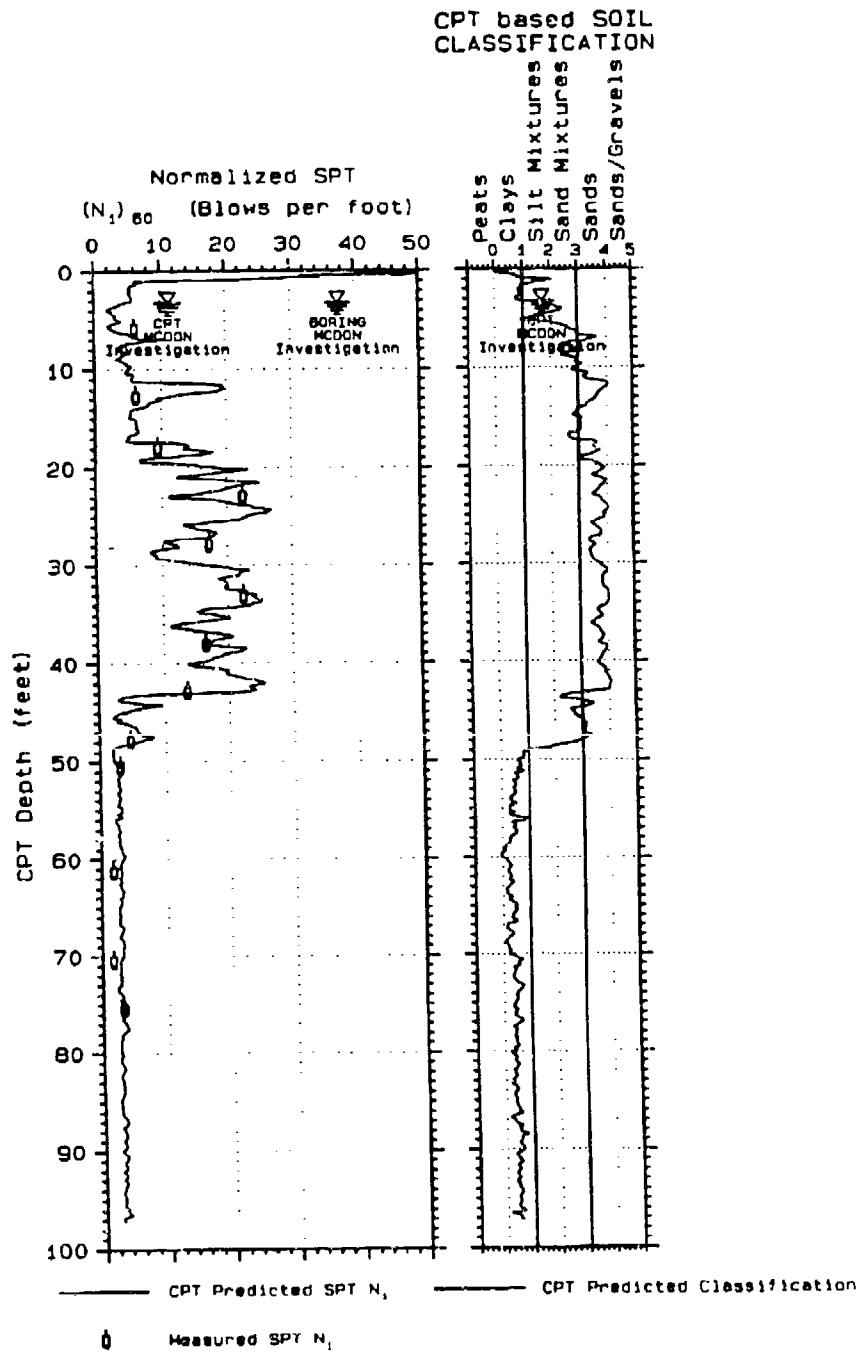
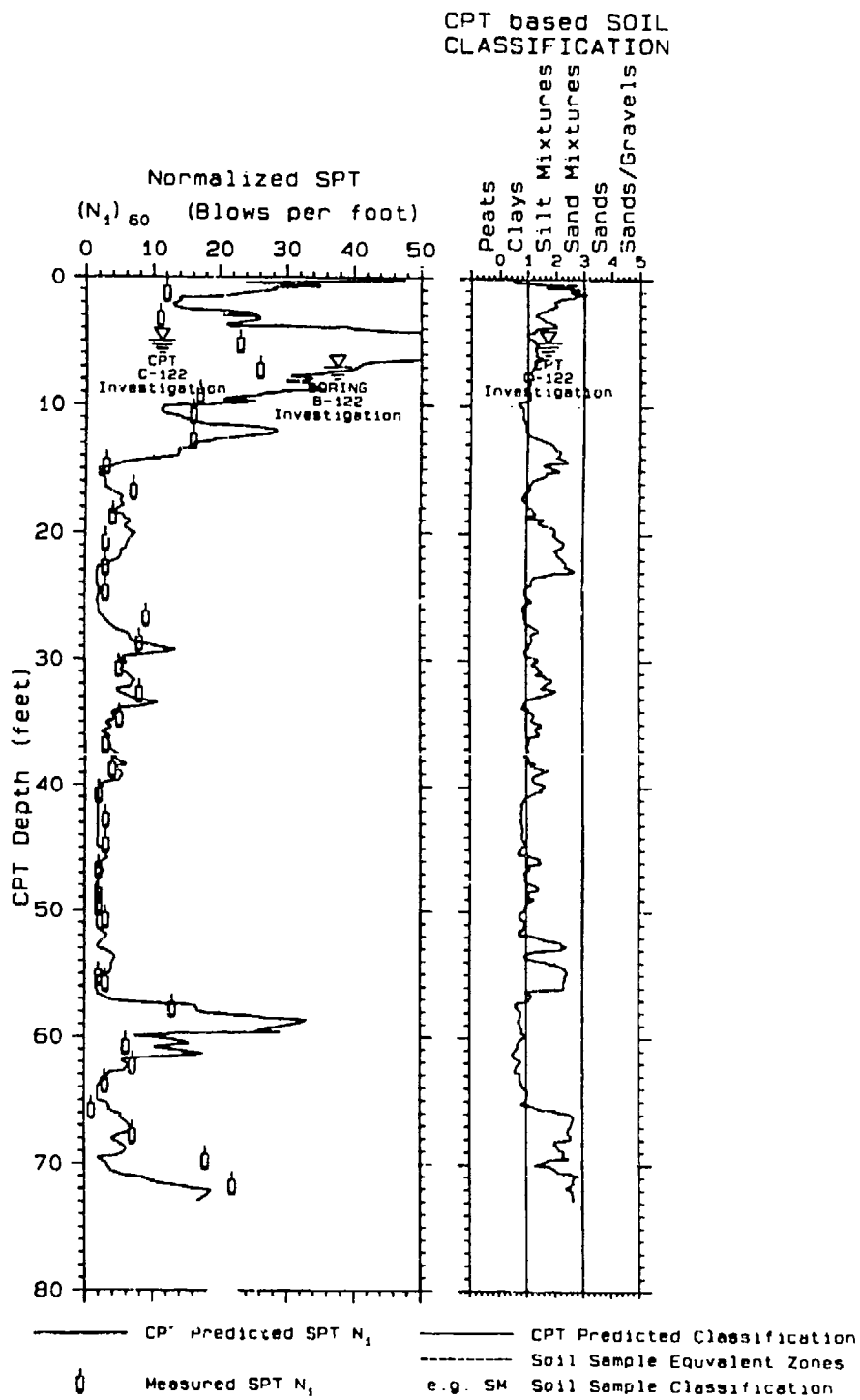


Figure 8.24 CPT predicted versus measured SPT  $N_1$  for a site composed of soil mixtures in Tracy California (project code WC-TSS)



**Figure 8.25** CPT predicted versus measured SPT  $N_1$  for McDonalds Farm, Sea Island, Richmond, British Columbia, Canada (University of British Columbia research site)(data from Campanella, et al, 1982)



**Figure 8.26** CPT predicted versus measured SPT  $N_1$  for the Arcadia Dam seismic evaluation study

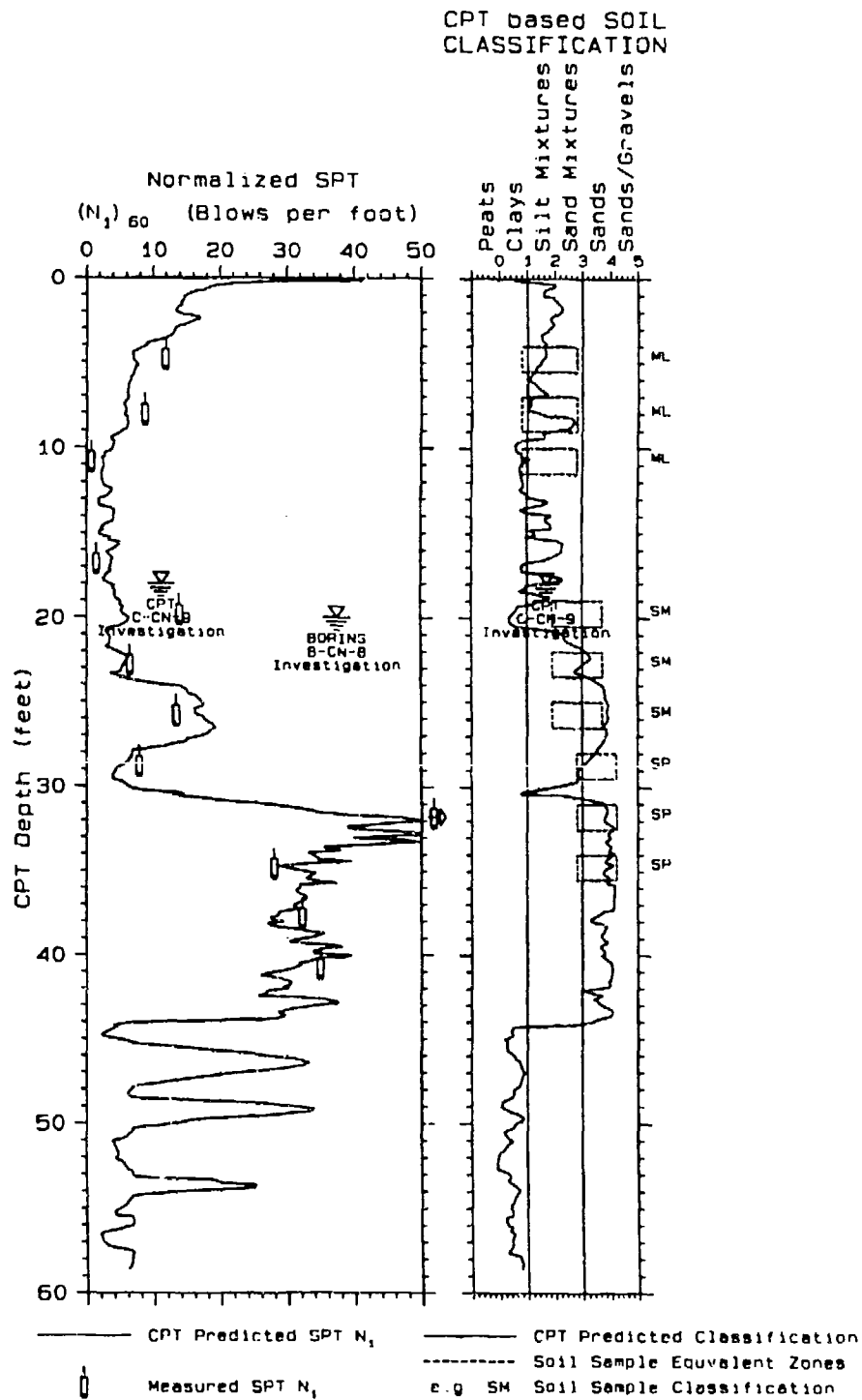


**Figure 8.27** CPT predicted versus measured SPT  $N_1$  at the Coyote North site (near San Jose) California (data from Martin & Douglas, 1980)

# CPT Prediction of Clay Undrained Strength, $S_u$

## *Introduction*

The undrained strength,  $S_u$ , of clay is one of the classic geotechnical properties and is critical for many design applications. In the U.S., the standard practice for obtaining clay undrained strength requires retrieval of relatively undisturbed soil samples, typically with a 3 inch Shelby tube, for unconsolidated undrained (UU) triaxial testing. However, only a few laboratory strength tests are typically performed for most geotechnical projects and it is assumed that they represent the character of the total site.

In Europe, the standard practice for obtaining the undrained strength of soft clays is the field vane shear test. However, the vane shear strength is always too high because of silting, overconsolidation effects, the high vane rotation rate, and/or vane geometric effects. A correction factor ( $\mu$ ) is required to reduce the field vane shear strength to the field strength level (typically the equivalent unconsolidated undrained triaxial test level). This correction factor ( $\mu$ ) is dependent on many factors, but generally established based on site specific correlations.

## *CPT Prediction of $S_u$*

Clay undrained strength was the first geotechnical property predicted using CPT data in the 1930's (reported by Broms and Flodin, 1988). For the last six decades, the literature has been filled with theoretical and case studies on the topic of

undrained strength prediction. It was difficult task then and is still a challenge today. Historically, the problem has been to select the correct bearing  $N_k$  factor in order to calculate the undrained strength from the CPT cone resistance measurement. This  $N_k$  factor, which ranges from 8 to 25 (Aas, Lacasse, Lunne, and Hoeg, 1986, Lunne and Kleven, 1981), depends on overconsolidation, clay type, sensitivity, silt content, reference testing device, and to a lesser degree on overburden stress. A new technique is developed in this chapter that uses both CPT measurements to directly predict the undrained strength without the need to estimate the  $N_k$  factor.

### *Historical Means of Estimating $N_k$ for CPT Prediction of $S_u$*

The classical means of predicting undrained strength using the CPT uses the  $N_k$  factor which can be estimated using Table 8.1 (Olsen, 1994). However, this procedure requires prior knowledge of the in situ state of the soil. The best procedure for calculating  $S_u$  is to estimate  $N_k$  assuming a medium stiff normally consolidated condition (i.e.  $N_k = 13$ ) then calculate  $S_u$  using Equation (8.1) and then calculate the  $\frac{S_u}{\sigma_v}$  ratio.

$$S_u = \frac{q_c - \sigma_{total}}{N_k} \quad (8.1)$$

Equation (8.1) was introduced in Chapter 4 during the development of the normalized cone resistance formulation. If the calculated  $\frac{S_u}{\sigma_v}$  is 0.29 to 0.33 and  $S_u$  is 250 to 500 psf (medium stiff condition) then the soil is probably normally consolidated with  $N_k$  equal to approximately 13 (within the range of 10 to 15). If



the calculated  $\frac{S_u}{\sigma_v}$  is high, than the clay is probably overconsolidated or a stiffer

condition prevails which requires a higher  $N_k$ . Iterations might be required until the conditions regarding  $N_k$  in Table 8.1 are matched. A few reference laboratory strength tests for each project should still be required. This discussion has shown the importance of the  $\frac{S_u}{\sigma_v}$  toward estimating the  $N_k$ .

### *Determining $S_{ul}$ using CPT Soil Characterization Chart*

The normalized undrained strength  $S_{ul}$  (i.e.  $\frac{c}{p}$  or  $\frac{S_u}{\sigma_v}$ ) can be correlated to CPT measurements using the CPT soil characterization chart. This section will introduce the concept of predicting  $S_{ul}$  based on bearing capacity formulation and the next section will describe the process of establishing  $S_{ul}$  contours on the CPT soil characterization chart.

The cone resistance bearing formulation (Equation (8.2)) was developed in Chapter 5 and is in terms of the normalized undrained strength ( $S_{ul}$ ), cohesive bearing factor ( $N_k$ ), and the normalized cone resistance ( $q_{cle}$ ):

$$S_{ul} = \frac{q_{cle}}{N_k} \quad (8.2)$$

This equation can be rearranged as shown below:

$$q_{cle} = S_{ul} N_k \quad (8.3)$$

Equation (8.3) can also be represented in a graphic form based on the CPT soil

**Table 8.1** Typical  $N_k$  values for estimating the unconsolidated undrained strength of clays using the CPT cone resistance (Olsen, 1994)

Clay condition	Unconsolidated Undrained (UU) Triaxial Test as the reference strength standard	
	$N_k$ range	$N_k$ average (typical)
Normally consolidated, normal sensitivity, soft to medium stiff	10 to 16	13
Normally consolidated, moderately sensitive, soft to very soft	9 to 13	11
Moderately over consolidated non-fissured	15 to 20	17
Highly over consolidated fissured	17 to 23	19

characterization chart as shown in Figure 8.28. The  $q_{c1e}$  in Equation (8.3) is equal to the combined effect of  $S_{u1}$  contours and  $N_k$  contours in Figure 8.28. For a given  $S_{u1}$  contour, increasing  $q_{c1e}$  (vertical axes) will correspond to an increasing contour of  $N_k$ . Increasing the overconsolidation or silt content will also increase the  $S_{u1}$  contour level as also shown with arrows and annotations. Therefore, any point on the CPT Soil Characterization Chart (for example point "A") has a  $N_k$  contour value, a  $S_{u1}$  contour value, and a  $q_{c1e}$  value from the vertical axis. Contours of  $S_{u1}$  can be established directly on the CPT Soil Characterization Chart using laboratory unconsolidated undrained triaxial strength data ( $(S_{u1})_{TxUU}$ ) or field vane shear strength data ( $(S_{u1})_{FV}$ ) together with the normalized CPT data. There is no need to determine the  $N_k$  contour because  $S_{u1}$  is the ultimate goal.

### *Establishment of $S_{u1}$ contours on the CPT soil characterization chart*

The procedure used for establishing contours of normalized undrained strength ( $S_{u1}$ ) for clays on the CPT soil characterization chart was the same as was used in the last section for prediction of the SPT blow count. Two sets of  $S_{u1}$  contours were established using measured undrained strength data from the database developed for this research program (and described in the Appendix). The first set of  $S_{u1}$  contours were based on data from laboratory unconsolidated undrained triaxial (TxUU) tests and the second set were based on data from field vane (FVane) shear tests. The  $S_{u1}$  contours were also established based on the knowledge (from the last section) that the contours should increase in value with increased  $q_{c1e}$  and  $f_{s1e}$  levels.

All measured strength data from the database, for all projects, were divided into unconsolidated undrained triaxial and field vane shear tests and then further divided into 6 strength ranges for the purpose of establishing individual correlation contours on the CPT soil characterization chart. Best fit contours of normalized unconsolidated undrained triaxial strengths are shown in Figure 8.29 to Figure 8.35

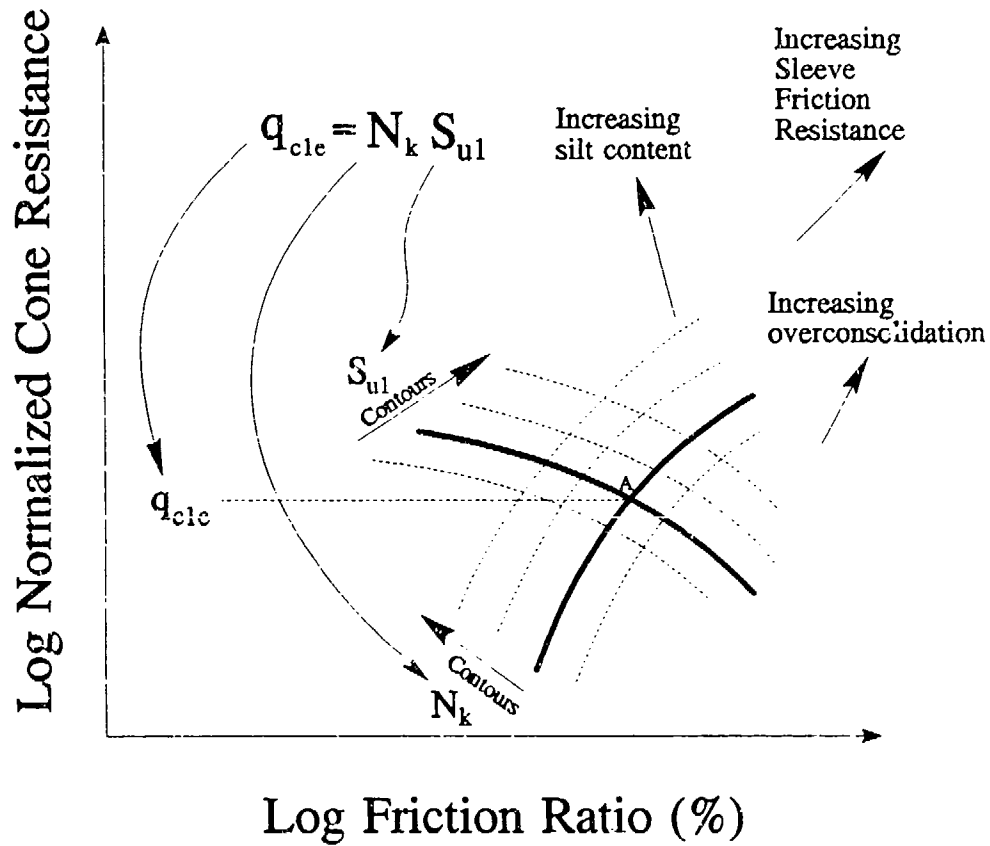


**Figure 8.28** Establishing  $S_{u1}$  (i.e.  $c/p$ ) contours on the CPT soil characterization chart based on bearing theory for clay penetration

based on the minimum inclusionary AQI levels for average  $(S_{ul})_{TxUU}$  levels of 0.15, 0.25, 0.31, 0.39, 0.54, and 2.0. The final plot having all the best fit  $(S_{ul})_{TxUU}$  contours is shown in Figure 8.36. The best fit contours of normalized field vane strength are shown in Figure 8.37 to Figure 8.41 for average  $(S_{ul})_{FVane}$  levels of 0.25, 0.31, 0.54, 0.80, and 2.0. The final plot having all  $(S_{ul})_{FVane}$  contours is shown in Figure 8.42.

Several examples of CPT predicted versus measured triaxial unconsolidated undrained (UU) test results  $((S_u)_{TxUU})$  are shown in Figure 8.43 to Figure 8.49. These examples represent sites composed of soft to stiff clay including several sites composed of sandy to silty clay. There are also several examples of desiccated layers with properly predicted  $(S_u)_{TxUU}$  levels.

Several examples of CPT predicted versus measured field vane shear test results  $((S_u)_{FVane})$  are shown in Figure 8.50 to Figure 8.56. These examples represent very soft to medium stiff clay sites and contain a few examples of desiccated strength. There is more field vane strength data compared to laboratory triaxial strength data, probably because the field vane test is easier to perform and less expensive.

The contours of  $(S_{ul})_{TxUU}$  and  $(S_{ul})_{FVane}$  have the same general contouring characteristics, namely increasing  $S_{ul}$  with increasing  $q_{c1c}$  and  $f_{s1c}$ . The differences between these contours is important. The ratio of  $(S_{ul})_{TxUU}$  to  $(S_{ul})_{FVane}$  is the historic Bjerrum vane shear correction factor,  $\mu$ . (Bjerrum, 1972) as shown:

$$\mu = \frac{(S_u)_{TxUU}}{(S_u)_{FVane}} = \frac{\left(\frac{S_u}{\sigma_v'}\right)_{TxUU}}{\left(\frac{S_u}{\sigma_v'}\right)_{FVane}} = \frac{(S_{ul})_{TxUU}}{(S_{ul})_{FVane}} \quad (8.4)$$

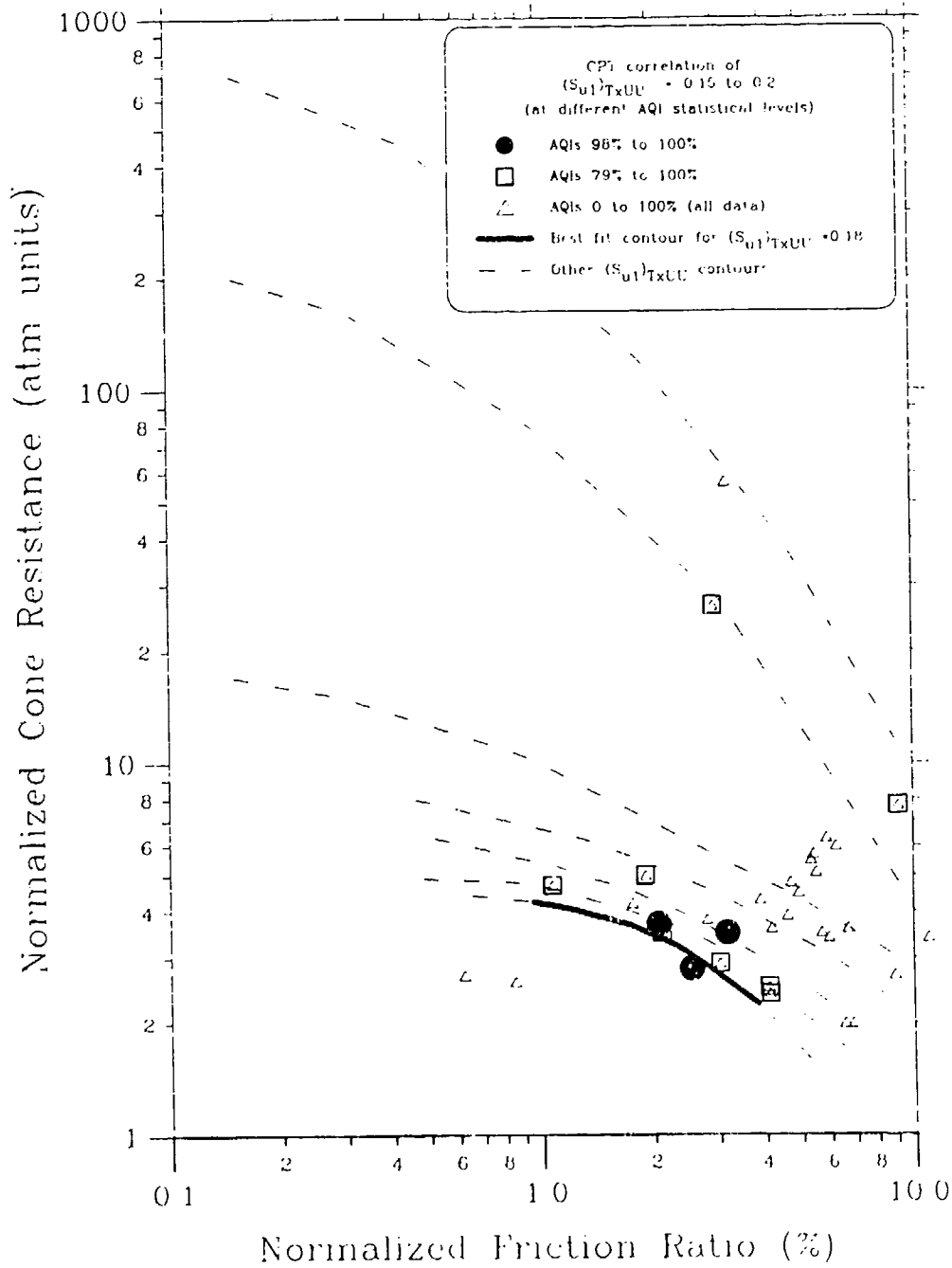


**Figure 8.29** Prediction of the  $(S_{u1})_{TxUU}=0.1$  contour on the CPT Soil Characterization Chart

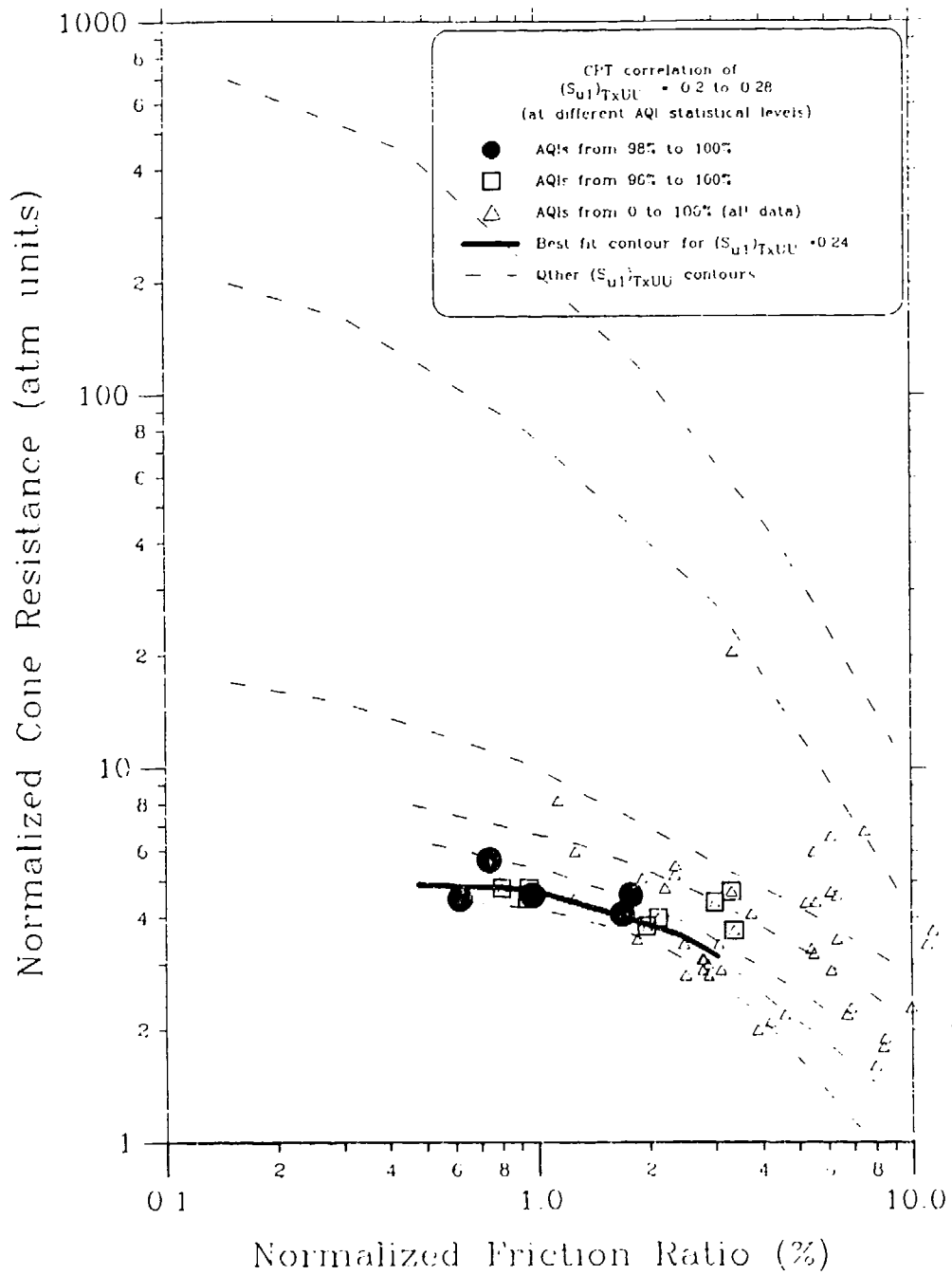


**Figure 8.30** Prediction of the  $(S_{u1})_{TxUU}=0.25$  contour on the CPT Soil Characterization Chart

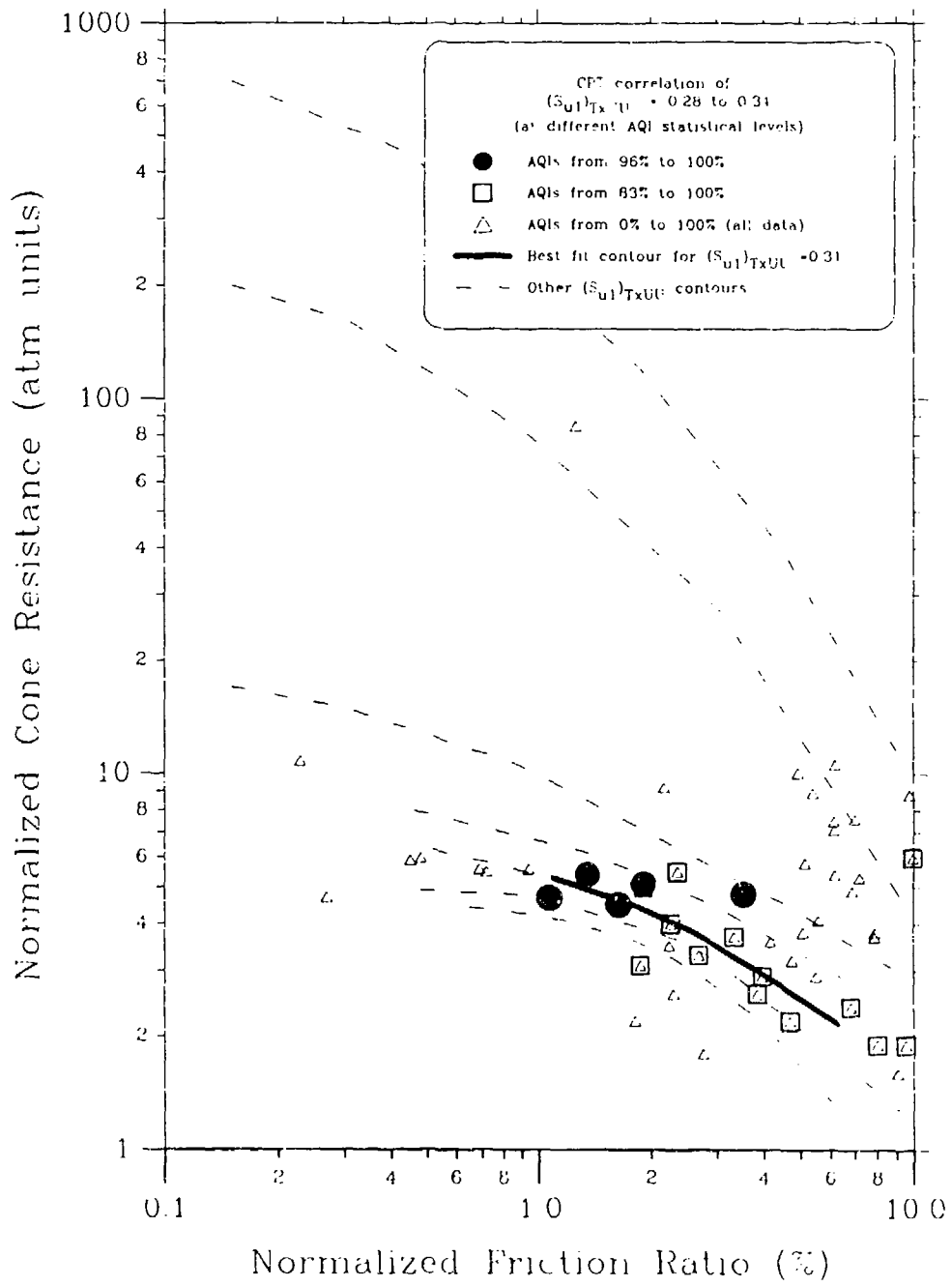


**Figure 8.31** Prediction of the  $(S_{u1})_{TxUU}=0.31$  contour on the CPT Soil Characterization Chart



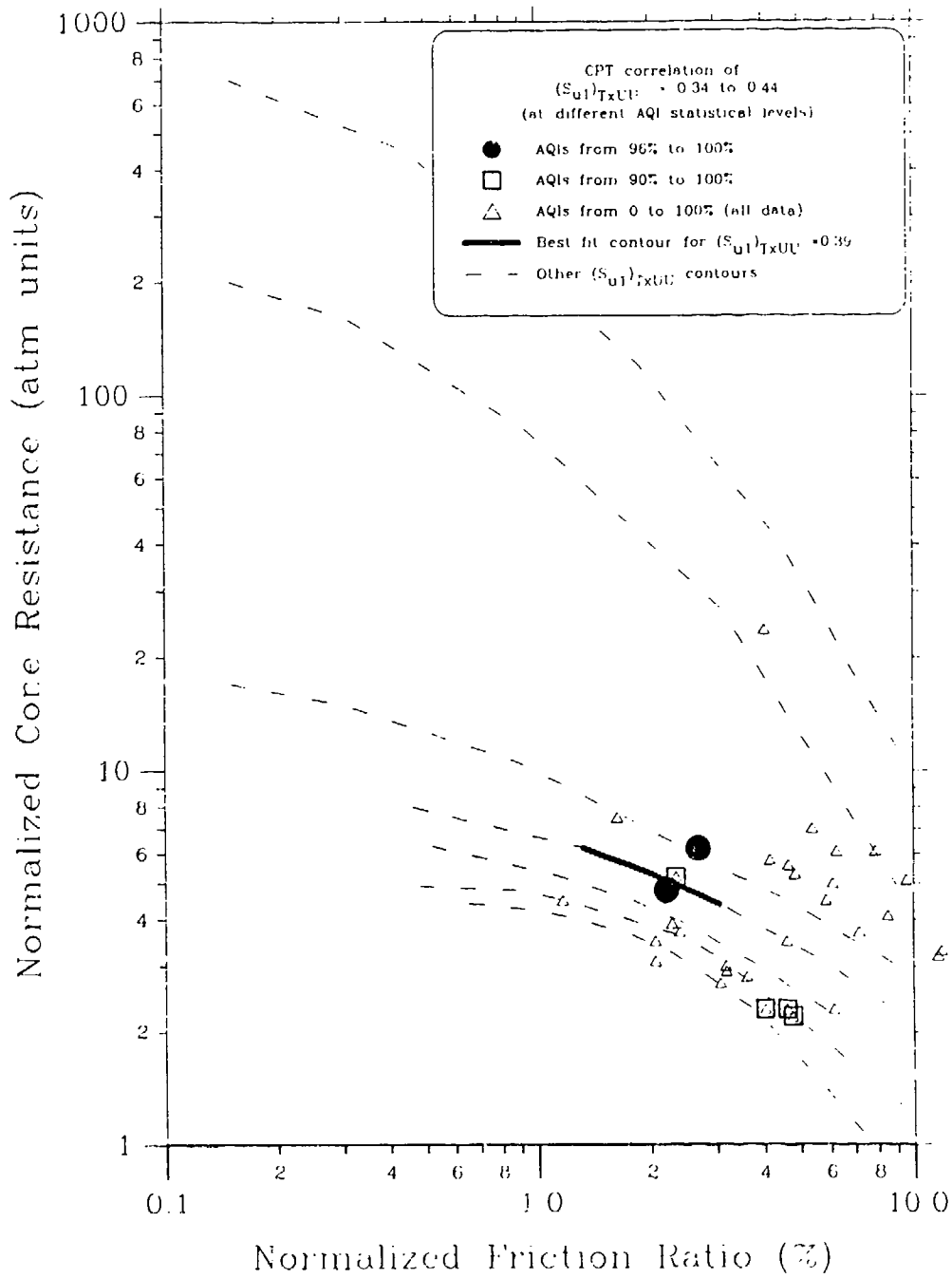


**Figure 8.32** Prediction of the  $(S_{u1})_{TxUU}=0.39$  contour on the CPT Soil Characterization Chart

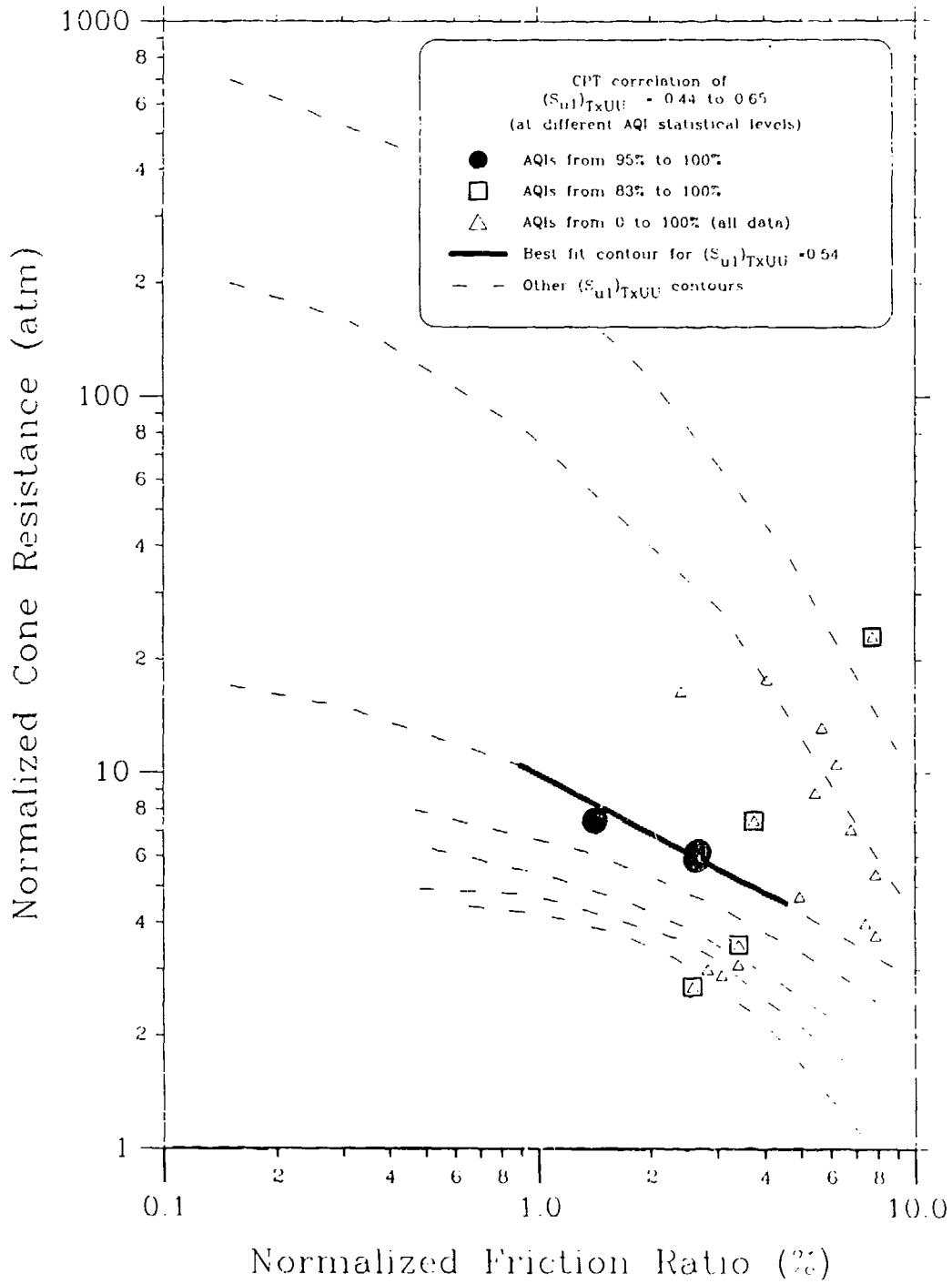


**Figure 8.33** Prediction of the  $(S_{u1})_{TxUU}=0.54$  contour on the CPT Soil Characterization Chart

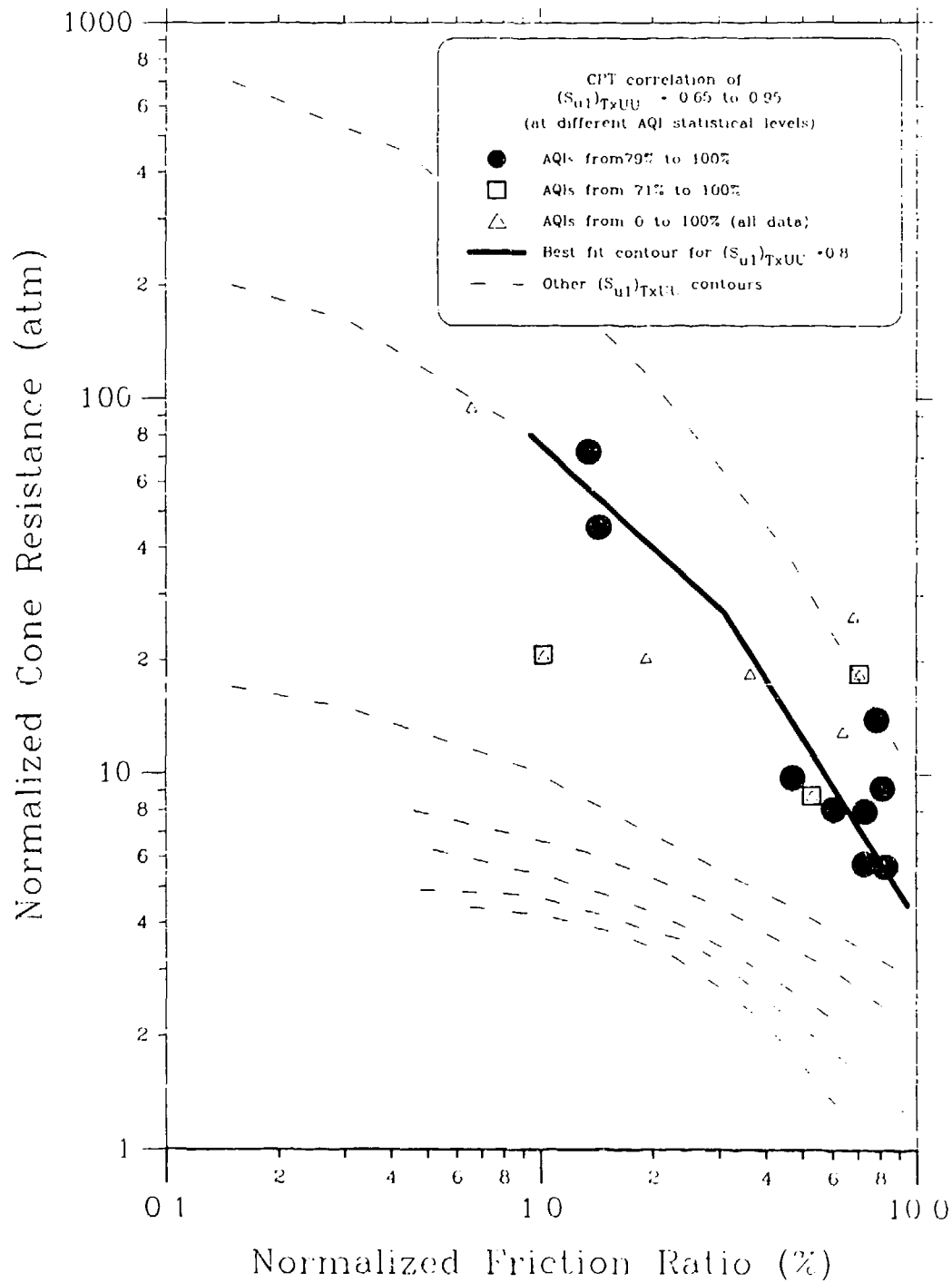


**Figure 8.34** Prediction of the  $(S_{u1})_{TxUU}=0.80$  contour on the CPT Soil Characterization Chart

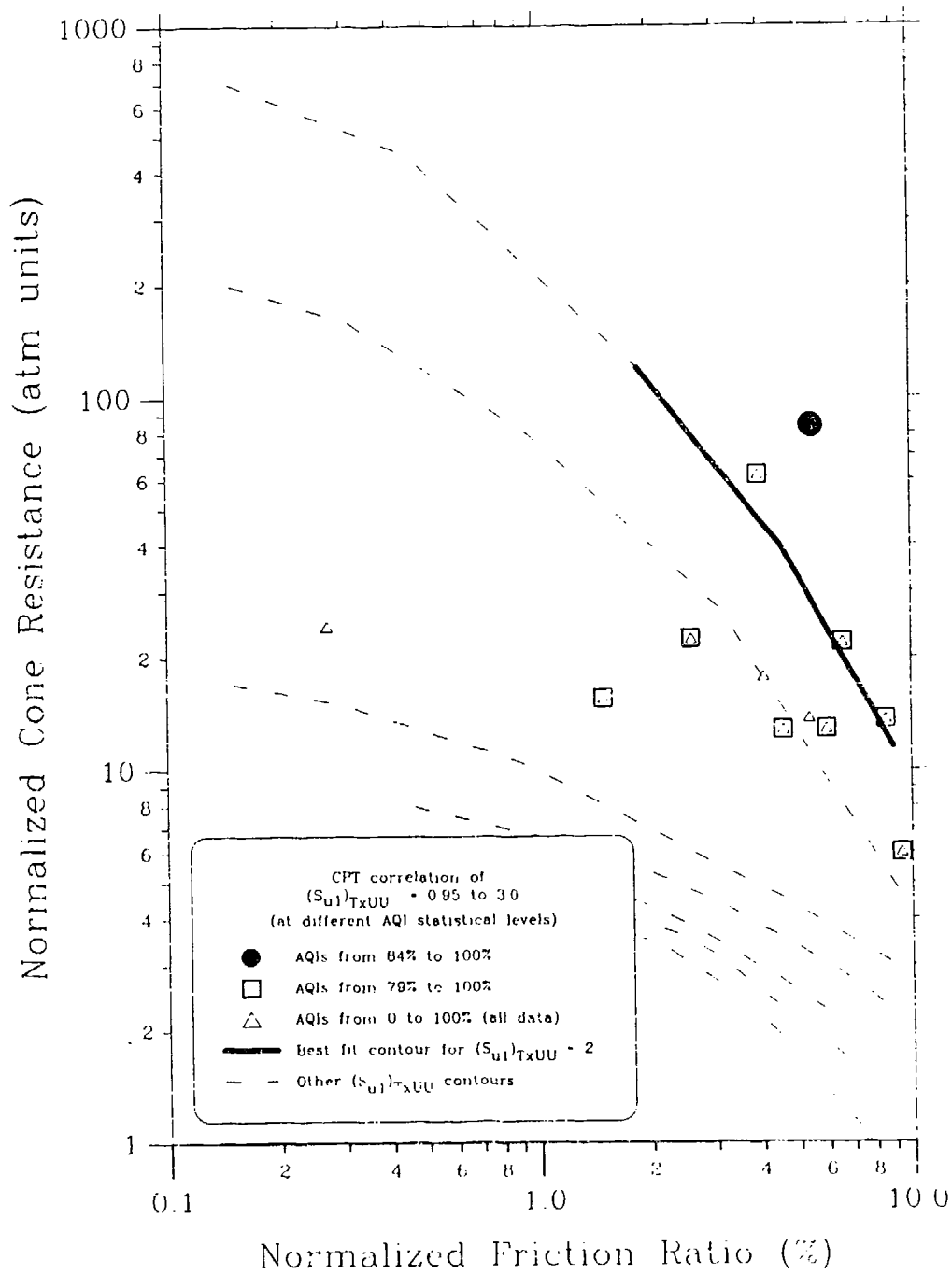


**Figure 8.35** Prediction of the  $(S_{u1})_{TxUU}=2$  contour on the CPT Soil Characterization Chart

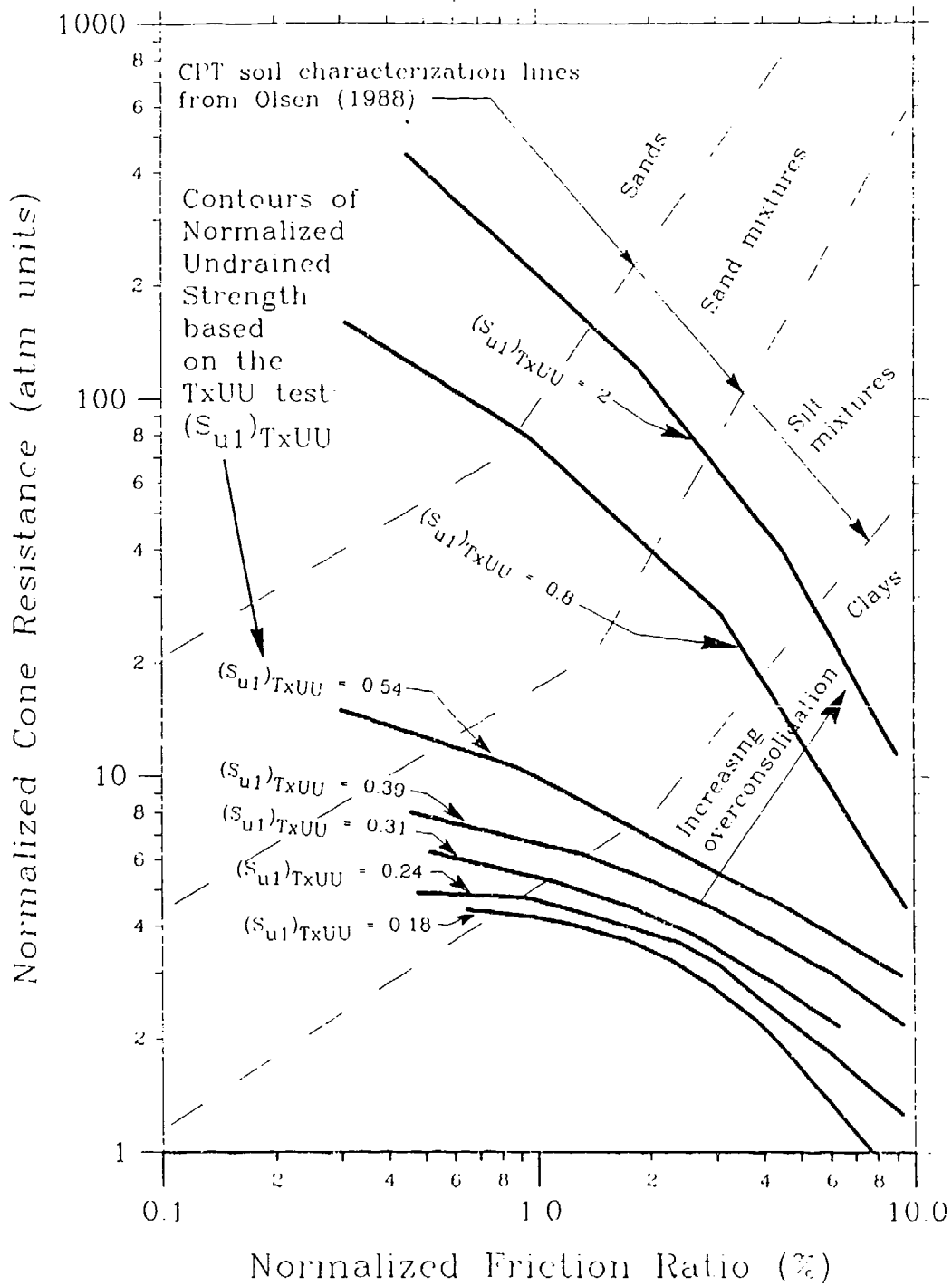


**Figure 8.36** Contours of normalized  $(S_{u1})_{TxUU}$  (i.e.  $(S_u)_{TxUU}/\sigma'_v$ ) on the CPT soil characterization chart for the unconsolidated undrained triaxial strength test

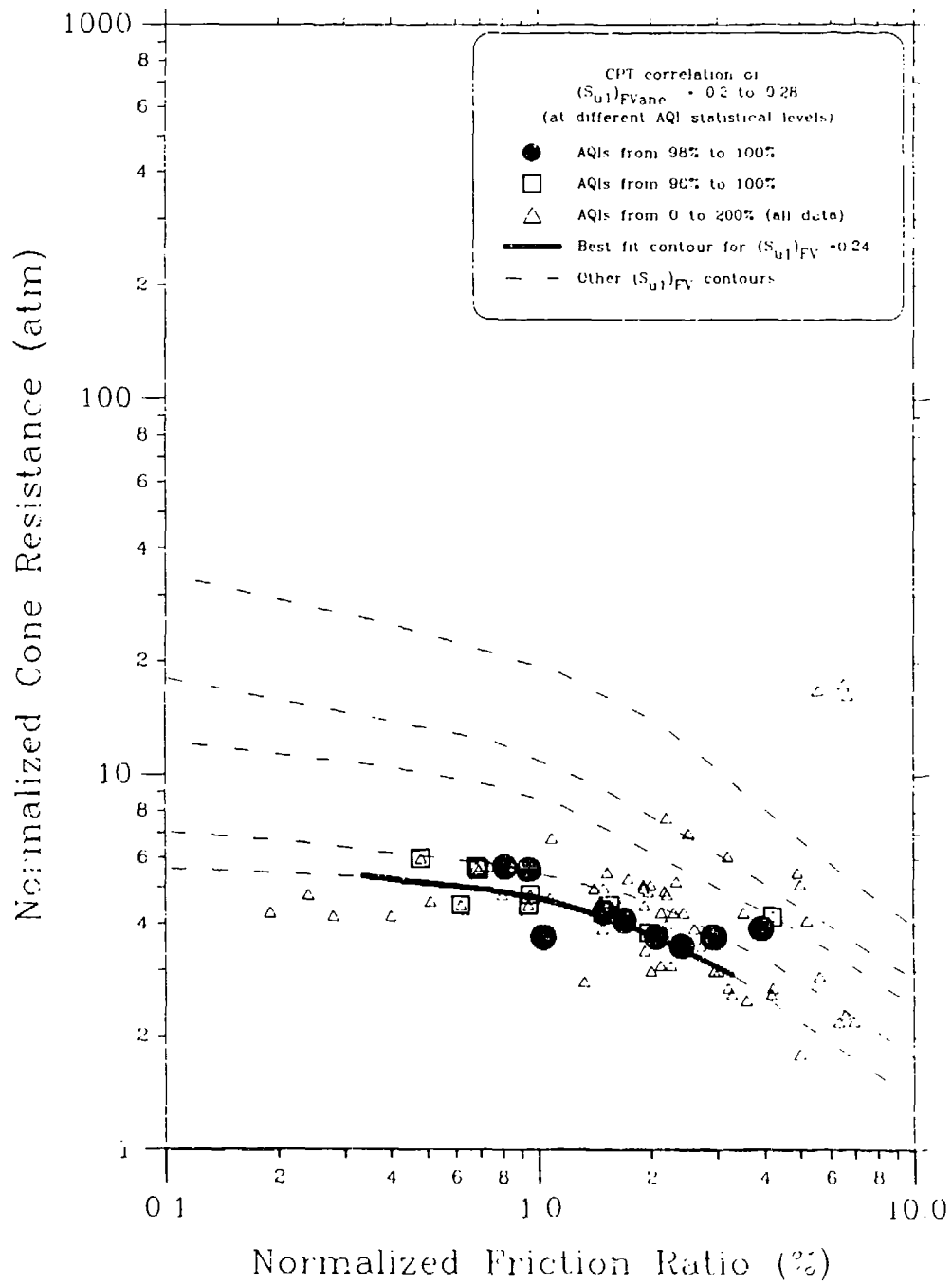


**Figure 8.37** Prediction of the  $(S_{u1})_{FVanc} = 0.25$  contour on the CPT soil characterization chart

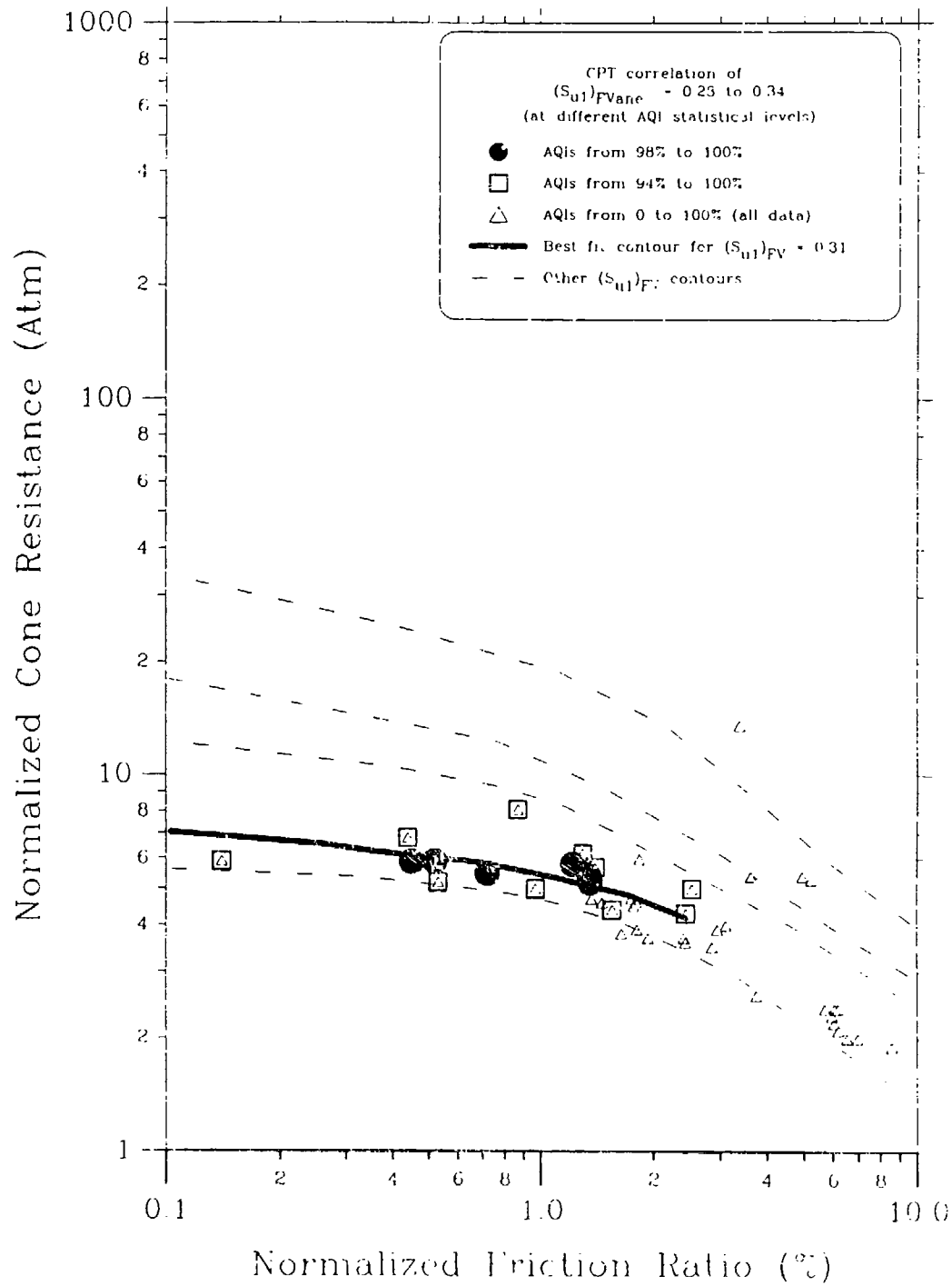


**Figure 8.38** Prediction of the  $(S_{u1})_{FVane} = 0.31$  contour on the CPT soil characterization chart

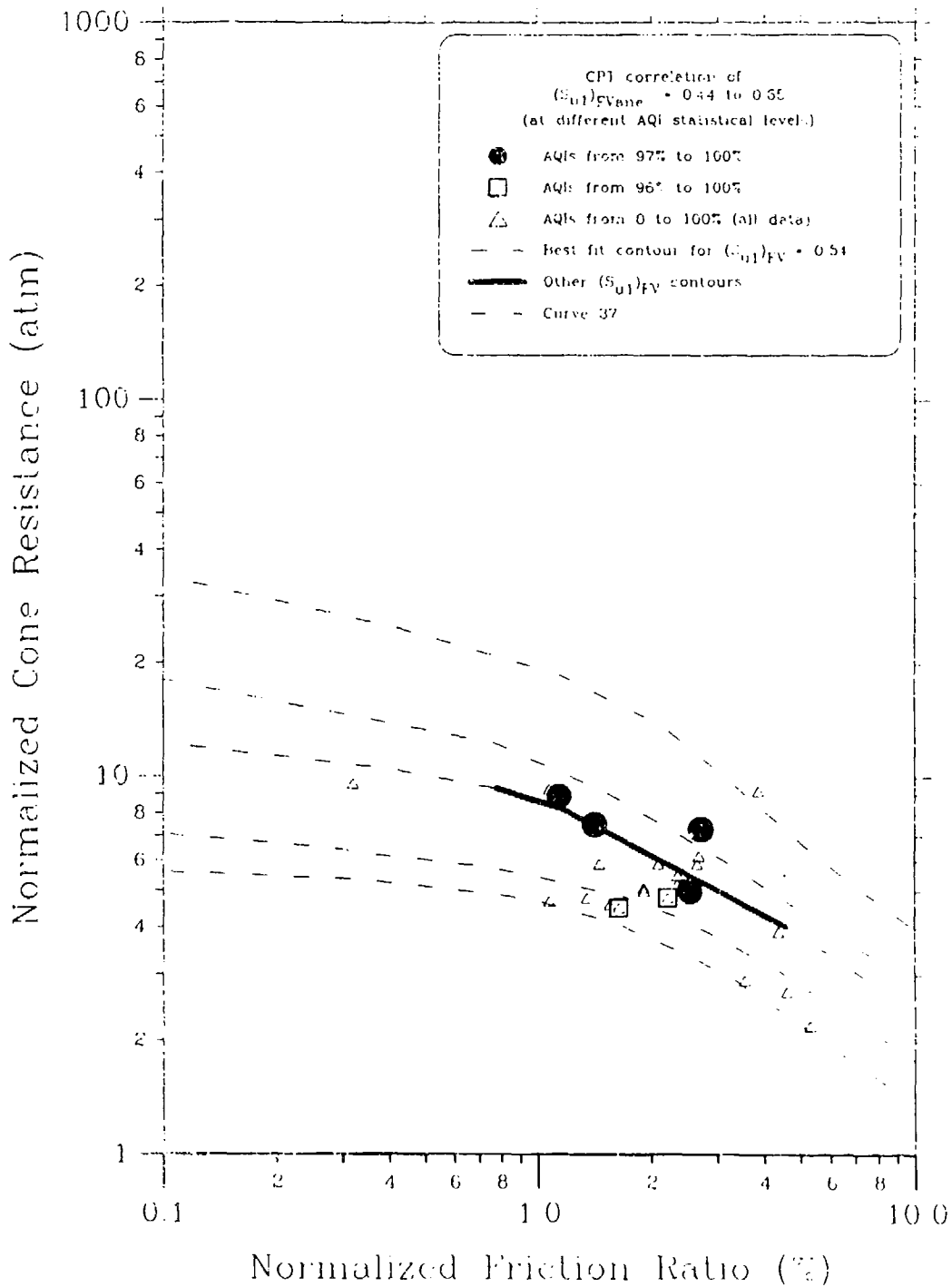


**Figure 8.39** Prediction of the  $(S_{u1})_{FVanc} = 0.54$  contour on the CPT soil characterization chart



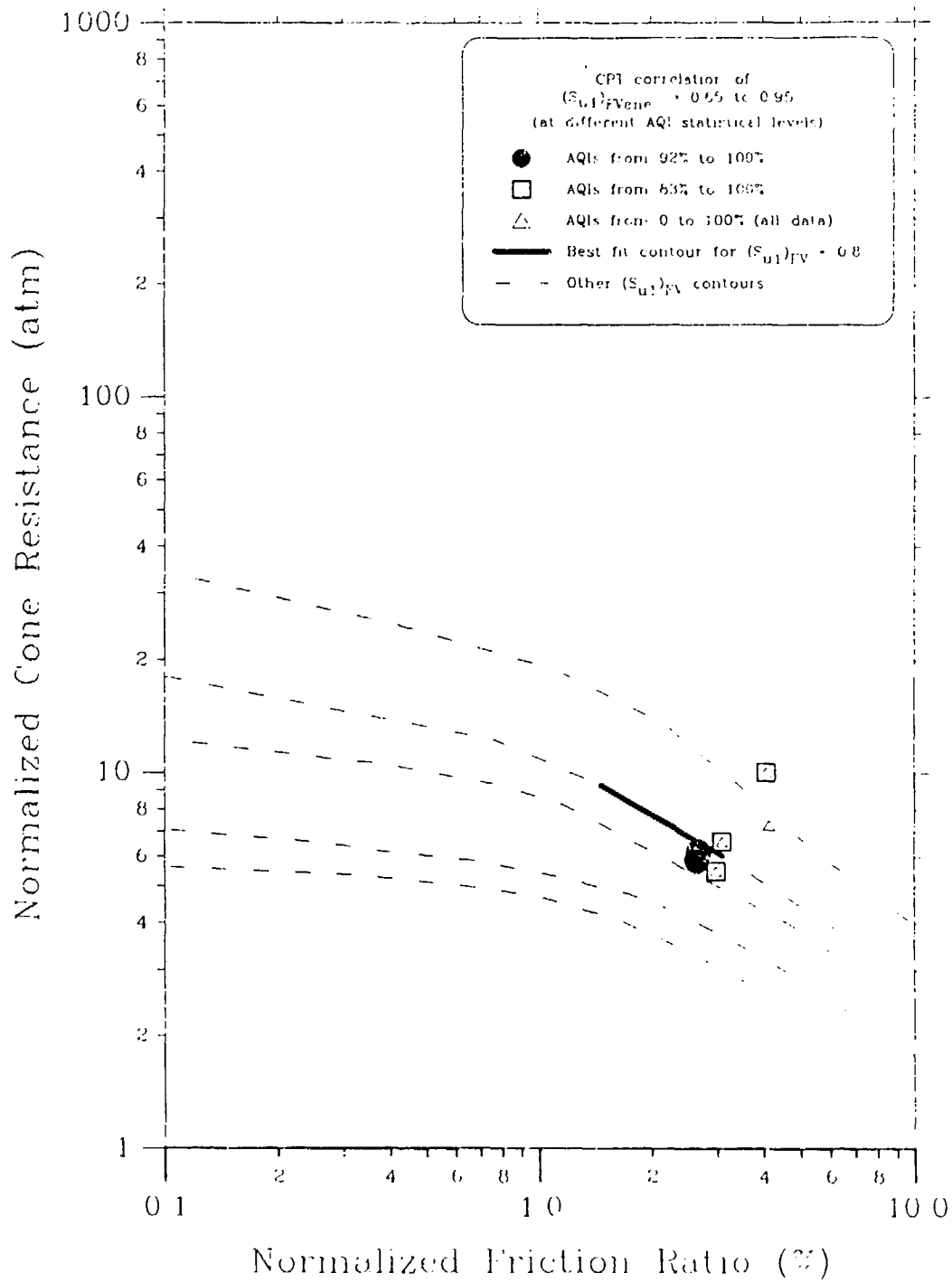


**Figure 8.40** Prediction of the  $(S_{u1})_{FVanc} = 0.80$  contour on the CPT soil characterization chart

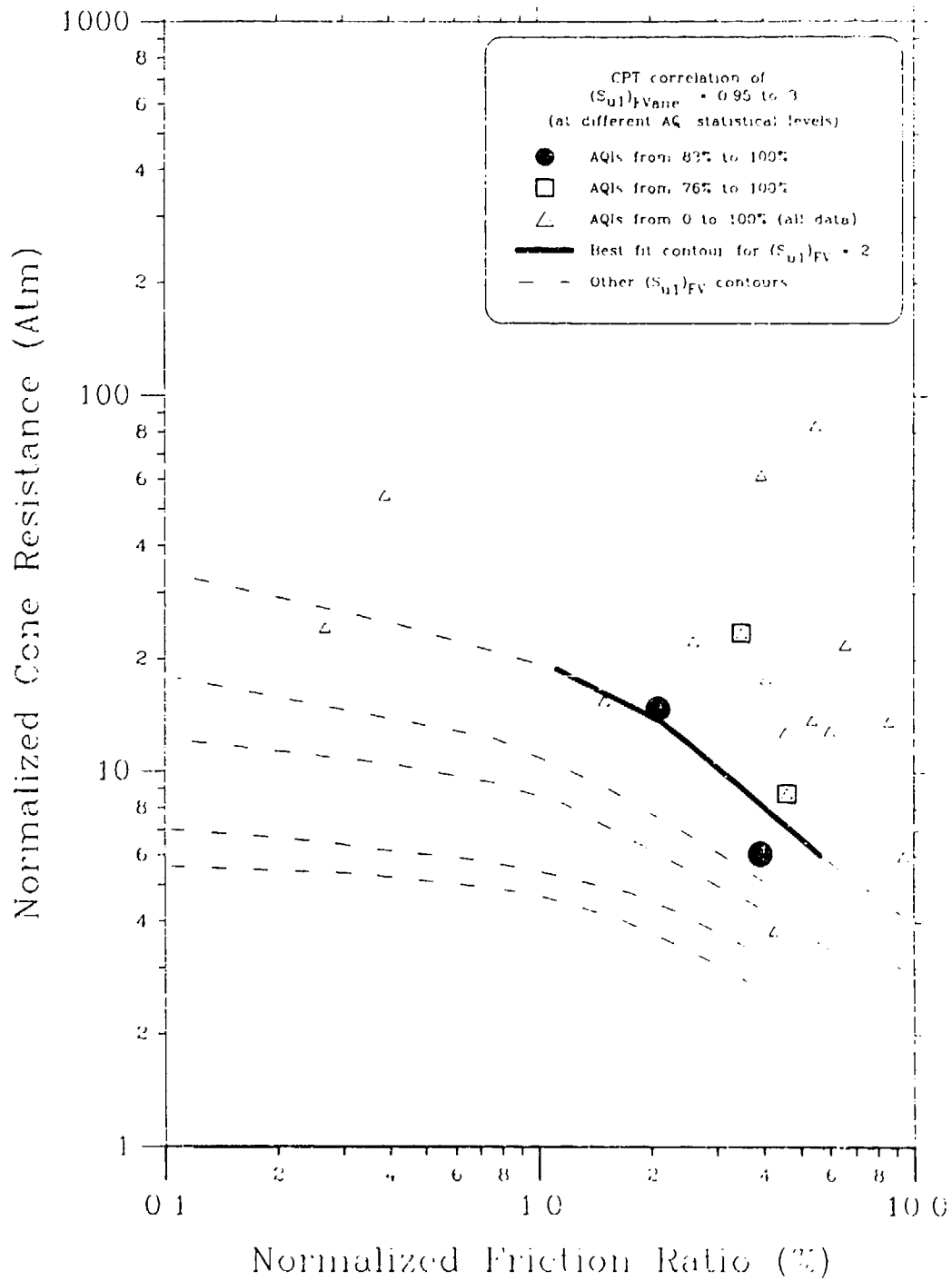


**Figure 8.41** Prediction of the  $(S_{u1})_{FVane} = 2$  contour on the CPT soil characterization chart

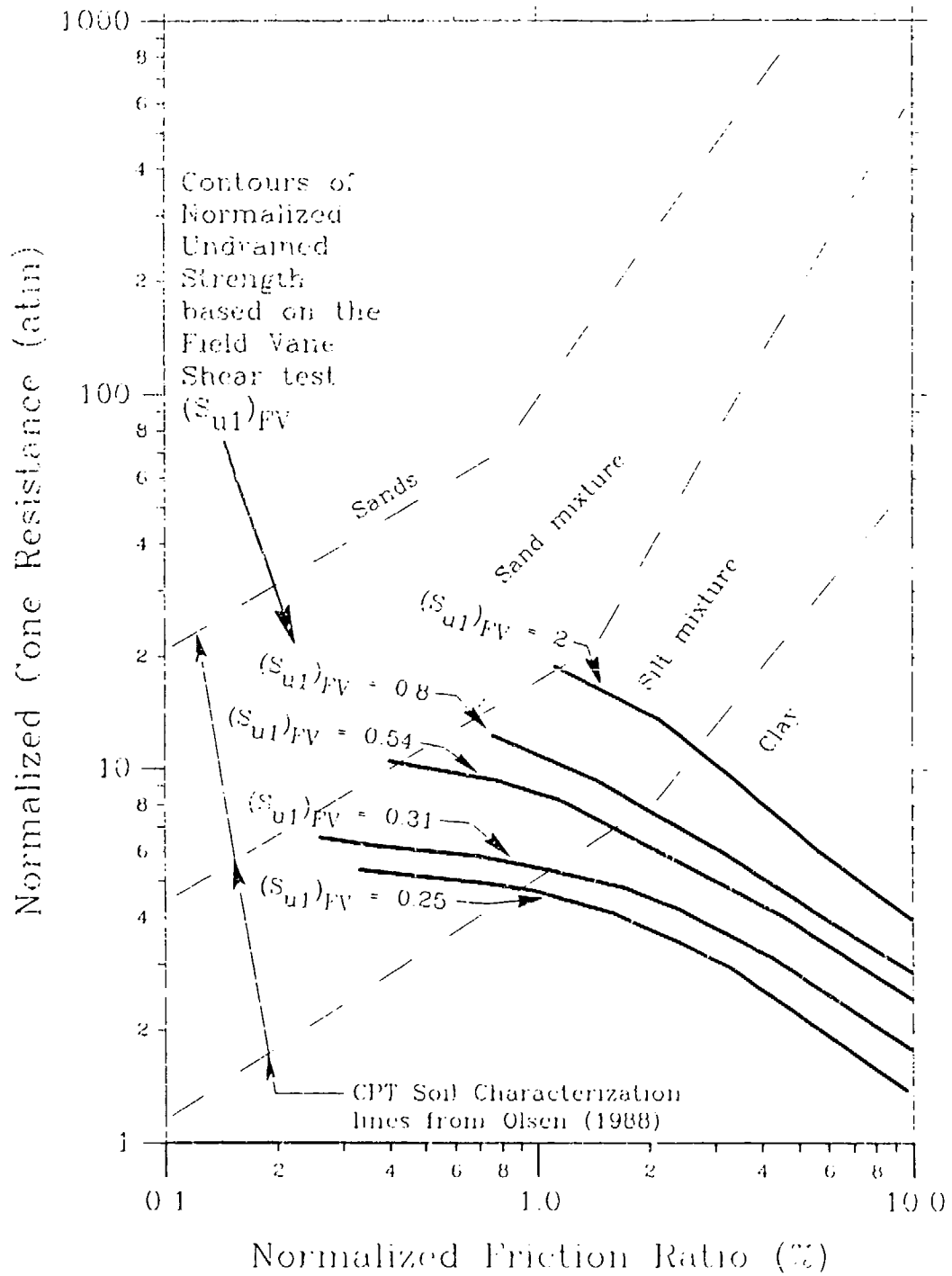


**Figure 8.42** Contours of  $(S_{u1})_{FVanc}$  (i.e.  $(S_u)_{FVanc} / \sigma'_v$ ) for the field vane shear on the CPT soil characterization chart

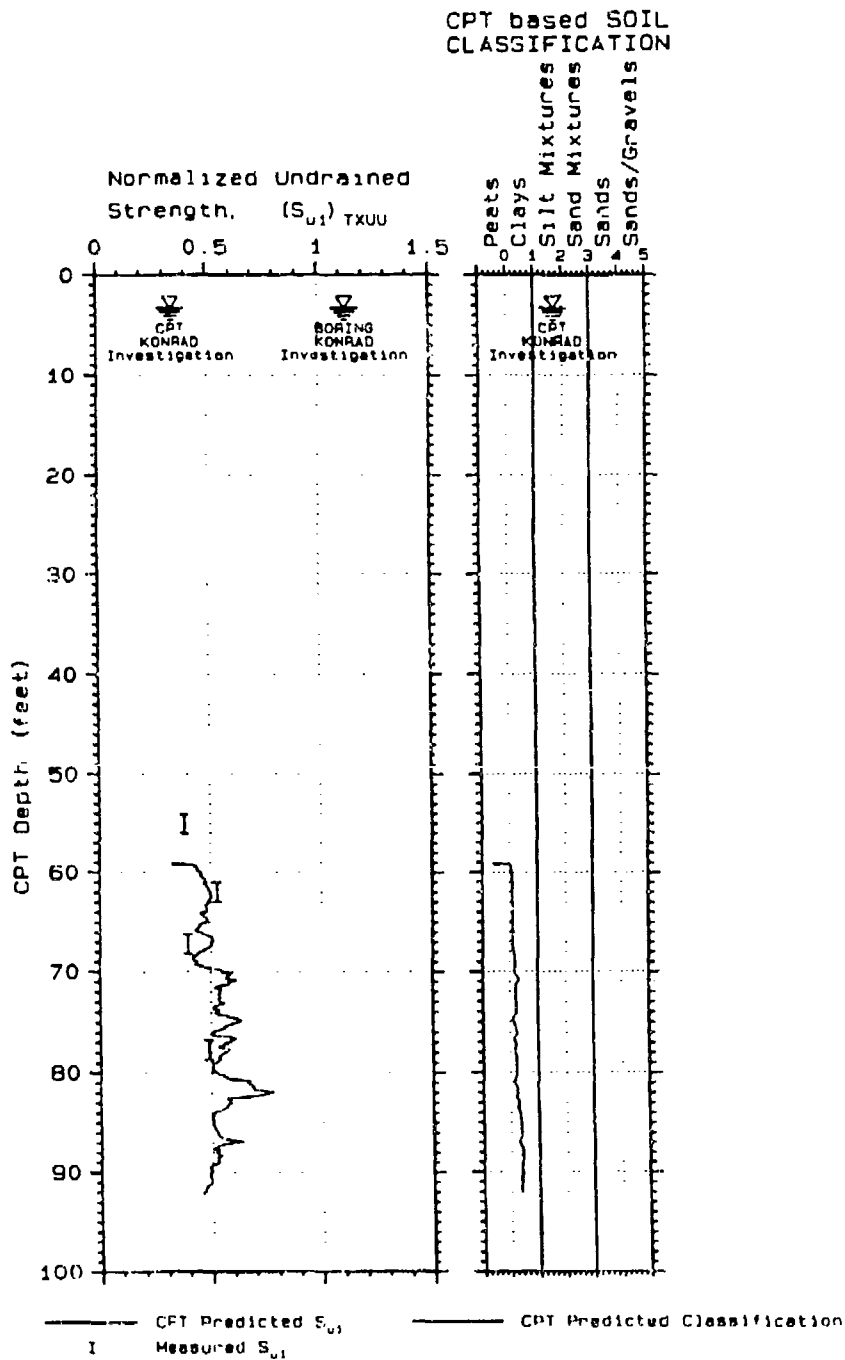


**Figure 8.43** CPT predicted versus measured  $(S_{u1})_{TXUU}$  for silty clays from a Fraser River site, Vancouver International Airport, Canada (data from Konrad, et al., 1985)

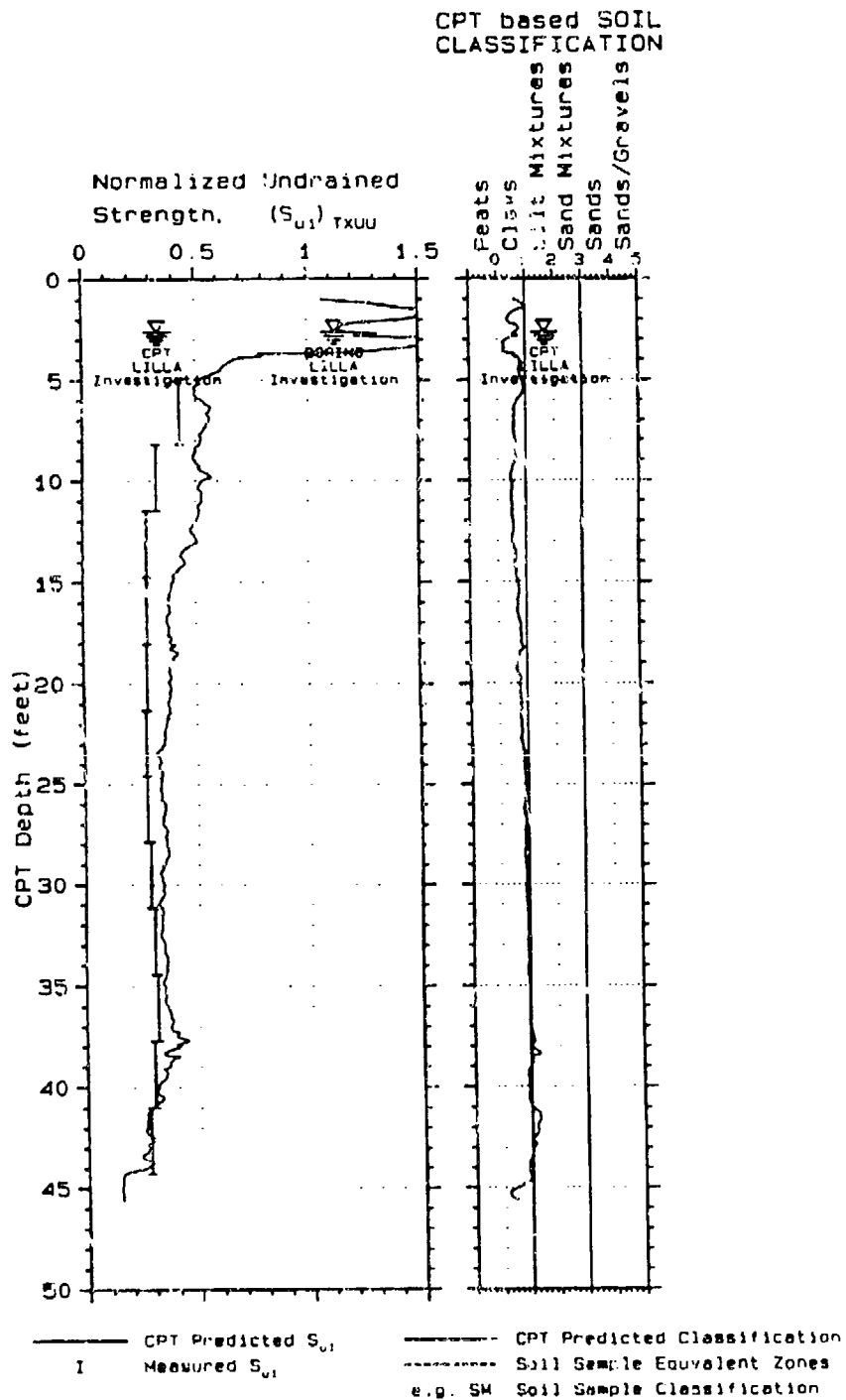


**Figure 8.44** CPT predicted versus measured  $(S_{U1})_{TXUU}$  for silty clay from Limna Mellösa, Sweden (40 km north of Stockholm) (data from Larsson & Mutabdic, 1991)



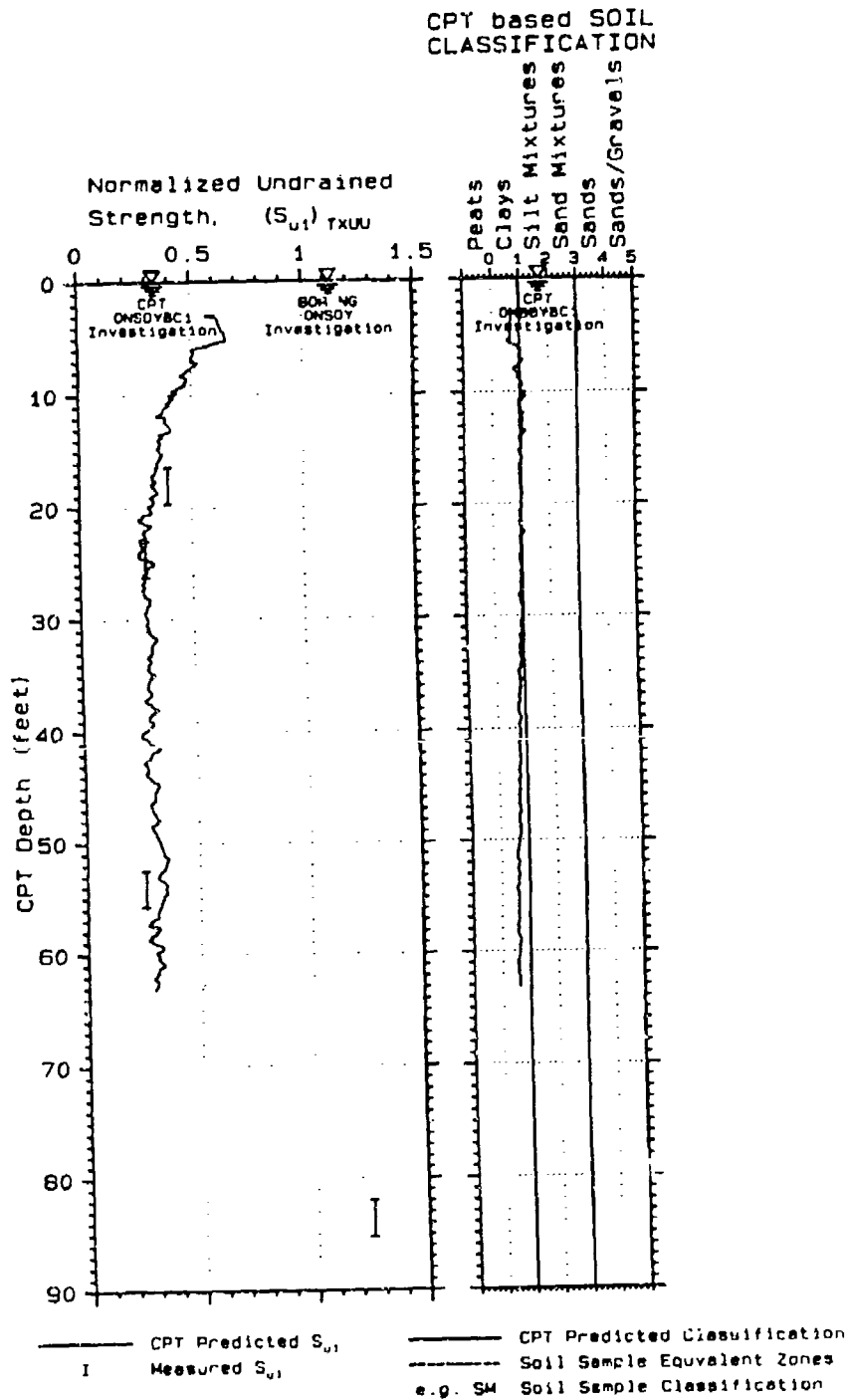


**Figure 8.46** CPT predicted versus measured  $(S_{u1})_{TxUU}$  for the Onsoy site in Norway (NGI research site) (the measured strength data are at four different depths) (data from Rad, et al., 1985, Gillespie, et al., 1985)

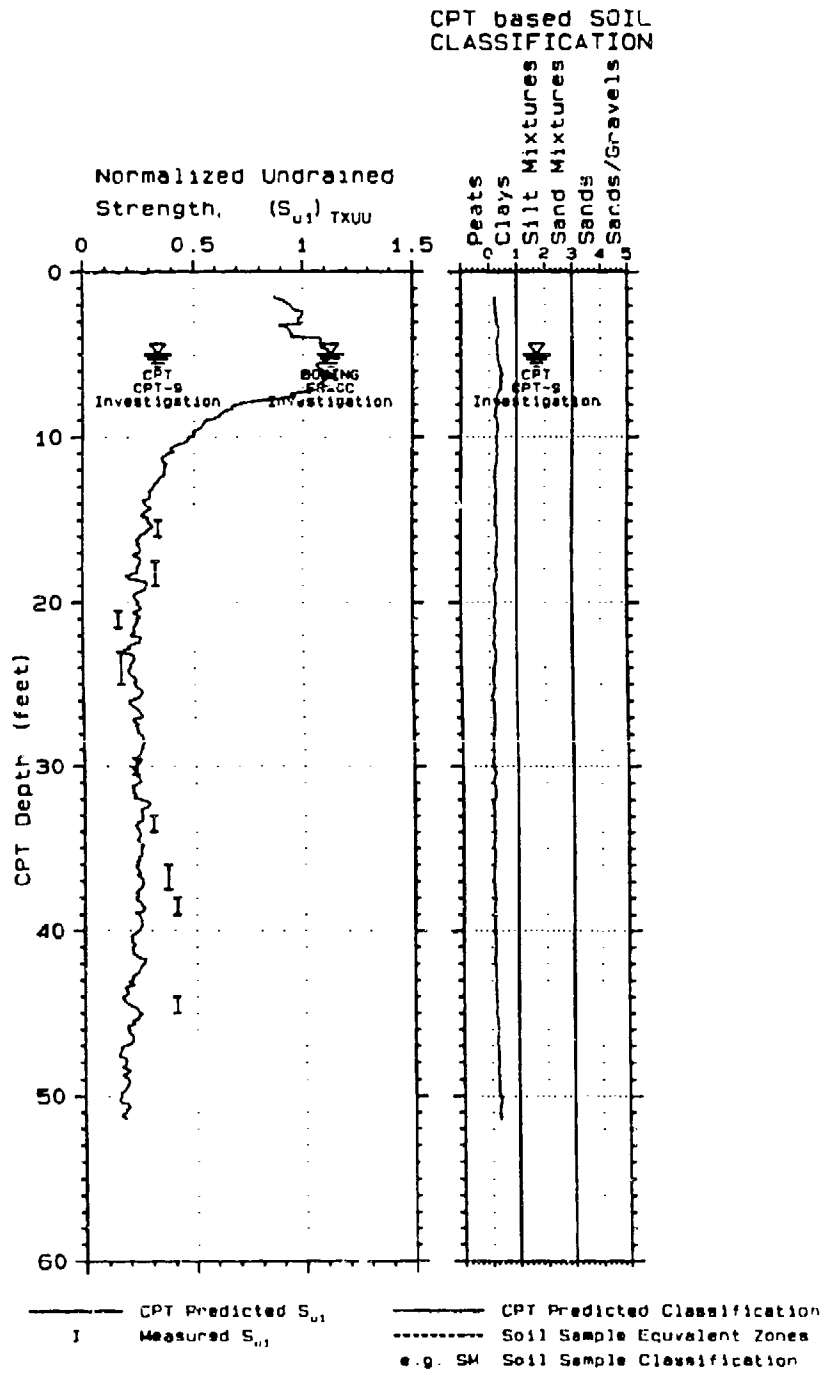


**Figure 8.47** CPT predicted versus measured  $(S_{u1})_{TxUU}$  for San Francisco Bay mud at Hamilton AFB (University of California at Berkeley research site) (data from project code ET-SE)



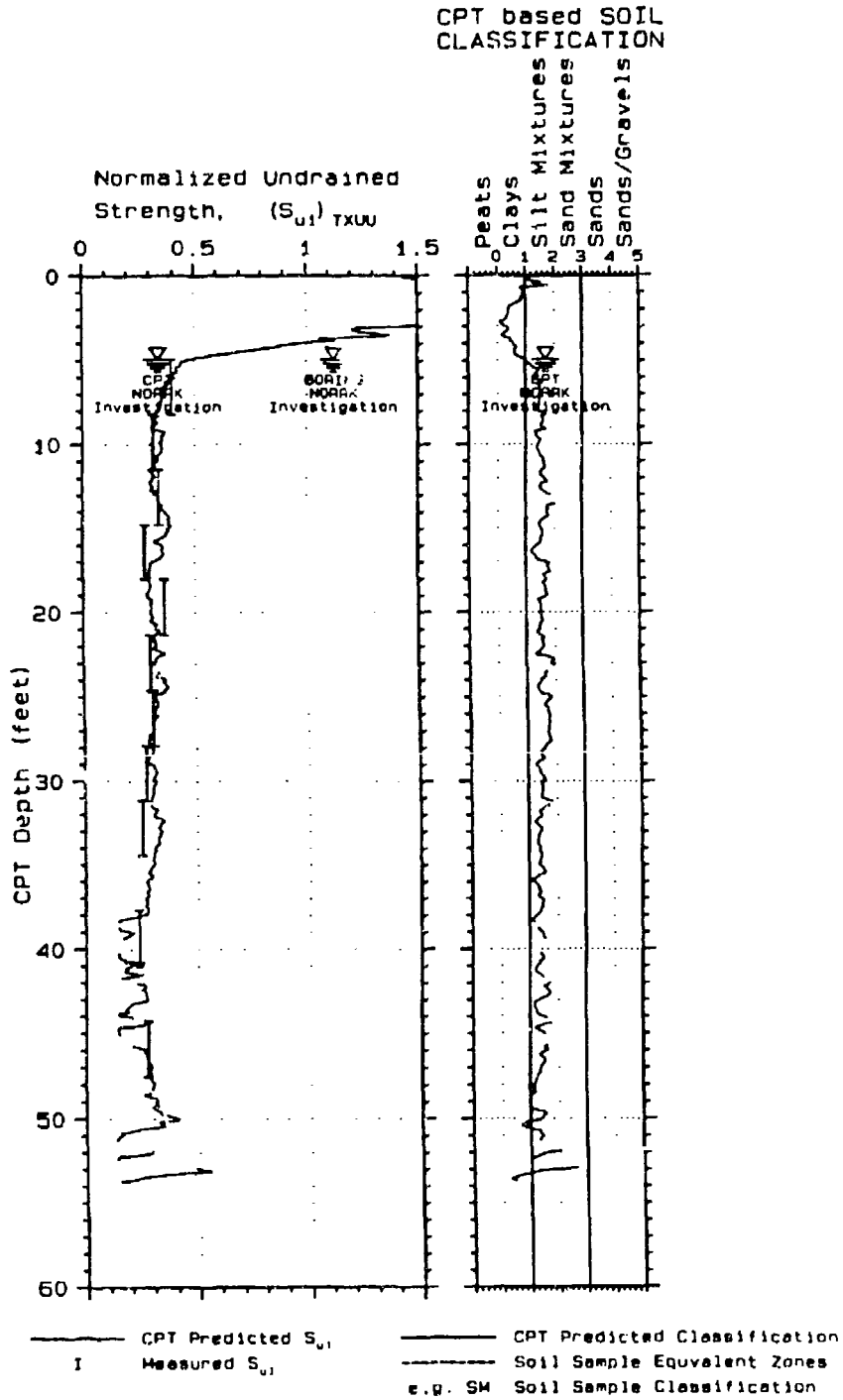


**Figure 8.48** CPT predicted versus measured  $(S_{u1})_{TXUU}$  from Norrköping, Sweden (with measurements at 11 different depths) (a Swedish Geotechnical Institute research site) (data from Larsson and Mu abdic, 1991)

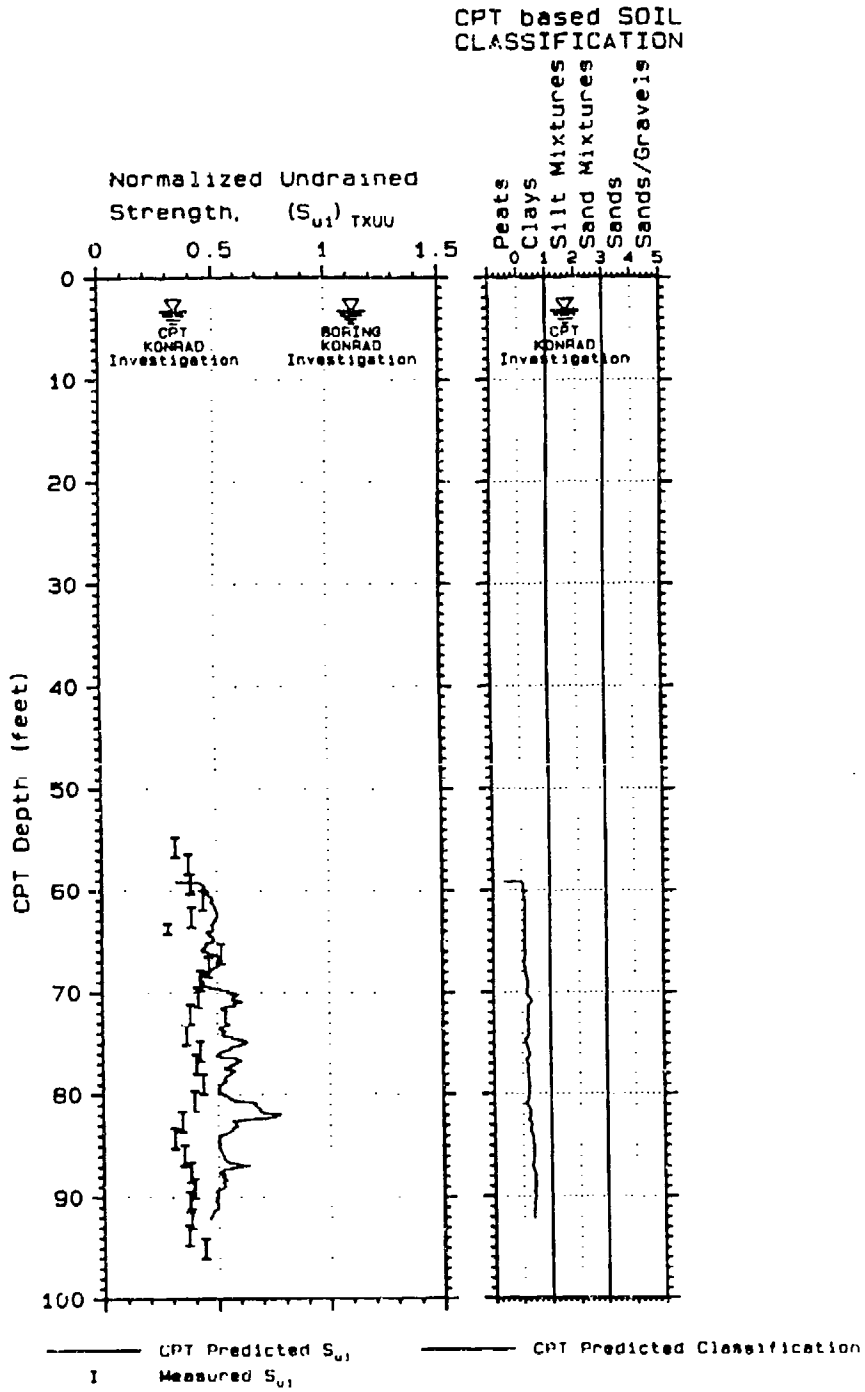


**Figure 8.49** CPT predicted versus measured  $(S_{u1})_{TxUU}$  from the Hibernia offshore investigation (data from Konrad, et al., 1991)

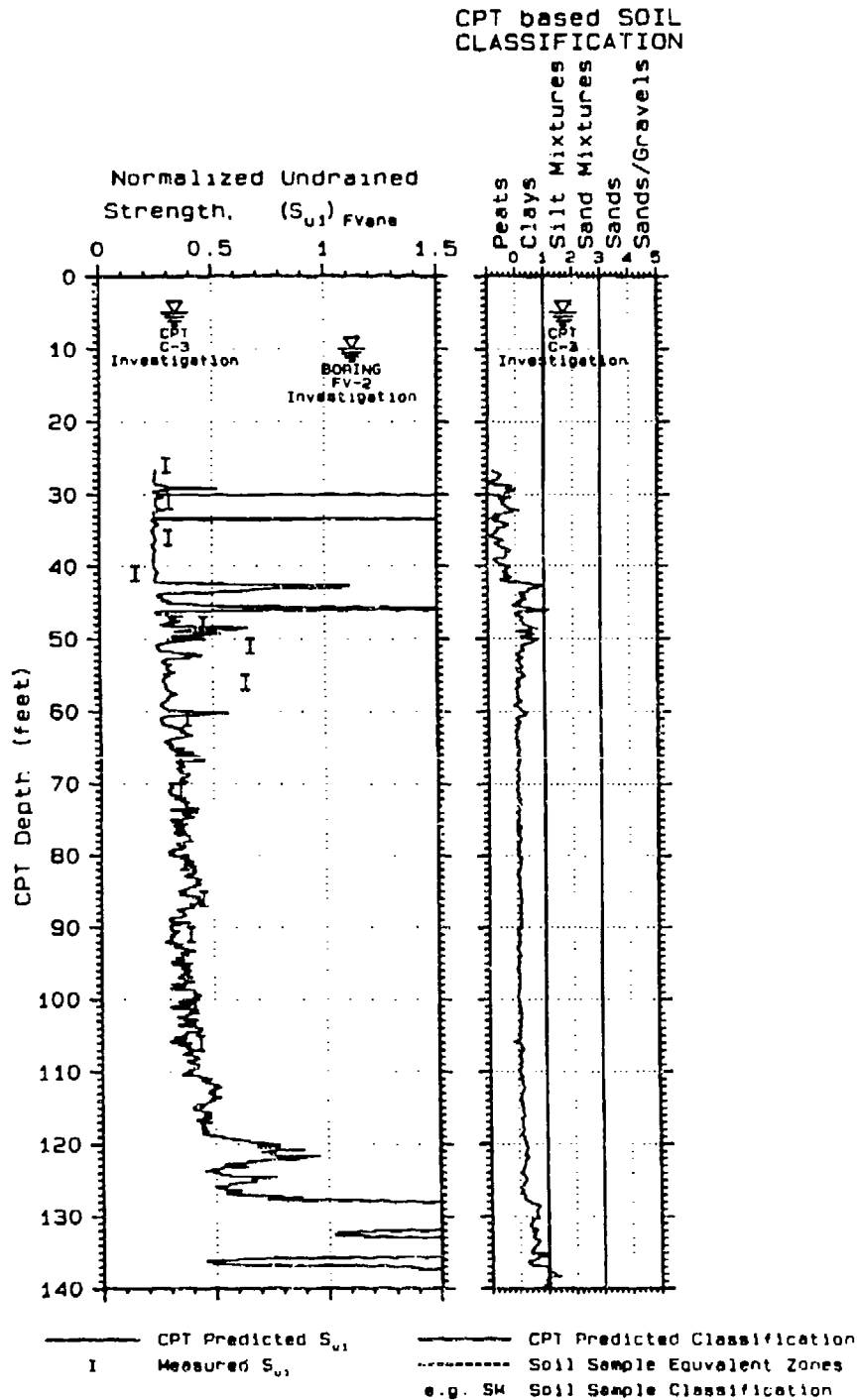


**Figure 8.50** CPT predicted versus measured  $(S_{UI})_{TxUU}$  for San Francisco bay mud at the muni metro turnaround facility (with measurements from 17 different depths) (data from Dames & Moore, 1985)

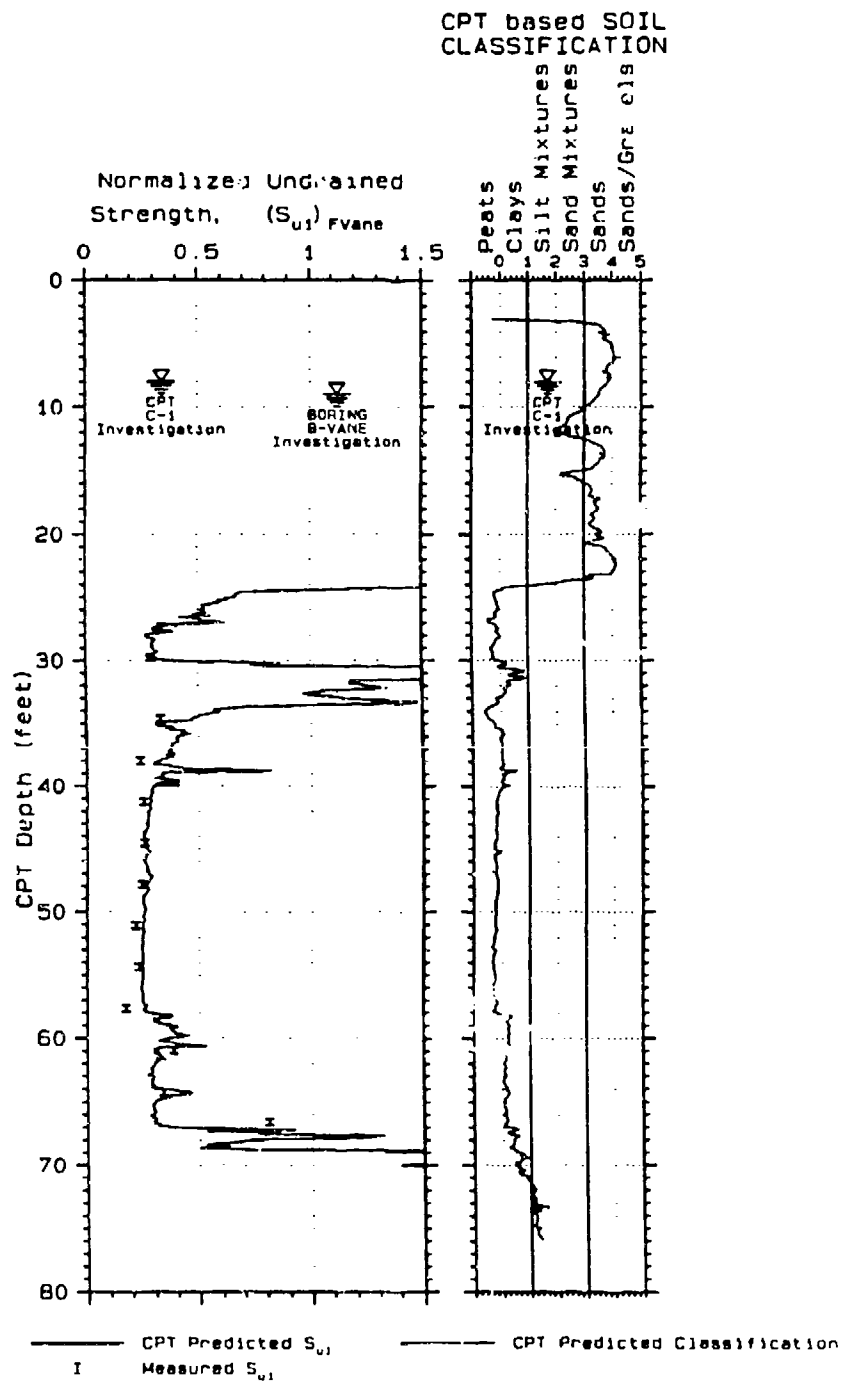


**Figure 8.51** CPT predicted versus measured  $(S_{u1})_{Fvane}$  for a conference pile load test at Northwestern University in 1988 (with measurements from 12 different depths) (data from Stratigraphics, Inc, 1988)

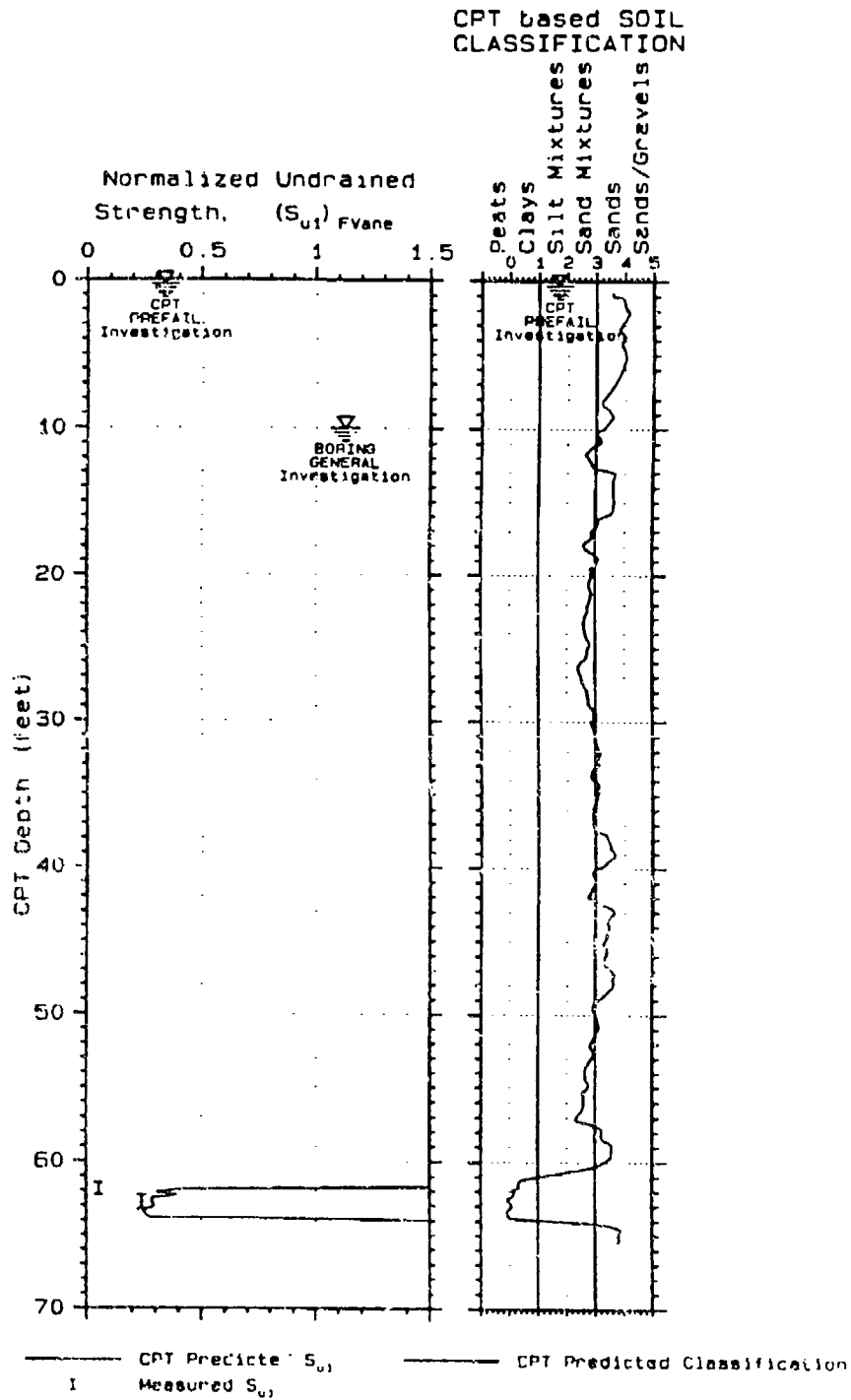


**Figure 8.52** CPT predicted versus measured  $(S_{u1})_{FVane}$  for a foundation clay layer for the Nerlerk Berm liquefaction slide study

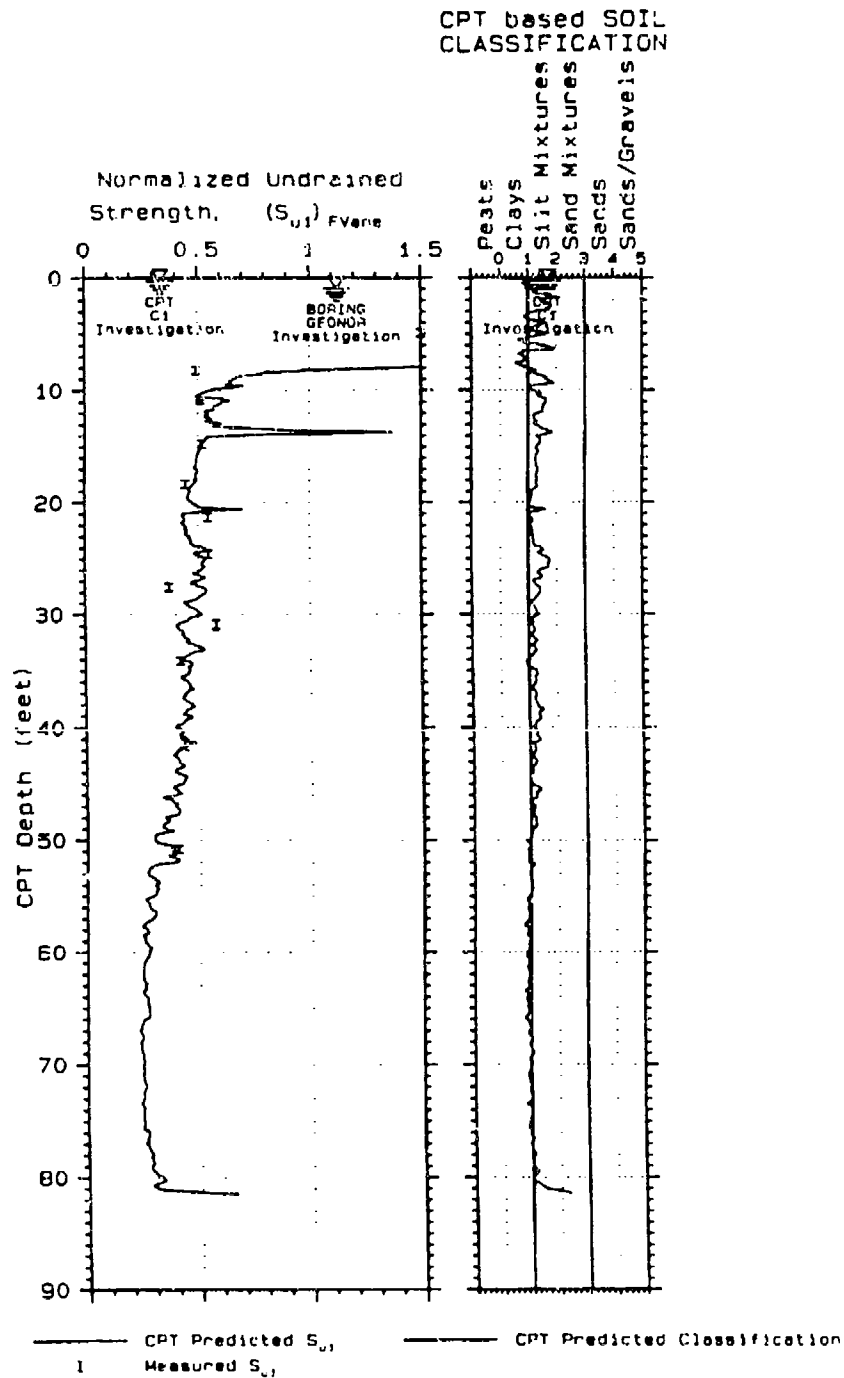


**Figure 8.53** CPT predicted versus measured  $(S_{u1})_{FVane}$  at the Fraser River Delta Bridge, 25 km SW of Vancouver, Canada (with measurements from 11 different depths) (Data from Crawford & Campanella, 1991)



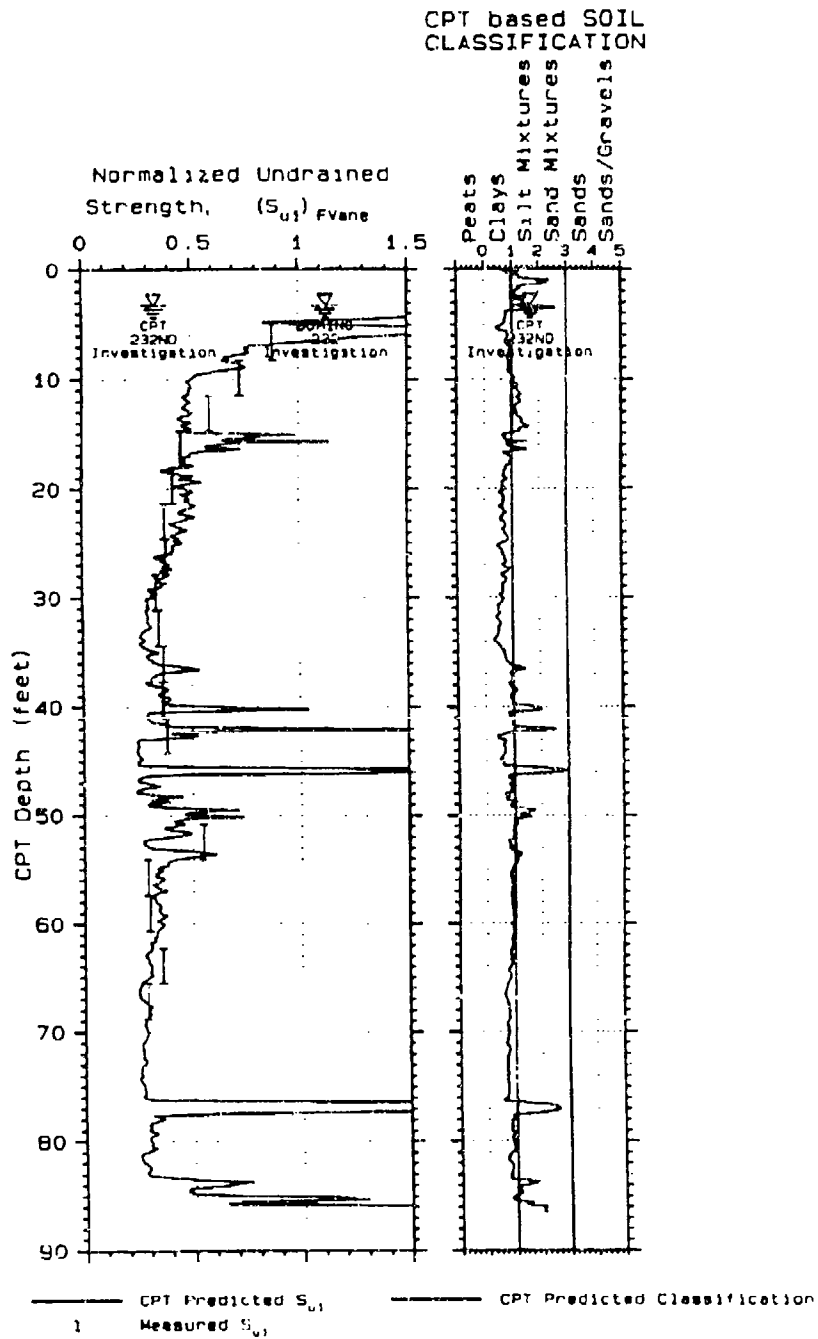


**Figure 8.55** CPT predicted versus measured  $(S_{u1})_{FVane}$  at Lower 232 Street, Langley, British Columbia, Canada (data from Campanella, et al., 1991)



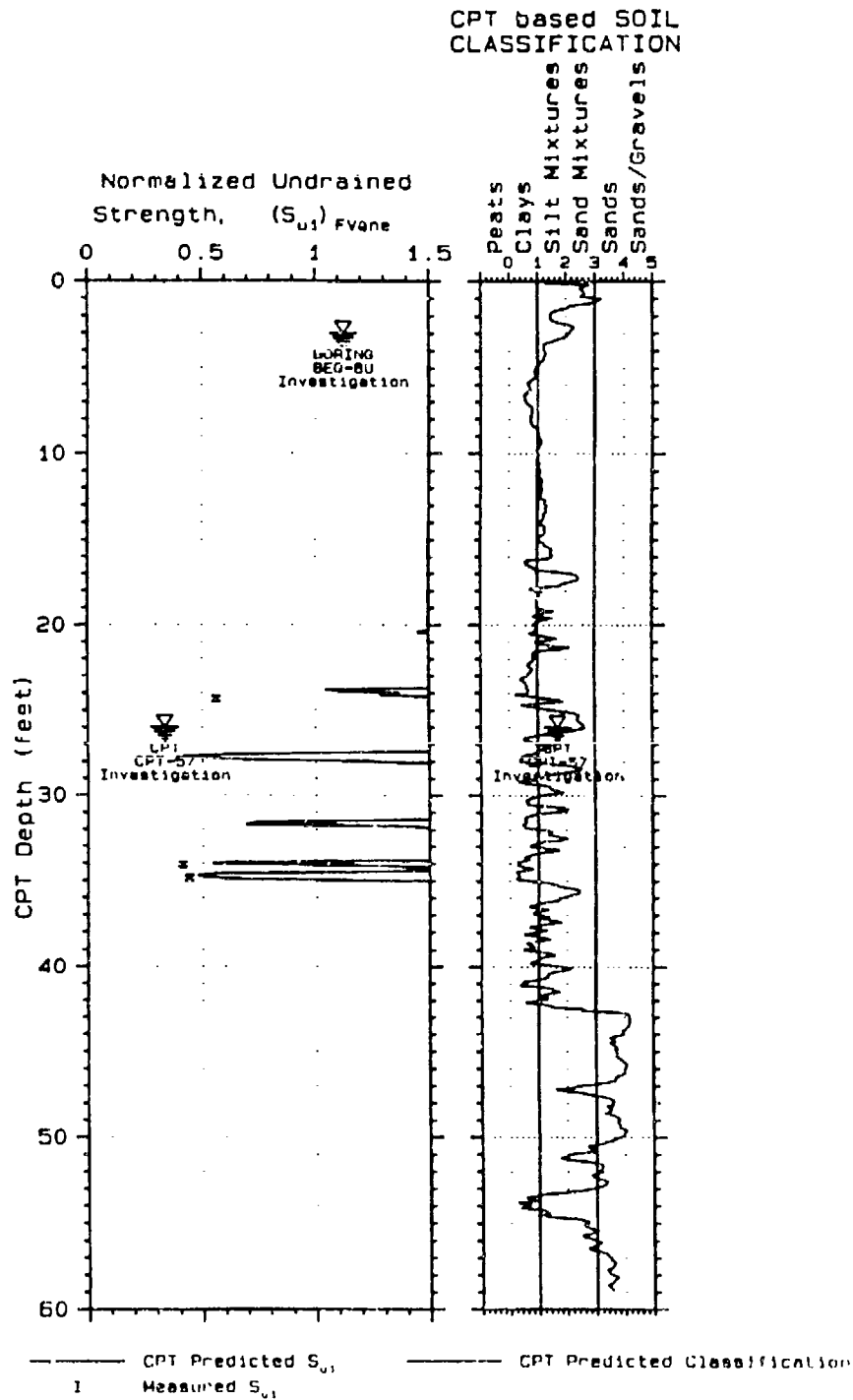


**Figure 8.56** CPT predicted versus measured  $(S_{u1})_{FVane}$  at Barkley dam, within clay lenses (data from Olsen, et al., 1989)

This  $\mu$  factor is used to reduce the measured field vane shear strength to an equivalent undrained triaxial test strength level (i.e. field strength value for slope stability evaluation). The  $\mu$  is therefore the ratio of  $(S_{ul})_{TxUU}$  contours in Figure 8.36 to the  $(S_{ul})_{FV}$  contours in Figure 8.42 as illustrated in Figure 8.57, with the results shown in Figure 8.58. The  $\mu$  contours in Figure 8.58 (i.e. 0.5 to 1.0) have the same general range as from historic observations in Figure 8.59 (i.e. 0.4 to 1.0). The Bjerrum  $\mu$  factor was historically indexed to Plasticity Index (PI) as shown in Figure 8.59 (Bjerrum, 1972). PI is now used only to index overconsolidation character as shown at the top of Figure 8.60 (Aas, Lacasse, Lunne, and Hoeg, 1985). After the overconsolidation character is estimated, the Bjerrum  $\mu$  factor is then estimated using the chart at the bottom of Figure 8.60. This figure shows that the  $\mu$  factor is approximately 0.6 to 1.0 for normally consolidated clay and 0.35 to 1.0 for overconsolidated clay. The contours in Figure 8.58 show a calculated  $\mu$  factor of about 0.9 to 1.0 for normally consolidated clays decreasing to 0.5 with increasing overconsolidation or increasing silt content. The lack of field vane shear data for highly overconsolidated clays prevents establishing  $\mu$  contours which are lower than 0.50.

### *Conclusions*

This section introduced a new technique for estimating undrained strength of clay which appears to be as accurate as methods which require estimating the cohesive  $N_c$  bearing factor. These correlations were shown to give good agreement between measured and predicted values for clays around the world.

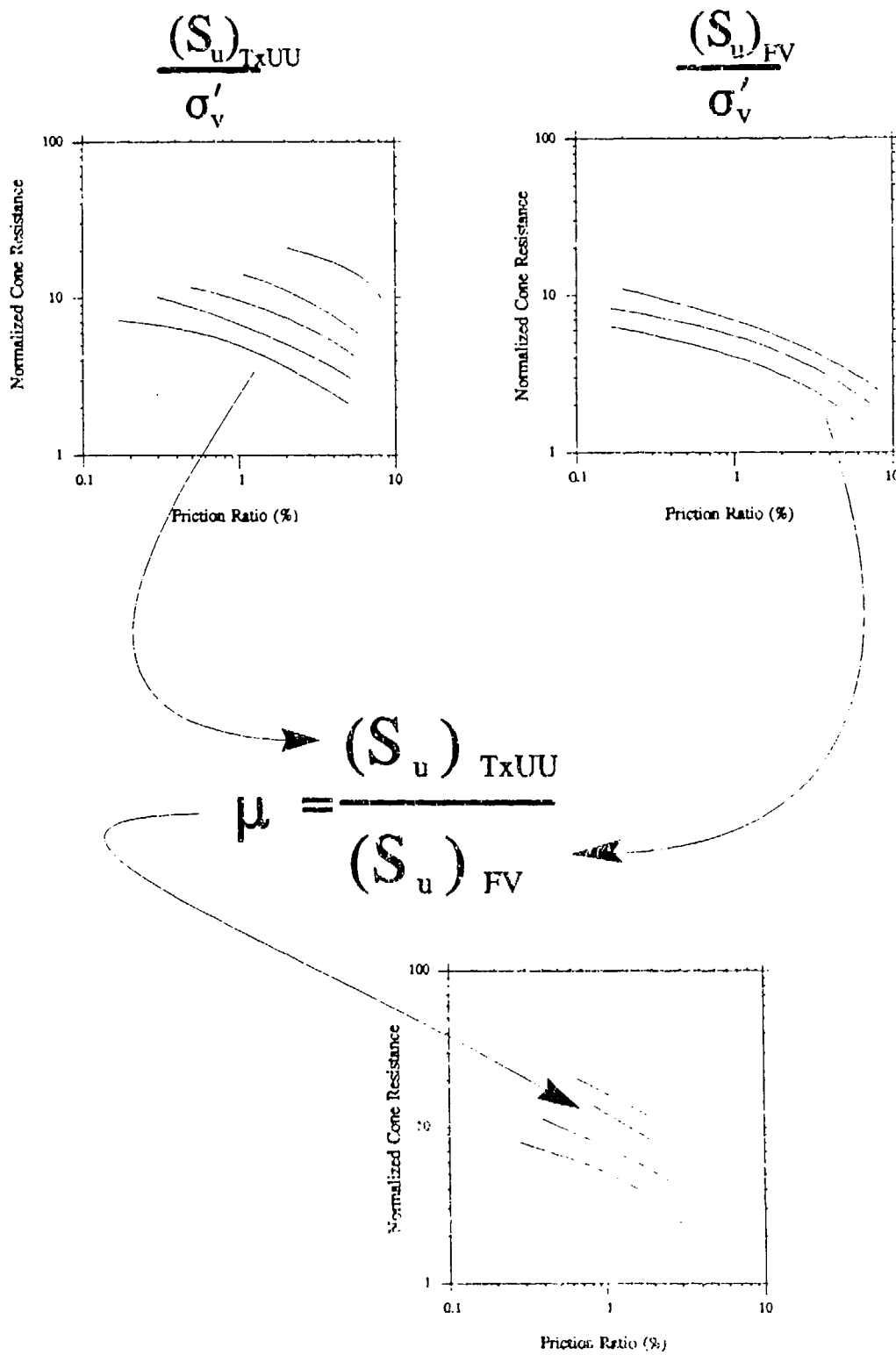


**Figure 8.57** Illustration on how to calculate the Bjerrum  $\mu$  correction factor using the predicted  $S_{u1}$  contours

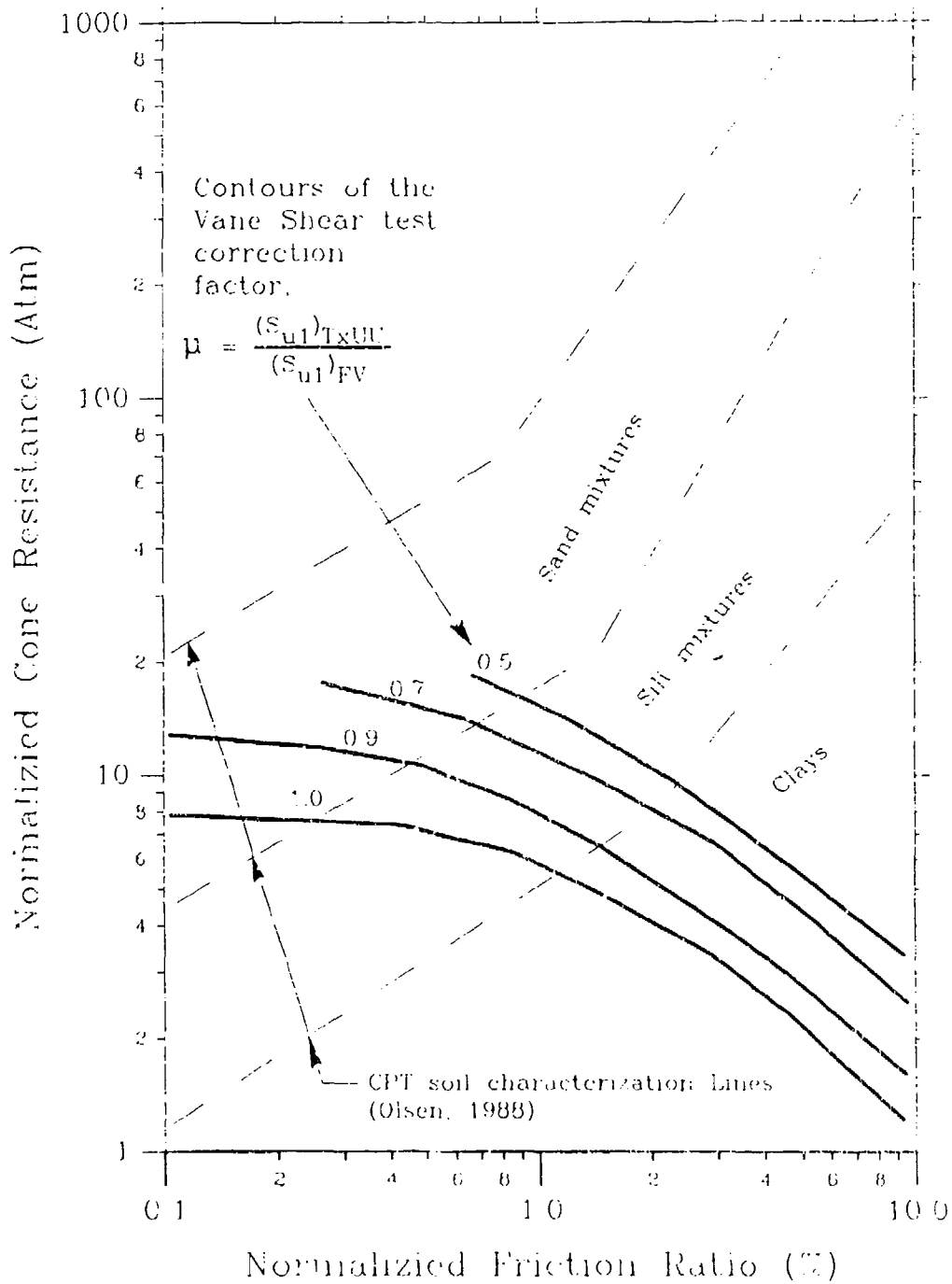


**Figure 8.58** Calculated contours of  $(S_u)_{T_{xUV}}/(S_u)_{FV}$  on the CPT soil characterization chart by taking a ratio of contours on Figure 8.36 to Figure 8.42

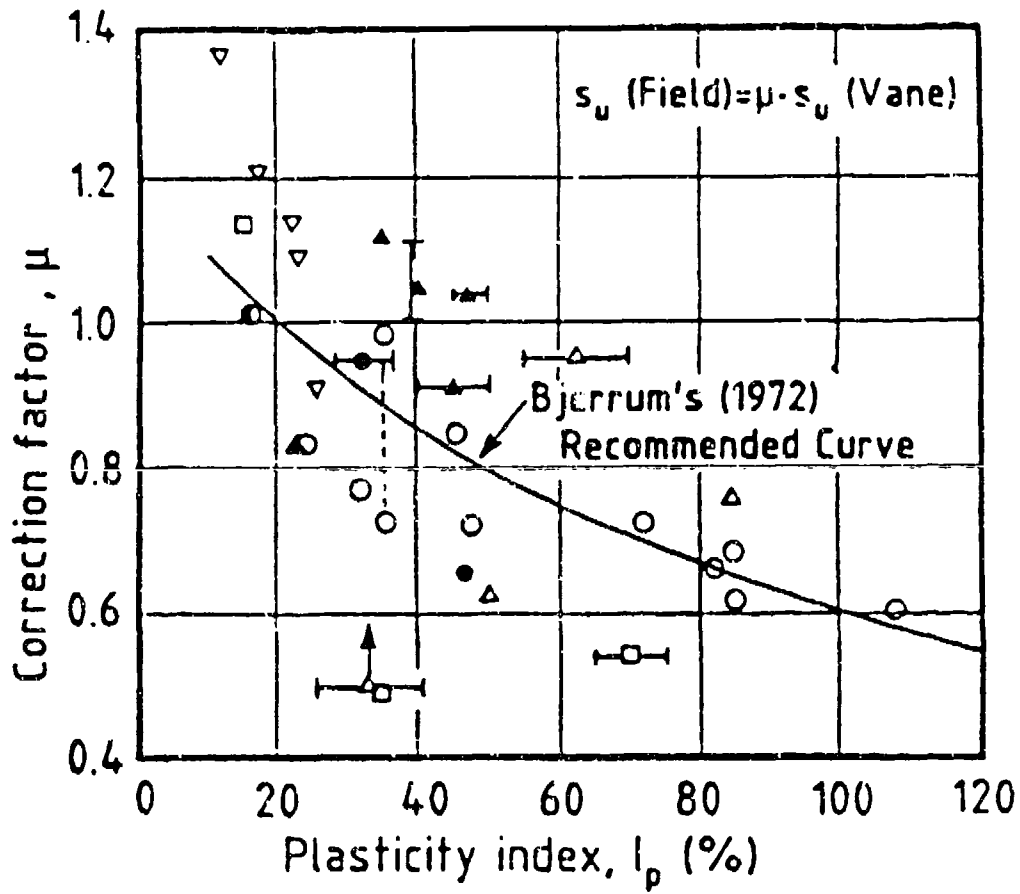


**Figure 8.59** Correlation of PI to the Bjerrum  $\mu$  correction factor for determining the undrained strength from field vane shear results (Bjerrum, 1972)

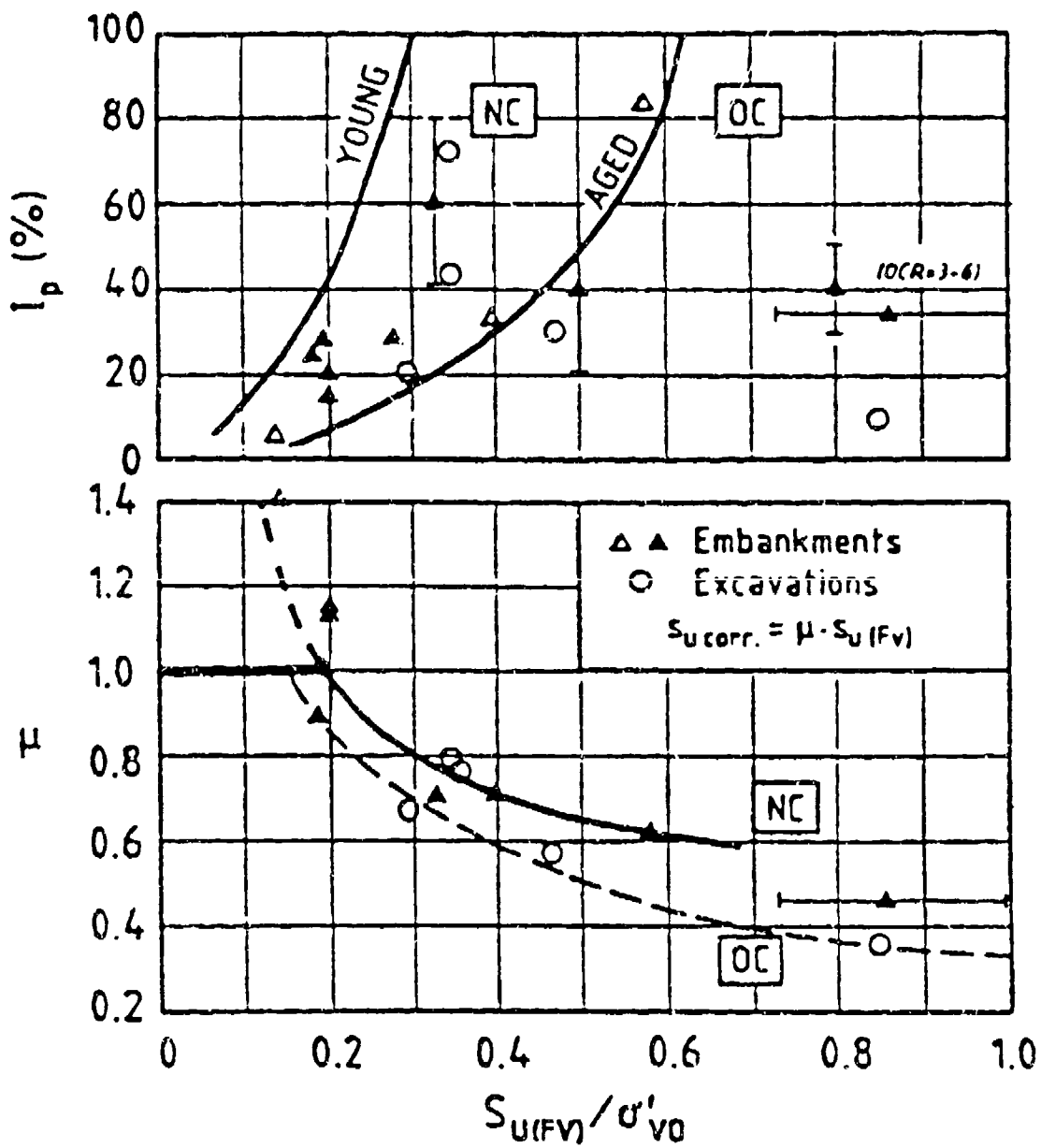


**Figure 8.60** Correlation of  $(S_u)_{FV}$  to  $PI$  to establish the overconsolidation character and then to get the Bjerrum  $\mu$  correction factor (Aas, Lacasse, Lunne, and Hoeg, 1985)

# CPT Prediction of Shear Wave Velocity ( $V_s$ )

## *Introduction*

As noted earlier, accurate prediction of the shear wave velocity,  $V_s$ , using the CPT results may not be possible because  $V_s$  is a low strain measurement while the CPT is a high strain measurement. Nonetheless, there have been several attempts to establish useful correlations. Typically,  $V_s$  has been predicted using the CPT cone resistance (Baldi, et.al., 1988) or more recently by using both CPT measurements (Olsen, 1988). The Olsen (1988) publication developed a technique for CPT prediction of the maximum shear modulus ( $G_{max}$ ) ( $G_{max}$  and  $V_s$  are theoretically related). This section will extend the Olsen (1988) technique for CPT prediction of  $V_s$  based on improved stress normalization techniques (Chapters 6 & 7) and use of the new larger database (Appendix A).  $V_s$ ,  $G_{max}$ ,  $(G_{max})_1$ , and  $V_{s1}$  were fully described in Chapter 7 during the development of the shear wave velocity normalization stress exponent ( $\nu$ ).

## *Minimal Stratigraphic Error when $V_s$ Measured by CPT sounding*

There are two general means of measuring shear wave velocity in the field: with borehole(s), or with the CPT probe. Borehole based shear wave measurements are performed either using crosshole (i.e. borehole-to-borehole) or downhole (surface energy source and geophones in the borehole) techniques. The CPT based shear wave velocity measurements use downhole measurement with the geophones inside the CPT probe (about 1 meter up from the cone tip) (FUGRO, 1980; Campanella and Robertson, 1984). During a shear wave test with a seismic CPT probe, the shear wave travels down through the soil directly adjacent to the probe. The soil tested by

the CPT probe is the same soil traversed by the shear waves, therefore, there should be little if any stratigraphic bias when establishing correlations. However, developing a correlation is still difficult because shear wave velocity is a low strain measurement and the CPT measurements are high strain measurements.

### *Historical use of both CPT Measurements to Predict $V_s$ or $G_{max}$*

The first technique for estimating  $V_s$  (i.e.  $G_{max}$ ) using the normalized cone and sleeve resistances is shown in Figure 8.61 (Olsen, 1988). The contours of  $(G_{max})_1$  in this figure are parallel to normalized sleeve resistance.  $G_{max}$  appears to be proportional to the sleeve friction resistance, more so than to the cone resistance. The proportionality of  $V_{s1}$  (i.e.  $(G_{max})_1$ ) to  $f_{s1e}$  was believed in 1987 because both parameters are influenced by horizontal stress. It will be shown in a later section that this proportionality is more likely because both parameters are dependent on void ratio and soil type.

### *CPT Prediction of $V_{s1}$ using Both CPT Measurements*

The procedures for establishing contours of normalized shear wave velocity ( $V_{s1}$ ) on the CPT soil characterization chart using the minimal inclusionary AQI technique is the same as used for establishing the  $N_1$  and  $S_{01}$  contours in previous sections of this chapter. All shear wave velocity data from the database, for all projects, were divided into five  $V_{s1}$  ranges for the purpose of establishing individual correlations contours on the CPT soil characterization chart. The best-fit contours of normalized shear wave velocity using the highest inclusionary AQI are shown in Figure 8.62 to Figure 8.66 for average  $V_{s1}$  levels of 150, 400, 650, 900, and 1200 feet/second. The final best fit  $V_{s1}$  contours are shown in Figure 8.67



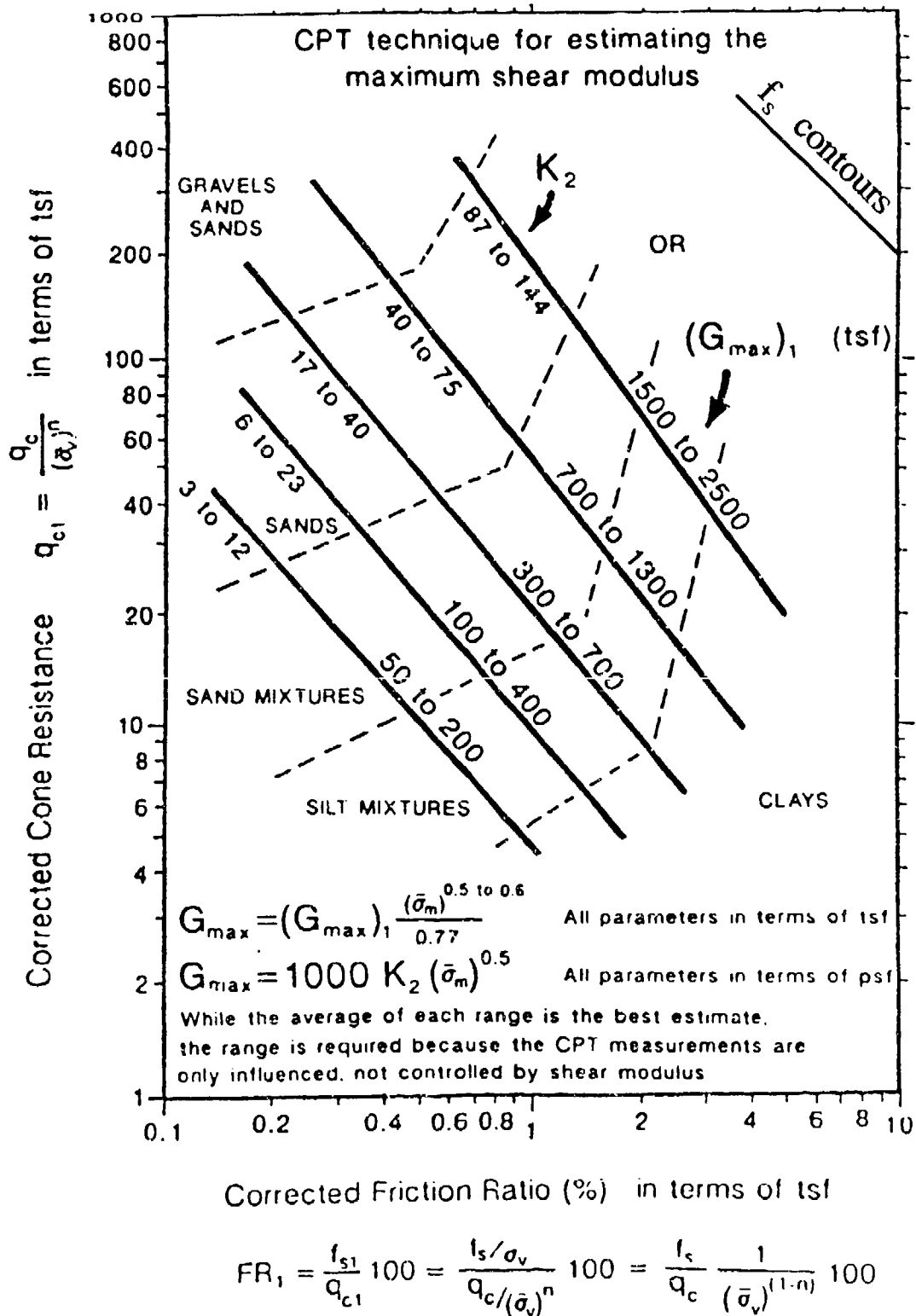


**Figure 8.61** CPT prediction of the maximum shear modulus using both of the CPT measurements (Olsen, 1988)

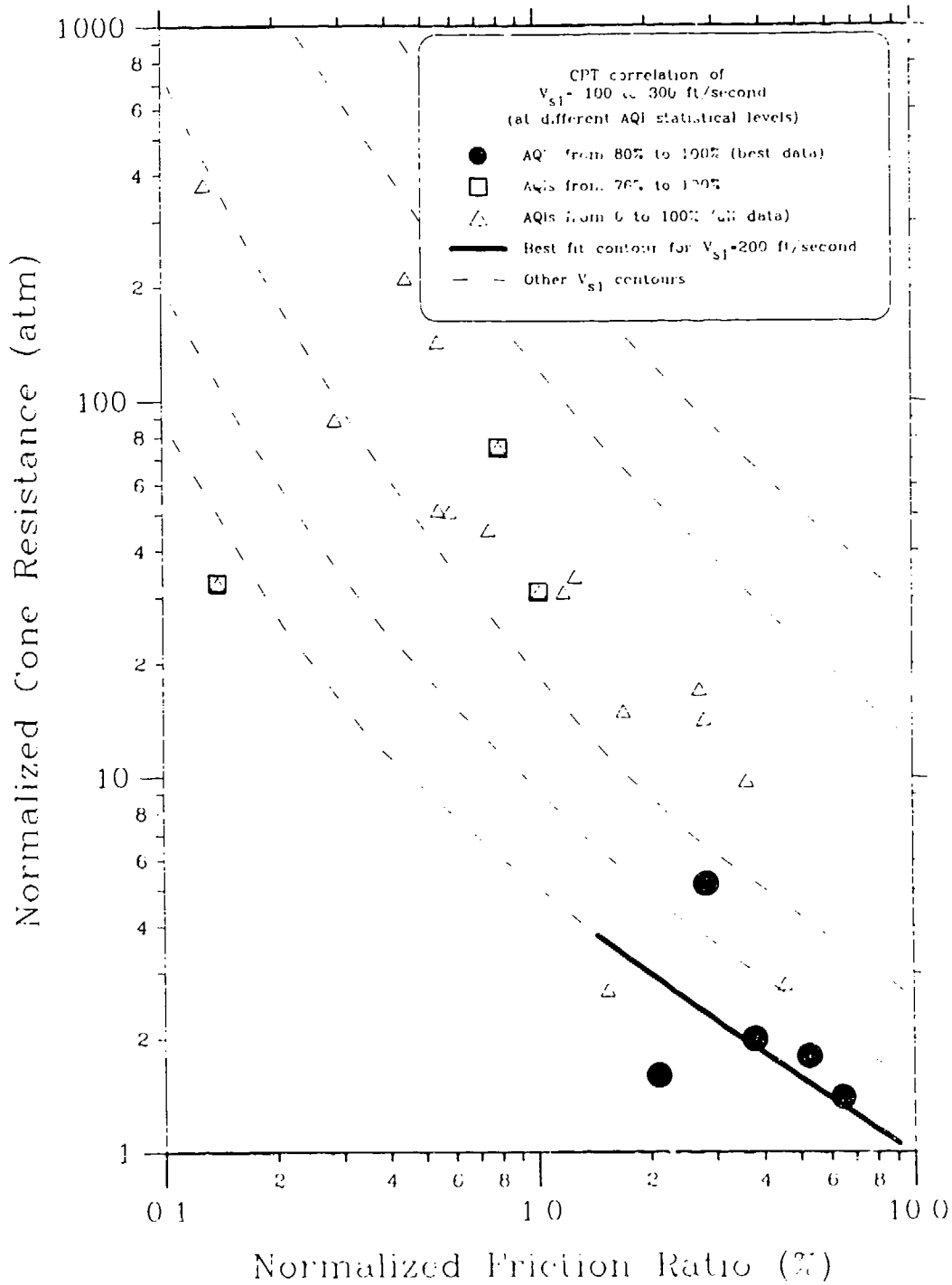


**Figure 8.62** Prediction of  $V_{s1} = 150$  ft/sec contour on the CPT soil characterization chart

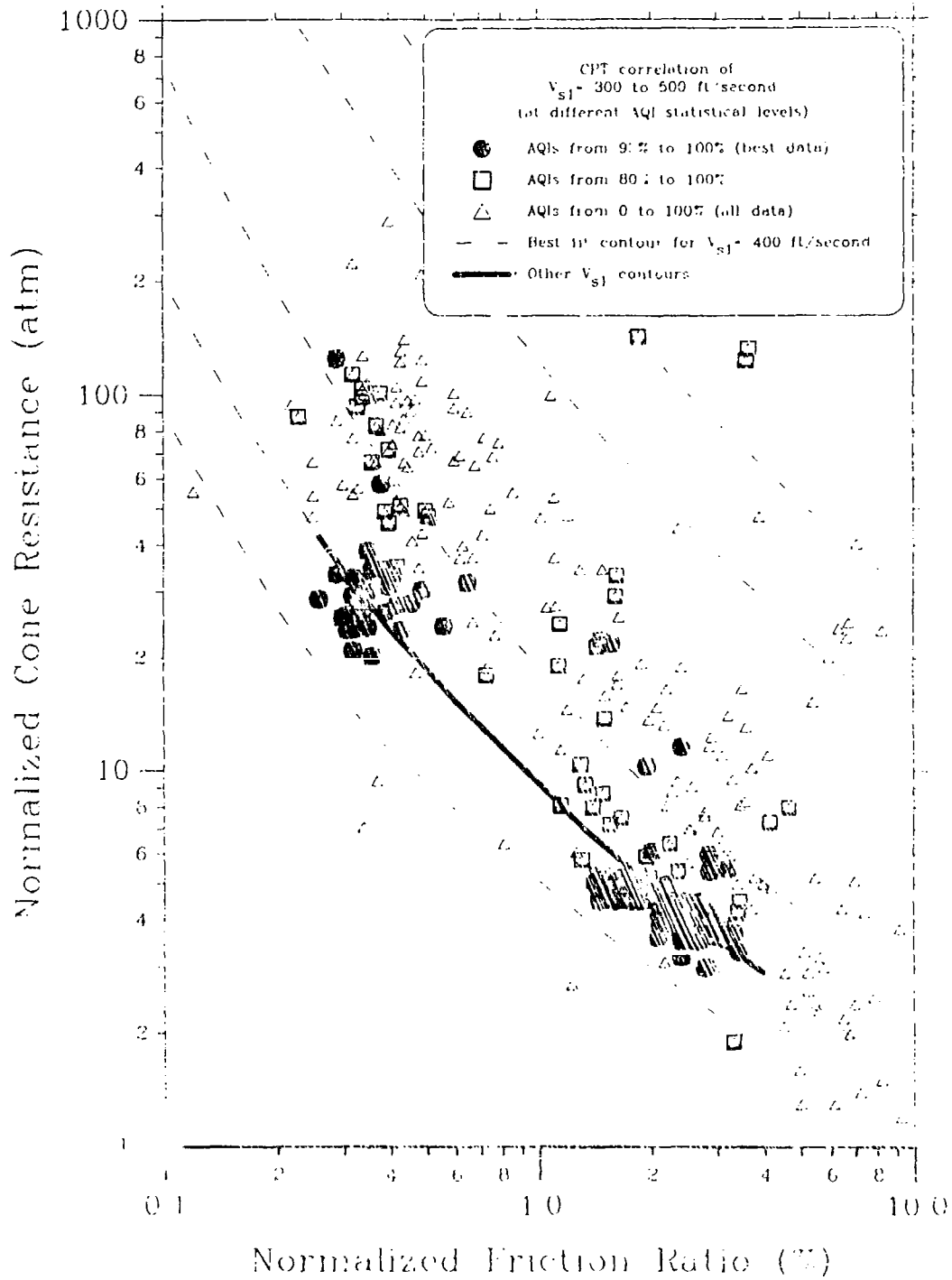


**Figure 8.63** Prediction of the  $V_{s1} = 400$  ft/sec contour on the CPT soil characterization chart

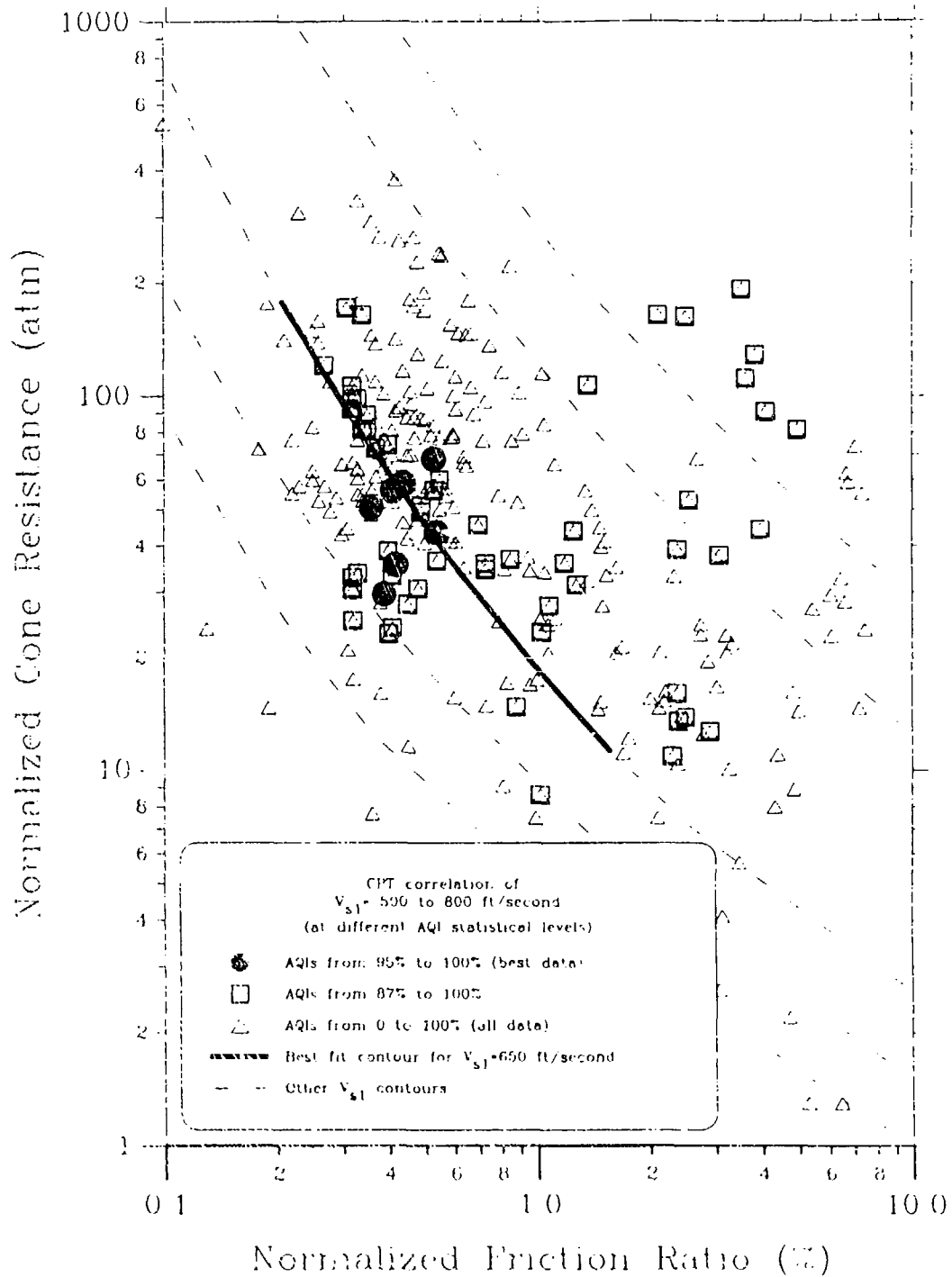


**Figure 8.64** Prediction of the  $V_{s1} = 650$  ft/sec contour on the CPT soil characterization chart.

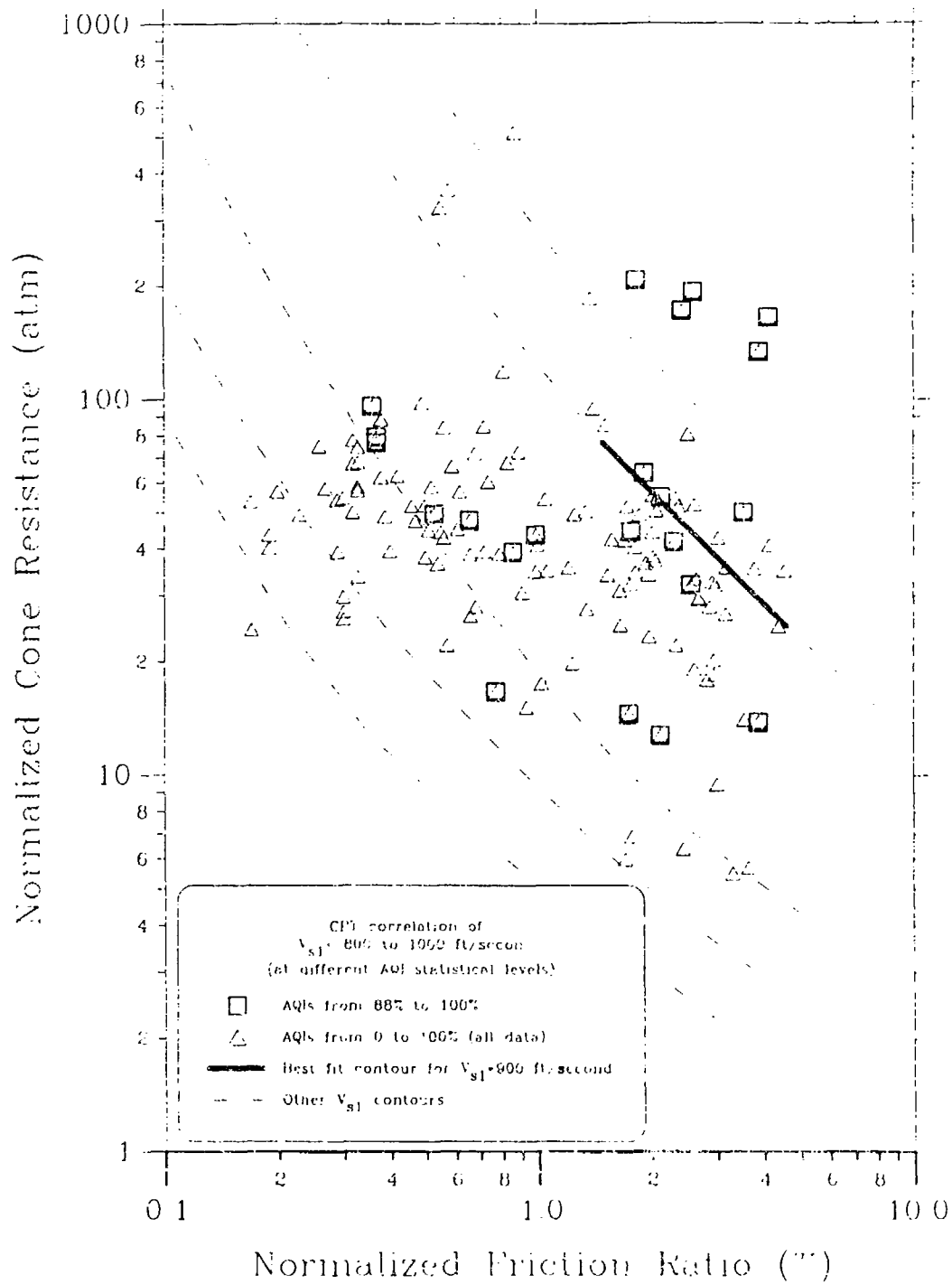


**Figure 3.65** Prediction of the  $V_{s1} = 900$  ft/sec contour on the CPT soil characterization chart

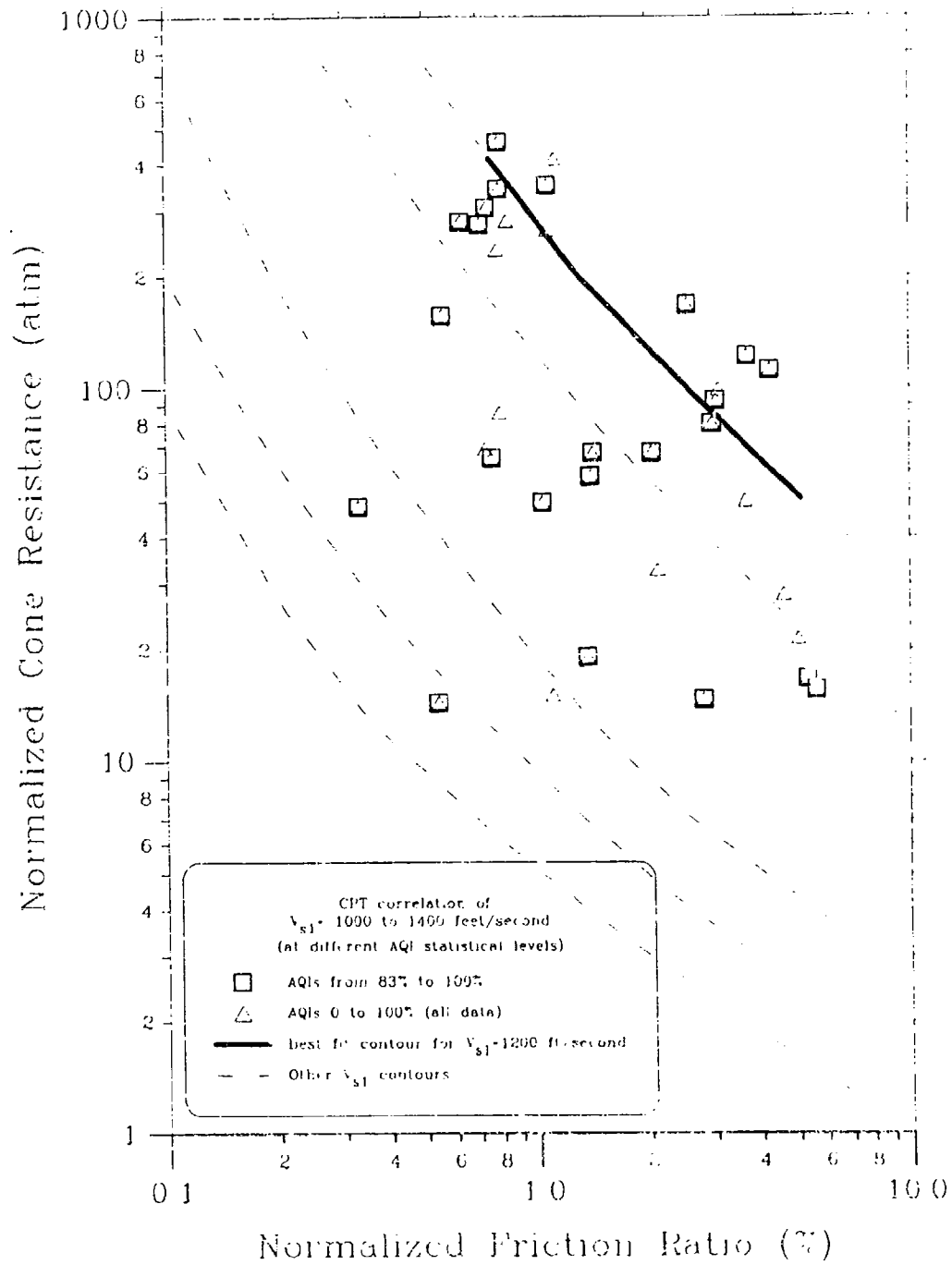


**Figure 8.66** Prediction of the  $V_{s1} = 1200$  ft/sec contour on the CPT soil characterization chart

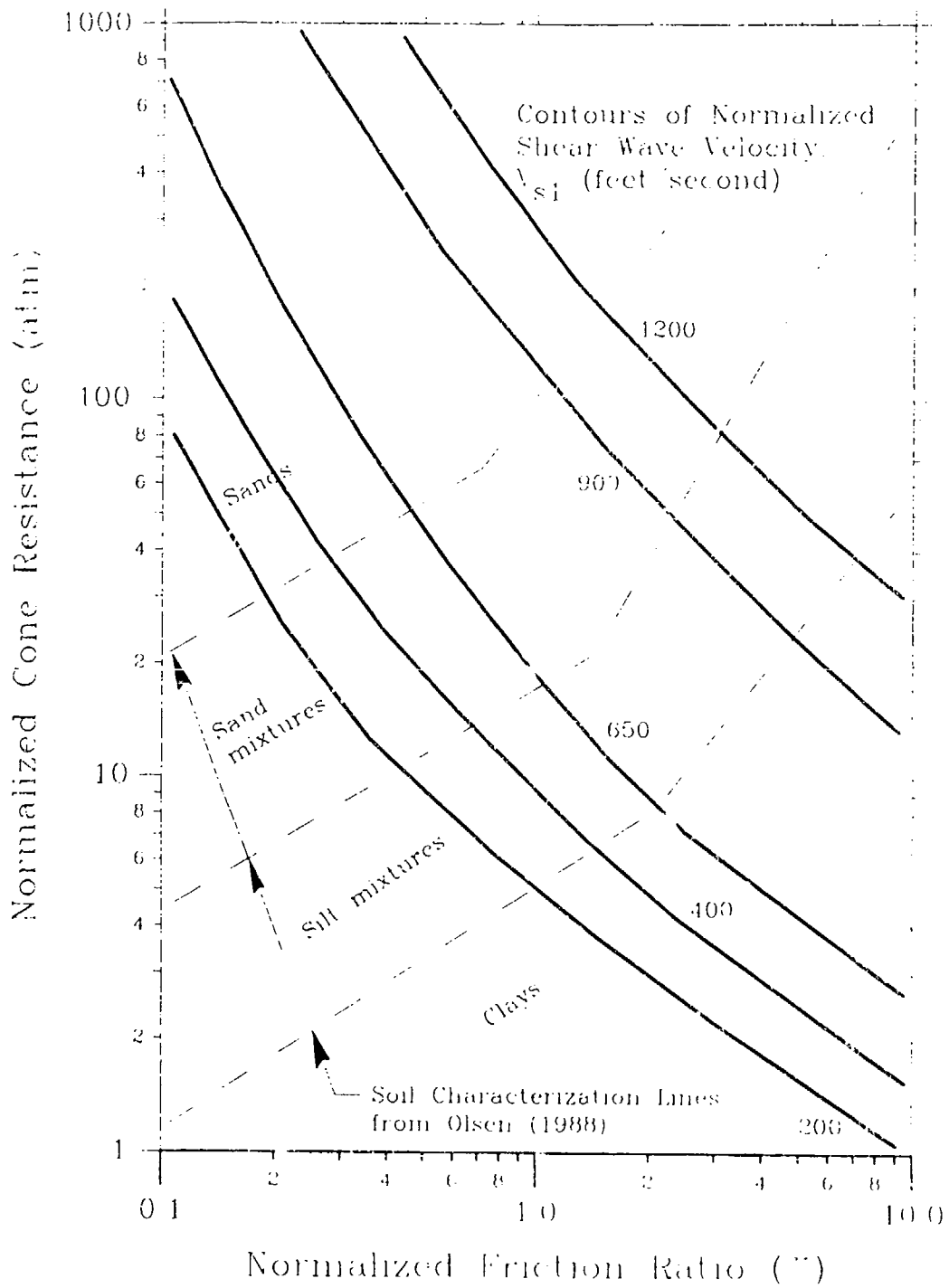


**Figure 8.67** Contours of normalized shear wave velocity ( $V_{s1}$ ) on the CPT soil characterization chart

Several examples of CPT predicted versus measured normalized shear wave velocity ( $V_{s1}$ ) are shown in Figure 8.68 to Figure 8.76. These plots represent all soil type and all relative strength levels. The important observation from these figures is that the CPT predicted  $V_{s1}$  agrees well with both the measured values and their variation with depth. It is also important to note that about 80% of the shear wave velocity data was measured using the seismic CPT probe so there is very little stratigraphic bias error.

### *Discussion of CPT prediction of $V_{s1}$*

For clays and silts, the normalized shear wave velocity ( $V_{s1}$ ) contours in Figure 8.67 are parallel to normalized sleeve friction,  $f_{s1c}$  ( $f_{s1e}$  contours are shown in Figure 8.18). This indicates that overburden stress similarly influences  $V_{s1}$  and  $f_{s1c}$ . However, sleeve friction resistance reflects a high-strain strength (Douglas and Olsen, 1981) while the shear wave velocity represents a modulus at extremely small strains ( $10^{-5}$  percent). Shear wave velocity is indexable to void ratio, confining stress and soil type (Richard, Hall, and Woods, 1970, Seed and Idriess, 1970). Sleeve friction resistance approaches steady state strength (if there is no volumetric shear) (Wahl, et.al., 1991, Castro, et.al., 1989). Sleeve friction resistance should be indexable to the same properties as steady state strength, namely; void ratio, confining stress and soil type (Castro, 1969, Schofield and Wroth, 1968). Because, the  $V_{s1}$  and  $f_{s1c}$  contours are parallel (for clayey soils), it suggests that they are also dependent to the same combination of geotechnical properties.

The  $V_{s1}$  contours bend within the sand zones of the CPT soil characterization chart (Figure 8.67) for loose and medium dense sands. CPT probing of these sands causes volume change due to the high bearing stresses which results in a denser soil. For loose clean sands, the measured cone resistance therefore reflect a denser state than the in situ condition because of grain rearrangement, grain crushing, and



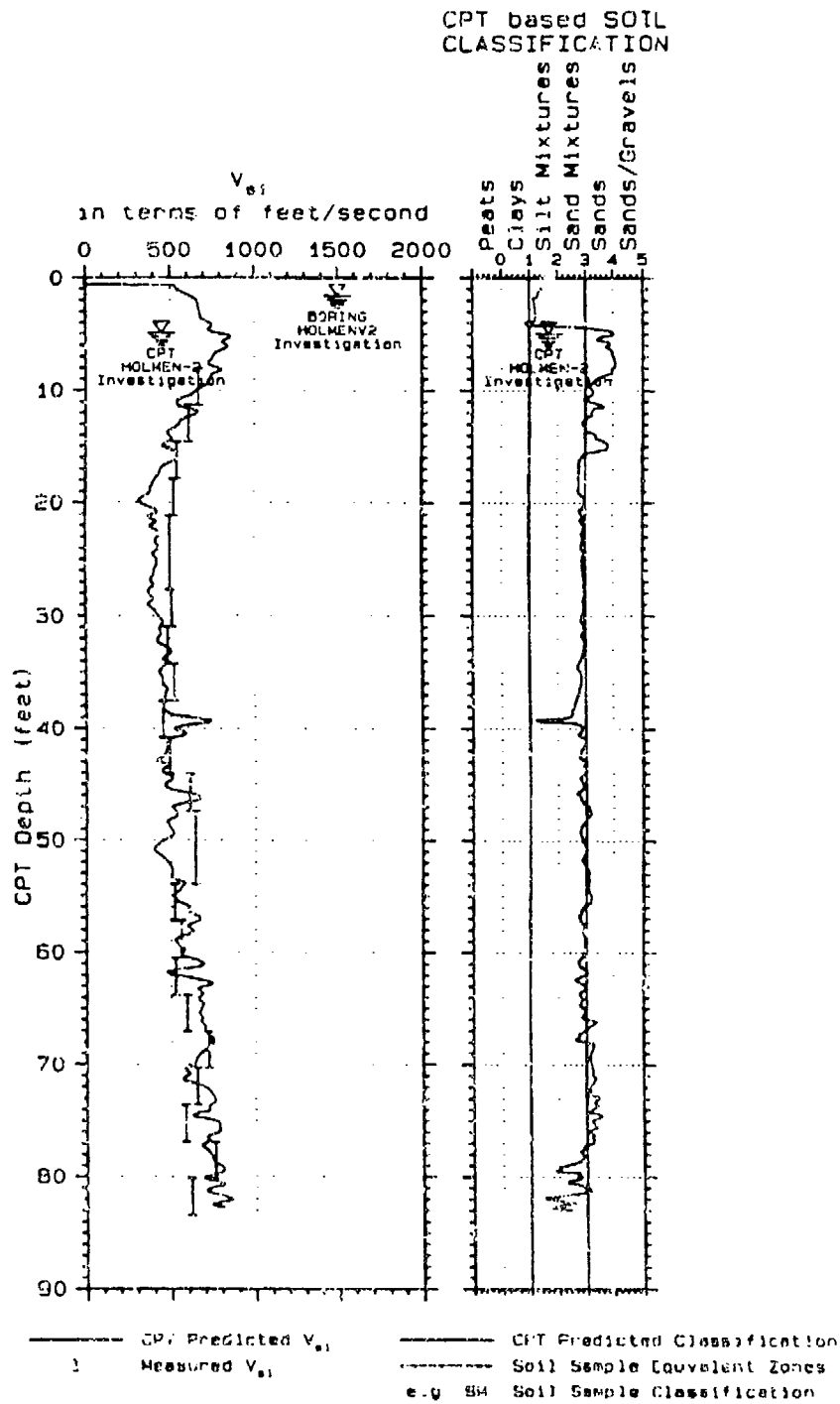


Figure 8.68 CPT predicted versus measured  $V_{s1}$  for the Holmen site, Drammen, Norway (NGI research site) (data from Christoffersen and Lunne, 1982; Gillespie, Lunne, and Eidsmoen, 1985)

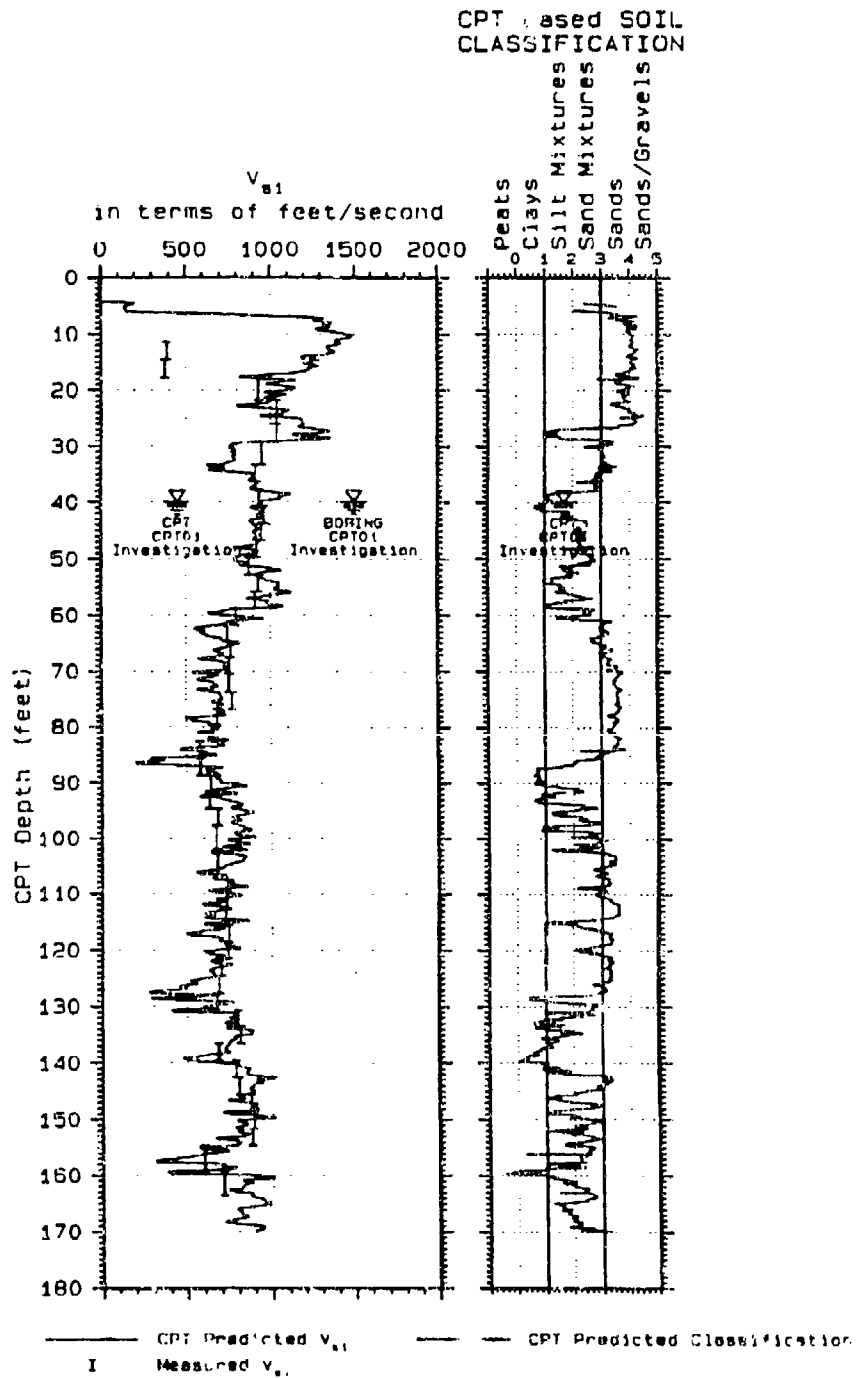
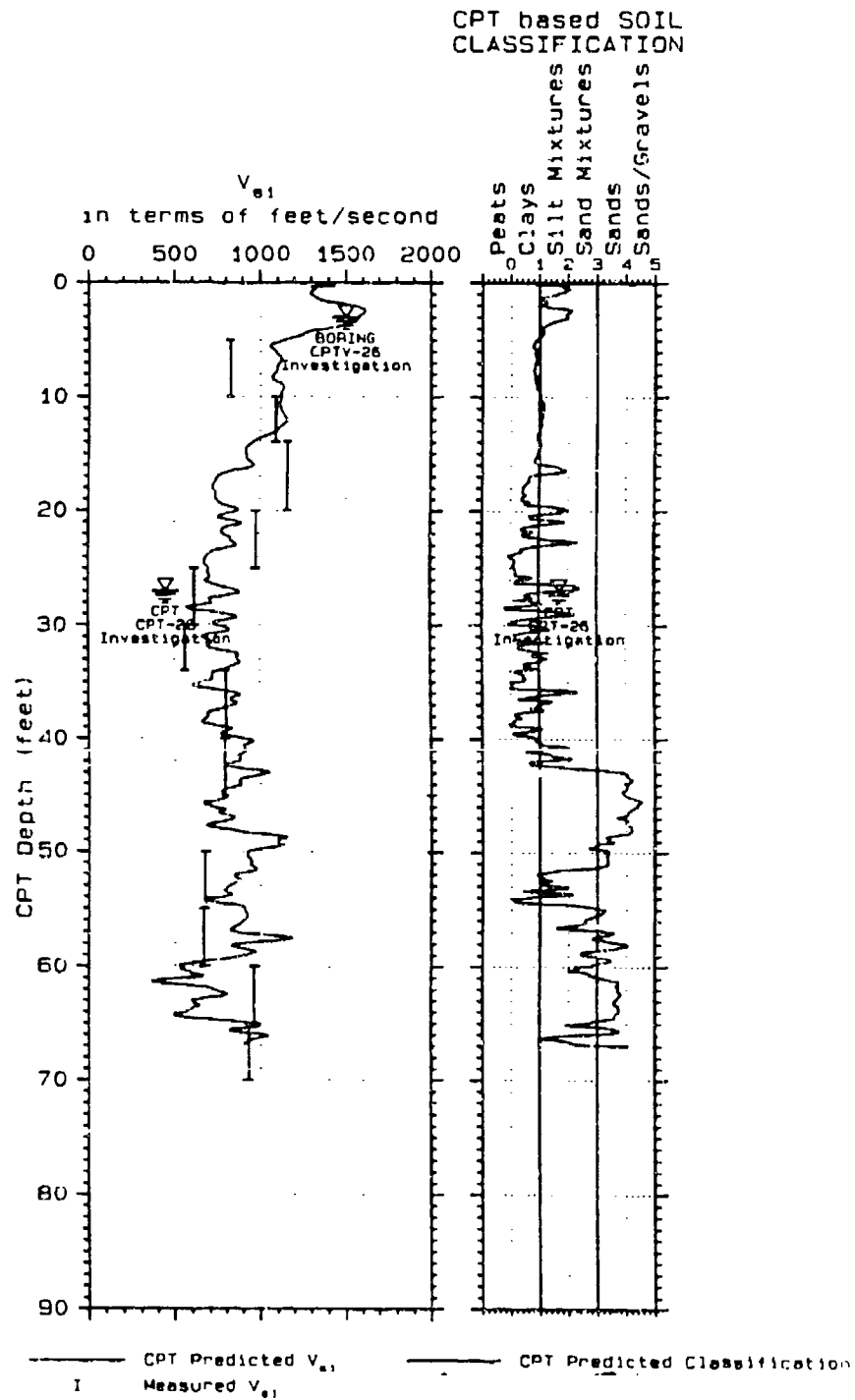
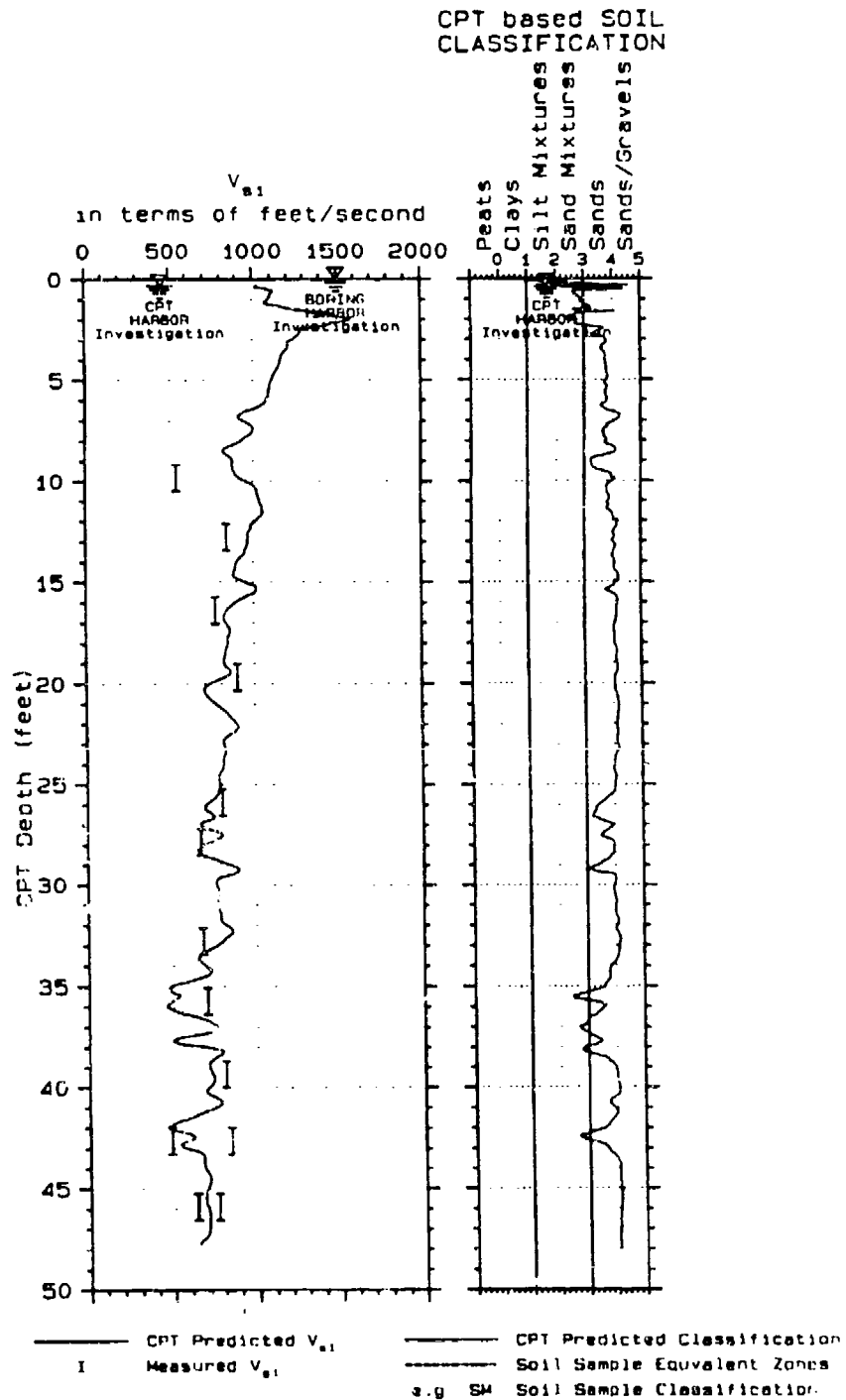


Figure 8.69 CPT predicted versus measured  $V_{s1}$  for a stiff/dense dirty sand site in the U.S. (project code DE-S-R)



**Figure 8.70** CPT predicted versus measured  $V_{s1}$  for the Barkley dam seismic evaluation study (data from Olsen, et al., 1989)



**Figure 8.71** CPT predicted versus measured  $V_{s1}$  for a site at Tuktoyaktule, Bugmallit Bay, Beaufort Sea, Canada (data from Campanella, et al., 1987)

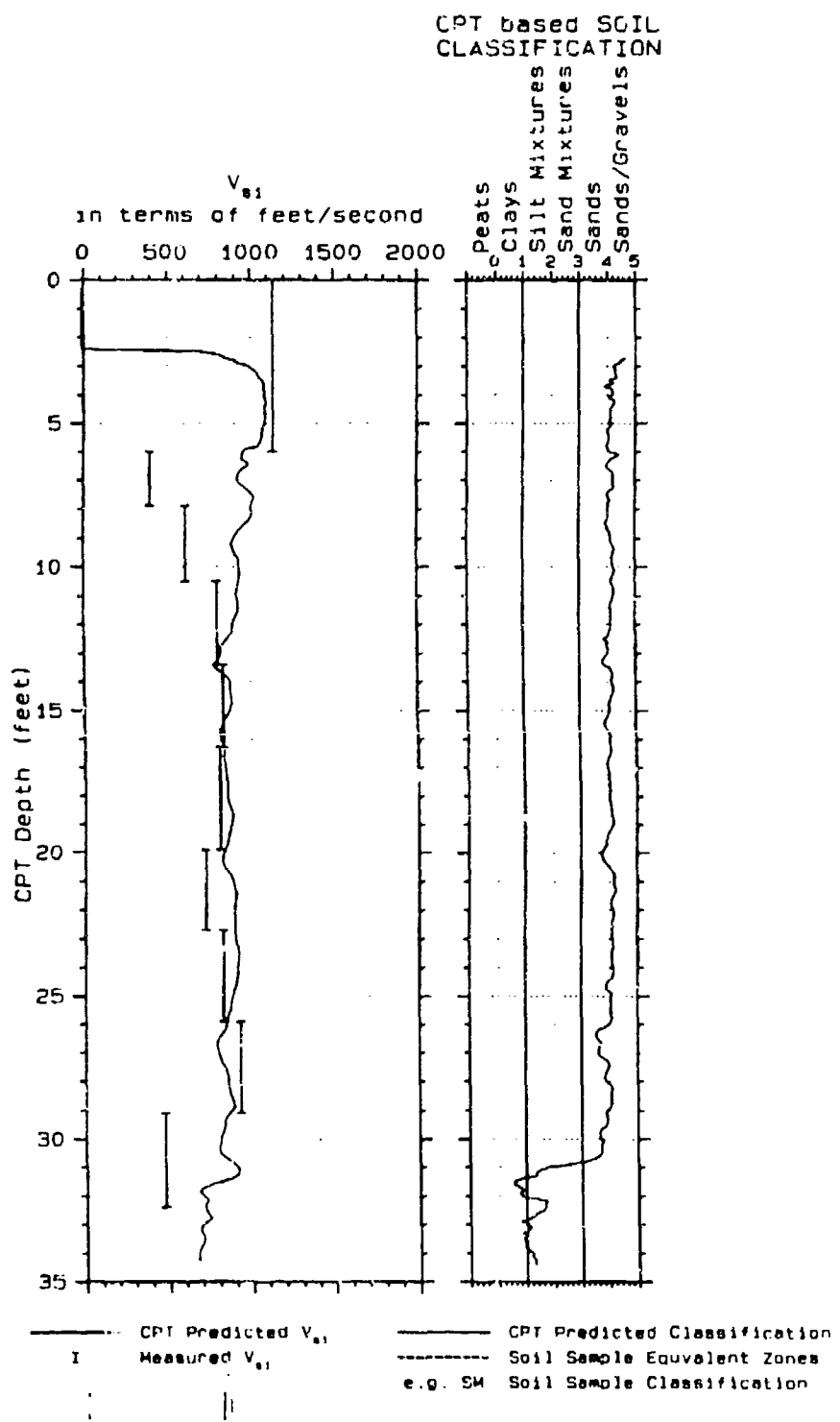


**Figure 8.72** CPT predicted versus measured  $V_{s1}$  for a uniformly compacted sand (data from project code DN-HJ2)

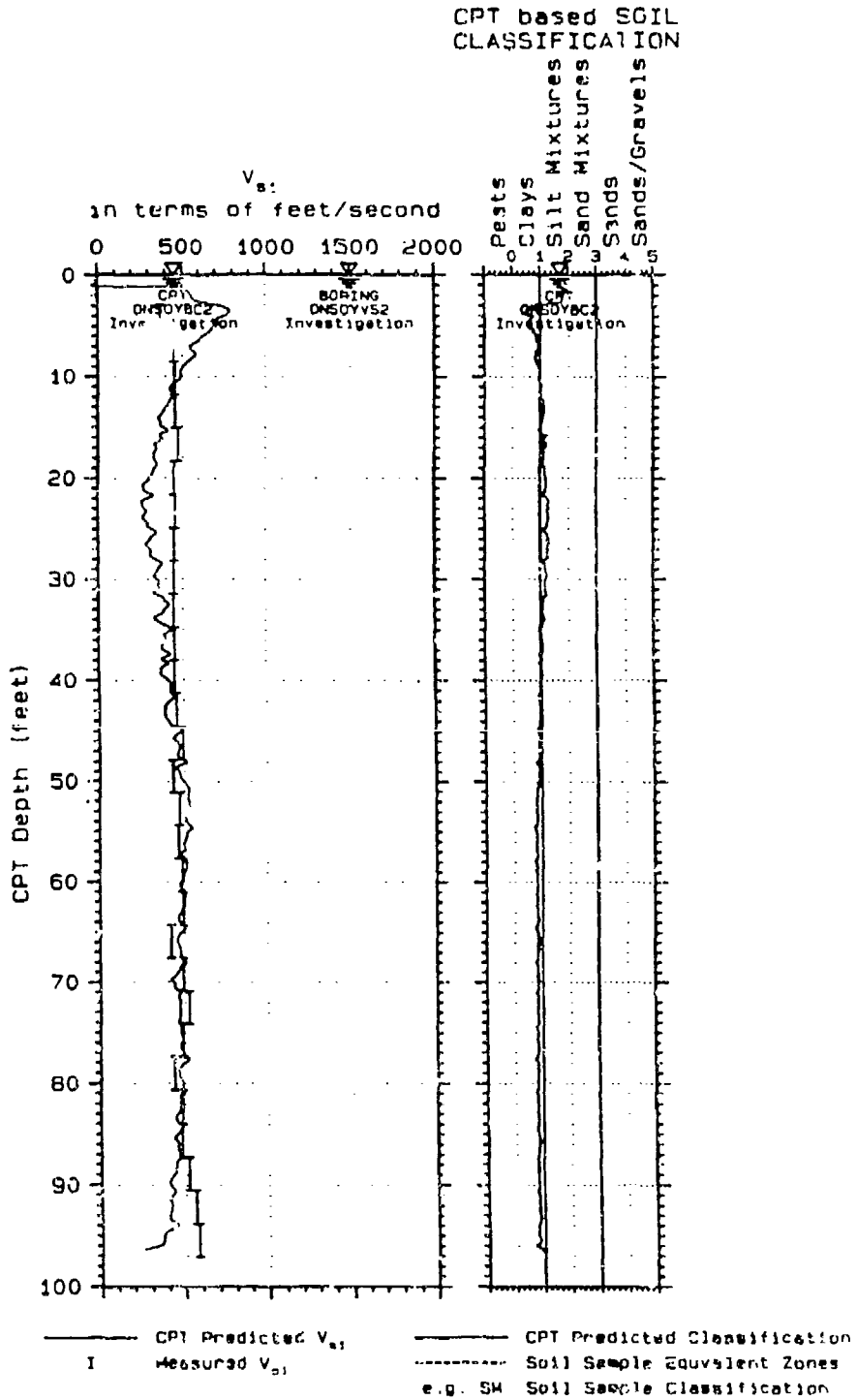


Figure 8.73 CPT predicted versus measured  $V_{s1}$  for a site at Onsoy, Norway (NGI research site)

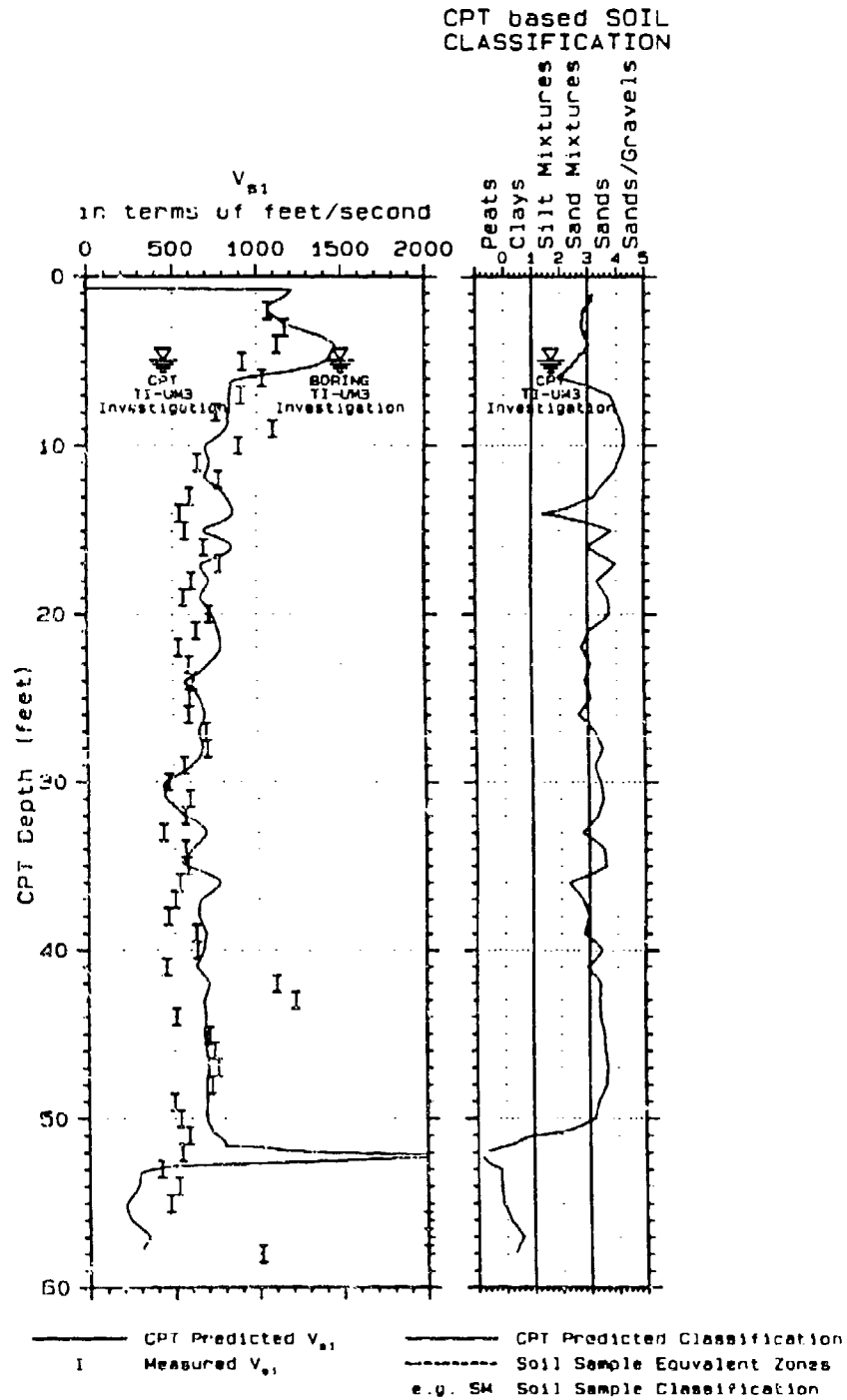
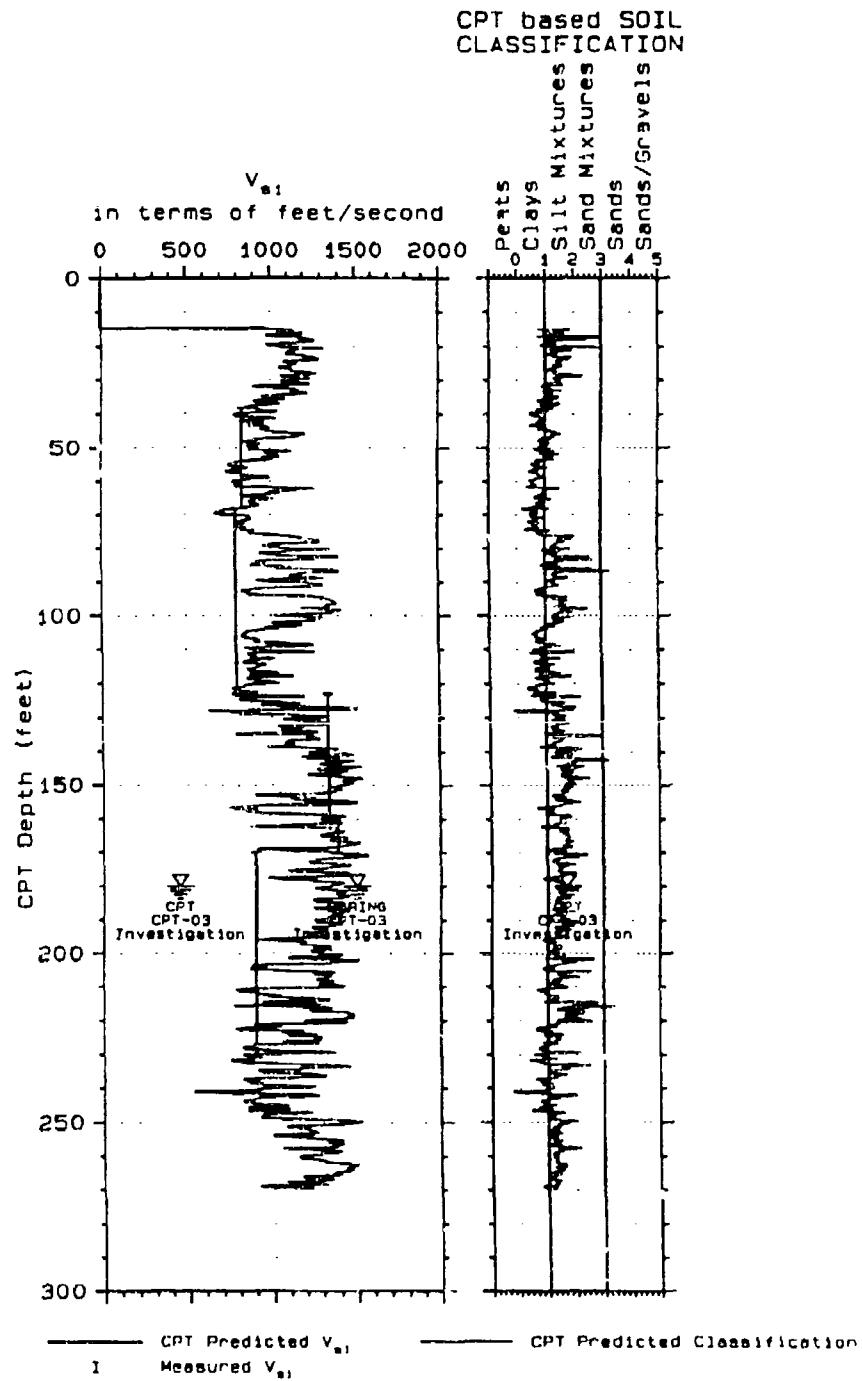


Figure 8.74 CPT predicted versus measured  $V_{s1}$  at Treasure Island, San Francisco, California (data from Hryciw, 1990)







**Figure 8.76** CPT predicted versus measured  $V_{s1}$  for the compacted silt core, Lucky Peak dam, Idaho

densification. However, for dense sand, the  $V_{s1}$  contours appear to be parallel to  $f_{s1c}$ . Dense sands do not densify during shear. Therefore, for dense sands, the in situ void ratio is approximately equal to (or even greater than) the void ratio surrounding the sleeve and cone units during penetration. The resultant is a  $V_{s1}$  contour which is approximately parallel to a  $f_{s1c}$  contour from clay to dense sand as shown in Figure 8.67 for  $V_{s1}=1200$  ft/second.

The  $V_{s1}$  contours in Figure 8.67 can also be generalized as shown in Figure 8.77 as a means to explain densification effects for loose to medium dense sand during penetration. A line of constant normalized sleeve friction resistance is shown as Line CF in Figure 8.77. Line CF would be parallel to the  $V_{s1}$  contour if there was no volume change in the clean sands. However, line VF is a typical  $V_{s1}$  contour. The difference between Lines CF and VF could be the effect of sand volume change during probing resulting in a denser soil for loose to medium dense sands. Point N is along a constant  $f_{s1c}$  contour (Line CF) representing no volume change for clean loose sand. Point S represents a denser sand condition due to probing and a higher measured  $f_{s1c}$  (and  $q_{c1c}$ ) because the sand surrounding the sleeve unit is denser. Therefore, CPT probing of clean loose to medium dense sand produces a denser condition than exists in situ which results in an explainable bending of the  $V_{s1}$  contours.

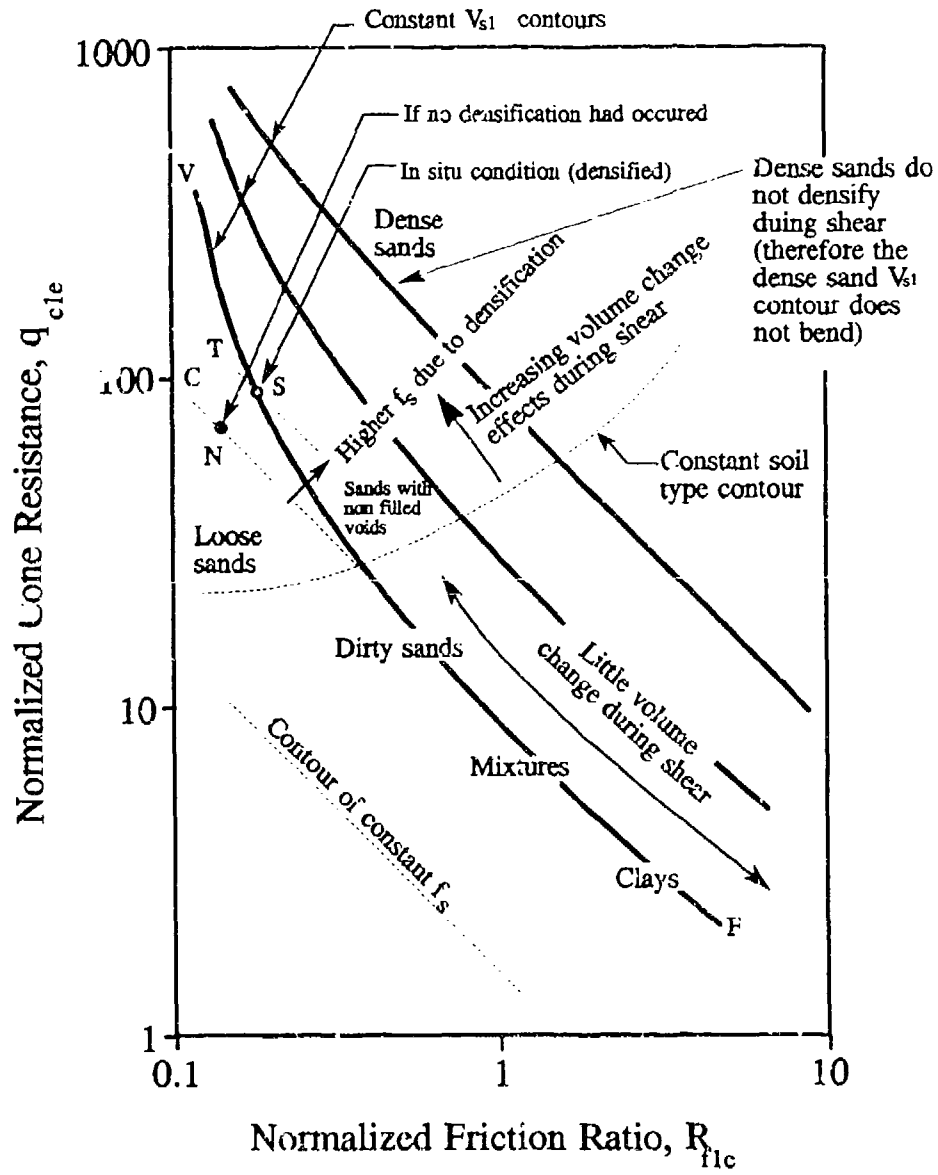


**Figure 8.77** Illustration why the predicted shear wave velocity contours on the CPT Soil Characterization chart are curved

# Chapter 9

## Conclusions

The primary objective of this research was to develop techniques and correlations for predicting geotechnical properties using CPT cone resistance and sleeve friction resistance measurements. Stress normalization provided the means for taking confining stress dependence into account when predicting geotechnical properties using CPT measurements.

A new concept, the Stress Focus, was discovered and confirmed which provides a basis for understanding strength behavior (e.g. friction angle, cone resistance, etc.,) as a function of confining stress. This study demonstrated that the relationships of sand friction angle to confining stress for different initial densities converge to a Stress Focus at high pressure, where the strength behavior is similar to that of a sedimentary rock. This convergence to a Stress Focus was also confirmed using the CPT cone resistance measurement. The paths of convergence to the Stress Focus are exponentially related to overburden stress and can be represented as straight lines on a log-log plot of strength versus vertical effective stress. A sand at a given relative density can be represented by a straight line on this log-log plot with all relative density lines converging to the Stress Focus. The slope of this line, termed the stress exponent, is inversely proportional to sand initial relative density.

The strength of dense sand is strongly influenced by dilation effects. Dilation effects for a dense sand will decrease with increased vertical effective stress until the Stress Focus is reached where its behavior is similar to that of a sedimentary rock.

The convergence of relative density lines to the Stress Focus for sand is caused by consolidation (i.e. decreasing void ratio) which is reflected in numerous geotechnical properties such as Mohr envelope curvature, grain crushing, compressibility, etc., Sands of all relative densities will have approximately the same bulk density (i.e. void ratio) at the Stress Focus and, as a result, approximately the same strength behavior. The Stress Focus should therefore be considered a fundamental geotechnical property. The Stress Focus concept replaces the variable soil type dependent stress exponent technique for normalizing cone resistance previously developed by the author (Olsen, 1984, 1988).

The Stress Focus concept was confirmed using historic high pressure triaxial test data in Chapter 2 (collectively shown by Figure 2.5). Sand strengths are shown to converge to a Stress Focus at a vertical effective stress of approximately 100 atmospheres. A simple yet unique CPT cone resistance normalization formula, which accounts for exponential stress dependence of the tip stress, has been derived in Chapter 4. The Stress Focus for CPT cone resistance is demonstrated using CPT laboratory chamber data in Chapter 5.

The Stress Focus location (i.e. vertical effective stress and strength level) was shown to be soil type dependent using field CPT data from uniform soil layers (Figure 6.24). For clay, the Stress Focus occurs at a vertical effective stress of approximately 9 atm. For sands the Stress Focus occurs at a vertical effective stress of approximately 70 to 200 atm.

A technique to estimate the stress exponent required for cone resistance normalization was also developed using CPT data from uniform soil layers. Contours of cone resistance stress exponent were established on the CPT soil characterization chart (Figure 6.16). These stress exponent contours also support the validity of the CPT soil characterization chart (Olsen, 1988) to characterize soil in terms of soil type and state.

The constant drilling mud height (i.e. constant pressure) used in SPT chamber tests, for all confining stress levels, reduces the confining stresses next to the SPT sampler (Chapter 7). All SPT chamber tests in the past have had this problem. This reduced confining stress results in a SPT based stress exponent which is too low if derived from the results of chamber tests. The SPT-N to  $N_1$  normalization concept, developed over 10-years ago, is based on SPT chamber test results and therefore uses stress exponents that are too low. The stress exponent for SPT borehole applications were shown to be equal to the CPT cone resistance stress exponents. Therefore, the CPT determined cone resistance stress exponent should be used for SPT normalization. To achieve the best SPT normalization, therefore, requires a nearby CPT sounding where the cone resistance stress exponent can be estimated.

The stress exponent for shear wave velocity is shown to be soil type dependent, and it can be approximated as 45% of the CPT cone resistance stress exponent as shown in Chapter 7.

Developing CPT correlations to geotechnical properties required a large database of CPT and tested soil sample data (described in the Appendix). The largest error during correlating of CPT measurements to nearby borehole soil samples is geological change of soil type. A change of soil type is considered a bias condition because it will skew the data trend. Bias data must therefore be discounted when developing correlations. A quality index was developed in an attempt to account for possible soil type difference between CPT soundings and boreholes—namely the Academic Quality Index (AQI). The overall AQI accounts for possible stratigraphic change and CPT measurement quality. Establishing predictive contour trends on the CPT soil characterization chart was accomplished with a new technique that uses the AQI quality index to account for bias error. Correlations were established for the following normalized geotechnical properties; SPT blow count, undrained cohesive strength from the unconsolidated undrained triaxial test, undrained cohesive strength from the field vane shear test, and the shear wave velocity.

The contours of normalized SPT blow count on the CPT soil characterization chart have a predictable trend (Figure 8.17). In loose to medium dense sands, the SPT sampler is primarily resisted by end bearing force (while the sampler side friction force is minor). On the other hand, for dense (and overconsolidated) sands and clays, SPT sampler side friction force dominates. This relative contribution of SPT sampler end bearing to side friction forces for different relative densities is confirmation of work by Schmertmann (1979a). The technique for predicting the SPT-N values based on the CPT cone resistance and sleeve friction resistance models the forces on the SPT sampler and demonstrates the potential for reliable prediction of SPT N values from knowledge of CPT cone and sleeve friction resistances.

Contours of normalized undrained cohesive strength (i.e.  $\frac{c}{p}$ ,  $\frac{S_u}{\sigma'_v}$ , or  $S_{u1}$ ) for unconsolidated undrained triaxial tests (Figure 8.36) and field vane shear tests (Figure 8.42) were established on the CPT soil characterization chart. Historically, the  $N_k$  (i.e. ratio of net cone resistance to measure undrained strength) must be either be estimated or developed as a site specific value. An estimation of the  $N_k$  bearing factor is not required with this new technique for CPT prediction of clay undrained strength. The ratio of the  $(S_u)_{TxUU}$  versus  $(S_u)_{FV}$  is the historic Bjerrum  $\mu$  correction factor used for reducing the field vane shear test results to unconsolidated undrained triaxial (TxUU) strength levels. The calculated  $\mu$  (Figure 8.58), based on these new correlations, has the same range published by NGI, namely 0.9 to 1 for normally consolidated clays and decreases to 0.5 for overconsolidation (or increased silt content).

Contours of normalized shear wave velocity were also established on the CPT soil characterization chart. These contours are parallel to the normalized sleeve friction resistance contours when there is no volume change during shear (e.g. clays, clayey silts, clayey sands, dense sands, etc.). It appears that the friction sleeve resistance and shear wave velocity are influenced by the same geotechnical properties

and in the same proportion. The normalized shear wave velocity contours were also observed to bend within the loose to medium dense clean sand area of the CPT soil characterization chart because volume change during shear causes a denser state. The predicted shear wave velocity agreed well with the measured values.

## Future Research

- Integration of the Stress Focus concept into critical state soil mechanics.
- Continue to evaluate chamber test results toward better understanding and definition of the Stress Focus.
- Evaluate man-compacted soils (e.g. earth dams, fills, etc.) toward establishing better techniques for stress normalization and prediction of geotechnical properties.
- Investigate the soil property and bulk density at the Stress Focus.
- Seek more verification of the CPT predicted geotechnical properties.
- Continue to develop the AQI as a subjective index for excluding bias error.
- Develop a computer technique for locating the Stress Focus using several relative density groups (this is an iterative procedure which searches for the optimum location for the Stress Focus by minimizing the relative density trend variances).
- Develop improved techniques for calculating the CPT stress exponents using field data.



## References

- Aas, G, Lacasse, S., Lunne, T., and Hoeg, K. (1984). "Use of In Situ Tests for Foundation Design in Clay," Norwegian Geotechnical Institute (NGI), Oslo, Norway.
- Al-Awkati, Z. A. (1975). "On Problems of Soil Bearing Capacity at Depth," Ph.D. Dissertation, Department of Civil Engineering. Duke University
- American Society for Testing and Materials (1980). "Standard Method for Penetration Test and Split-Barrel Sampling of Soils, " Designation: D 1586-67, ASTM 1980 Annual Book of Standards, Part 19, Soils and Rock; pp. 283-285.
- American Society for Testing and Materials (1986). "Standard Test Method for Deep Quasi-static, Cone and Friction Cone Penetration Tests of Soil, D 3441-86," ASTM Committee D-18 on Soil and Rock.
- Arulanadan, K., Yogachandran, C., and Meegoda, N. J. (1986). "Comparison of the SPT, CPT SV and Electrical Methods of Evaluating Earthquake Induced Liquefaction Susceptibility in Ying City During the Haicheng Earthquake," Proceedings of In Situ 86 - Use of In Situ Tests in Geotechnical Engineering, Geotechnical Special Publication Number 6, S. P. Clemence, ed., ASCE, New York, 389-415.
- Baldi, G., Bruzzi, D., Superbo, S., Battaglio, M., and Jamiolkowski, M. (1988). "Seismic Cone in Po River Sand," Proceedings of the First International Symposium on Penetration Testing (ISOPT-1), A. A. Balkema, Rotterdam, Netherlands, ed. J. de Ruiter, 887-893.
- Baldi, G., Bellotti, R., Ghionna, V., Jamiolkowski, M. and Pasqualini, E. (1982). "Design Parameters for Sands from CPT," Proceedings of the Second European Symposium on Penetration Testing, ESOPT II, Amsterdam, Vol. 2, pp. 425-438, May.
- Baldi, G., Bellotti, R., Ghionna, V., Jamiolkowski, M. and Pasqualini, E. (1981). "Cone Resistance of a Dry Medium Sand," 10th International Conference on Soil Mechanics and Foundation Engineering, Stockholm, Vol. 2, pp. 427-432.
- Baligh, M. M. (1976). "Cavity Expansion in Sand with Curved Envelopes," Journal of the Geotechnical Engineering Division, ASCE, Vol. 102, No. GT11, November 1976, pp. 1131-1146.

- Barton, N. (1971). "Estimation of In Situ Shear Strength from Back Analysis of Failed Rock Slopes," Proceedings of the International Symposium on Rock Mechanics, Nancy, Paper II-27.
- Barton, N. (1976). "Rock Mechanics Review: The Shear Strength of Rock and Rock Joints," International Journal of Rock Mechanics, minerals, and Geomechanics, Vol. 13, pp 255-279.
- Been, K., Conlin, B. H., Crooks, J. H. A., Fitzpatrick, S. W., Shinde, S. (1987). "Back Analysis of the Nerlerk Berm Liquefaction Slide: Discussion of a paper by J. A. Sladen, R. D. D'Hollander, J. Krahn, and D. E. Mitchell, 22, Canadian Geotechnical Journal," 24(1), February, Canadian Geotechnical Journal, 170-179.
- Been, K., Crooks, J. H. A., Becker D. E., and Jefferies, M. G. (1986). "The Cone Penetration Test in Sands: Part I, State Parameter," *Geotechnique*, 36(2), 239-249.
- Bellotti, R., Bizzi, G., Enel Cris, M., Ghionna, V. Jamiolkowski, M. (1979). "Preliminary calibration test of electrical cone and flat dilatometer in Design parameters in Geotechnical Engineering", ECSMFE VII, pp.195-200.
- Bennett, M.J., McLaughlin, P.V., Sarmiento, J.S., and Youd, T.L. (1984) "Geotechnical Investigation of Liquefaction Sites, Imperial Valley, California," Open file report 84-252, U.S. Geological Survey, Menlo Park, California
- Bieganousky, W. A., and Marcuson III, W. F. (1976). "Liquefaction Potential of Dams and Foundations, Report 1, Laboratory Standard Penetration Test on Reid Bedford, Model and Ottawa Sands," U.S. Army Waterways Experiment Station, Research Report, S76-2, October, 156 p.
- Bieganousky, W. A., and Marcuson III, W. F. (1977). "Liquefaction Potential of Dams and Foundations, Report 2, Laboratory Standard Penetration Test on Flat Platte River and Standrad Concrete Sands," U.S. Army Waterways Experiment Station, Research Report, S76-2, February, 87 p.
- Bjerrum, L. (1954). "Geotechnical Properties of Norwegian Marine Clays," *Geotechnique*, 4(2), 49-69.
- Bjerrum, L. (1972). "Embankment on Soft Grounds," ASCE Proceedings of the Specialty Conference on Performance of Earth and Earth-Supported Structures," Vol. 2, pp. 1-54, Lafayette.

- Bouckovalas, G., Kalteziotis, N., Sabatakakis, N., and Zervogiannis, C. (1989). "Shear Wave Velocity in a Very Soft Clay - Measurement and Correlations," 12th International Conference on Soil Mechanics and Foundation, Balkema, Rotterdam, Vol. 4, pp 191-194.
- Box, G. E. P., and Draper, N. R. (1987). *Empirical Model-building and Response Surfaces*, John Wiley and Sons, New York.
- Brandon, T. L., Clough, G. W., and Rahardjo, P. P. (1990) "Evaluation of Liquefaction Potential of Silty Sands based on Cone Penetrometer Test," NSF Grant Number ECE-8614516, Geotechnical Engineering, Department of Civil Engineering, Virginia Tech (VPI), Blacksburg, Virginia.
- Broms, B.B., Flodin, N. (1988) "History of soil penetration testing", Proceedings of the First International Symposium on Penetration Testing (ISOPT-1), A. A. Balkema, Rotterdam, Netherlands, ed. J. de Ruiter, pp 157-220
- Bruce, W.F., Paulding, B.W., and Scholz, C. (1966) "Dilatancy in the Fracture of Crystalline Rock," *Journal of Geophysics*, No. 71, pp 3939-3953.
- Casagrande, Arthur. (1932) "The structure of clay and its importance in foundation engineering," *Contributions to Soil Mechanics 1925-1940*, Boston Society of Civil Engineers, pp. 257-276
- Coulson, J.H. (1972). "Shear Strength of Flat Surfaces on Rock," *Proceedings of the 13<sup>th</sup> Symposium on Rock Mechanics*, Urbana, IL, pp. 77-105.
- Campanella, R. G. and Robertson, P. K. (1984). "A Seismic Cone Penetrometer to Measure Engineering Properties of Soil," 54th Annual International Meeting and Exposition of the Society of Exploration Geophysicists, Atlanta, GA., pp 138-141
- Castro, G., Keller, T. O., Boynton, S. S. (1989). "Re-Evaluation of the Lower San Fernando Dam - Report 1 - An Investigation of the February 9, 1971 Slide - Volume I: Text," Contract Report GL-89-2, U.S. Army Engineer Waterways Experiment Station, Vicksburg, MS.
- CH<sub>2</sub>M Hill (1988). "Great American Parkway Interchange and SR-237 Re-alignment Santa Investigation," Report for the California Department of Transportation, Oakland, CA.
- Christophersen, H.P., and Lacasse, S. (1985) "In Situ Site Investigation Techniques and Interpretation for Offshore Practice," Report 40019-8, Norwegian Geotechnical Institute, Oslo, Norway, July.

Christophersen, H P., and Lunne, T. (1982) "Offshore Site Exploration Techniques, Laboratory Tests on Sand Samples from Holmen," Report 40019-8, Norwegian Geotechnical Institute, Oslo, Norway, July.

Cooper, S. S., Malone, P. G., Olsen, R. S. and Douglas, D. H. (1988). "Development of a Computerized Penetrometer System for Hazardous Waste Sites Soils Investigations," Final Report Number AMXTH-TR-TE-88242, U.S. Army Toxic and Hazardous Material Agency.

Cooper, S. S., Malone, P. G., Olsen, R. S., and Mohrman, G. B. (1988). "Use of an instrumented cone penetrometer in monitoring land disposal sites," Proceedings of the 5th National Conference on Hazardous Wastes and Hazardous Material, Las Vegas, NV.

Crawford, C. R., Campanella, R. G. (1991). "Comparison of Field Consolidation with Laboratory and In Situ Tests," Canadian Geotechnical Journal, 28(1), 103-112.

Dames and Moore. (1982). "Replacement Airport at Chek Lap Kok - Civil Engineering Design Studies Report No. 1 - Site Investigation - Volume I - Main Report," D. Koutsoftas and R. Foott, ed., June, Kowloon, Hong Kong.

Dames and Moore. (1982). "Replacement Airport at Chek Lap Kok - Civil Engineering Design Studies Report No. 1 - Site Investigation - Volume II - Appendix - Geology and Field Testing," D. Koutsoftas and R. Foott, ed., June, Kowloon, Hong Kong.

Dames and Moore. (1982). "Replacement Airport at Chek Lap Kok - Civil Engineering Design Studies Report No. 1 - Site Investigation - Volume III - Appendix - Laboratory Testing," D. Koutsoftas and R. Foott, ed., June, Kowloon, Hong Kong.

Dames and Moore. (1985). "Factual Report - Site Investigation for Completion of Preliminary Design - Phase I - MUNI Metro Turnaround Facility," Job No. 185-215-03, San Francisco, CA.

Douglas, B.J. and Martin, G. R. (1980). "In Situ Testing in Regions Liquefied during the 1979 Imperial Valley Earthquake," for U.S. Geological Survey, Contract No. PFR-8007419, March, Project No. 80-220-05, Long Beach, CA.

Douglas, B. J. (1982). "SPT Blowcount Variability Correlated to the CPT," Proceedings of the 2nd European Symposium on Penetration Testing. ESOPT II, Amsterdam, Vol. 1, pp. 41.

Douglas, B. J., and Olsen, R. S. (1981). "Soil Classification Using the Electric Cone Penetrometer," Proceedings of a Session Entitled Cone Penetration Testing and Experience - ASCE Fall Convention, ASCE, New York, 209-227.

Douglas, B. J., Olsen R. S., and Martin, G. R. (1981). "Evaluation of the Cone Penetrometer Test for SPT Liquefaction Assessment," Proceedings of In Situ Testing to Evaluate Liquefaction Susceptibility, ASCE, New York.

Draper, H. R., and Smith H. (1981). *Applied Regression Analysis*, John Wiley and Sons, New York, New York, 1981.

Durgunoglu, H. T. and Mitchell, J. K. (1973). "Static Penetration Resistance of Soils", General Report, University of California, April 1973

Durgunoglu, H. T. and Mitchell, J. K. (1975). "Static Penetration Resistance of Soils: I-Analysis," Proceeding ASCE, Specially Conference on In-Situ Measurements of Soil Parameters Raleigh, Vol. I.

Durgunoglu, H. T. (1972), "Static Penetration Resistance of Soils," PhD Dissertation, Department of Civil Engineering, University of California at Berkeley

Earth Technology Corporation. (1985). "Cone Penetrometer Testing - Lower San Fernando Dam - Los Angeles, California," Project No. 86-140-03, for Waterways Experiment Station, Long Beach, CA.

Earth Technology Corporation. (1986). "Cone Penetrometer Testing - Lucky Peak Dam - Idaho," for Walla Walla District of the Corps of Engineers, Project No. 86-141-01, Long Beach, CA.

Earth Technology Corporation. (1985). "Cone Penetrometer Testing - Ririe Dam - Ririe Idaho," Project No. 85-140-05, Report for Waterways Experiment Station, Long Beach, CA.

Earth Technology Corporation. (1985). "In Situ Testing II - Peoples Republic of China," Project No. 84-141-13, Report for the National Science Foundation (NSF), NSF Grant No. CEE 831873, Long Beach, CA.

Earth Technology Corporation. (1985). "Cone Penetrometer Testing - Ririe Dam, Ririe, Idaho," for Walla Walla District of the Corps of Engineers, Project No. 85-140-05, Long Beach, CA., Jan.

Earth Technology Corporation. (1983). "Cone Penetrometer Testing - Blackfoot Dam - Blackfoot, Idaho," Project No. 83-100-68, for Walla Walla Corps of Engineers, Long Beach, CA., July.

- Earth Technology Corporation. (1982). "Cone Penetrometer Testing and Design Strengths, Great Highway, San Francisco, CA," Contract W-1 of 80-266
- Eidsmoen, T., Gillespie, D., Lunne, T., and Campanella, R. G. (1985). "Tests with UBC Seismic Cone at Three Norwegian Research Sites," Report 59040-1, November, Norwegian Geotechnical Institute, Oslo, Norway.
- Eidsmoen, T., Howland, J., and Kjesbu, E. (1985). "Laboratory and Field Evaluation of Cone Penetrometers, Statistical Evaluation of CPTs in Holmen Sand," Report 40015-9, Norwegian Geotechnical Institute, Oslo, Norway, May
- FUGRO Inc (1981). "Evaluation of the Cone Penetrometer for Liquefaction Hazard Assessment," USGS Open File Report No. 81-284.
- FUGRO Inc. (1981). "Cone Penetrometer Testing - Copper City No. 2 Tailing Dam - Globe, Arizona," Project No. 80-225, February, for the Utah State University, Long Beach, CA.
- FUGRO Inc (1980). "Cone Penetration Testing of the Arcadia Dam Site," for Tulsa District of the Corps of Engineers, Long Beach, CA, Aug.
- FUGRO Inc. (1980). "Intermountain Power Project (IPP) - Site Specific Geotechnical Studies - Volume I - Plant Site," Project No: 80-164-10, July, For the Los Angeles Department of Water and Power FUGRO Inc., Long Beach, CA.
- FUGRO Inc. (1980). "Internal report on the design, fabrication, and testing of the first seismic CPT probe," Long Beach, CA. March.
- Gibbs, H .J. and Holtz W.H. (1957). "Progress Report of Research on Penetrometer Resistance Method of Subsurface Exploration," EM-314, Bureau of Reclamation, U.S. Department of the Interior, Denver, CO
- Gibbs, H.J. and Holtz, W.H. (1957). "Research on Determining the Density of Sands by Spoon Penetration Testing, " Proceedings of the 4th International Conference on Soil Mechanics and Foundation Engineering, London, Vol. I, pp. 35-39.
- Gillespie, D., Lunne, T., and Eidsmoen, T. (1985). "In Situ Site Investigation Techniques and Interpretation for Offshore Practice - Cone Penetrometer Tests in Onsoy Clay - Field Report and Data Reduction," Internal Report (Preliminary), Report 40019-7, Norwegian Geotechnical Institute, Oslo, Norway, July.

Gillespie, Lunne, T., and Eidsmoen, T. (1985). "In Situ Site Investigation Techniques and Interpretation - Cone Penetration Tests in Sands at Holmen, Drammen - Field report and Data Reduction," Internal Report, Report 40019-13, Norwegian Geotechnical Institute, Oslo, Norway, June.

Harder, L.F. (1988). "Use of Penetration Tests to determine the Cyclic loading Resistance of Gravelly Soils during Earthquake Shaking", PhD Dissertation, University of California at Berkeley

Hardin, B. O. and Black W.L. (1969) "Sand Stiffness under Various Triaxial Stresses," Journal of the Soil Mechanics and Foundations Division, ASCE, Vol. 92, No. SM2, March, pp 27-43.

Hardin, B. O. and Drnevich, V. P. (1972). "Shear Modulus and Damping in Soils: Design Equations and Curves," Proceedings of ASCE, Journal of the Soil Mechanics and Foundation Division, Vol. 98, SM7, pp. 667-692.

Hardin, B. O. and Richart, F.E., Jr. (1963) "Elastic wave velocities in Granular Soils," Journal of the Soil Mechanics and Foundation Division, ASCE, Vol. 89, No. SM1, February, Pp 33-65.

Harding Lawson Associates (1989) "Site Investigation, Medical/Dental Clinic, Treasure Island, San Francisco," San Francisco, CA. Project report. December.

Harding-Lawson Associates (1987) "Site Investigation, Proposed Terminal Building, John Wayne Airport, Orange County, CA.," Project report, April.

Harding-Lawson Associates (1978) "Geotechnical Studies, Intake Structure, Water tanks, Diesel Fuel Storage Tanks, Diablo Canyon Nuclear Power Plant, San Luis Obispo County, California," for Pacific Gas & Electric Company, Project report, April.

Hirschfield, R.C. and Poulo, S.J. (1963) "High Pressure Tests on a Compacted Sand and an Undisturbed Silt," Laboratory Shear Testing of Soils, Special Technical Publication No. 361, ASTM, pp 329-341

Hoaglin, D.C., Mosteller F., and Tukey, J.W. (1983). *Understanding Robust and Exploratory Data Analysis*, John Wiley & Sons, Inc. New York

Hryciw, R. D. (1990) "Post Loma Prieta Earthquake CPT, DMT and Shear Wave Velocity Investigation of Liquefaction Sites in Santa Cruz and on Treasure Island," for U.S. Geological Survey (Award No. 14-08-0001-G1865), Report, University of Michigan.

- Hobbs, D.W. (1970) "The Behavior of Broken Rock under Triaxial Compression," International Journal of Rock Mechanics and Material Science, Vol. 7, pp 125-148.
- Hutchinson, J.N. (1972). "Field and Laboratory Studies of a Fall in Upper Chalk Cliffs at Joss Bay, Isle of Thanet," Proceedings of the Roscoe Memorial Symposium, Cambridge University, pp 692-706.
- Jamiolkowski, M. (1988), computer output and descriptions of chamber test results
- Jamiolkowski, M., Baldi, G., Bellotti, R., Ghionna, V. and Paqualini. (1985). "Penetration Resistance and Liquefaction of Sands," Proceedings of the 11th International Conference on Soil Mechanics and Foundation, Balkema, Rotterdam, Volume 4, 1891-1895.
- Jamiolkowski, M., Ghionna, V. N., Lancellotta, R. and Pasqualini. (1988). "New Correlations of Penetration Test for Design Practice," Invited lecture, ISOPT-I, Disney World, March, Balkema Publ., pp. 263-296.
- Jamiolkowski, M., Ladd, C. C., Germaine, J. T., and Lancellotta, R. (1985). "New Developments in field and Laboratory Testing of Soils," Proceeding of 11th International Conference on Soil Mechanics and Foundations, Balkema, Rotterdam, Volume 1, 617-634 or 57-154.
- Janbu, N. and Senneset, K. (1974). "Effective Stress Interpretation of In situ Static Penetration Tests," Proceedings of the European Symposium on Penetration Testing, ESOPT 1, Stockholm, Sweden, Vol. 2.2, pp. 181-193.
- Jefferies, M. G, Crooks, J. H. A., Becker, D. E., and Hill, P. R. (1988). "Independence of Geostatic Stress from Overconsolidation in some Beaufort Clays: Reply to Discussion by P. W. Mayne and F. H. Kulhawy; G. Mesri and T. W. Feng, 1988, Canadian Geotechnical Journal," Canadian Geotechnical Journal, 25, 624-630.
- Jefferies, M. G, Crooks, J. H. A., Becker, D. E., and Hill, P. R. (1987). "Independence of Geostatic Stress from Overconsolidation in some Beaufort Clays," Canadian Geotechnical Journal, 24(3), 342-356.
- Juran, I., Mahmoodzadegan, B., Tumay, M. T. (1989). "Geotechnical Investigation and Piezocone Testing in Well Documented Liquefiable Sites in California," Department of Civil Engineering, Louisiana State University, Baton Rouge, LA.
- Keaveny, J.M. (1985). "In-Situ Determination of Drained and Undrained Soil Strength Using the Cone Penetration Test," PhD Dissertation, University of California at Berkeley.



Kerisel, J. (1964) "Deep Foundations - Basic Empermental Facts," Proceedings of the North American Conference on Deep Foundations, Mexico City.

Konrad, J. M. (1991). "Hibernia Geotechnical Investigation and Site Investigation: Discussion of a paper by G. R. Thompson and L. G. Long, 1989, Canadian Geotechnical Journal," Canadian Geotechnical Journal, 24, 168-170.

Konrad, J. M., Bozozuk, M., and Law, K. T. (1985). "Study of In Situ Test Methods in Deltaic Silt," Proceedings of the 11th International Conference on Soil Mechanics and Foundation, Volume 4, Balkema, Rotterdam, 879-886.

Konstantinidis, B., Pacal, A.J., and Shively, A.W. (1987) "Uplift Capacity of Drilled Piers in Desert Soils," Proceedings of Foundations for Transmission Line Towers, Geotechnical Special Publication number 8

Kovacs, W.D., Salomone, L.A. (1984) "Energy Evaluation of SPT Energy, Equipment and Methods in Japan comparied with SPT in the United States," U.S. Department of Commerce, report NBSIR 84-2910, Aug.

Kovacs, W.D., Salomone, L.A., and Yokel, F.Y. (1981) "Energy Measurements in the Standard Penetration Test," NBS Building Science Series No. 135, National Bureau of Standards, August.

Kulhaway, F. H., and Mayne, P. W. (1990). "Manual on Estimating Soil Properties for Foundation Design," Manual EL-6800, Electric Power Research Institute, Palo Alto, CA.

Lacasse, S. and Vage, T. (1985). "In Situ Site Investigation Techniques and Interpretation for Offshore", Norwegian Geotechnical Institute, Olso, Norway, 1985.

Lambe, T. W. and Whitman, R. V. (1969). *Soil Mechanics*, John Wiley and Sons, New York, New York. Soil Mechanics, 1969.

Larsson, P., and Mutabdic, M. (1991) "Piezocone tests in clay," Swedish Geotechnical Institute, Report number 42, Linkoping, Sweden.

Lee, K.L., and Seed, H.B. (1967) "Drained Strength Characteristics of Sands," Journal of the Soil Mechanics and Foundations Division, ASCE, Vol. 93, No. SM6, Proceeding paper 5561, Nov 1967, pp 117-141

Lee, M. M. and Campbell, K. W. (1985). "Relationship between Shear Wave Velocity and Depth of Overburden," Proceedings of Measurements and Use of Shear Wave Velocities, ASCE Fall convention, ASCE, Denver, CO, 63-76.

Lee, S.H.H. and Stokoe K.H. (1986) "Investigation of Low-Amplitude Shear Wave Velocity in Anisotropic Material," Geotechnical Engineering Report GR86-6 Civil Engineering Department, University of Texas at Austin.

Lieberman S. H., Theriault, G. A., Cooper, S. S., Malone, P. G., Olsen, R. S., and Lurk, P. W. (1991). "Rapid, Subsurface, In Situ Field Screening of Petroleum Hydrocarbon Contamination Using Laser Induced Fluorescence Over Optical Fibers," Proceedings of the Second International Symposium - Field Screening Methods for Hazardous Wastes and Toxic Chemicals, Las Vegas, NV, 57-63.

Lunne, T. (1991). Personal written communication, February.

Lunne, T., Eidsmoen, T., Gillespie, D., and Howland, J. D. (1988). Laboratory and Field Evaluation of Cone Penetrometers, Norwegian Geotechnical Institute (NGI), Oslo, Norway, 1988.

Lunne, T., and Kleven, A. (1981) " Role of CPT in North Sea Foundation Engineering", Proceedings of a Session Entitled Cone Penetration Testing and Experience - ASCE Fall Convention, ASCE, New York, 209-227.

Marcuson, W.F. III and Bieganousky, W.A. (1977), "SPT and Relative Density in Coarse Sands," Journal of Geotechnical Engineering Division, ASCE, Vol. 103, No. GT11, pp. 1295-1309.

Martin, G. R., and Douglas, B. J. (1980). "Evaluation of the Cone Penetrometer for Liquefaction Hazard Assessment," for U.S. Geological Survey, Contract No. 14-08-0001-17790, October, Project No. 79-153, Long Beach, CA.

Masood, T. (1990). "Comparison of In situ Methods to Determine Lateral Earth Pressure at Rest in Soils," Ph.D. Dissertation, University of California, Department of Civil Engineering, Berkeley, USA.

Masood, T., Mitchell, J. K., Lunne, T. and Hauge, E. A. (1988). "Joint U.C. Berkeley and Norwegian Geotechnical Institute in-situ testing at Hamilton Air Force Base and Bay Farm Island, California," Department of Civil Engineering, Berkeley, USA.

McLean, F.G., Franklin, A.G., and Dahlstrand, T.K., (1975). "Influence of Mechanical Variables on the SPT," Proceedings of the conference on In Situ Measurements of Soil Properties, ASCE, Vol II, pp 287-318

Meyerhof, G. G. (1961). "The Ultimate Bearing Capacity of Wedge Shaped Foundations," Proceedings of 5th International Conference on Soil Mechanics and Foundation Engineering, Paris, Vol. 2.

- Mitchell, J. K. (1978). "In-Situ Techniques for Site Characterization," Proceedings on Site Characterization and Exploration, ASCE, 107-129.
- Mitchell, J.K. (1993). *Fundamentals of Soil Behavior*, John Wiley & Sons, Inc., New York.
- Mitchell, J. K. and Gardner, W. S. (1975). "In situ Measurement of Volume Change Characteristics," State-of-the-art report, Proceedings of the Conference on In situ Measurement of Soil Properties, Specialty Conference of the Geotechnical Division, North Carolina State University, Raleigh, Vol. 11.
- Mosteller, F., and Tukey J.W. (1977). *Data Analysis and Regression*, Addison-Wesley Publishing Company.
- Olsen, R. S. (1984). "Liquefaction analysis using the cone penetrometer test," Proceedings of the Eighth World Conference on Earthquake Engineering, Volume III, Prentice-Hall Inc., Englewood Cliffs, NJ, 247-254.
- Olsen, R. S. (1988). "Using the CPT for Dynamic Site Response Characterization," Proceedings of the Earthquake Engineering and Soil Dynamic II Conference, Geotechnical Special Publication Number 2, J. Lawrence Von Thun, ed., ASCE, New York, 374-388.
- Olsen, R. S. (1992). "CPT Evaluation of the Midnight Hour II and Husky Jaguar I projects," internal report for Geomechanics Division, WES, November 1992.
- Olsen, R. S. (1994). "Use and interpretation of the Cone Penetrometer Test (CPT)," Engineering manual prepared for the Office of Engineers, Corps of Engineers, Washington D.C., manual designation EM 1110-2-359
- Olsen, R. S., Bluhm, P. F., Hynes, M. E., Yule, D. E., and Marcuson III, W. F. (1989). "Seismic Stability Evaluation of Alben Barkley Lock and Dam Project - Volume 3 - Field and Laboratory Investigation," Technical Report GL-86-7, U.S. Army Engineer Waterways Experiment Station, Vicksburg, MS.
- Olsen, R. S. and Farr, J. V. (1986). "Site Characterization using the Cone Penetrometer Test," Proceedings of In Situ 86 - Use of In Situ Tests in Geotechnical Engineering, Geotechnical Special Publication Number 6, S. P. Clemence, ed., ASCE, New York, 854-868.
- Parkin, A. K., Holden, J., Aamot, K., Last, N. and Lunne, T. (1980). "Laboratory Investigations of CPT's in Sand," Norwegian Geotechnical Institute, Report 52108-9, Oslo.

- Parkin, A. K., Holden, J., Aamot, N. and Lunne, T. (1980). "Laboratory Investigation of CPTs in Sand," Norwegian Geotechnical Institute, Report 52108-9, Oslo.
- Parkin, A. K. and Lunne, T. (1982). "Boundary Effects in the Laboratory Calibration of a Cone Penetrometer in Sand," Proceedings of the Second European Symposium on Penetration Testing, ESOPT II, Amsterdam, May 1982, Vol. 2, pp. 761-768.
- Peck, R. B., Hanson, W. E., and Thornburn, T. H. (1974). *Foundation Engineering*, 2nd Ed., John Wiley and Sons, New York, NY.
- Rahardjo, P.P. (1989) "Evaluation of Liquefaction Potential of Silty Sand based on Cone Penetrometer Test," Ph.D. Dissertation, Department of Civil Engineering, Virginia Polytechnic Institute and State University, Blacksburg, Virginia.
- Richart, F.E., Hall, J.R., and Woods, R.D. (1970) *Vibrations of Soils and Foundations*, Prentice-Hall, New Jersey
- Ripley, C. F. and Lee, K. L. (1962). "Sliding Friction Tests on Sedimentary Rock Specimens," Translations of the 7<sup>th</sup> International Congress on Large Dams, Rome, Vol. 4, pp. 657-671.
- Rad, N.S., Eidsmoen, T., and Lunne, T. (1985) "In Situ Investigation Techniques and Interpretation for Offshore Practice, Interpretation of Piezocone tests in Onsoy and Haga Clays," Norwegian Geotechnical Institute, Report 40019-23, Progress report, December
- Rahardjo, P.P. (1989) "Evaluation of Liquefaction Potential of Silty Sand based on Cone Penetrometer Test" Dissertation submitted in partial fulfillment of the requirement for the degree of Doctor of Philosophy, Virginia Polytechnic Institute, Virginia
- Robertson, P. K., Campanella, R. G., Gillespie D., and Greig, J. (1986). "Use of Piezometer Cone Data," Proceedings of In Situ 86 - Use of In Situ Tests in Geotechnical Engineering, Geotechnical Special Publication Number 6, S. P. Clemence, ed., ASCE, New York, 1263-1280.
- Robertson, P. K., and Campanella, R. G. (1984). "Guidelines for Use and Interpretation of the Electric Cone Penetrometer," Hogentogler and Co., Gaithersberg, MD.
- Robertson, P. K. and Campanella, R. G. (1983). "Interpretation of Cone Penetration Tests - Part I (Sand)," Canadian Geotechnical Journal, Vol. 20, No. 4, pp. 734-745.

- Robertson, P. K. and Campanella, R. G. (1983). "Interpretation of Cone Penetration Tests - Part 11 (Clay)," Canadian Geotechnical Journal, Vol. 20, No. 4.
- Robertson, P. K., Campanella, R. G., and Wightman, A. (1983). "SPT-CPT Correlations," Journal of the Geotechnical Division, ASCE, Vol. 109, November.
- Rowe, P.W. (1962) "The Stress-Dilatancy Relation for Static Equilibrium of an Assembly of Particles in Contact", Proceedings of the Royal Society, Vol. A269, pp. 500-527
- Rowe, P.W. (1962) "The Relevance of Soil Fabric to Site Investigation Practice," Geotechnique, Vol. 22, No. 2, pp. 195-300.
- Schmertmann, J. H. (1976). "Predicting the  $q_c/N$  Ratio," Final Report D-636, Engineering and Industrial Experiment Station, Department of Civil Engineering, University of Florida, Gainesville.
- Schmertmann, J. H. (1978a). "Guidelines for Cone Penetration Test, Performance and Design," U.S. Department of Transportation, Federal Highway Administration, Report FHWA-TS-78-209, Washington, July 1978, 145 pgs.
- Schmertmann, J. H. (1978b). "Study of Feasibility of Using Wissa-Type Piezometer Probe to Identify Liquefaction Potential of Saturated Sands," U.S. Army Engineer Waterways Experiment Station, Report S-78-2.
- Schmertmann, J. H. (1979a). "Statics of SPT," Journal of the Geotechnical Engineering Division, ASCE, Vol. 105, No. GT5, May.
- Schmertmann, J. H. (1979b). "Energy Dynamics of SPT," Journal of the Geotechnical Engineering Division, ASCE, Vol. 105, No. GT8, August.
- Schofield, A., and Wroth, P. (1968). *Critical State Soil Mechanics*, McGraw-Hill, Berkshire, England
- Seed, H. B. (1976). "Evaluation of Soil Liquefaction Effects on Level Ground During Earthquakes," Liquefaction Problems in Geotechnical Engineering, ASCE Preprint 2752, Philadelphia, PA.
- Seed, H. B. and De Alba, P. (1986). "Use of SPT and CPT tests for evaluating the liquefaction resistance of soils," Proceedings of the Specialty Conference on the Use of In Situ Tests in Geotechnical Engineering, Blacksburg, VA, ASCE Geotechnical Special Publication No. 6, pp. 120-134.

- Seed, H. B. and Idriss, I. M. (1970). "Soil Moduli and Damping Factors for Dynamics Response Analysis," Report No. EERC 70-10, Univ. of California, Berkeley, December.
- Seed, H. B. and Idriss, I. M. (1981). "Evaluation of Liquefaction Potential of Sand Deposits Based on Observations of Performance in Previous Earthquakes," Geotechnical Engineering Division, ASCE National Convention, St. Louis, Session No. 24.
- Seed, H. B. and Idriss, I. M. (1982). *Ground Motions and Soil Liquefaction during Earthquakes*, Earthquake Engineering Research Institute, Berkeley, CA.
- Seed, H. B., Idriss, I. M. and Arango, T. (1983). "Evaluation of Liquefaction Potential Using Field Performance Data," Journal of Geotechnical Engineering Division, ASCE, Vol. 109, No. 3, March 1983, pp. 458-492.
- Seed, H. B., Seed, R. B., Harder, L. F., and Jong, H. L. (1988). "Re-Evaluation of the Slide in the Lower San Fernando Dam in the Earthquake of February 9, 1971," Report No. UCB/EERC-88/04, April, Earthquake Engineering Research Center, University of California at Berkeley, Berkeley, CA.
- Seed, H. B., Seed, R. B., Harder, L. F., and Jong, H. L. (1989). "Re-Evaluation of the Lower San Fernando Dam - Report 2 - Examination of the Post-Earthquake Slide of February 9, 1971," Contract Report GL-89-2, U.S. Army Engineer Waterways Experiment Station, Vicksburg, MS.
- Singh R.D. and Gardner, W.S. (1979). "Characterization of Dynamic Properties of Gulf of Alaska Clays, Proceedings of the ASCE Fall convention session entitled "Soil Dynamics in Marine Environment", Boston, Preprint 3604.
- Skempton, A.W. (1986) "Standard Penetration Test Procedures and the Effects in Sands of Overburden Pressure, Relative Density, Particle Size, Aging, and Overconsolidation," *Geotechnique*, Vol. 36, No. 3, pp 425-447.
- Stokoe, K.H., Lee, S.H.H., and Knox D.P. (1985) "Shear Moduli Measurements under True Triaxial Stresses", Proceedings of a session sponsored by the Geotechnical Engineering Division, ASCE, Edited by Khosia, October 24, 1985
- Stokoe, K.H., II, Lee, S.H.H., and Chu, H.Y.F. (1985) "Effects of Stress State on Velocity of Low-Amplitude Compression and Shear of Non-nuclear munitions with structures," Proceedings of the second symposium on the Interaction of Non-nuclear munitions iwth structures, Eglin AFB, Florida, April 1985
- Stratigraphics Inc (1988). "Piezocone Penetration Testing, Northwestern University, Pile Load Test Site, Evanston, IL," Project report, Job 088-03, June.

- Taylor, J. K. (1990). *Statistical Techniques for Data Analysis*, Lewis Publisher, Inc., Chelsea, MI,
- Telford, W.M., Geldart, L.P., Sheriff, R.E., and Keys, D.A. (1967). *Applied Geophysics*, Cambridge University Press, Cambridge
- Terzaghi, K. (1943). *Theoretical Soil Mechanics*, John Wiley and Sons, Inc., New York, NY.
- Terzaghi, K. and Peck, R. B. (1967). *Soil Mechanics and Engineering Practice*, John Wiley and Sons, New York.
- Torrey, V. H. (1988). "Retrogressive Failures in Sand Deposites of the Mississippi River - Report 2 - Empirical Evidence in support of the Hypothesized Failure Mechanism and Development of the Levee Safety Flow Slide Monitoring System," Technical Report GL-88-9, U.S. Army Waterways Experiment Station, Vicksburg, MS.
- Torrey, V. H., Dunbar, J. B., and Peterson, R. W. (1988). "Retrogressive Failures in Sand Deposites of the Mississippi River - Report 1 - Field Investigations, Laboratory Studies and Analysis of the Hypothesized Failure Mechanism," Technical Report GL-88-9, U.S. Army Waterways Experiment Station, Vicksburg, MS.
- Tseng, D-J. (1989). "Prediction of Cone Penetration Resistance and Its Application to Liquefaction Assessment," PhD Dissertation, University of California at Berkeley
- Tulsa District of the Corps of Engineers. (1982). "Arcadia Lake - Deep Fork River - Design Memorandum No. 9 - Supplement No. 1 - Embankment and Spillway," Corps of Engineers, Tulsa, OK.
- Tumay, M. T. (1985). Field Calibration of Electrical Cone Penetrometer in Soft Clay- Executive, Louisiana Department of Transportation and Development, Baton Rouge, LA, 1985.
- Tumay, M. T., and DeSeze, E. (1983). Correlations of Undrained Shear Strength  $S_u$  and QCPT results using, Department of Civil Engineering, Louisiana State University, Baton Rouge, LA, 1983.
- Tumay, M. T., Acar, Y. and Deseze, E. (1982). "Soil Exploration in Soft Clays with the Quasi-static Electric Cone Penetrometer," Proceedings of the Second European Symposium on Penetration Testing, ESOPT II, Amsterdam, Vol. 2, pp. 915-921.

Updike, R. G., Olsen, H. W., Schmoll, H. R., Kharaka, Y. K. and Stokoe II, K. H. (1988). "Geologic and Geotechnical Conditions Adjacent to the Turnagain Heights Landslide, Anchorage, Alaska," U.S. Geological Survey Bulletin No. 1817, Denver, CO.

Updike, Randall G. (1984). "The Turnagain Heights Landslide," State of Alaska, Department of Natural Resources, Division of, Alaska, 1984.

Vesic, A. S. (1972). "Expansion of Cavities in Infinite Soil Masses," Journal of the Soil Mechanics and Foundation Division, ASCE, Vol. 98, SM3, pp. 265-290.

Vesic, A. S. (1963). "Bearing Capacity of Deep Foundations in Sand," Highway Research Report 39, Highway Research Board, National Research Council, Washington, DC.

Vesic, A.S., and Barksdale R. D. (1964). "On Shear Strength of sands at very high pressures," Symposium on Laboratory Shear Testing of Soils, Ottawa, 1963, ASTM Special technical publication, No. 361, pp 301-305.

Vesic, A. S., and Clough, G. W. (1968). "Behaviour of Granular Materials under High Stresses," Journal of the Soil Mechanics and Foundations Division, ASCE, vol. 94, no. SM3, May 1968, pp. 661-688.

Vicksburg District of the Corps of Engineers. (1988). "Cone Penetrometer Testing - Atchafalaya River - Dredging Studies," Report, Corps of Engineers, Vicksburg, MS.

Vicksburg District of the Corps of Engineers. (1988). "Levee Failure Investigation at St. Marin and Jefferson Parish, LA," Corps of Engineers, Vicksburg, MS.

Wahl, R. E., Olsen, R. S., Bluhm, P. F., Yule, D. E., and Hynes, M. E. (1991). "Stratigraphy Evaluation of the Foundation Soils for the Dynamic Analysis of the Alben Barkley Dam, KY," *Proceedings of the 1991 Geotechnical Engineering Congress*, ASCE, New York.

Wahl, R. E. Olsen, R. S., Hynes, M. E., Yule, D. E. and Bluhm, P. (1989). "Seismic Evaluation of Alben Barkley Dam: Volume 4 - Liquefaction Susceptibility Evaluation and Post-Earthquake Strength Determination," Technical Report GL-865-7, U.S. Army Waterways Experiment Station, Vicksburg, MS.

Webster's The New Collegiate Dictionary (1975). G & C Merriam Company, Springfield, Massachusetts.



Woodward-Clyde Consultants. (1987). "Subsurface Investigation and Geotechnical Reports - Oakland Federal building," for Kaplan-McLaughlin-Diaz Corp., Project No. 16864A, Oakland, CA.

Yareshenko, V.A. (1964). "Interpretation of the Results of Static Penetration of Sands," Fundamety Proekt, No. 3.

Yilmaz, R. (1991). FUGRO Corporation, Houston, TX, Personal written communication

# Appendix

## The Database Contents

### *Introduction*

Collecting the CPT and boring data represented the single largest effort (and longest time effort) for the purpose of developing CPT correlations of geotechnical properties. There were three major sources for this data, namely, 1) the author's project files, 2) requests for data by letter, and 3) requests for data after a lecture was presented. Overall, the best CPT and boring data originated from the author's project files. This data base represents the largest coherent accumulation of CPT cone and sleeve with boring/laboratory project/research data in the world (1994). This collection of data also contains two types of data: field CPT/boring data and laboratory large diameter chamber test data. Most of the collection emphasis was directed toward field CPT/boring data.

### *Requesting Data by Letter*

From 1986 to 1988, about 120 letters were sent to government, utility and consulting firms requesting CPT and boring data. Only 15% of the requests for data resulted in data and only 5% of the total database came from these blind requests for data. Only 60% of the data received during this research program was usable. Less than 15% of the geotechnical engineering publications which describe projects having CPT data actually show a CPT sounding log. When a CPT sounding log was

presented in a publication, less than 10% of the total also show sleeve friction measurements. Therefore, only a small fraction of this database originated from publications.

### *Requesting Data by Presenting Lectures*

Approximately half of the geotechnical data came from professional contacts and as a result of presentation lectures on CPT technology. A total of 23 lectures were presentations by the author to consulting engineering companies and state/federal organizations from 1988 to 1992. Engineers typically felt obligated after a lecture was presented to search for and copy at least one geotechnical project for this research program.

### *The Data in the Database*

This database contains approximately 670 CPT records and 580 borings from 90 projects. The CPT records represent approximately 51,000 ft of data and there are at least 1,200 boring soil samples with a total of approximately 8,100 laboratory and field test values. The following is a partial list of the types of data in the database: CPT measurements (cone resistance, sleeve friction resistance, and dynamic pore pressure), SPT blow count, measured shear wave velocity, water content, plastic limit, liquid limit, total density, percent passing #200 sieve,  $D_{50}$ , field vane shear strength, laboratory triaxial strength test results (and testing method), Unified Soil Classification System designation, word descriptor based soil classification, consolidation parameters (e.g.  $C_c$ ,  $C_s$ , OCR,  $P_{max}$ , etc.), void ratio, etc.,

## *Test Chamber Data*

Data from several large diameter test chambers are also included in the database for establishing new CPT and SPT normalization techniques. The CPT chamber data was provided by Jamiolkowski (1988). SPT chamber data by Bieganousky and Marcuson (1976, 1977) and Gibbs and Holtz (1952) were also included in this data base collection. A complete listing and description of the CPT and boring data base are shown in Table A-1. The soil conditions column provides a general descriptor only for comparison between sites.

## *Data Sensitivity*

Most of the data used in this research program originated from military, sensitive security, or sensitive private projects where the data source must be kept confidential. Much of the private project data (classified as sensitive private sites) were provided by geotechnical engineering consulting firms with the understanding that the data and source would be kept confidential. In all cases, the data could be used to establish data correlations and the data points on the correlation plots could be published; however, the provider would not allow the site name to be published.

Table A-1 Summary of CPT projects contained in the data base

Project	Soil conditions	Number of CPT soundings / boreholes (in database)	General Stratigraphic AQI	Laboratory tests	Reference
Afchafalaya River, Dredge Study (Corps of Engineers)	River sediments	157 / 0		none	Olsen Files (1985)
Arcadia Dam Deep Fork River, Oklahoma	Medium dense sands and clay mixtures	5 / 9	76%	SPT, index, and strength	Tulsa District, Corps of Engineers (1982)
China, Five Sites which liquefied during the 1989 Earthquake	Liquefiable dirty sands and soil mixtures	4 / 5	76%	SPT, index, and $V_s$	Brown, Strutynsky, and Douglas (1985) (Research Report to NSF)
Barkley Dam, Seismic Evaluation (Corps of Engineers, Nashville District)	medium stiff clayey and silty sands	65 / 30	76%	SPT, index, steady state, and $V_s$	Olsen, Bluhm, Hynes, Yule, and Marcuson, (1989) WES report
Blackfoot Dam, Seismic Evaluation, Idaho (Corps of Engineers, Walla Walla District)	Medium stiff silty sands	2 / 2	76%	$V_s$	Olsen files ERTEC report (1987)

Agios Stefanos Bridge Piers Liquefaction Evaluation, Greece	loose sands	1 / 1	65%	$S_u$ and $V_s$	Boukvalas, Kalteziotis, Sabtakakis, and Zervogiann (1989)
Private, project code CC*, Liquefaction evaluation of a tailing dam	tailing material	2 / 2	76%	index tests	Olsen Files
Private, project code LC-V* Liquefaction evaluation of a Hospital addition	medium dense sands	2 / 2	78%	SPT and index tests	Olsen Files
Fraser River Delta Bridge, Canada, Consolidation data comparison	Compressible silts and clays	1 / 2	95%	index tests, consolidation, and $V_s$	Crawford and Campanella (1991)
Government. project code C-CG*	Silts and sensitive silts	19 / 3	79%	SPT, index tests, $S_u$	Olsen Files (1993)
Private, project code ET-SE* Pile capacity	San Francisco Bay mud	1 / 1	95%	index test, $S_u$	Olsen Files (1981)
Grays Harbor, Seattle. Liquefaction Evaluation (Seattle District, Corps of Engineers)	River sediments, dirty sands and clayey silts	9 / 6	71%	index tests and SPT	Olsen Files (1993)
Great America Parkway (California Department of Transportation)	soft to medium stiff clays and silt mixtures	6 / 6	76%	SPT, index tests, $S_u$ (torvane), consolidation	Caltran contractor reports (1987)
Private, project code HL-GH* Excavation evaluation	sands	4 / 0			Olsen files

Government, project code DN-HJ1*	compacted uniform sand	7 / 0			Olsen files
Government, Project code DN-HJ2*	compacted uniform sand	12 / 12		$V_s$	Olsen files
Government, Project code DN-MH*	compacted uniform sand	8 / 8		$V_s$	Olsen files
Government, project code DE-S-R*	medium stiff clays and medium dense sands	12 / 11	88%	SPT, index tests, Strength, $V_s$	Olsen files
Government, project code DE-S-K*	Medium stiff clays and medium dense sands	4 / 9	40%	SPT, index tests, $V_s$	Olsen files
Private, Project code HL-JW Airport expansion investigation	medium stiff clays and medium dense sands	17 / 15	70%	SPT, index tests, $S_u$	Olsen files
Lower San Fernando dam Seismic Evaluation in 1985	Desiccated hydraulic material, and foundation	11 / 6	70%	SPT, index tests, $S_u$ , steady state	Seed, et.al. (1985) Castro, et.al. (1985) ERTEC (1984)
Hong Kong Sha Tsui Tau at Tung Chung Bay, Replacement airport	soft bay deposits	5 / 12	79%	$S_u$ , index tests, consolidation	Dames & Moore (1982) Koutsoflas and Foot (1982)
USGS Post Loma Prieta Earthquake at Santa Cruz & Treasure Island	Loose to medium dense Dirty sands	11 / 16	77%	SPT and $V_s$	Hryciw (1990) report for USGS

Intermountain Power Project Delta, Utah (foundation investigation)	Very stiff clays and very dense sands	4 / 4	85%	SPT, index tests, $V_s$	Olsen files
Private, project code RP-IT* dike evaluation over soft clay	soft clay	7 / 8	75%	index tests, $S_u$ , consolidation	Olsen files
Jackson Lake Bureau of Reclamation	loose dirty sand	19 / 0			Olsen files
Vancouver Airport, Canada Sea Island	soft silts and clay	1 / 1	83%	$S_u$ index tests	Konrad, Bozozuk, and Law (1985)
Private, project code LE-JN	medium stiff soil mixtures	2 / 2	60%	SPT, index test	Olsen files
Heber road & Wildlife sites, California Liquefaction evaluation study	loose to medium density sand	2 / 2	85%	SPT, index tests	Juran, Mahmoudzadegan, and Tumay (1989) Research report
Lorco, Louisiana Research on soft sediments	very soft clays	3 / 3	78%	Index tests, $S_u$ and consolidation	Tumay and Deseze (1992)
Lucky Peak Dam, Liquefaction Evaluation	Medium dense clay silt	2 / 4	78%	$V_s$	Olsen files
Mackenzie Delta bay Beaufort Sea, Canada 3 sites	Soft to medium stiff silts	3 / 4	80%	$V_s$	Campanella, Robertson, Gillespie, Racing, Kurfurst (1987)
Private, project code DM-MT* Excavation evaluation	soft clay	5 / 12	84%		Olsen files



Nerlerk Berm, Beaufort Sea Liquefaction slide evaluation	Soil mixtures	2 / 1	79%	Index tests, $S_u$	Been, Conlin, Crooks, Fitzpatrick, Jefferies, Rogers. Shinde (1987)
Ririe Dam Seismic Evaluation Corps of Engineers	Compacted silts and sands	1 / 1	90%	$V_s$	ERTEC (1987) Olsen files
Tarsiut P-45, Beaufort Sea, Canada	Sand and soil mixtures	1 / 1	90%	index tests, consolidation	Jefferies, Crooks, Beecker, and Hill (1988)
Norwegian Geotechnical Institute (NGI) Research Sites	loose to medium dense sand	3 / 5			
	soft clays	2 / 3		index tests, $S_u$ , $V_s$ , and consolidation	Numerous NGI reports (from 1980 to 1988)
	soft clays	3 / 6	90%		
Northwestern University Pile study	Sand (fill) and clay	1 / 3	80%	Index test, $S_u$ , and SPT	Strutynsky (1989)
Pinto Dam study. Liquefaction Evaluation Bureau of Reclamation	Silts and sand	8 / 4	76%	SPT and index tests	Olsen files
Sardis Dam Liquefaction Evaluation, Mississippi	Hydraulic sand and river sediments	76 / 256	55%	index tests, SPT, $S_u$	Olsen files

Swedish Geotechnical Institute (SGI) Research sites	Sara Road 6-900	soft clays	1 / 1	96%	Index tests, $S_u$ , and consolidation	Larsson and Mulabdic (1991) SGI report 42		
	Sara Road 7-600	soft clays	1 / 1	96%				
	Backebol, Hisingen Island	soft clays	1 / 1	96%				
	Limma Mellosa	very soft clays and organic clays	1 / 1	96%				
	Norrkoping	clays	1 / 1	96%				
	Ska-Edeby	very soft clay	1 / 1	96%				
	Tuve	soft clays	1 / 1	96%				
	Valen	organic clay	1 / 1	96%				
	Bonnet Carre Points	sands and silts	2 / 2	60%			Index tests, SPT	Torrey, Dunbar, Peterson (1988) (WES report)
	Montz	sands and silts	4 / 5	60%				
Foundations for transmission line towers	Almo, NV	Very stiff clays and mixture	1 / 1	65%		Konstatindis et.al. (1986)		
	Baker, California	Very stiff clays and dense sands	1 / 1	85%				
	Caliente	Very dense sands	1 / 1	65%				
	Delta	medium dense dirty sand	1 / 1	65%				

Private project code HL-TI	medium dense sands old hydraulic sand	3 / 3	70%	Index tests, SPT, consolidation, S <sub>u</sub>	Olsen files
Turnagain Heights Landslide, Anchorage, AL	clays and silts	3 / 3	67%	Index tests and S <sub>u</sub>	Updike, Olsen H, Schmoll, Kharaka and Stokoe (1988)
Lower 232 Street British Columbia, Canada	Clay and silt	1 / 1	90%	Index tests and S <sub>u</sub>	Campanella, Robertson, and Gillespie (1982)
McDonald Farm, University of British Columbia Research site	Sand and silt	1 / 1	90%	Index tests, V <sub>s</sub> , and S <sub>u</sub>	Campanella, Robertson, and Gillespie (1982)
Heber Road, El Centro, California (Liquefaction evaluation)	Sands	5 / 0			Douglas and Martin (1982) (NSF research report)
Evaluation of CPT for Liquefaction Hazard Assessment (California sites)	Coyote North	2 / 3	78%		
	Coyote South	2 / 2	71%		
	Moss Landing	2 / 2	76%	SPT and index tests	Martin and Douglas (1980)
	Salinas Landing	4 / 4	85%		research report to USGS
	San Diego NAS	7 / 8	84%		

Wildlife, California Site characterization for liquefaction potential evaluation	sands, silts and clay	15 / 11	79%	SPT and index tests	Bennett, et.al. (1984) USGS research report
Mississippi River dike failure, w-46 and W-52 sites	Clay	23 / 4	76%	SPT, index tests, and $S_u$	Olsen files
Private, project WC-FOK*	Clays and silts	2 / 3	78%	SPT, $S_{up}$ , $V_s$ , & index tests	Olsen files
Private, project WC-HY*	Stiff clays and silts	4 / 4	74%	SPT, $S_{u'}$ , consolidation, & index tests	Olsen files
Private, project code WC-HRB*	Medium stiff clays and silts	3 / 3	70%	SPT, $S_{u'}$ , and index tests	Olsen files
Private, project code WC-TSS*	Stiff clay and some sands	2 / 2	77%	Index tests and SPT	Olsen files

\* Sensitive project, data origin must be confidential

# REPORT DOCUMENTATION PAGE

Form Approved  
OMB No. 0704-0188

Public reporting burden for this collection of information is estimated to average 1 hour per response, including the time for reviewing instructions, searching existing data sources, gathering and maintaining the data needed, and completing and reviewing the collection of information. Send comments regarding this burden estimate or any other aspect of this collection of information, including suggestions for reducing this burden, to Washington Headquarters Services, Directorate for Information Operations and Reports, 1215 Jefferson Davis Highway, Suite 1204, Arlington, VA 22202-4302, and to the Office of Management and Budget, Paperwork Reduction Project (0704-0188), Washington, DC 20503.

<b>1. AGENCY USE ONLY (Leave blank)</b>	<b>2. REPORT DATE</b> August 1994	<b>3. REPORT TYPE AND DATES COVERED</b> Final report	
<b>4. TITLE AND SUBTITLE</b> Normalization and Prediction of Geotechnical Properties Using the Cone Penetrometer Test (CPT)		<b>5. FUNDING NUMBERS</b>	
<b>6. AUTHOR(S)</b> Richard S. Olsen		<b>8. PERFORMING ORGANIZATION REPORT NUMBER</b>  Technical Report GL-94-29	
<b>7. PERFORMING ORGANIZATION NAME(S) AND ADDRESS(ES)</b> U.S. Army Engineer Waterways Experiment Station 3909 Halls Ferry Road Vicksburg, MS 39180-6199		<b>10. SPONSORING/MONITORING AGENCY REPORT NUMBER</b>	
<b>9. SPONSORING/MONITORING AGENCY NAME(S) AND ADDRESS(ES)</b> U.S. Army Corps of Engineers Washington, DC 20314-1000		<b>11. SUPPLEMENTARY NOTES</b>  Available from the National Technical Information Service, 5285 Port Royal Road, Springfield, VA 22161.	
<b>12a. DISTRIBUTION/AVAILABILITY STATEMENT</b>  Approved for public release; distribution is unlimited.		<b>12b. DISTRIBUTION CODE</b>	
<b>13. ABSTRACT (Maximum 200 words)</b>  <p>This research was to develop techniques for (1) stress normalization of CPT measurements (and geotechnical properties) and (2) CPT prediction of geotechnical properties using cone and sleeve friction resistance values. Stress normalization allows a variable geotechnical property to be reduced to an equivalent value at a standard confining stress.</p> <p>A new concept, the Stress Focus, was identified which provides a basis for understanding soil strength as a function of confining stress. This study demonstrated that sand friction angles for different initial relative densities converge to a Stress Focus at high confining stress (approximately 100 atm), where the strength behavior is similar to that of a sedimentary rock. Dilation of dense sands decreases with increased confining stress until the Stress Focus is reached, as confirmed using historic high pressure triaxial test data as well with CPT measurements from laboratory chamber tests and uniform soil layers. The paths of convergence to the Stress Focus are exponentially related to confining stress and are the basis for development of CPT cone and sleeve friction resistance normalization techniques. The overburden stress at the Stress Focus is soil type dependent.</p> <p style="text-align: right;">(Continued).</p>			
<b>14. SUBJECT TERMS</b>  See reverse.		<b>15. NUMBER OF PAGES</b>  322	
		<b>16. PRICE CODE</b>	
<b>17. SECURITY CLASSIFICATION OF REPORT</b>  UNCLASSIFIED	<b>18. SECURITY CLASSIFICATION OF THIS PAGE</b>  UNCLASSIFIED	<b>19. SECURITY CLASSIFICATION OF ABSTRACT</b>	<b>20. LIMITATION OF ABSTRACT</b>

13. (Concluded).

The stress exponent for SPT normalization was shown to be equal to the CPT derived stress exponent.

CPT correlations to geotechnical properties were established using both CPT cone resistance and friction ratio. These correlations were based on a large database which was developed for this research effort. Statistical evaluation during the development of these correlations concentrated on excluding biased data. CPT based correlations were established for the following geotechnical properties: SPT blow count, unconsolidated undrained triaxial test strength, field vane shear test strength, and shear wave velocity.

14. (Concluded).

Geotechnical properties  
Sand friction angles  
Soil strength

Stress exponent  
Stress normalization